UNIVERSITÀ DEGLI STUDI DELL'INSUBRIA

Dipartimento di Scienza ed Alta Tecnologia (DISAT)

PhD in Chemical Sciences, cycle XXVIII

Synthesis and biomedical applications of novel RGD- and *iso*DGR-integrin ligands

Silvia Panzeri

720558

Tutor: Prof. Umberto Piarulli

A.Y. 2014/2015

The work herein described was performed at the University of Insubria (Como) in the period from November 2012 to October 2014 under the supervision of Prof. Umberto Piarulli, and at the Institute of Organic Chemistry at the University of Regensburg in the period from October 2014 to October 2015 in Prof. Dr. Oliver Reiser's research group.

Doctoral Final Oral Examination: February, 5th 2016

Examination Committee:

Prof. Oliver Reiser,

Prof. Daniele Passarella

Prof. Andrea Goti

TABLE OF CONTENTS

CHAPTER 1

INTEGRIN LIGANDS

1.1 Targeting integrins

1.1.1 Introduction

Integrins are the major family of adhesion receptors in the *Animalia* kingdom. This family was first recognized around 25 years ago[1] and since then have become attractive pharmacological targets[2]. In the last decade research focused on the discovery and development of integrin antagonists for clinical applications because of their roles in pathological conditions.[3] A turning point for class-selective or promiscuous integrin inhibitor was provided by rational design based on the discovery of the structural basis of the integrin-ligand recognition. This aim has been achieved by means of studies on short amino acid sequences[4] and crystallographic, electron microscopy, computational analysis[5] on selected integrin subfamilies.

Integrins are involved in the regulation of many aspects of cell behavior,[6] in cell adhesion to the ECM proteins, they provide anchorage for endothelial cells and they make transmembrane connections between the ECM and the cytoskeleton, mediating dynamic linkages. In addition, they activate many intracellular signaling pathways. Moreover in vertebrates, these proteins play a role in mediating cell-cell adhesion processes. Thanks to their involvement in all these functions, integrins are involved both in physiological processes and pathological conditions. These receptors and their ligands play a key role in pathogenesis of inflammatory diseases, leukocyte traffic, aggregation, tumor progression, osteoporosis and macular degeneration.

[1] Hynes, R. O., *Cell* **1987**, *48*, 549-554
[2] Millard, M.; Odde, S.; Neamati, N., *Theranostics* **2011**, *1*, 154-188
[3] (a) Shimaoka, M.; Springer, T. A., *Nature Rev. Drug. Discov.* **2003**, *2*, 703-716; (b) Gottschalk, E.-K.; Kessler, H., *Angew. Chem. Int. Ed.* **2002**, *41*, 3767-3774; (c) Miller, W. H.; Keenan, R. M.; Willette, R. N.; Lark, M. W., *Drug Discovery Today* **2000**, *5*, 397-408; (d) Ojima, I., *Bioorg. Med. Chem.* **1995**, *3*, 337-360
[4] (a) Rouslahti, E., *Matrix Biol.* **2003**, *22*, 459-465; (b) For a review on the *iso*DGR-motif see: Rouslahti, E., Annu. *Rev. Cell. Dev. Biol.* **1996**, *12*, 967-715
[5] (a) Xiong, J. P.; Stehle, T.; Diefenbach, B.; Zhang, R.; Dunker, R.; Scott, D. L.; Joachimiak, A.; Goosman, S. L.; Amaout, M. A., *Science* **2001**, *294*, 339-345; (b) Xiong, J. P.; Stehle, T.; Diefenbach, B.; Zhang, R.; Dunker, R.; Scott, D. L.; Joachimiak, A.; Goosman, S. L.; Amaout, M. A., *Science* **2002**, *296*, 151-155; (c) Chen, W.; Chang, C.; Gilson, M. K., *J. Am. Chem. Soc.* **2006**, *128*, 4675-4684; (d) Marinelli, L.; Meyer, A.; Heckmann, D.; Lavecchia, A.; Novellino, E.; Kessler, H., *J. Med. Chem.* **2005**, *48*, 4204-4207; (e) Marinelli, L.; Gottschalk, K.-E.; Meyer, A.; Novellino, E.; Kessler, H., *J. Med. Chem.* **2004**, *47*, 4166-4177; (f) Xiao, T.; Tagaki, J.; Coller, B. S.; Wang, J.-H.; Sprinmger T. A., *Nature* **2004**, *432*, *59-67*; (g) Springer, T. A.; Zhu, J.; Xiao, T., *J. Cell. Biol.* **2008**, *182*, 791-800; (h) You, T. J.; Maxwell, D. S.; Kogan, T. P.; Chen, Q.; Li, J.; Kassir, J.; Holland, G. W.; Dixon, R. A. F., *Biophys. J.* **2002**, *82*, 447-457
[6] Barczyk, M.; Carracedo, S.; Gullberg, D., *Cell Tissue Res.* **2010**, *339*, 269-280

1.1.2 Integrins: family, structure, function

1.1.2.1 Integrins structure and subfamilies

Integrins are a heterodimeric membrane glycoproteins composed by non-covalently associated α- and β–subunits (Figure 1.1). In mammals 18 α and 8 β subunits, giving rise to 24 different heterodimers, are present but their diversity varies among species.[7]

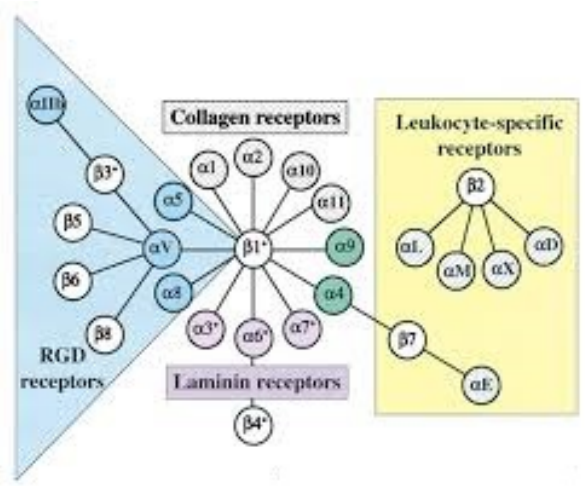

Figure 1.1 – Mammalian integrins subunits and their associations

Selectivity for ECM proteins, cell surface molecules, plasma proteins, or microorganism is determined by the combination between the α- and the β-chain.[8] Although some integrins recognize primarily a single ECM protein ligand, others can bind several ligands (e.g., $\alpha_v\beta_3$ binds vitronectin, fibronectin, fibrinogen, denatured or proteolyzed collagen, and other matrix proteins).[8b,9]

[7] Hynes, R. O., *Cell* **2002**, *110*, 673-687

[8] (a) Loftus, J. C.; Smith, J. W.; Ginsberg, M. H., *J.Biol. Chem.* **1994**, *269*, 25235-25238; (b) Plow. E. F.; Haas, T. A.; Zhang, L.; Loftus, J. C.; Smith, J. W., *J. Biol. Chem.* **2000**, *275*, 21785-21788; (c) Van der Flier, A.; Sonnenberg, A., *Cell. Tissue Res.* **2001**, *305*, 285-298

[9] (a) Humphries, J. D.; Byron, A.; Humphries, M. J., *J. Cell Sci.* **2006**, *119*, 3901-3903; (b) Pankov, R.; Yamada, K. M., *J. Cell Sci.* **2002**, 115, 3861-3863

Each subunit consists of an extracellular domain, a single transmembrane region and a short (30-40 amino acids) cytoplasmic region (Figure 1.2, $\alpha v\beta_3$ integrin). The *N*-terminus of the α-subunit consists of a β-propeller, which is a domain made of seven repeated sequences of 60 amino acids each.[10] Between the Thigh and Calf-1 domains is present a highly flexible region. In addition, in half of the α-subunits the I-domain, 200 additional amino acids, is inserted between the second and third repeated sequences in the β-propeller.[11] In integrins with an I-domain, this region is a major binding-site for ligands whereas in all the other integrins the β-propeller is the binding-site.[12] Cytoplasmic tail domains of individual α-subunits are well-conserved across species boundaries.[13] This subunit has also a flexible "knee" region, formed by the hybrid domain and the first EGF-like repeats.[12] In the β subunit the *N*-terminus region consist of a Cys-rich region (plexinsemaphorin-integrin domain). This domain has a C-terminus evolutionary conserved I-like domain flanked on either side by hybrid domains (immunoglobulin folds). These cytoplasmic tails in the β-chain play key roles in regulating integrin activity.[5b] A metal ion-dependent adhesion site (MIDAS), which is important in the ligand-protein interaction[14], is present across their extracellular α/β subunits interface.

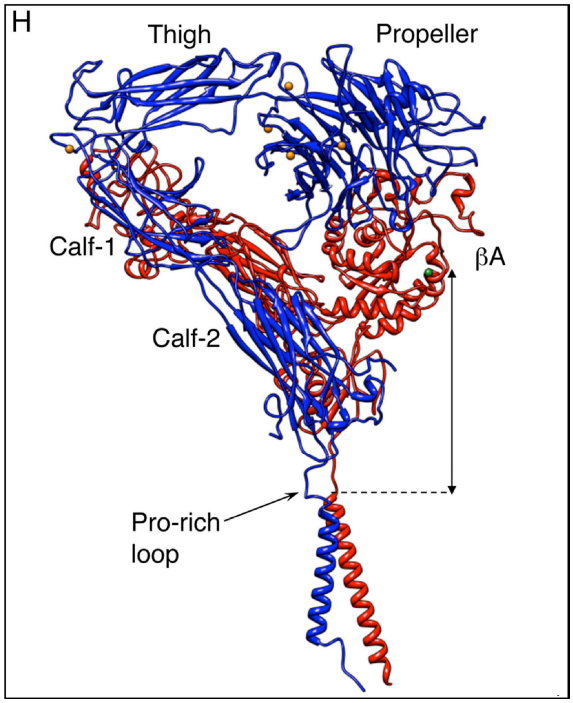

Figure 1.2 – $\alpha v\beta_3$ integrin structure

[10] Springer, T. A., *Proc. Natl. Acad. Sci. USA* **1997**, *94*, 65-72
[11] Humphries, M. J., *Biochem. Soc. Trans.* **2000**, *28*, 311-339
[12] Shimaoka, M; Takagi, J; Springer A. T., *Annu. Rev. Biophys. Biomol. Struct.* **2002**, *31*, 485-516
[13] Fagerholm, S. C.; Hilden, T. J.; Gahmberg, C. G., *Trends Biochem. Sci.* **2004**, *29*, 504-512
[14] Plow, E. F.; Haas, T. A.; Zhang, L.; Loftus, J.; Smith, J. W., *J. Biol. Chem.* **2000**, *275*, 21785-21788

1.1.2.2 Integrins action mechanism

Integrins are not constitutively active[15] and their activation status is regulated by a delicate balance. The interaction between integrins and ligands is regulated by conformational changes.[16] Signal transfer is allosterically coupled to three major equilibrium conformational states, including the 1) inactive bent state, 2) intermediate extended state with a closed headpiece, and 3) active extended form with an open headpiece.[17] Recognition ligand-integrin, and consequently integrin activation, is mediated by peptidic sequences contained in the ligands. Many integrins recognize the RDG sequence (Aspartic acid, Glycine, Arginine) in their endogenous or exogenous ligands. (while other integrins recognize alternative short peptide sequences).

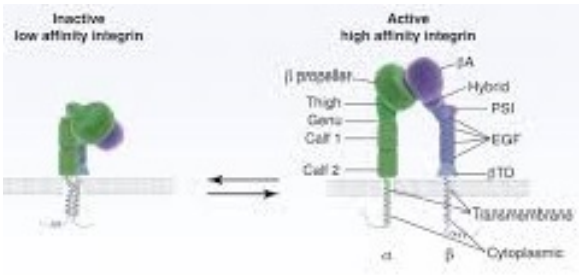

Figure 1.3 - Representation of integrin activation states

Integrins are defined bidirectional receptor because they mediate both the outside-in signaling and the inside-out signaling[17] to promote cell adhesion, motility, and migration. As a consequence, their activation status is regulated both by extra- and intra-cellular stimuli (Figure 1.3).[7,16a] Extracellular factors that influence integrin activation are ligand binding, divalent cation concentration (since integrins bind to their ligands in a divalent cation-dependent manner[18]), chemokine signaling, and mechanical stress. When a signal is transmitted to the cell interior, the organization of the cytoskeleton is regulated, kinase signaling cascades are activated, and the cell cycle and gene expression are modulated. The out-in signaling, following ligand binding, and the consequent switch from the inactive to active state is accompanied by an outwards movement of the β-hybrid domain, characterized by a swing-out angle varying between 10° and 80°.[19] In the inside-out signaling, intracellular events alter the tertiary and quaternary structure of the extracellular region, making the integrin ligand-competent.

[15] Moser, M.; Legate, K. R.; Zent, R.; Fässler, R., *Science* **2009**, *324*, 895-899
[16] (a) Arnaout, M. A.; Mahalingam, B.; Xiong, J. P., *Annu. Rev. Cell Dev. Biol.* **2005**, *21*, 381-410; (b) Luo, B. H.; Carman, C. V.; Springer, T. A., *Annu. Rev. Immunol.* **2007**, *25*, 619-647
[17] For a review see: Asakai, J. A.; Buckley, P. A.; Mould, A. P.; Humphries, M. J., *J. Cell. Sci.* **2009**, *122*, 165-170
[18] (a) Smith, J. W.; Piotrowicz, R. S.; Mathis, D., *J. Biol. Chem.* **1994**, *269*, 960-967; (b) Mould, A. P.; Akiyama, S. K.; Humphries, M. J., *J. Biol. Chem.* **1995**, *270*, 26270-26277
[19] (a) Puklin-Faucher, E.; Gao, M.; Schulten, K.; Vogel, V., *J. Cell Biol.* **2006**, *175*, 349-360; (b) Puklin-Faucher, E.; Vogel, V., *J. Biol. Chem.* **2009**, *284*, 36557-36568; (c) Provasi, D.; Murcia, M.; Coller, B. S.; Filizola, M., *Proteins Struct. Funct. Genet.* **2009**, *77*, 477-489

There is a strong similarity between many integrins stimulated pathways and those triggered by growth factors. Moreover, there is a significant cross-talk in the regulation of angiogenesis between integrin operated pathways and growth factors operated pathways (e.g.: VEGF route[20]). In adhesion dependent cells, an ECM privation results in anoikis and apoptotic cell death[5f,21] because the signal generated from focal adhesions have been shown to promote cell survival, differentiation, and proliferation (Figure 1.4).[22]

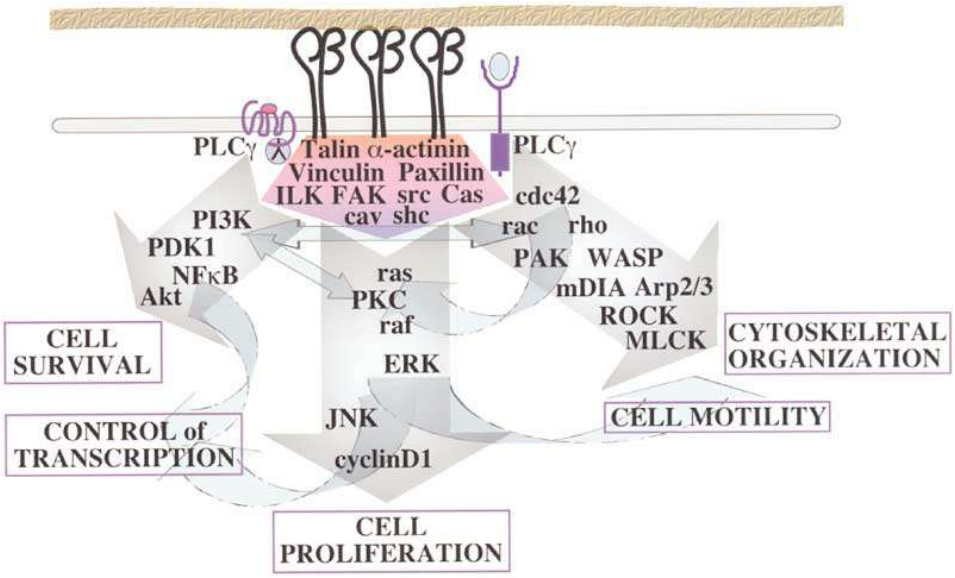

Figure 1.4 – Integrin signaling

Integrins behave as mechanochemical transducers. For the whole receptor family (except for $\alpha_6\beta_4$), the linkage is to the actin-based microfilament system.

Since these receptors serve as a site for docking of various kinases and related adaptor proteins, among which focal adhesions, integrin ligation is essential to block apoptosis (via PI3-kinase and Akt) and to stimulate cell cycle progression (e.g., via ERK and cyclin D) in normal cells.[7] As a consequence, prolonged integrin inhibition prevents cells from survival. So pharmacological inhibition of integrin ligation is of great interest for the therapy of numerous diseases resulting from aberrant integrin mediated signaling.

[20] Reynolds, A. R.; Hart, I. R.; Watson, A. R.; Welti, J. C.; Silva, R. G.; Robinson, S. D.; Da Violante, G.; Gourlaouen, M.; Salih, M.; Jones, M. C.; Jones, D. T.; Saunders, G.; Kostourou, V.; Perron-Sierra, F. J. C.; Tucker, G. C.; Hodivala-Dilke, K. M., *Nat. Med.* **2009**, *15*, 392-400

[21] Desgrosellier, J.; Cheresh, D., *Nat. Rev. Cancer.* **2010**, *10*, 9-22

[22] Legate, K.; Wickström, S.; Fässler, R., *Genes Dev.* **2009**, *23*, 397-418

1.1.2.3 Integrins functions

As mentioned before, integrins are involved in a number of physiological and pathological situations (Table 1.1)[23].

Integrin class	Clinically target in	Main ligands*
α_4-Family		
$\alpha_4\beta_1$	MS, autoimmune, Chron's, IBD	VCAM-1, FN
$\alpha_4\beta_7$	MS, autoimmune, Chron's, arthritis	Mad-CAM-1
$\alpha_9\beta_1$	Cancer	VCAM-1, Opn, VEGF-C, D
Leukocyte cell adhesion		
$\alpha_L\beta_2$	Inflammation, psorisasis, stroke, ischemia, fibrosis	ICAM-1, -2, -3
$\alpha_M\beta_2$	Inflammation, autoimmune	iC3b, Fbg
$\alpha_X\beta_2$	Inflammation	iC3b, Fbg
$\alpha_D\beta_2$	Inflammation	ICAM-3, VCAM-1
$\alpha_E\beta_7$	Inflammation	E-cadherin
RGD-binding		
$gp_{IIbIIIa}$	Thrombosis, stroke, myocardial ischemia	Fbg, vWf
$\alpha_5\beta_1$	Cancer, AMD	FN
$\alpha_8\beta_1$	None	Npn, FN, VN
$\alpha_v\beta_1$	Cancer	VN, FN
$\alpha_v\beta_3$	Cancer, osteoporosis	VN, Opn, vWf, FN, Fbg**
$\alpha_v\beta_5$	Cancer	VN
$\alpha_v\beta_6$	Fibrosis, transplant rejection, cancer	FN, TGF-b1, -3
$\alpha_v\beta_8$	Cancer	FN, TGF-b1, -3
I domain: collagen binding		
$\alpha_1\beta_1$	Fibrosis, cancer	Col
$\alpha_2\beta_1$	Fibrosis, cancer	Col
$\alpha_1\beta_1$, $\alpha_{11}\beta_1$	None	Col
LN binding		
$\alpha_3\beta_1$	None	LN-5
$\alpha_6\beta_1$, $\alpha_7\beta_1$	None	LN-1, -2
$\alpha_6\beta_4$	None	LN-2, -4, -5

Table 1.1 – Integrin subfamilies cluster major therapeutic indications and main ligands (* = see the list of abbreviations for acronyms; ** = among many other ligands)

As an example, the growth of new blood vessels (angiogenesis) from pre-existing vasculature promotes embryonic development, wound healing, the female reproductive cycle but it has also a key role in various pathological events such as development of solid tumor cancers, hemangiomas, diabetic retinopathy, age-related macular degeneration, psoriasis, gingivitis rheumatoid arthritis, and possibly osteoarthritis and inflammatory bowel

[23] Teicher, B. A.; Ellis, L. M.; Eds., Antiangiogenic Agents in Cancer Therapy, HumanPress, **2008**, *3*, 49-71

disease.[24] A deep analysis of all these different profiles is beyond the scope of this thesis and only the aspects concerning tumor growth and metastasis spreading will be taken into consideration. As previously mentioned, VEGF is a growth factor that induces blood vessel growth and it is strictly connected with integrins. Angiogenesis is known to play a major role in tumor growth and so inhibiting angiogenesis can inhibit tumor progression and metastasis.

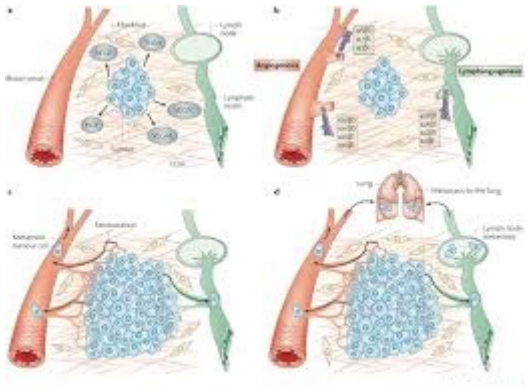

Figure 1.5 – Angiogenesis promoted by secreted growth factors and chemokines

A second key factor for tumor growth and metastasis spreading is adhesion to the ECM. As a matter of fact, formation of new vasculature requires endothelial cell attachment and migration on ECM proteins. Among all the ECM proteins, fibronectin in particular is associated with proliferation.[25] As already explained, integrins are critical for the cell to bind ECM and in regulating vascular growth. Since proliferating endothelial cells overexpress integrins that are not expressed in quiescent vessels (e.g., $\alpha_V\beta_3$[26]) a selective inhibition of these ones is interesting from a therapeutical point of view. Antibody or peptide antagonists of $\alpha_V\beta_3$ were proved to block angiogenesis and tumor growth in animal models and to stimulate tumor regression related to apoptosis.[27]

Also $\alpha_5\beta_1$ integrins are up-regulated in tumor angiogenesis (mice and humans) but not in quiescent endothelium. Also in this case, tumor regression[23] in chicks and mice is induced by $\alpha_5\beta_1$-antagonist (through the activation of protein kinase A and caspase-8) as a consequence of angiogenesis inhibition and induced apoptosis.[28] These antagonists suppress signal transduction for cell survival, cell migration on vitronectin, but not attachment to vitronectin. These data show a dependence of the migration process and cell survival from $\alpha_5\beta_1$-antagonists but not a relation to integrin receptors for vitronectin.[23,28]

[24] Carmeliet, P., *Nat. Med.* **2003**, 9, 653-660
[25] Kim, S.; Bell, K.; Mousa, S. A.; Varner, J. A., *Am. J. Pathol.* **2000**, *156*, 1345-1362
[26] Brooks, P.C.; Clark, R. A.; Cheresh, D. A., *Cell*, **1994**, *270*, 1500-1502
[27] Brooks, P.C.; Montgomery, A. M.; Rosenfeld, M.; Reisfeld, R. A.; Hu, T.; Klier, G.; Cheresh, D. A., *Cell*, **1994**, *270*, 1500-1502
[28] Kim, S; Bakre, M.; Yin, H.; Varner, J. A., *J. Clin. Invest.* **2002**, *110*, 933-941

The 3D structure of the ligand-binding site of $\alpha_5\beta_1$ complexed with fibronectin was determined.[29] Integrins $\alpha_v\beta_5$ are closely related to $\alpha_v\beta_3$ for what concern the structure. Differences were found in the β_3 subunit (residues 159-188) and explains why a few $\alpha_v\beta_3$ inhibitor display selectivity over $\alpha_v\beta_5$[5e,30] but specific inhibitors of $\alpha_v\beta_3$ have not been described yet.

1.1.2.4 RGD recognition motif

The RGD sequence (Figure 1.6) is a tripeptide sequence composed by Aspartic acid, Glycine and Arginine identified as the endogenous recognition motif for cell attachment to proteins. This recognition motif was discovered in fibronectin in 1984.[31] Among the large amounts of recognized proteins, such as fibrinogen, vitronectin, and thrombospondin, it recognizes and binds numerous integrin subfamilies.[31]

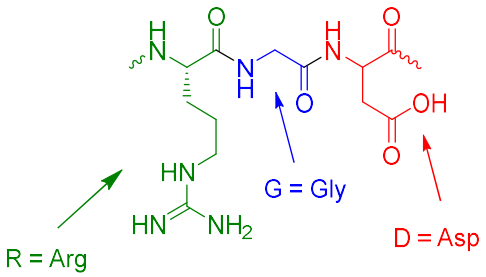

Figure 1.6 – The RGD sequence

Naturally RGD-ligands have a varied selectivity and potency in targeting RGD-recognized integrins. The structure of these compounds was analyzed and it seems that in order to inhibit integrins, a proper restriction of the RGD flexibility is required.[32] In the ligand recognition the RGD sequence is primary involved while the flanking residues are important for the selectivity.[8a,b] The binding mode of RGD sequence to integrins was deeply studied (Figure 1.7), thanks to the crystal structure of extracellular segment of the $\alpha_v\beta_3$ complexed with the cyclic pentapeptide *Cyclo*[*N*-MeVal-D-Phe-Arg-Gly-Asp] (Cilengitide) (Figure 1.8).[33] The analysis revealed for this compound a conformation featuring an inverse γ-turn centered on Asp and an ectodomain receptor conformations of a distorted βII'-turn with Gly and Asp at the *i*+1 and *i*+2 positions respectively. The measured distance C^{β}(Arg)-C^{β}(Asp) was around 8.9 Å, that accounts for an almost extended RGD sequence conformation.

[29] Takagi, J.; Strokovich, K.; Springer, T. A.; Waltz, T., *EMBO J.* **2003**, *22*, 4607-4615
[30] Meyer, A.; Auernheimer, J.; Modlinger, A.; Hessler, H., *Curr. Pharm. Des.* **2006**, *12*, 2723-2747
[31] Pierschbacher, M. D.; Ruoslahti, E., *Nature* **1984**, *309*, 30-33
[32] (a) Swenson, S.; Ramu, S.; Markland, F. S., *Curr. Pharm. Des.* **2007**, *13*, 2860-2871; (b) Calvete, J. J.; Marcinkiewicz, C.; Monleón, D.; Esteve, V.; Celda, B.; Juárez, P.; Sanz, L., *Toxicon* **2005**, *45*, 1063-1074; (c) Fujii, Y.; Okuda, D.; Fujimoto, Z., *J. Mol. Biol.* **2003**, *332*, 1115-1122; (d) Gould, R. J.; Polokoff, M. A.; Friedman, P. A.; Huang, T. F.; Holt, J. C.; Cook, J. J.; Niewiarowski, S., *Proc. Soc. Exp. Biol. Med.* **1990**, *195*, 168-171
[33] Xiong, P. J.; Stehle, T.; Zhang, R.; Joachimiak, A.; Frech, M; Goodman, S. L.; Arnaout, M. A., *Science* **2002**, *296*, 151-155

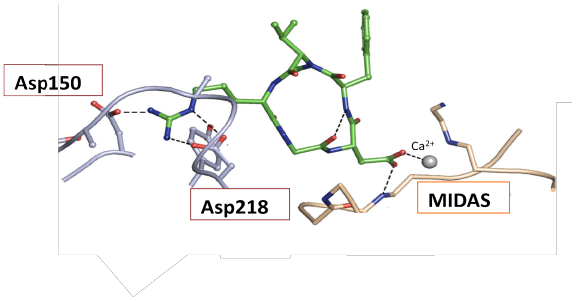

Figure 1.7 – Mode of binding for RGD sequence to integrins

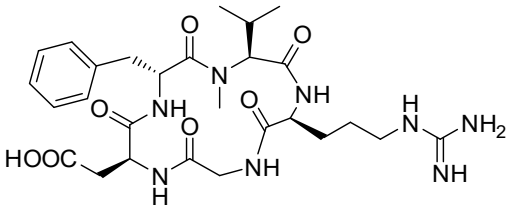

Figure 1.8 – Cilengitide

The main interactions involve the guanidinium group of the Arg in the RGD sequence with the Asp^{218} and Asp^{150} in the α-subunit (salt bridges), one of the oxygen of the carboxylic group of the Asp side chain in the RGD sequence with the Mn^{2+} ion at the MIDAS region in the β-subunit and the second oxygen of the carboxylic group of the Asp side chain in the RGD sequence with the backbone amides of Asn^{215} and Tyr^{122}. In addition, there are several hydrophobic interactions involving the Gly residue, at the interface between the two integrin subunits.

1.1.2.5 *iso*DGR recognition motif

Beside the well-known RGD sequence, also the *iso*DGR (Figure 1.9) sequence was identified as a binding site for integrins.[34]

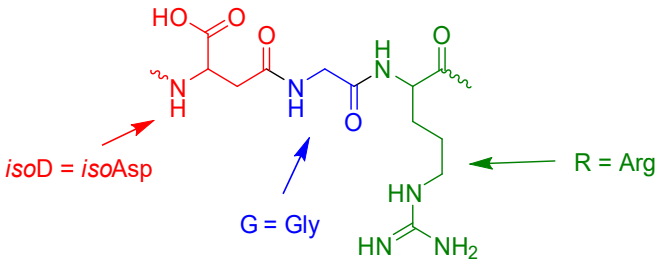

Figure 1.9 – *iso*DGR sequence

[34] Curnis, F.; Sacchi, A; Gasparri, A.; Longhi, R.; Bachi, A.; Doglioni, C.; Bordignon, C.; Traversari, C.; Rizzardi, G.-P.; Corti, A., *Cancer Res.* **2008**, *68*, 7073-7082

NGR (Asn-Gly-Arg) and DGR (Asp-Gly-Arg) motifs, as well as other integrin recognition sequences,[4b] contain Asp or Asn that can spontaneously undergo post-translational modifications to form *iso*Asp (both *in vitro* and *in vivo*[35]). Evidences show the formation of this non-standard β-amino acid during tissue aging in the ECM and in proteins with a slow turn over.[35b,36] Even if usually this reaction causes a loss of the protein activity (it might cause a change in the charge or the length of the peptide bond), in the case of fibronectin a gain of function was observed: the switch creates a new binding-site for integrins because the resulting *iso*DGR motif can mimic RGD and recognize the RGD-binding site.[37] For example, it has been suggested that at the NGR site of FN-I_5, a naturally occurring reaction leads to the formation of the *iso*DGR and the DGR, activating a latent $\alpha v\beta_3$-integrin-binding site. It has also been proposed that the *iso*Asp formation can provide a sort of molecular indicator of protein damage because the switch (which might occur faster in proteins that have a lost their structural integrity) is able to activate selective degradation mechanisms.[35,36,38]

The formation of *iso*Asp in proteins is obtained by a non-enzymatic Asn deamidation or Asp isomerization reactions (Scheme 1.1).[37,38b, 39 , 40] Asn deamidation occurs by a nucleophilic attack of the backbone NH center at the carbonyl group of Asn side chain, which leads to formation of a succinimide ring. The succinimide ring is also the first intermediate formed in the Asp isomerization. Both carbonyl groups of the succinimide ring are susceptible to hydrolysis, that leads a mixture of Asp and *iso*Asp residues (ratio of approximately 1:3). Racemization and hydrolysis of the succinimide intermediate can also lead to the formation of Asp and *iso*Asp in D-configuration. However the resulting Asp and *iso*Asp in L-configuration are more relevant because the formation of the D-isomers occur with much lower efficiency.[39,41] These deamidation and isomerization reactions can take hours, days or even years, depending on several factors (the presence of secondary or tertiary or quaternary structural elements[38b, 42], the pH, the ionic strength, and the temperature[38b]). For example, NGR deamidation in the FN-I_5 fragment is very rapid,[37] probably because a Gly residue follows the Asn, and because of the position of the Asn side chain that is favorable to a nucleophilic attack.[43] Notably, *iso*DGR can be converted into succinimide intermediate by protein-L-*iso*Asp-*O*-methyltransferase (PIMT), which catalyzes the transfer of a methyl group from S-adenosyl-L-methionine to the free carboxyl

[35] (a) Reissner, K. J.; Aswald, D. W., *Cell Mol. Life Sci.* **2003**, *60*, 1281-1295; (b) Weber, D. J.; McFadden, P. N., *J. Protein Chem.* **1997**, *16*, 269-281
[36] (a) Lanthier, J.; Desrosiers, R. R., *Exp. Cell Res.* **2004**, *293*, 96-105; (b) Linder, H.; Helliger, W., *Exp. Gerontol.* **2001**, *36*, 1551-1563; (c) Weber, D. J.; McFadden, P. N., *J. Protein Chem.* **1997**, *16*, 269-281
[37] Curnis, F.; Longhi, R.; Crippa, L.; Cattaneo, A.; Dondossola, E.; Bachi, A.; Corti, A., *J. Biol. Chem.* **2006**, *281*, 36466-36476
[38] (a) Robinson, N. E.; Robinson, A. B., *Proc, Natl. Acad. Sci. USA* **2001**, *98*, 94-949; (b) Weintraub, S. J.; Deverman, B. E., *Sci. STKE* **2007**, *2007*, re7
[39] Geiger, T.; Clarke, S., *J. Biol. Chem.* **1987**, *262*, 785-794
[40] Takahashi, S.; Leiss, M.; Moser, M.; Ohashi, T.; Kitao, T.; Heckmann, D.; Pfeifer, A.; Kessler, H.; Takagi, J.; Erickson, H. P.; Fässler, R., *J. Cell Biol.* **2007**, *178*, 167-178
[41] (a) Stephenson, R. C.; Clarke, S., *J. Biol. Chem.* **1989**, *264*, 6164-6170; (b) Tyler-Cross, R.; Schirch, V., *J. Biol. Chem.* **1991**, *266*, 22549-22556
[42] (a) Robinson, N. E., *Proc. Natl. Acad. Sci. USA* **2002**, *99*, 5283-5288; (b) Robinson, N. E.; Robinson, Z. W.; Robinson, B. R.; Robinson, A. L.; Robinson, J. A.; Robinson, M. L.; Robinson, A. B., *J. Pept. Res.* **2004**, *63*, 426-436
[43] Di Matteo, P.; Curnis, F.; Longhi, R.; Colombo, G.; Sacchi, A.; Crippa, L.; Protti, M. P.; Ponzoni, M.; Toma, S.; Corti, A., *Mol. Immunol.* **2006**, *43*, 1509-1518

group of D-Asp and L-*iso*Asp residues[38a]. The resulting methyl ester can then form the cyclic succinimide intermediate that could generate the DGR motif, inactivating the *iso*DGR site.[40]

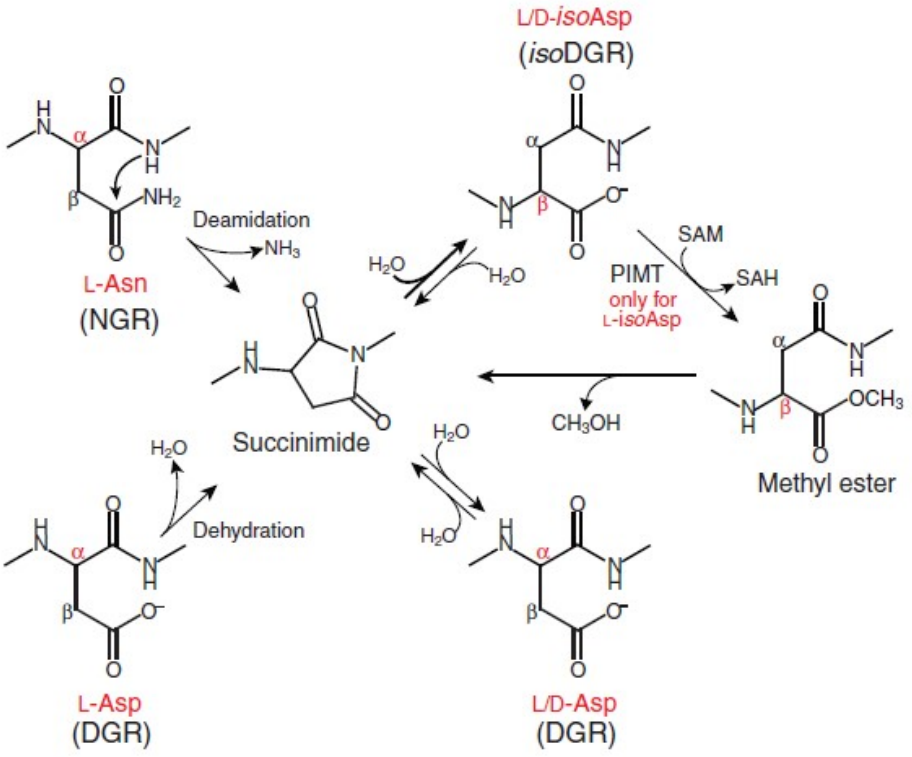

Scheme 1.1 – Naturally occurring pathways for *iso*Asp generation

It has been suggested that both NGR and DGR sequences can function as a latent integrin-binding site, that is differentially activated depending on its molecular context and conditions, because they can be converted into *iso*DGR by the isomerization of Asp. As a matter of facts, *iso*DGR containing peptides can recognize only some members of the RGD-dependent integrin family, such as $\alpha v\beta_3$, $\alpha v\beta_5$, $\alpha v\beta_6$, $\alpha v\beta_8$, and $\alpha_5\beta_1$.[44] The affinity and specificity of the interaction depend on the molecular scaffold of *iso*DGR.[44] Also in that case, the context (flanking residues and 3D presentation) influences activity and selectivity for integrins. A marked loss of binding affinity is caused by the replacement of *iso*Asp with Asp or with D-*iso*Asp, indicating the highly selective and stereospecific interactions.[40,44] NMR structure analysis of correspondent cyclic *iso*DGR-, RGD-, DGR-, and NGR- peptides showed that *iso*DGR but not DGR and NGR fit into the RGD-binding pocket interacting favorably with integrins (Figure 1.10).[34,40]

[44] Curnis, F.; Cattaneo, A; Longhi, R.; Sacchi, A.; Gasparri, A. M.; Pastorino, F.; Di Matteo, P.; Traversari, C.; Bachi, A.; Ponzoni, M.; Rizzardi, G.-P.; Musco, G., *J. Biol. Chem* **2010**, *285*, 9114-9123

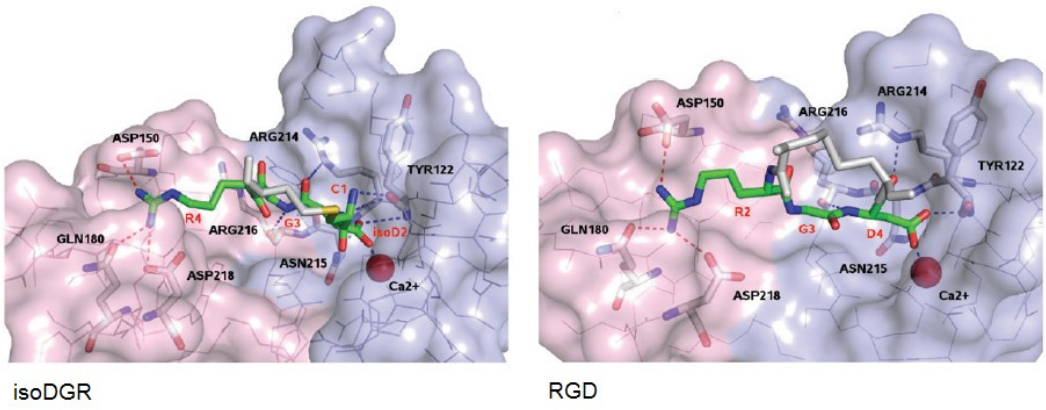

Figure 1.10 – Model for the interaction of *iso*DGR and RGD-binding site of $\alpha_v\beta_3$ integrin

The *iso*DGR sequence mimics the RGD sequence and it docks in the RGD integrin binding-site in an inverted orientation with respect to the RGD sequence, thus allowing the formation of the classic electrostatic clamp as for the RGD motif.[45] The binding mode to the integrin pocket of $\alpha_v\beta_3$ is maintained: the acid and basic residues are at the correct distance and orientation to generate stabilizing interactions with the polar region of integrins. Also for the *iso*DGR sequence, the *iso*Asp carboxylic side chain interacts with MIDAS, Asn^{215}, Tyr^{122}, and Arg^{214} while the guanidinium group of the Arg interacts with Asp^{218}, Asp^{150}, and Gln^{180}. Further stabilizing interactions are present and involve the Gly residue: it recognizes the receptor via polar interactions and, thanks to its amide group, forms an H-bond with the carbonyl of Arg^{216}.

Although *iso*DGR and RGD-containing ligands share the same integrin binding-site, they might act in different ways on integrins because RGD-ligands and *iso*DGR ligands could activate different conformational changes (regulating integrin activation).[46] Even if the binding affinity of the two classes of ligands is similar, the kinetic data of binding might differ. Since this is an important parameter for biological properties, kinetics analysis are needed to define the extent to which *iso*DGR differs from or mimics RGD.[46] For instance, the MolMed group discovered that the *iso*DGR ligand C*iso*DGRC can block the integrin in the bent, inactive conformation acting as a true antagonist.[47]

[45] Spitalieri, A.; Mari, S.; Curnis, F.; Traversari, C.; Longhi, R.; Bordignon, C.; Corti, A.; Rizzardi, G.-P.; Musco, G., *J. Biol. Chem.* **2008**, *283*, 19757-19768
[46] Corti, A., Curnis, F.; *J. Cell Sci.* **2011**, *124*, 515-522
[47] Ghitti, M.; Spitalieri, A.; Valentinis, B.; Mari, S.; Asperti, C.; Traversari, C.; Rizzardi, G.-P.; Musco, G., *Angew. Chem. Int. Ed.* **2012**, *51*, 7702-7705

1.2 RGD- and *iso*DGR-integrin ligands

Nowadays, many linear or cyclic peptidic and peptidomimetic integrin ligands have been developed and a few potent compounds are in different phases of clinical trials as anticancer drugs or in clinical use for antithrombotic therapy.[48]

1.2.1 RGD-integrin ligands

1.2.1.1 Linear RGD-integrin ligands

Examples of linear RGD-containing integrin ligands are present in the literature.[49] However they have shown lower activity than the correspondent cyclic derivatives.[49] This low activity is probably due to the reduced rigidity (since the RGD sequence requires a proper conformation to interact optimally with the receptor) and also to an increase of the degradation compared to cyclic correspondent ligands.[50] In fact it is know in the literature that cyclization increases stability towards *in vivo* enzymatic peptide degradation.[51] In addition, the Asp residue, known to be susceptible to chemical degradation, in the linear derivative is less protected.[52]

1.2.1.2 Cyclic RGD-integrin ligands

Many cyclic peptides and peptidomimetics RGD-containing integrin ligands have been developed. In these compounds different flanking residues are present and they are characterized by different 3D presentation of the RGD sequence.[48c] Semipeptidic $\alpha v\beta_3$ inhibitors, bearing a non-peptidic and rigid turn-inducing scaffold to appropriately constrain the RGD motif, and various peptides are validating their use as preferred conformation-inducing scaffolds.[53]

In 1991, Kessler and co-workers identified RGD-based cyclic peptide, c(RGDfV) (Figure 1.11), an early example of $\alpha v\beta_3$ integrin ligands ($\alpha v\beta_3$ IC_{50} = 3.2 ± 1.3 nM, value calculated as the concentration required for 50% inhibition of biotinylated vitronectin binding as estimated by GraphPad Prism software).[54] This derivative targets selectively $\alpha v\beta_3$ integrins

[48] (a) Avraamides, C. J.; Garmy-Susini, B.; Varner, J. A., *Nat. Rev. Cancer* **2008**, *8*,604–617; (b) D'Andrea, L. D.; Del Gatto, A.; Pedone, C.; Benedetti, E., *Chem. Biol. Drug Des.* **2006**, *67*, 115–126; (c) Auzzas, L.; Zanardi, F.; Battistini, L.; Burreddu, P.; Carta, P.; Rassu, G.; Curti, C.; Casiraghi, G., *Curr. Med. Chem.* **2010**, *17*, 1255–1299

[49] Samenen, J.; Ali, F.; Romoff, T.; Calvo, R.; Sorenson, E.; Vasko, J.; Storer, B.; Berry, D.; Bennett, D.; Strohsacker, M.; Powers, D.; Stadel, J.; Nichols, A., *Bioorg. Med. Chem.* **2014**, *14*, 4158-4181

[50] Bogdanowich-Knipp, S. J.; Chakrabarti, S.; Williams, T. D.; Dillman, R. K.; Siahaan, T. J., *J. Peptide Res.* **1999**, *53*, 530-541

[51] (a) Hruby, V. J., *Life Sci.* **1982**, *31*, 189-199; (b) Cody, W. L.; Mahoney, M.; Knittel, J. J.; Hruby, V.J.; Castrucci, A. M. De L.; Hadley, M. E., *J Med. Chem.* **1985**, *28*, 583-588; (c) Hruby, V. J., *Epilepsia* **1989**, S42-S50; (d) Hadley, M. E.; Marwan, M. M.; Hruby, F.; Castrucci, A. M., *Pigment Cell Res.* **1989**, *2*, 478-484

[52] (a) Clarke, S., *Int. J. Peptide Protein Res.* **1987**, *30*, 808-821; (b) Geiger, T.; Clarke, S., *J. Biol. Chem.* **1987**, *262*, 785-794; (c) Manning, M.C.; Patel, K; Borchardt, R. T., *Pharm. Res.* **1989**, *6*, 903-918

[53] (a) Hanessian, S.; Auzzas, L., *Acc. Chem. Res.* **2008**, *41*, 1241-1251; (b) Trabocchi, A.; Scarpi, D.; Guarna, A., *Amino Acids* **2008**, *34*, 1-24; (c) Cowell, S. M.; Lee, Y. S.; Cain, J. P.; Hruby, V. J., *Curr. Med. Chem.* **2004**, *11*, 2785-2798

[54] Aumailley, M.; Gurrath, M.; Müller, G.; Calvete, J.; Timpl, R.; Kessler, H., *FEBS Lett.* **1991**, *291*, 50-54

and is commercially available thus providing an useful reference standard compound. Later, the same group developed a potent $\alpha_v\beta_3$ RGD-containing integrin ligand (the *N*-methylated derivative) named Cilengitide (EMD121974, Figure 1.8)[3b,55]. This ligand opened the era of investigation of integrin inhibitor as anticancer and antiangiogenic agents.

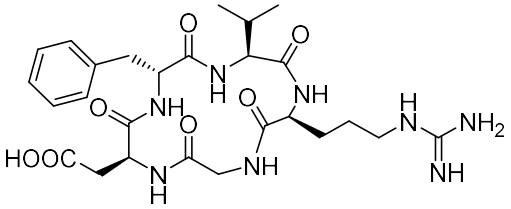

Figure 1.11 – c(RGDfV) integrin ligand

In Kessler's research group also azabicycloalkane and spyrocyclic systems, traditionally known as β-inducers, were to be inserted into RGD cyclic peptidomimetics were developed.[56] The most active and less constrained compound of the series was a fully promiscuous antagonist (Figure 1.12) with IC_{50} 43 nM on $\alpha_v\beta_3$ and 550 nM on $\alpha_{IIb}\beta_3$.

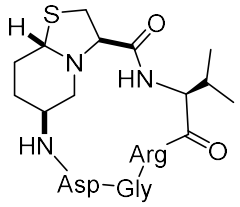

Figure 1.12 – Kessler's RGD- azabicycloalkane ligand

Kessler inserted also an amino pyrrolidinone-based scaffold in a RGD cyclic peptidomimetics (Figure 1.13).[56] Both these derivatives showed a nanomolar affinity for $\alpha_v\beta_3$ integrins, but the most active (**a**) was also the less selective towards $\alpha_{IIb}\beta_3$ integrins while ligand **b** was more selective but with higher IC_{50}. The main difference between the two ligands is the orientation of the lactam bond that is rotated by 180° in the two isomers. This amide bond was proved to be involved in an H-bond with the receptor. As a consequence the interaction is different in the two cases.

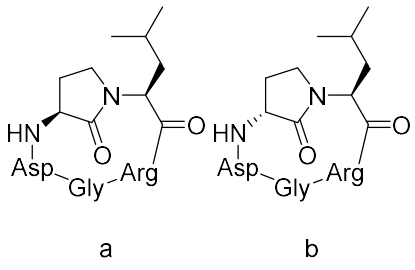

Figure 1.13 – Kessler's RGD- azabicycloalkane ligand

[55] (a) Schaffner, P.; Dard, M. M., *Cell. Mol. Life Sci.* **2003**, *60*, 119.132; (b) Dechantsreiter, M.; Planker, E.; Mathä, B.; Lohof, E.; Hölzelmann, G.; Jonczyk, A.; Goodman, S. L.; Kessler, H., *J. Med. Chem.* **1999**, *42*, 3033-3040

[56] Haubner, R.; Schmitt, W.; Hölzemann, G.; Goodmann, S. L.; Jonczyk, A.; Kessler, H., *J. Am. Chem. Soc.* **1996**, *118*, 7881-7891

Kessler and Overhand have inserted pyranoid and furanoid sugars as scaffolds in the δ- and ε-amino acid-based cyclic compounds (representative members of the class are shown in Figure 1.14).[57] These molecules have a high flexibility which cancel selectivity towards the different integrin subfamilies (Pyranoid-derivative: $\alpha_v\beta_3$ 25 nM, $\alpha_v\beta_5$ >10^4, $\alpha_{IIb}\beta_3$ 13.4 nM; furanoid-derivative: $\alpha_v\beta_3$ 1.4 μM, $\alpha_v\beta_5$ 0.38 μM), as confirmed by conformational analysis.

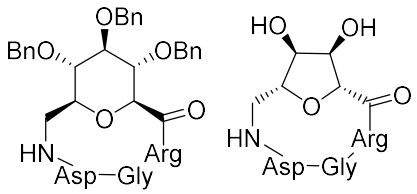

Figure 1.14 – Pyranoid and furanoid RGD-peptidomimetics

In a similar approach, Casiraghi and coworkers synthesized γ-amino acid, generating four stereoisomeric 14-membered macrocycles (representative members of the family are depicted in Figure 1.15).[58] The activity was slightly improved compared to the previous sugar derivatives ($\alpha_v\beta_3$ IC_{50}: **a** = 5.6 ± 0.1 nM, **b** = 7.2 ± 0.07 nM and $\alpha_v\beta_5$ IC_{50}: **a** = 4.56 ± 0.13 nM, **b** = 13.1 ± 0.05 nM). In these ligands the distance C^{β}(Asp)-C^{β}(Arg) is in the range of 8.0-8.4 Å. The conformation, according to NMR, is a γ-turn centered on the Asp residue. Analogue **c** was the best candidate (IC_{50} = 1.5 nM vs $\alpha_v\beta_3$ and 0.59 nM vs $\alpha_v\beta_5$).

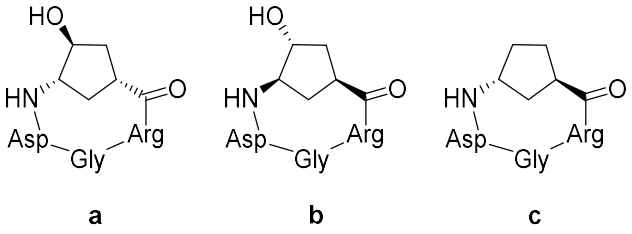

Figure 1.15 – Casiraghi's compounds

The same research group used the 4-amino proline (Amp) as scaffold in cyclic RGD peptidomimetics (Figure 1.16).[59] All the synthesized compounds displayed a really high affinity towards $\alpha_v\beta_3$ and $\alpha_v\beta_5$ integrins (nanomolar values and picomolar values in the high affinity status of the integrin). In all the cyclic derivatives the C^{β}(Asp)-C^{β}(Arg) distance was measured with values in the range of 7.8-8.2 Å. All the key interactions were maintained in the most active analogues and if R is an hydrogen, a further H-bonding between this NH and the Tyr178 is present. On the other hand, alkyl and acyl chains provided additional

[57] (a) Van Well, R. M.; Marinelli, M.; Altona, C.; Erkelens, K.; Siegal, G.; Van Raaij, M.; Liamas-Saiz, A. L.; Kessler, H.; Novellino, E.; Lavecchia, A.; Van Boom, J. H.; Overhand, M., *J. Am. Chem. Soc.* **2003**, *125*, 10822-10829; (b) Van Well, R. M.; Overkleeft, H. S.; Van der Marel, G. A.; Bruss, D.; Thibault, G.; De Groot, P. G.; Van Boom, J. H.; Overhand, M., *Bioorg. Med. Chem. Lett.* **2003**, *13*, 331-334; (c) Lohof, E.; Planker, E.; Mang, C.; Burkhart, F.; Dechantsreiter, M. A.; Haubner, R.; Wester, H.-J.; Schwaiger, M.; Hölzemann, G.; Goodman, S.L.; Kessler, H., *Angew. Chem. Int. Ed.* **2000**, *39*, 2761-2764

[58] Casiraghi, G.; Rassu, G.; Auzzas, L.; Burreddu, P.; Gaetani, E.; Battistini, L.; Zanardi, F.; Curti, C.; Nicastro, G.; Belvisi, L.; Motto, I.; Castorina, M.; Giannini, G.; Pisano, C., *J. Med. Chem.* **2005**, *48*, 7675-7687

[59] Zanardi, F.; Burreddu, P.; Rassu, G.; Auzzas, L.; Battistini, L.; Curti, C.; Sartori, A.; Nicastro, G.; Menchi, G.; Cini, N.; Bottoncetti, A.; Raspanti, S.; Casiraghi, G., *J. Med. Chem.* **2008**, *51*, 1771-1782

contacts in an aromatic rich hydrophobic hollow of the receptor. NMR conformational analysis detected a preferred inverse γ-turn motif centered on Asp for macrocycles containing a *cis*-disposed γ-amino acid. On the contrary, more flexibility is associated with *trans*-γ-amino acids.

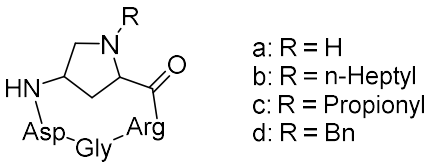

Figure 1.16 – Cyclic RGD containing the Amp scaffold

Pepidomimetics developed by Sewald, Reiser, and co-workers are very close to this class. These 16-membered cyclic peptidomimetics contain a *cis*-β-aminocyclopropanecarboxylic acid as scaffolds, and the RGDV (Arg-Gly-Asp-Val) sequence. These compounds will be treated in Chapter 4.

Guarna and coworkers have replaced the *N*-Me-Val moiety of Cilengitide with D- and L-morpholines (Figure 1.17).[60] Derivative **a** showed a ten time higher affinity for $\alpha v\beta_5$ integrins (IC_{50} = 15.1 nM) versus $\alpha v\beta_3$ integrins (IC_{50} = 157 nM), while derivative **b** has nanomolar IC_{50} values for both the integrin families (32.6 nM for $\alpha v\beta_3$ and 21 nM for $\alpha v\beta_5$). The two cyclic derivatives show distinct structural arrangements because of the D-Phe-morpholine peptide bond which has different conformations in the two derivatives. According to the docking analysis, ligand **b** has a *cis* conformation in which the RGD sequence adopts an arrangement comparable to the one of the RGD-complexed Cilengitide.

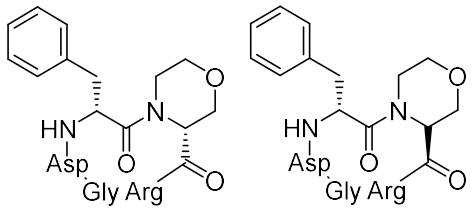

Figure 1.17 – Morpholine-based RGD ligands

The group of Scolastico, synthesized and tested a library of RGD cyclopentapeptides incorporating a 5,6- and 5,7-fused azabicycicloalcane amino acid (Figure 1.18).[61] The most active one, **ST1646** (15-membered cycle), has a low nanomolar affinity for $\alpha v\beta_3$ and $\alpha v\beta_5$ integrins (3.8 ± 0.9 nM and 1.39 ± 0.2 nM respectively, tested in a solid-phase receptor

[60] Sladojevich, F.; Trabocchi, A.; Guarna, A., *J. Org. Chem.* **2007**, *72*, 4254-4257

[61] (a) Belvisi, L.; Bernardi, A.; Colombo, M.; Manzoni, L.; Potenza, D.; Scolastico, G.; Giannini, G.; Marcellini, M.; Riccioni, T.; Castorina, M.; LoGiudice, P.; Pisano C., *Bioorg. Med. Chem.* **2006**, *14*, 169-180; (b) Manzoni, L.; Belvisi, L.; Arosio, D.; Civera, M.; Pilkington-Miksa, M.; Potenza, D.; Caprini, A.; Araldi, E. M. V.; Monferrini, E.; Mancino, M.; Podestà, F.; Scolastico, C., *ChemMedChem* **2009**, *4*, 615-632

assay for their ability to compete for the binding of [^{125}I]echistatin to either purified $\alpha_v\beta_3$ or $\alpha_v\beta_5$) and it is selective towards $\alpha_{IIB}\beta_3$ and $\alpha_5\beta_1$ integrins. *In vitro* cell tests on this compound demonstrated the inhibition of endothelial cells proliferation indicator of an antiangiogenic activity.[62] Docking studies, showed a γ-turn conformation centered on the Asp residue, maintaining the main contacts already seen in the X-ray for Cilengitide.

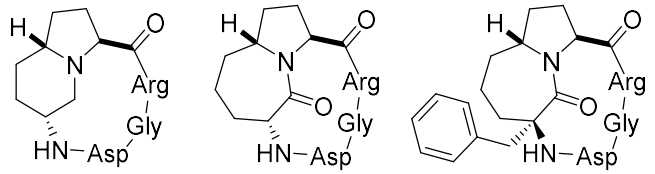

ST1646

Figure 1.18 – Scolastico's RGD-azabicycloalkane ligands

Tests performed on these compounds were indicative of a strong dependence of the activity on the lactam ring size and on the stereochemistry as these parameters influence the overall conformation. Conformational studies performed on the library showed for **ST1646** a C^{β}(Arg)-C^{β}(Asp) distance of 8.8 Å and the same interactions found in the complexed structure of Cilengitide.[63]

Sewald and coworkers examined the application of β-amino acids in the design of cyclic peptides. The insertion of these amino acids allows the control of the peptide backbone conformation such that these non-native building blocks clearly prefer to adopt Ψ_γ-turns. Among the various cyclic RGD-containing peptides studied, the 13-membered derivative depicted in Figure 1.19 resulted a selective $\alpha_v\beta_3$ nanomolar antagonist (IC_{50} $\alpha_v\beta_3$ = 63 nM; IC_{50} $\alpha_{IIb}\beta_3$ > 300 nM).[64]

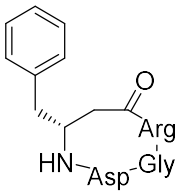

Figure 1.19 – Sewald's best ligand

[62] Belvisi, L.; Riccioni, T.; Marcellini, M.; Vesci, L.; Chiarucci, I.; Efrati, D.; Potenza, D.; Scolastico, C.; Manzoni, L.; Lombardo, K.; Stasi, M. A.; Orlandi, A.; Ciucci, A.; Nico, B.; Ribatti, D.; Giannini, G.; Presta, M.; Carminati, P.; Pisano, C., *Mol. Cancer Ther.* **2005**, *4*, 1670-1680

[63] Arosio, D.; Belvisi, L.; Colombo, L.; Invernizzi, D.; Manzoni, L.; Potenza, D.; Serra, M.; Castorina, M.; Pisano, C.; Scolastico, C., *ChemMedChem* **2008**, *3*, 1589-1603

[64] Schumann, F.; Müller, A.; Koksch, M.; Müller, G.; Sewald, N., *J. Am. Chem. Soc.* **2000**, *122*, 12009-12010

The synthesis of a library of 17-membered ring cyclic peptidomimetics containing a diketopiperazine scaffold has already been reported by our research group.[65] These compounds will be deeply considered in Chapter 2.

1.2.2 *iso*DGR-integrin ligands

A few examples of constrained cyclic peptides or pseudo-peptides containing the *iso*DGR sequence can be found in the literature.[66] Early evidences of the interest of this family of molecules date back to 2006.[37] Corti and co-workers discovered the first ligand of the class (Figure 1.20, compound **a**)[34] and then a derivative of this (Figure 1.20, compound **b**) was prepared in the same research group. This second compound showed an increased affinity towards the majority of integrins tested.[44] However the competitive binding test has been performed against a weak $\alpha_v\beta_3$ ligand and so the data obtained cannot be compared to all the previous ones.

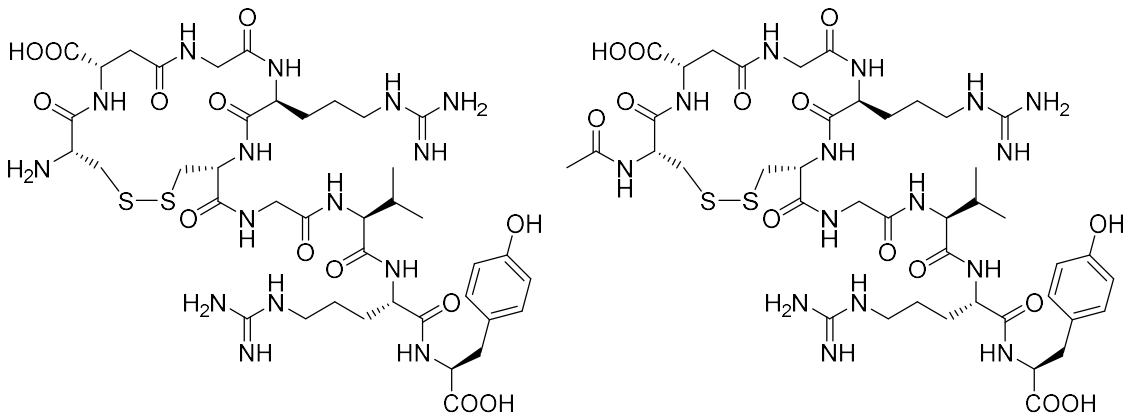

a **b**

Figure 1.20 – Corti's *iso*DGR ligands

A further attempt has been pursued by Kessler's research group working on the retrosequence of c(RGDfV), thus synthesizing for example c(V*f*isoDGR). Results were not significant. A more interesting result was obtained with compounds depicted in Figure 1.21.[66b] In these derivatives have been highlighted an interesting selectivity towards integrins $\alpha_v\beta_3$ and $\alpha_{IIb}\beta_3$ (**a**: $\alpha_5\beta_1$ = 83 nM, $\alpha_v\beta_3$ = 410 nM; **b**: $\alpha_5\beta_1$ = 19 nM, $\alpha_v\beta_3 > 10^3$ nM; **c**: $\alpha_5\beta_1$ = 57 nM, $\alpha_v\beta_3$ = 753 nM; **d**: $\alpha_5\beta_1$ = 406 nM, $\alpha_v\beta_3$ = 89 nM). This example furnished an idea of how much the effects of a *iso*DGR-flanking aromatic moiety is important. However,

[65] (a) Resurreiçao, A. S. M.; Vidu, A.; Civera, M.; Belvisi, L.; Potenza, D.; Manzoni, L.; Ongeri, S.; Gennari, C.; Piarulli, U., *Chem. Eur. J.* **2009**, *15*, 12184-12188; (b) Marchini, M.; Mingozzi, M.; Colombo, R.; Guzzetti, I.; Belvisi, L.; Vasile, F.; Potenza, D.; Piarulli, U.; Arosio, D.; Gennari, C., *Chem. Eur. J.* **2012**, *18*, 6195-6207

[66] (a) Spitaleri, A.; Ghitti, M.; Mari, S.; Alberici, L.; Traversari, C.; Rizzardi, G.-P.; Musco, G., *Angew. Chem. Int. Ed.* **2011**, *50*, 1832–1836; (b) Frank, A. O.; Otto, E.; Mas-Moruno, C.; Schiller, H. B.; Marinelli, L.; Cosconati, S.; Bochen, A.; Vossmeyer, D.; Zahn, G.; Stragies, R.; Novellino, E.; Kessler, H., *Angew. Chem. Int. Ed.* **2010**, *49*, 9278–9281

none of these first *iso*DGR-containing ligands showed an high affinity for $\alpha v\beta_3$ integrins in competitive binding assays.[66]

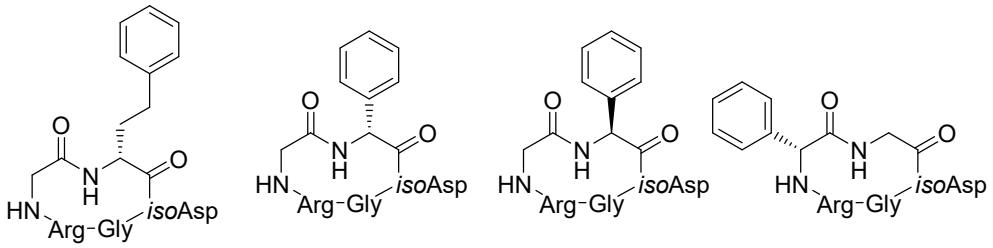

Figure 1.21 – *iso*DGR ligands

The synthesis and biological evaluation of cyclic peptidomimetics containing a bifunctional diketopiperazine scaffold (DKP2 and DKP3) was already reported by our research group [67] and the library was recently extended with two more members (containing the DKP5 and DKP7).[68] These compounds will be deepened in Chapter 2.

[67] Mingozzi, M.; Dal Corso, A.; Marchini, M.; Guzzetti, I.; Civera, M.; Piarulli, U.; Arosio, D.; Belvisi, L.; Potenza, D.; Pignataro, L.; Gennari, C., *Chem. Eur. J.* **2013**, *19*, 3563–3567

[68] Panzeri, S.; Zanella, S.; Arosio, D.; Vahdati, L.; Dal Corso, A.; Pignataro, L.; Paolillo, M.; Schinelli, S.; Belvisi, L.; Gennari, C.; Piarulli, U., *Chem. Eur. J.* **2015**, *21*, 6265 – 6271

1.3 RGD- and *iso*DGR-integrin ligands mode of action

1.3.1 Receptor pharmacology: general definitions

Drugs that bind to physiological receptors and mimic the regulatory effects of the endogenous signaling compounds are termed **agonists**. Agents that are only partly as effective as agonists no matter the amount employed (even at saturating concentrations) are termed **partial agonists**. Drugs that bind to receptor without regulatory effect but only blocking the binding of the endogenous ligand (for example by competition for agonist-binding site) are called **antagonists** and those who stabilize the receptor in its inactive conformation are termed **inverse agonists** (Figure 1.22).[69] Inverse agonism may be measured only in systems where an equilibrium between the active and inactive receptor state in absence of drugs exists, and this is not the case of integrins which are constitutively in the inactivated state.[15] The whole concept is much more clear as depicted in Figure 1.22. Named D the studied drug and R the receptor, R_a is the active receptor state, R_i is the inactive receptor state and DR_a/DR_i is the complex ligand-receptor.

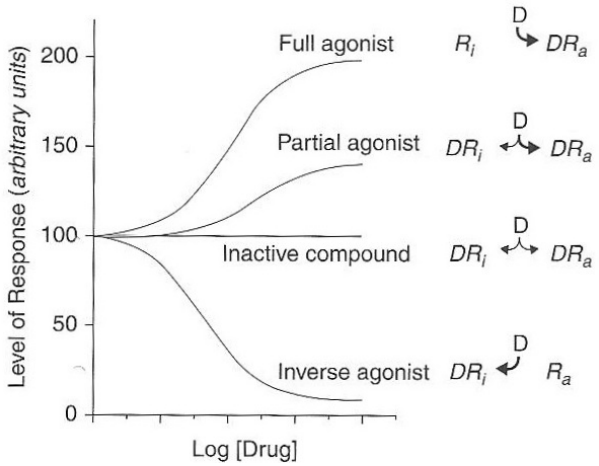

Figure 1.22 – Regulation of the activity of a receptor with conformation-selective drugs

1.3.2 Cilengitide pharmacological activity

Cilengitide (Figure 1.8) is a 15-membered cyclic RGD-pentapeptide (c-RGD-(D-Phe)-*N*-Methyl-Val) developed by Kessler and coworkers[3b,55]. It is a potent $\alpha_v\beta_3/\alpha_v\beta_5$ binder (IC_{50} $\alpha_v\beta_3$ = 0.6 nM, IC_{50} $\alpha_{IIb}\beta_3$ = 860 nM). As mentioned before, the crystal structure of this compounds complexed with integrins has already been studied.[34] The calculated distance C^{β}(Asp)-C^{β}(Arg) is around 9 Å, thus allowing an extended conformation of the RGD sequence that guarantee an optimal ligand-receptor interaction.

[69] Brunton, L. L.; Lazo, J. S.; Parker, K. L. in "The Pharmacological Basis of Therapeutics – Goodman & Gilman's" (11th edition), **2006**, 23

Preclinical models have indicated a synergistic effect in combination with radiotherapy[70] or with an alkylating agent. For example in a rat xenograft model, it potentiated the cytotoxic effects of radiation when the compound was administered prior to the radiation therapy (differently from classical radiosensitizers[71]).[69a] Cilengitide has demonstrated its potential as antiangiogenic agent in cancer therapy in various clinical trials (in different clinical phases according to the kind of cancer).[72] For example phase I and phase II trials of Cilengitide as single-agent in *glioblastoma multiforme* demonstrated little toxicity and promising antitumor activity.[73] In a phase I/IIa study, the addition of Cilengitide to the standard chemoradiotherapy for newly diagnosed *glioblastoma multiforme* demonstrated to be safe, well tolerated, and to improve progression-free survival and overall survival in patients with MGMT promoter methylation (status of the gene encoding for the repair enzyme O^6-methylguanine-DNA methyltransferase). [74] However, in a subsequent study, Cilengitide was not proven to alter the tumor progression[75] and in a phase III clinical trial (CENTRIC) the addition of Cilengitide to the standard of care did not improve overall patient survival.[76]

Cell studies on Cilengitide are controversial. This RGD-ligand was proven to induce anoikis and to inhibit FAK phosphorylation in glioblastoma and endothelial cells in the micromolar concentration range (1–80 μm).[77] On the other hand, the same compound showed, at nanomolar concentrations an agonist-like activity and adverse paradoxical integrin activation effects.[20] Moreover, Cilengitide was shown to promote angiogenesis in human umbilical vein endothelial cells (HUVEC) at nanomolar concentrations while, in the same cellular model, it was reported to induce FAK phosphorylation at clinically-relevant concentration (i.e. 10 μm).[78] These different data seem to indicate that experimental conditions and cellular model affect the activity of Cilengitide.

This evidenced paradoxical pro-angiogenic activity of RGD-mimetic agents at low concentrations have raised concerns about the efficacy of RGD compounds as true integrin antagonists and raise questions concerning the use of antiangiogenetic drugs as single therapy agent.[20,47,79] In summary, one major problem with integrin inhibitors is their

[70] (a) Mikkelsen, T; Brodie, C.; Finniss, S.; Berens, M. E.; Rennert, J. L.; Nelson, K.; Lemke, N.; Brown, S. L.; Hahn, D.; Neuteboom, B.; Goodman, S. L., *Int. J. Cancer* **2009**, *124 (11)*, 2719-2727; (b) MacDonald, T. J.; Taga, T.; Shimada, H., *et. al., Neurosurgery*, **2001**, *48*, 151-157

[71] Miller R. A.; Woodburn, K.; Fan, Q.; Renschler, M. F.; Sessler, J. L.; Koutcher, J. A., *Int. J. Radiat. Oncol. Biol. Phys.* **1999**, *45*, 981-989

[72] Mas-Moruno, C.; Rechenmacher, F.; Kessler, H., *Anti-Cancer Agents Med. Chem.* **2010**, *10*, 753-768

[73] (a) Reardon, D. A.; Fink, K. L.; Mikkelsen, T.; Cloughesy T. F.; O'Neill, A.; Plotkin, S.; Glantz, M.; Ravin, P.; Raizer, J. J.; Rich, K. M.; Schiff., D.; Shapiro, W. R.; Burdette-Radoux, S.; Dropcho, E. J.; Wittemer, S. M.; Nippgen, J.; Picard, M.; Nabors, L. B., *J. Clin. Oncol* .**2008**, *26(34)*, 5610-5617; (b) Gilbert, M.; Lamborn, K.; Lassman, A., et. al, Preliminary data from NABTC protocol 03-02, presented at the 12th Annula Meeting of the Society for Neuro-Oncology, Dallas, TX, November 15-18, 2007 (abstr. MA39); (c) Nabors, L. B.; Mikkelsen, T.; Rosenfeld, S. S., et. al, *J. Clin. Oncol.* **2007**, *25*, 1651-1657

[74] Stupp, R.; Hegi, M. E.; Neyns, B.; Goldbrunner, R.; Schlege, U.; Clement, P. M. J.; Grabenbauer, G. G.; Ochsenbein, A. F.; Simon, M.; Dietrich, P.-Y.; Pietsch, T.; Hicking, C.; Tonn, J.-C.; Diserens, A.-C-; Pica, A.; Hermisson, M.; Krueger, S.; Picard, M.; Weller, M., *J. Clin. Oncol.* **2010**, *28(16)*, 2712-2718

[75] Eisele, G.; Wick, A.; Eisele, A.-C.; Clément, P.M.; Tonn, J.; Tabatabai, G.; Ochsenbein, A.; Schlegel, U.; Neyns, B.; Krex, D.; Simon, M.; Nikkhah, G.; Picard, M.; Stupp, R.; Wick, W.; Weller, M., *J. Neurooncol.* **2014**, *117(1)*, 141-145

[76] Merck Group, CENTRIC trials (news release, March, the 24rd 2014)

[77] Oliveira-Ferrer, L.; Hauschild, J.; Fiedler, W.; Bokemeyer, C.; Nippgen, J.; Celik, I.; Schuch, G., *J. Exp. Clin. Cancer Res.* **2008**, *27*, 86–99

[78] Alghisi, G. C.; Ponsonnet, L.; Rüegg, C., *PLoS ONE* **2009**, *4*, e4449

[79] (a) Weiss, S. M.; Stupack, D. G.; Cheresh, D. A., *Cancer Cell* **2009**, *15*, 359-361; (b) Robinson, S. D.; Hodivala-Dilke, K. M., *Curr. Opin. Cell Biol.* **2011**, *23*, 630-637

potential to activate conformational changes, which can initiate unwanted signals that induce agonist-like activities and adverse paradoxical effects.[3a,80]

1.3.3 *iso*DGR-integrin ligands act as true integrin antagonists

In order to design new integrin blockers could be very useful to get information defining the receptor allosteric events induced by ligand binding. In this context, Musco and co-workers exploited a combination of computational (all-atom MD simulations) and biochemical studies to describe the dynamic changes of $\alpha_V\beta_3$ upon ligand binding.[47] Simulations were carried out on the $\alpha_V\beta_3$ headpiece alone and in the presence of cyclopeptidic ligands: RGDf(NMe)V, C*iso*DGRC, and $_{ac}$C*iso*DGRC. Collected data showed that the three ligands anchor to the α_V and β_3 domains through an electrostatic clamp. However, the three interaction patterns are similar but not identical (Figure 1.23).[47] In particular, a relevant difference was registered in the coordination pattern of the second carboxylate oxygen. In the case of *iso*DGR-containing peptides (C*iso*DGRC and $_{ac}$C*iso*DGRC) this oxygen interacts with residue $N^{215}{}_{\beta3}$, whereas the very same oxygen in RGDf(NMe)V stably binds to residues $S^{121}{}_{\beta3}$-$S^{123}{}_{\beta3}$. These interactions play a crucial role as the trigger of the integrins activation mechanism operated by endogenous ligands.[81] Remarkably, these interactions are barely present in the simulations with *iso*DGR-containing cyclopeptides.[47]

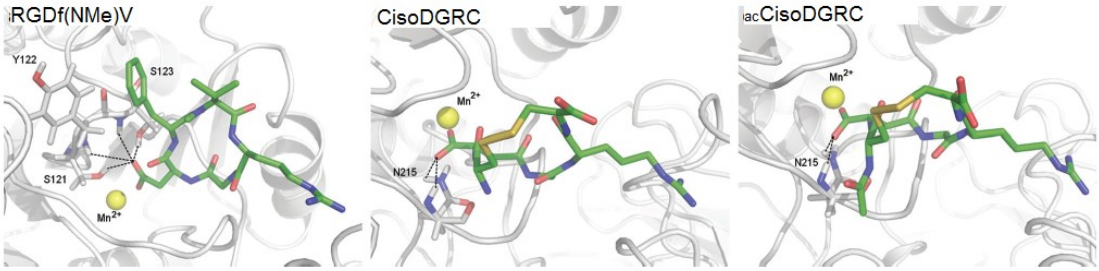

Figure 1.23 – Interactions patterns of the ligands tested

The $\alpha_V\beta_3$ binding pocket is in grey and the cyclopeptides ligands are depicted in green (blue = nitrogen, red = oxygen, yellow = sulfur). Sticks are used to represent $\alpha_V\beta_3$ residues (one-letter code) directly coordinating the carboxylate groups of Asp/*iso*Asp residue of the ligand. MIDAS is represented as a yellow sphere. Dotted lines highlight the different ligand-receptor interaction patterns.

[80] (a) Cox, D.; Brennan, M.; Moran, N., *Nat. Rev. Drug. Discovery* **2010**, 9, 804-820; (b) Ahrens, I.; Peter, K., *Thromb. Haemostasis* **2008**, 99, 803-804
[81] Zhu, J.; Zhu, J.; Negri, A.; Provasi, D.; Filizola, M.; Coller, B. S.; Springer, T. A., *Blood* **2010**, *116*, 5050-5059

As presented in paragraph 1.1.2.2 (Integrin action mechanism), the activation of integrins involves an outwards movement of the β-hybrid domain. None of the movements for $\alpha_V\beta_3$, either free or bound to *iso*DGR-containing ligands, matches the typical features of the swing-out movement. Therefore, it seems that *iso*DGR-containing cyclopeptides, unlike RGDf(NMe)V, do not induce the $\alpha_V\beta_3$ headpiece-opening.[47]

The same research group carried out a further investigation to see whether *iso*DGR-containing cyclopeptides could also act as inhibitors of $\alpha_V\beta_3$ allostery in receptors already bound to the cell surface. Receptor activation changes the conformation of the β_3 subunit[47] resulting in the exposure of epitopes called ligand-induced binding sites (LIBS). These could be specifically recognized by LIBS-specific monoclonal antibodies (such as AP5mAb). As expected, only RGDf(NMe)V induces a significant exposure of LIBS on HUVEC. In contrast, *Ciso*DGRC and $_{ac}$*Ciso*DGRC fail to induce the exposure of these epitopes. All the data collected seem to indicate that *iso*DGR-containing cyclopeptides inhibit integrin activation unlike RGDf(NMe)V, which induces integrin activation.[47]

Additional studies on $\alpha_V\beta_3$-expressing HUVEC were carried out with the aim of investigating if the allosteric movement of $\alpha_V\beta_3$ could influence the pathways usually triggered by ligand-induced $\alpha_V\beta_3$ activation. Once again, the effect of RGDf(NMe)V was compared to the effect of *iso*DGR-containing cyclopeptides. Both $_{ac}$*Ciso*DGR and *Ciso*DGRC did not induce accumulation of $\alpha_V\beta_3$ at the cell border while RGDf(NMe)V promoted the redistribution of $\alpha_V\beta_3$ from focal adhesion to the cell periphery,[77] an event critical for cell migration[82]. These data prove that $\alpha_V\beta_3$ relocalization at the cell edge is induced by RGDf(NMe)V (Figure 1.24) and, as a consequence, that this RGD-containing ligand stimulates the conversion of an inactive integrin into a multifaceted signaling machine causing undesired receptor clustering, activation, and redistribution.[47] All these experimental evidences support the hypothesis that *iso*DGR-containing cyclopeptides compete with the ligand binding without inducing integrin activation.[83]

[82] Kiosses, W. B.; Shattil, S. J.; Pampori, N.; Schwartz, M. A., *Nat. Cell Biol.* **2001**, *3*, 316-320
[83] Caswell, P. T.; Vadrevu, S.; Norman, J. C., *Nat. Rev. Mol. Cell Biol.* **2009**, *10*, 843-853

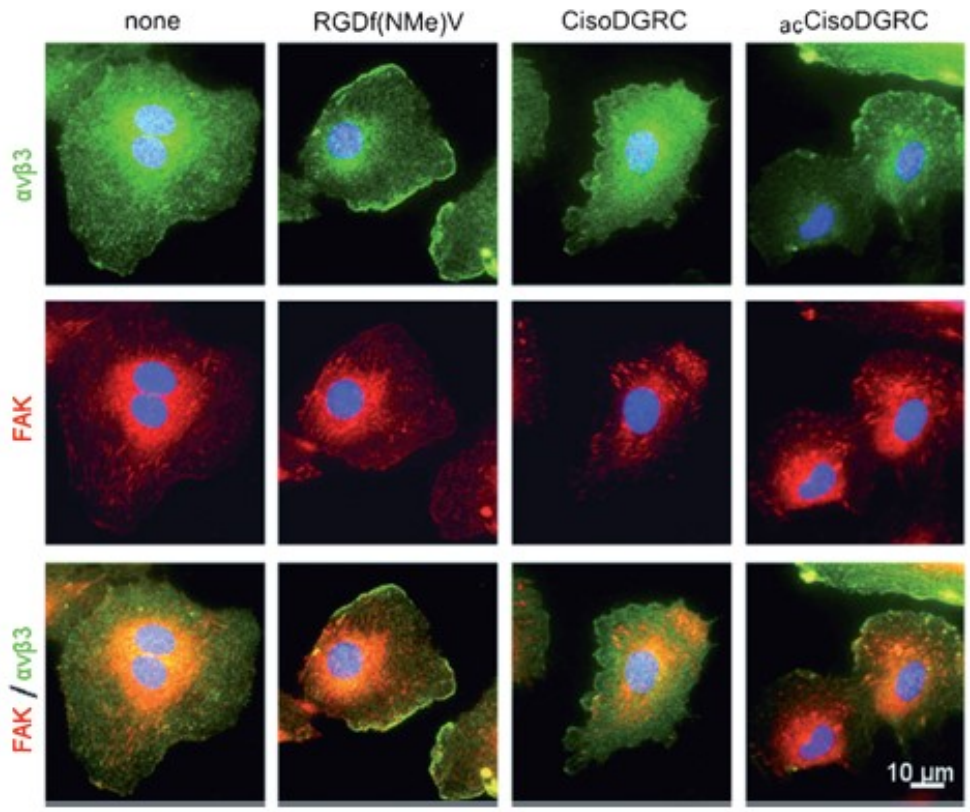

Figure 1.24 – Localization of $\alpha v\beta_3$ integrin (green) and FAK (red) was monitored by immunoflorescence staining
In this test, HUVEC were plated on fibronectin and treated with saturating amounts of RGDf(NMe)V, *Ciso*DGR, or $_{ac}$*Ciso*DGRC. Only RGDf(NMe)V caused disappearance of $\alpha v\beta_3$ (stained with focal adhesion kinase antibodies) from focal adhesion and promoted relocalization at the cell periphery.

Summarizing, Musco and co-workers demonstrated that *iso*DGR-based cyclopeptides unexpectedly inhibit receptor allosteric activation acting as true antagonist of $\alpha v\beta_3$ integrin. The intrinsic ability of the *iso*DGR motif to block receptor allosteric activation is interesting for drug development: *iso*DGR-based drugs represent promising integrin antagonist class, devoid of intrinsic paradoxical activation effects.[78]

CHAPTER 2

DKP-INTEGRIN LIGANDS

2.1 Aim of the project

The aim of this project was the synthesis of a small collection of *Cyclo*[DKP-*iso*DGR] peptidomimetics active as integrin ligands. According to the evidences reported in Chapter 1.3, the *iso*DGR library was synthesized to see whether the new compounds maintain the affinity and selectivity of the RGD-ligands analogues with the advantage of pure antagonist activity on integrins. The synthesis was planned with a mixed solid phase/solution phase approach.

2.2 2,5-Diketopiprazines as privileged scaffolds

2.2.1 Introduction

2,5-Diketopiperazines (DKPs) (Figure 2.1) are biologically active constrained cyclic peptides[84] with a wide spectrum of properties[85] and applications. These compounds are six-membered heterocyclic scaffolds that differ for the substitution on up to four positions (N1, N4, C3, C6) and for the configuration at the two stereocenters (C3, C6). DKPs are formally derived from two α-amino acids.

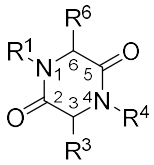

Figure 2.1 – DKP general structure and numbering

DKPs are characterized by a rigid structure embedding amide groups and, because of this, they are poorly soluble in organic solvents. The nitrogen atom of the α-amino amide is constrained into a ring and therefore the susceptibility to bond cleavage is reduced, the physical properties are altered and conformational rigidity is induced. Because of their properties, DKPs can be used to circumvent some limitations of peptides.[86] In addition, interactions with biological targets are supported by the presence of groups acting as donors and acceptors of hydrogen bonds.

DKPs were once believed to be only protein artifacts or degradation products. Nowadays they are considered privileged structures[87] in medicinal chemistry, in heterocyclic diversity-oriented synthesis and in combinatorial biomedical chemistry[88], to provide high-affinity ligands to specific receptors and for the *de novo* design of proteins[89]. Moreover they find applications also in organocatalysis: they were used in the hydrocyanation of aldehydes,[90] imines[91] (even if the result in this last case was questioned[92]) and in the addition reaction of several aldehydes to β-nitrostyrene and (E)-2-(furan-2-yl)nitroethene.[93]

---

[84] (a) Witiak, D. T.; Wei, Y. in: *Progress in Drug Discovery* (Ed.: E.Jucker, BirkhäuserVerlag: Basel), **1990**, *35*, 249–363; (b) González, J. F.; Ortín, I.; De la Cuesta, E.; Menéndez, *J. C. Chem. Soc. Rev.* **2012**, *41*, 6902-6915; (c) Martins, M. B.; Carvalho, I., *Tetrahedron*, **2007**, *63*, 9923-9932; (d) Liebscher, J.; Jin, S., *Chem. Soc. Rev.* **1999**, *28*, 251-259

[85] McCleland, K.; Milne, P. J.; Lucieto, F. R.; Frost, C.; Brauns, S. C.; Van De Venter, M.; Du Plessis, J.; Dyason, K. J., *Pharm. Pharmacol.* **2004**, *56*, 1143-1153

[86] Borthwick, A. D., *Chem. Rev.* **2012**, *112*, 3641-3716

[87] Evans, B. E.; Rittle, K. E.; Bock, M. G.; Di Pardo, R. M.; Freidinger, R. M.; Whitter, W. L.; Lundell, G. F.; Veber, D. F.; Anderson, P. S.; Chang, R. S. L.; Lotti, V. J.; Cerino, D. J.; Chen, T. B.; Kling, P. G.; Kunkel, K. A.; Springer, J. P.; Hirshfield, J., *J. Med. Chem.* **1988**, *31*, 2235–2246

[88] (a) Horton, D. A.; Bourne, G. T.; Smythe, M. L., *Mol. Divers.* **2000**, *5*, 289-304; (b) Spatola, A. F.; Romanovskis, P. in *"Combinatorial Peptide and Nanopeptide Libraries"* (Ed: G. Jung, VHC, Weinheim), **1996**, 327-347

[89] Tuchscherer, G.; Mutter, M., J. *Biotechnol.* **1995**, *41*, 197-210

[90] (a) Oku, J. I.; Inoue, S., *J. Chem. Soc., Chem. Commun.* **1981**, 229-230; (b) Kogut, E. F.; Thoen, J. C.; Lipton, M. A., *J. Org. Chem.* **1998**, *63*, 4604-4610

[91] Iyer, M. S.; Gigstad, K. M.; Namedev, N. D.; Lipton, M., *J. Am. Chem. Soc.* **1996**, *118*, 4910-4911

[92] Becker, C; Hoben, C.; Schollmeyer, D.; Scherr, G.; Kunz, H., *Eur. J. Org. Chem.* **2005**, 1497-1499

[93] Durini, M.; Sahr, F. A.; Kuhn, M.; Civera, M.; Gennari, C.; Piarulli, U., *Eur. J.Org. Chem.* **2011**, *20*, 5599-5607

2.2.2 Applications to medicinal chemistry

The DKP heterocycle can be found as part of complex molecules in natural products[84c,94] (fungi[95] or bacterial[96] origin) or alone. They show various therapeutic properties[97] and a widespread applications as biologically active compounds. Among all these activities, the most important are probably the inhibitor of plasminogen activator inhibitor-1 (PAI-1)[98], the regulation of the P-glycoprotein activity, and the effects on cardiovascular and blood-clotting functions[85]. DKPs are also antitumor[99], antifungal[100], antibacterial[101], antihyperglycaemic[102], and antiviral agents[103]. It is well known their affinity for calcium channels and opioid receptors[104], as well as for GABAergic[105], for serotoninergic 5-HT_{1A}[106] and oxytocin receptors.[107] Several example concerning pharmacologically active compounds (both synthetic or natural) containing DKPs can be found in the literature. In the following section will be discussed only some examples to give an idea of their wide spectrum of applications.

[94] (a) Huang, R.; Zhou, X.; Xu, T.; Yang, Liu, Y., *Chem. Biodiv.* **2010**, *7*, 2809-2829; (b) Gou, H.; Sun, B.; Gao H.; Chen, X.; Liu, S.; Yao, X.; Liu, X.; Che, Y., *J. Nat. Prod.* **2009**, *72*, 2115-2119

[95] For example see: (a) Ding, J.; Jiang, L.; Guo, L.; Chen, X.; Zhang, H.; Che, Y., *J. Nat. Prod.* **2008**, *71*, 1861-1865; (b) Cui, C.; Kakeya, H.; Osada, H., *Tetrahedron* **1996**, *52*, 12651-12666

[96] For example see: (a) Ameur, R. M.-B.; Mellouli, L.; Chabchoub, F.; Fotso, S.; Bejar, S., *Chem. Nat. Compd.* **2004**, *40*, 510-513; (b) Raju, R.; Piggott, A. M.; Huang, X.-C.; Capon, R., *J. Org. Lett.* **2011**, *13*, 2770-2773

[97] Long, D. D.; Tennant-Eyles, R. J.; Estevez, J. C.; Wormald, M. R.; Dweck, R. A.; Smith, M. D.; Fleet, G. W. J., *J. Chem. Soc., Perkin Trans. 1* **2001**, 807-813

[98] (a) Folkes, A.; Roe, M. B.; Sohal, S.; Golec, J.; Faint, R.; Brooks, T.; Charlton, P., *Bioorg. Med. Chem. Lett.* **2001**, *11*, 2589-2592; (b) Wang, S.; Golec, J.; Miller, W.; Milutinovic, S.; Folkes, A.; Williams, S.; Brooks, T.; Hardman, K.; Charlton, P., *Bioorg. Med. Chem. Lett.* **2002**, *12*, 2367-2370; (c) Brooks, T. D.; Wang, S. W.; Brünner, N.; Charlton, P. A., *Anti-Cancer Drugs* **2004**, *15*, 37-44; (d) Einholm, A. P.; Pedersen, K. E.; Wind, T.; Kulig, P.; Overgaard, M.T.; Jensen, J. K.; Bodker, J. S.; Christensen, A., *Biochem. J.* **2003**, *373*, 723-732; (e) Cheng, Y.; Manwell, J., U. S. Pat. Appl. Publ. 130, 281, 2005, *Chem. Abstr.* **2005**, *142*, 411381

[99] (a) Kanoh, K.; Kohno, S.; Katada; J., Takahashi, J.; Uno, I., *J. Antibiot.* **1999**, *52*, 134-141; (b) Nicholson, B.; Lloyd, G. K.; Miller, B. R.; Palladino, M. A.; Kiso, Y.; Hayashi, Y.; Neuteboom, S. T. C., *Anti-Cancer Drugs* **2006**, *17*, 25-31; (c) Kanzaki, H.; Imura, D.; Nitoda, T.; Kawazu, K., *J. Biosci. Bioeng.* **2000**, *90*, 86-89

[100] (a) Asano, N., *Glycobiology* **2003**, *13*, 93R-104R; (b) Houston, D. R.; Synstad, B.; Eijsink, V. G. H.; Stark, M. J. R.; Eggleston, I. M.; Van Aalten, D. M. F., *J. Med. Chem.* **2004**, *47*, 5713-5720; (c) Byun, H.-G.; Zhang, H.; Mochizuki, M.; Adachi, K.; Shizuri, Y.; Lee, W.-J.; Kim, S. K., *J. Antibiot.* **2003**, *56*, 102-106

[101] (a) Fdhila, F.; Vázquez, V.; Sánchez, J. L.; Riguera, R., *J. Nat. Prod.* **2003**, *66*, 1299-1301; (b) Kanokmedhakul, S.; Kanokmedhakul, K.; Phonkerd, N.; Soytong, K.; Kongsaree, P.; Suksamrarn, A., *Planta Med.* **2002**, *68*, 834-836; (c) Sugie, Y.; Hirai, H.; Inagaki, T.; Ishiguro, M; Kim, Y. J.; Kojima, Y.; Sakakibara, T.; Sakemi, S.; Sugiura, A.; Suzuki, Y.; Brennan, L.; Duignan, J.; Huang, L. H.; Sutcliffe, J.; Kojima, N., *J. Antibiot.* **2001**, *54*, 911-916; (d) De Kievit, T. R.; Iglewski, B. H., *Infect. Immun.* **2000**, *68*, 4839-4849; (e) Kozlovsky, A. G.; Zhelifonova, V. P.; Adanin, V. M.; Antipova, T. V.; Ozerskaya, S. M.; Ivanushkina, N. E.; Grafe, U., *Appl. Biochem. Microbiol.* **2003**, *39*, 393-397

[102] (a) Kwon, O. S.; Park, S. H.; Yun, B. S.; Pyun, Y. R.; Kim, C. J., *J. Antibiot.* **2000**, *53*, 954-958; (b) Song, M. K.; Hwang, I. K.; Rosenthal, M. J.; Harris, D. M.; Yamaguchi, D. T.; Yip, I.; Go, K. V. L. W., *Exp. Biol. Med.* **2003**, *228*, 1338-1345; (c) Hwang, I. K.; Harris, D. M.; Yip, I.; Kang, K. W.; Song, M. K., *Diabetes Obes. Metab.* **2003**, *5*, 317-324

[103] Sinha, S.; Srivastava, R.; De Clercq, E.; Singh, R. K., *Nucleotides Nucleic Acids* **2004**, *23*, 1815-1824

[104] Kilian, G.; Jamie, H.; Brauns, S. C. A.; Dyason, K.; Milne, P., *J. Pharmazie* **2005**, *60*, 305-309

[105] Imamura, M.; Prasad, C., *Peptides* **2003**, *24*, 445-448

[106] López-Rodríguez, M. L.; Morcillo, M. J.; Fernández, E.; Porras, E.; Orensanz, L.; Beneytez, M. E.; Manzanares, J.; Fuentes, J. A., *J. Med. Chem.* **2001**, *44*, 186-197

[107] (a) Wyatt, P. G.; Allen, M. J.; Borthwick, A. D.; Davies, D. E.; Exall, A. M.; Hatley, R. J. D.; Irving, W. R.; Livermore, D. G.; Miller, N. D.; Nerozzi, F.; Sollis, S. L.; Szardenings, A. K., *Bioorg. Med. Chem. Lett.* **2005**, *15*, 2579-2583; (b) Liddle, J., PCT Int. Appl. CODEN: PIXXD2; WO 2005000840; A1 20050106; 2005; *Chem. Abstr.* **2005**, *142*, 114102; (c) Brooks, D. P., PCT Int. Appl. CODEN: PIXXD2 WO 2005000311; A1 20050106, 2005; *Chem. Abstr.* **2005**, *142*, 114098; (d) Dömling, A.; Huang, Y., *Synthesis* **2010**, 2859-2883

2.2.2.1 Examples of biological active compounds containing DKPs

Acyl-CoA cholesterol transferase enzyme is the rate-limiting enzyme in the absorption of cholesterol and, because of this, its inhibition has a potential in moderating the effect of elevated cholesterol level. Gypsetin (Figure 2.2) was found to be a competitive acyl-CoA cholesterol transferase inhibitor with respect to oleoyl-CoA.[108]

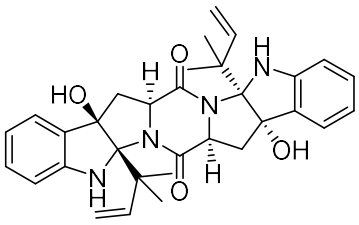

Figure 2.2 – Gypsetin

Some examples of DKPs as antimicrobial active compounds (identified and isolated from microorganism) are depicted in Figure 2.3: a series of DD-DKPs (**2.1** isolated from *Pectenmaximus* bacterial strains)[102a], roquefortine (**2.2**)[101e] and 3,12-dihydroroquefortine (**2.3**)[101e].

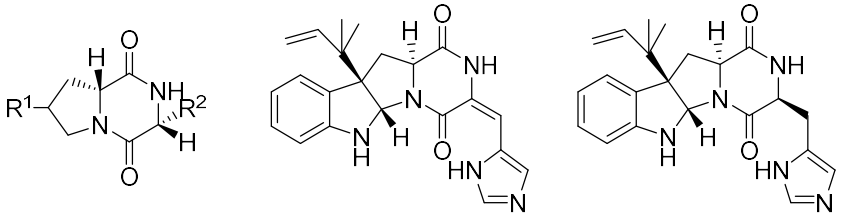

2.1 **2.2** **2.3**

Figure 2.3 – DKPs with antimicrobial activity

It is also worth mentioning Pestalazine A (Figure 2.4), which presents inhibitory activity against HIV-1 replication.[99c]

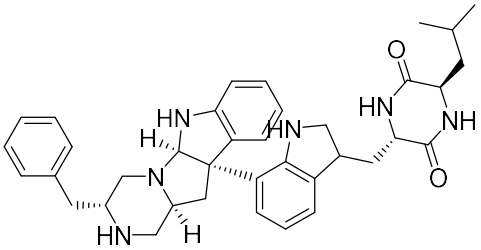

Figure 2.4 – Pestalazine A

Several examples of DKP-containing compounds show cytotoxicity. In Figure 2.5 are reported some molecules as a representative set of derivatives with this action. For example, (-)-Phenylahistin (**2.4**) is a metabolite isolated from *Aspergillus ustus* which

[108] Schkeryantz, J. M.; Woo, J. C. G.; Danishefsky, S. J., *J. Am. Chem. Soc.***1995**, *117*, 7025-7026

resulted cytotoxic for several lines of tumor cells.[99a] Diketopiperazine (**2.5**) is a synthetic analogue of **2.4** and it is a promising agent for cancer treatment. Both these molecules bind to microtubules. Compound **2.5** showed antitumor activity *in vitro* against human tumor cell lines from prostate, breast, lung, leukemia and colorectal tumors.[99b] Moreover **2.5** is able to induce rapidly microtubule depolymerization already at low concentration in an *in vitro* model for vascular endothelial tumor cells.

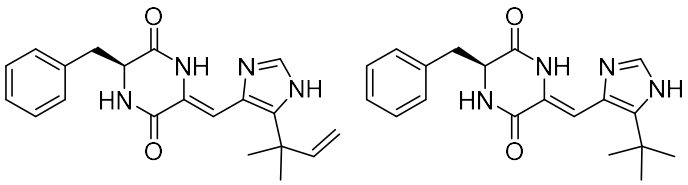

2.4: (-)-Phenylahistin **2.5**

Figure 2.5 – Cytotoxic DKPs

Another biological activity of DKPs is related to the inhibition of plasminogen activator inhibitor (PAI-1) and to alterations of cardiovascular and blood-clotting functions.[98d] In Figure 2.6 are depicted four molecules that were designed structurally based on DKPs as inhibitors of PAI-1.[98]

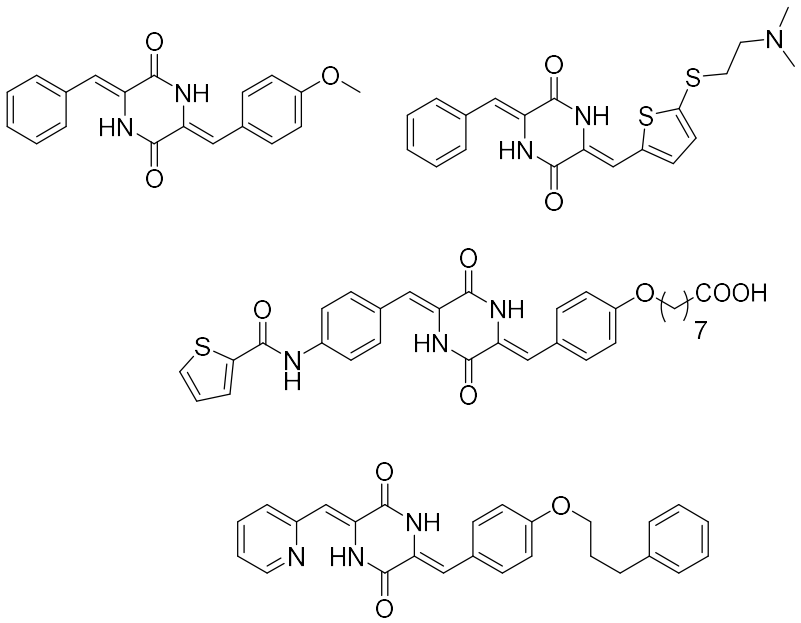

Figure 2.6 – DKPs as PAI-1 inhibitors

It seems that tumor malignant cells are protected from the host immunological system because of a fibrin coat stimulated by the same tumor cells (pro-coagulant activity). As a consequence, inhibition of tumor growth and circumvention of metastasis could be reached by targeting components of the blood-clotting system. *Cyclo*(L-His-L-Tyr) DKP **2.6** (Figure 2.7) significantly increased clotting time, prevented platelet adhesion and

aggregation induced by adenosine diphosphate, and increased the heart rate in isolated rodent hearts. On the other hand, *Cyclo*(L-His-L-Phe) DKP **2.7** (Figure 2.7) showed antitumor activity by significantly reducing the viability of HeLa cells (from cervical carcinoma), WHCO3 cells (from oesophageal carcinoma) and MFC-7 cells (from mammary carcinoma) and it also decreased the cardiac output and the level of coronary blood flow.[85]

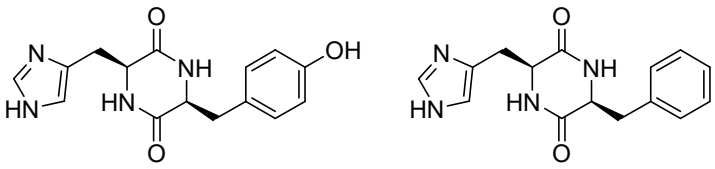

2.6 **2.7**

Figure 2.7– DKPs which interfere in cardiovascular and blood-coagulation functions

2.2.2.2 Applications as templates

DKPs have been used as templates in order to induce a defined secondary structure in peptide sequences. These constrained heterocyclic scaffolds were employed in the selective recognition of anions and small peptides, and in peptidomimetics as secondary structure-mimics (e.g., β-turns, β-hairpins, and α-helices mimics). Thanks to their peptide functionalities (e.g., an amine and a carboxy groups) and their well-defined spatial properties, DKPs can reproduce the desired orientation in the growing peptide.

Several examples in which DKPs are used as β-turn inducers are reported in the literature. A β-turn is a four residue turn showing a 10-membered intramolecular H-bonded ring (general structure in Figure 2.8). β-turn inducers are grouped in three classes (Figure 2.9): a) internal β-turn mimics, b) β-hairpin mimics (when a rigid scaffold, incorporated into a peptide or pseudo-peptide chain, causes a reversal of the chain.[109]), c) external β-turn inducers (where a rigid template is used to constrain the backbone of a cyclic peptide in order to stabilize the peptide residue into a β-turn conformation).

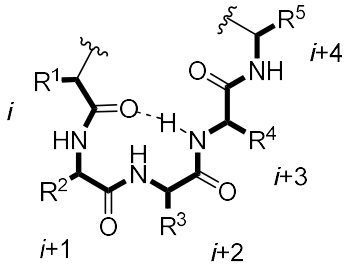

Figure 2.8 – β-turn structure

[109] Robinson, A. J., *Acc. Chem. Res.* **2008**, *41*, 1278-1288

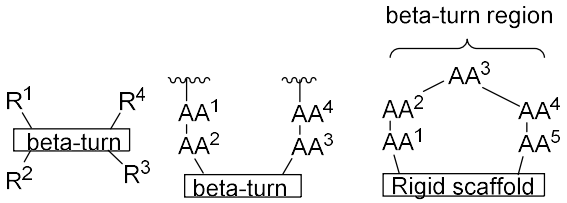

Figure 2.9 – β-turn classes

To mention some interesting applications in this field, Golebiowski and co-workers developed a solid-supported high-throughput synthesis of bicycle DKPs and synthesized a library to mimic type I β-turn (**2.8**, Figure 2.10)[110]. A further example is the conformationally restricted β-turn mimic **2.9** presented by Khan and co-workers (Figure 2.10).[111]

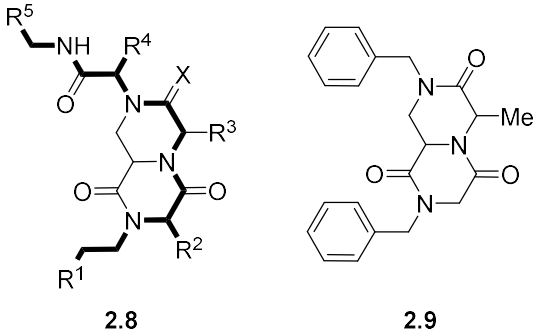

Figure 2.10 - Examples of diketopiperazine-based β-turn mimics

Burgess and co-workers synthesized antagonists for tropomysin C containing a DKP substituted at N1 and C3 (general structure in Figure 2.11) where these substituents, according to calculations, overlay with the side chains of the *i*+1 and *i*+2 of a type I β-turn.[112]

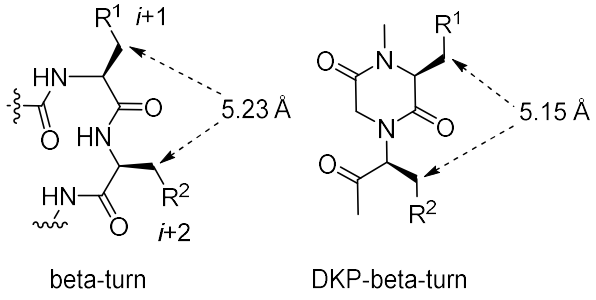

Figure 2.11 – General structure of the tropomysin C antagonist of Burgess and co-workers

[110] Golebiowski, A.; Klopfenstein, S. R.; Chen, J. J.; Shao, X., *Tetrahedron Lett* .**2000**, *41*, 4841-4844
[111] Kim, H.-O.; Nakanishi, H.; Lee, M. S.; Khan, M., *Org. Lett.* **2000**, *2*, 301-302
[112] Liu, J.; Brahimi, F.; Saragovi, H. U.; Burgess, K., *J. Med. Chem.* **2010**, *53*, 5044-5048

As β-hairpin inducers, the DKP scaffold can promote the formation of parallel or antiparallel β-sheets depending whether the side chains contain the same or complementary functionalities. For example, a protected optically pure DKP scaffold (Figure 2.12) was synthesized by Gellerman and co-workers.[113]

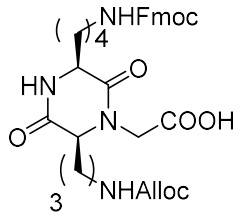

Figure 2.12 – DKP-based β-turn mimic

Examples of external β-turn inducers, based on DKP scaffold, have been reported by Robinson and co-workers.[114] The Pro-based DKP templates were used to stabilize turn and hairpin conformations in cyclic peptides containing the Asn-Pro-Asn-Ala sequence (which seemed important for immune recognition of the folded circumsporozoite surface protein in *Plasmodium falciparum*). The same scaffold was also introduced into a cyclic RGD-containing peptidomimetic (Figure 2.13).[114] Unfortunately, from ^{1}H-NMR studies, emerged that the compound was present in more conformational states in aqueous solution because of the rapid interconversion of the peptide backbone.

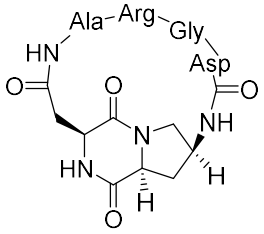

Figure 2.13 – DKP-based external β-turn mimic

[113] (a) Gellerman, G.; Hazan, E.; Brider, T.; Traube, T.; Albeck, A.; Shatzmiler, S., *Int. J. Pept. Res. Ther.* **2008**, *14*, 183-192; (b) Gellman, G.; Hazan, E.; Kovaliov, M.; Albeck, A.; Shatmiler, S., *Tetrahedron* **2009**, *65*, 1389-1396

[114] Bisang, C.; Weber, C.; Robinson, J. A., *Helv, Chim. Acta* **1996**, *79*, 1825-1842

Schafmeister and co-workers have synthesized a "molecular rod" (Figure 2.14) starting from a "bis-amino acid", the 4-amino-4-carboxy Pro.[115] Bis-peptide are defined as "synthetic oligomers assembled from cyclic, stereochemically pure monomers coupled through pairs of amide bonds to form rigid spiroladder oligomers with predefined and programmable three-dimensional structures"[116].

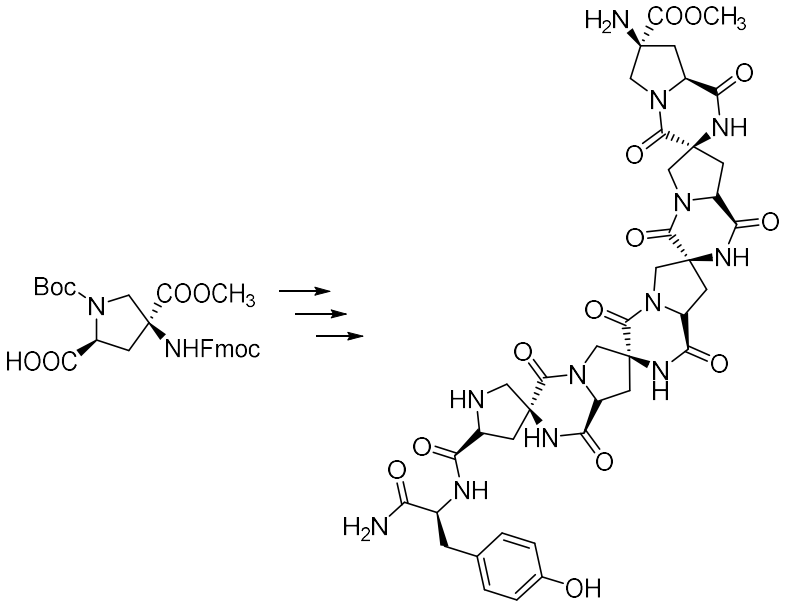

Figure 2.14 – Molecular rod

2.2.2.3 DKPs as two armed receptors

Two-armed receptors are structures composed of a central scaffold and two arms, generally symmetrical, that contain several binding sites that bind different kinds of guests (e.g., anions, cations, small molecules, amino acids and short peptides). The central scaffold has two roles: create a cleft with an adequate size to accommodate the guest and link two-side arms with correct geometry to tie up the guest with a sufficient number of binding points. DKPs, having a flat core and lateral chains of diverse size and nature, are suitable for this purpose. For example, Wennemers and co-workers synthesize a class of symmetrical DKP-based two-armed receptors derived from 4-aminoproline (five different molecules) with two tripeptide chains in *cis* relative configuration (Figure 2.15).[117] In these structures, the scaffold avoids also intramolecular recognition between the two tripeptide arms and collapse of the receptor. The screening against a resin-bound tripeptide library revealed for each of the five structurally similar prototypes selectivity for different

[115] Levins, G. C.; Schafmeister, C. E., *J. Am. Chem. Soc.* **2003**, *125*, 4702-4703
[116] Schafmeister, C. E.; Brown, Z. Z.; Gupta, S., *Acc. Chem. Res.* **2008**, *41*, 1387-1398
[117] (a) Wennemers, H.; Conza, M.; Mold, M.; Krattiger, P., *Chem. Eur. J.* **2001**, *7*, 3342-3347; (b) Conza, M.; Wennemers, H., *J. Org. Chem.* **2002**, *67*, 2696-2698

tripeptides.[118] These two-armed receptors were evaluated also as selective and sensitive coatings for gravimetric gas sensors and to detect and differentiate simple alcohols.[119]

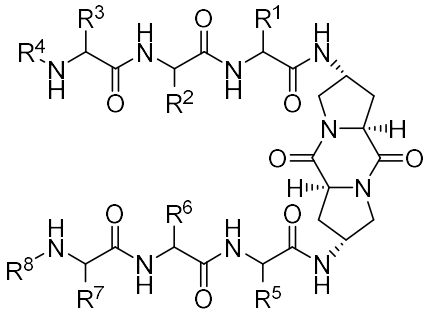

Figure 2.15 - General structure of di-(2*S*,4*R*)-4-aminoproline DKP two-armed receptors

2.2.2.4 Previous work of our group on DKPs field

In 2008 our research group has reported the synthesis of a new class of DKPs.[120] The bifunctional *cis*-DKP scaffold **2.10**, can be seen as a β-hairpin inducer and promoter of antiparallel β-sheet. This compound seemed to have promising properties and it when inserted into several peptidomimetics (synthesis performed in solution with a Boc strategy). ^{1}H-NMR spectroscopy (chemical shift and NOE studies), IR spectroscopy, CD spectroscopy and molecular modeling were employed to clarify the conformation of the derivatives depicted in picture 2.16.[120] These analysis revealed the formation of β-hairpin mimics involving 10- and 18-membered H-bonded rings and a reverse turn of the growing peptide chain. The high stability of the β-hairpin conformation and the turn-inducing ability of **2.10** scaffold was demonstrated by NMR experiments and it was detected also in competitive, dipolar and even protic solvents on **2.11** and **2.12** (Figure 2.16).[120]

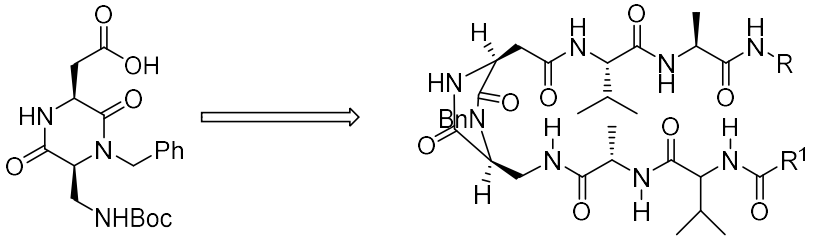

2.10 **2.11**: R = O-tBu; **2.12**: R = CH_3

Figure 2.16 - Bifunctional 2,5-DKP β-hairpin mimic

[118] (a) Ohlmeyer, M. H. J.; Swanson, R. N.; Dillard, L. W.; Reader, J. C.; Asouline, G.; Kobayashi, R.; Wigler, M. H.; Still, W. C., *Proc. Nat. Acad. Sci. USA*, **1993**, *90*, 10922-10926; (b) Nestler, H. P.; Bartlett, P.; Still, W. C., *J. Org. Chem.* **1994**, *59*, 4723-4724

[119] Emery, F.; Bisang, C.; Favre, M.; Jiang, L.; Robinson, A., *Chem. Commun.* **1996**, 2155-2156

[120] Resurreiçao, A. S. M.; Bordessa, A.; Civera, M.; Belvisi, L.; Gennari, C.; Piarulli, U., *J. Org. Chem.* **2008**, *73*, 652-660

An evidence of the DKP1 turn-inducing ability arose also from investigations on the trimerBoc-(DKP1)$_3$-NH*n*Bu (Figure 2.17), and on the correspondent tetramer (Boc-(DKP1)$_4$-NH*n*Bu).[121] ^{1}H-NMR and CD spectroscopy of the trimeric structure in solution suggest the possible formation of two turns for the first and third residues. On the other hand, the tetramer is best described as a β-bond ribbon conformation which means a succession of β-turns forming a linear peptide with a ribbon-like shape.

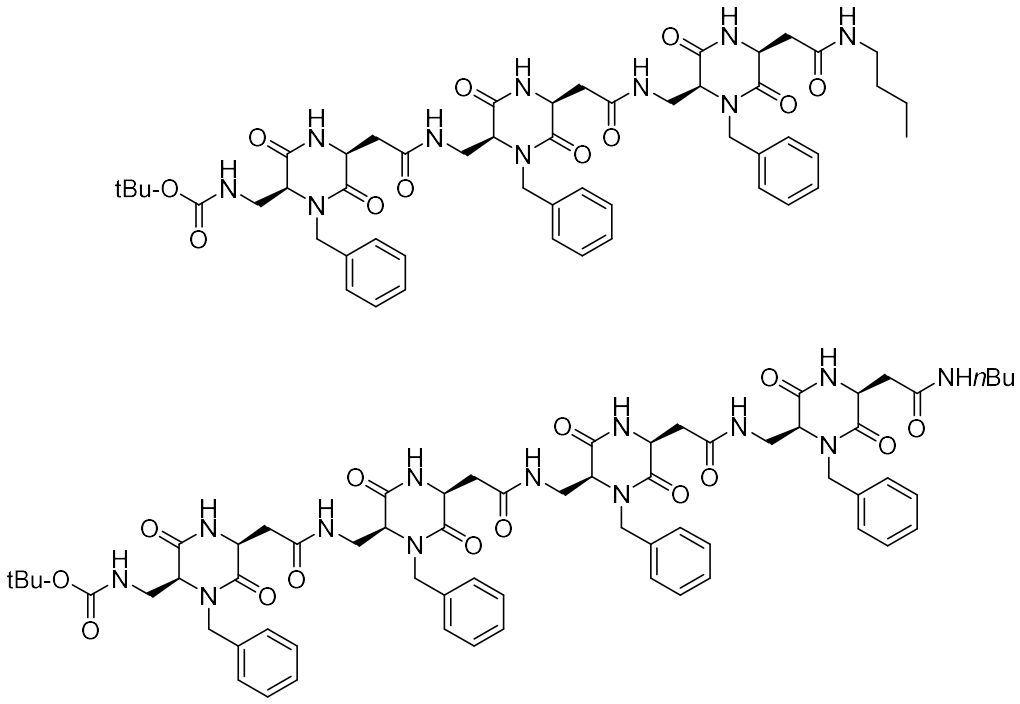

Figure 2.17 – Boc-(DKP1)$_3$-*n*Bu trimer and Boc-(DKP1)$_4$-*n*Bu tetramer

As already mentioned in Chapter 1, several cyclic peptides and peptidomimetics containing the RGD sequence or the *iso*DGR sequence active as integrin ligands have been synthesized and tested: if the ring-size and conformational properties of the cyclic ligand are properly chosen, nanomolar receptor binding affinities could be observed. From this point of view, DKPs have well-defined conformational properties which confer them unique feature as scaffolds to constrain cyclic ligands. Our research group has synthesized a collection of RGD-[65] and *iso*DGR-[67,68] cyclic peptidomimetics active as integrin ligands containing various DKPs as scaffolds to induce the proper RGD-/*iso*DGR-conformation. The whole topic will be further discussed in Paragraph 2.3.

[121] Delatouche, R.; Durini, M.; Civera, M.; Belvisi, L.; Piarulli, U., *Tetrahedron* **2010**, *51*, 4278-4280

2.2.3 Synthesis

In nature the 2,5-DKPs head-to-tail dipeptides are a common structural motif and, as a consequence, most of the biologically active DKPs can be isolated from natural sources. They are also common by-products/degradation products in oligopeptides synthesis. However DKPs can be easily accessed from commercial α-amino acids through different synthetic pathways both in solid phase[122] or in solution phase by conventional synthetic procedures[123] or using microwave-assisted organic synthesis[124].

The main logical sites of disconnections of a 2,5-DKP ring are three (Figure 2.18): the amide bond (**A**) and the C−N bond (**B**), both frequently used, and the C−C bond (**C**), more recent as approach. Also tandem cyclizations forming N1−C2/C3−N4 (**D**) and C2−N1−C6 (**E**) bonds are mentioned in the literature but not commonly used.

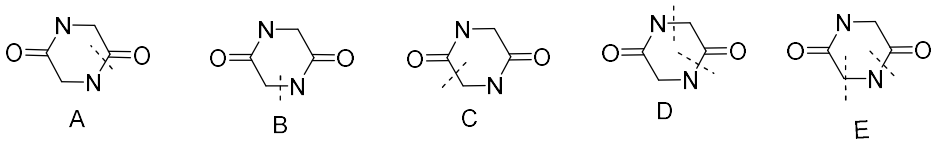

Figure 2.18 - Possible disconnections of the 2,5-DKP ring

In addition, DKP formation in reactions involving amino acids is quite a common side reaction. For example, attempts to employ ethyl glycine chloride in the presence of a strong base to perform nucleophilic substitutions in pyrimidinic rings, resulted in the DKP produced by predominant auto-condensation of ethyl glycine.[125]

Since a comprehensive review an DKPs synthesis is beyond the scope of this thesis, only some interesting conventional synthetic procedures will be shortly examined while more attention will be given to the synthetic pathway used for *Cyclo*[DKP-RGD] and *Cyclo*[DKP-*iso*DGR] ligands.

[122] (a) Li, W. R.; Yang, J. H., *J. Comb. Chem.* **2002**, *4*, 106-108; (b) For a review, see: Fischer, P. M., *J. Pept. Sci.* **2003**, *9*, 9-35

[123] Rodionov, I. L.; Rodionova, L. N.; Baidakova, L. K.; Romashko, A. M.; Balashova, T. A.; Ivanov, V. T., *Tetrahedron* **2002**, *58*, 8515-8523; (b) For a review on synthetic approaches to all three DKP isomers (2,3-, 2,5-, and 2,6-), see: Dinsmore, C. J.; Beshore, D. C., *Tetrahedron* **2002**, *58*, 3297-3312 and references therein

[124] (a) Lopez-Cobenas, A.; Cledere, P.; Sanchez, J. D.; Lopez-Alvaro, P.; Ramos, M. T.; Avendano, C.; Menendez, J. C., *Synthesis* **2005**, *19*, 3412-3422; (b) For a review, see: O'Neill, J. C.; Blackwell, H. E.; *Comb. Chem. High Throughput Screening* **2007**, *10*, 857-876 and references therein

[125] Ermolat'ev, D. S.; Babaev, E. V., *Molecules* **2003**, *8*, 467-471

2.2.3.1 Conventional synthetic procedures

It is possible to prepare symmetrical DKPs simply by heating the free amino acid methyl esters (even with reactive chains) in a sealed tube. However, it is generally better to use protected precursors to avoid the formation of by-products (the corresponding pyrrolidone, piperidone and homopiperidone). For unsymmetrical DKPs, the oldest synthetic procedure consists in the dipeptide ester treatment with methanolic ammonia. Unfortunately this strategy can lead to epimerization because of the strong basic conditions. Boc-dipeptidyl methyl ester *N*-deprotection with formic acid followed by reflux of the dipeptidyl ester formate salt in 2-butanol/toluene (and removal of formic acid through azeotropic distillation is a method less prone to loss of stereointegrity. For many DKPs is enough the simple reflux the dipeptidyl methyl esters in low-boiling solvents, such as MeOH (Scheme 2.1).[126]

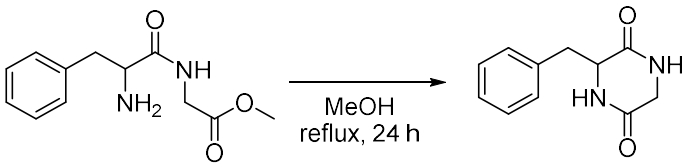

Scheme 2.1 – Solution phase synthesis in refluxing MeOH

DKPs can be synthesized also through a Ugi reaction with the advantage of possible direct substitutions on the secondary amino group (Scheme 2.2).[88]

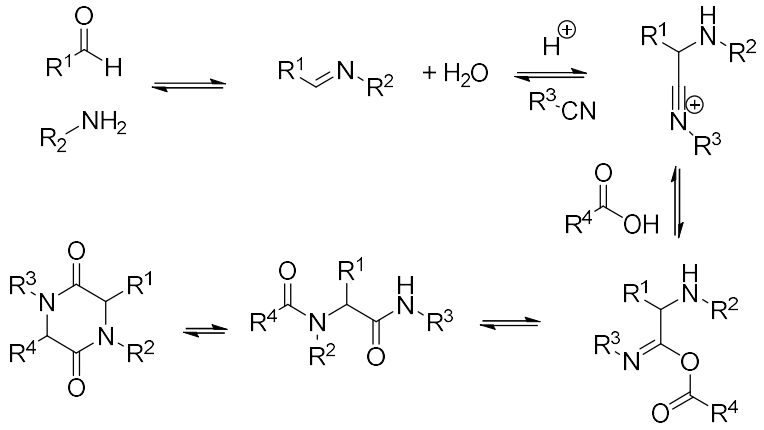

Scheme 2.2 – Ugi reaction mechanism and following cyclization

An example is depicted in Scheme 2.3, a stereospecific synthesis proposed as an alternative in the preparation of trisubstituted DKPs. Unfortunately, the stereochemistry on the stereocenter located on the α-carbon of the tertiary ammine which could not be controlled.[127]

[126] Nitecki, D. E.; Halpern, B.; Westley, J. W., *J. Org. Chem.* **1968**, *33*, 864-866
[127] Sollis, S. L., *J. Org. Chem.* **2005**, *70*, 4735-4740

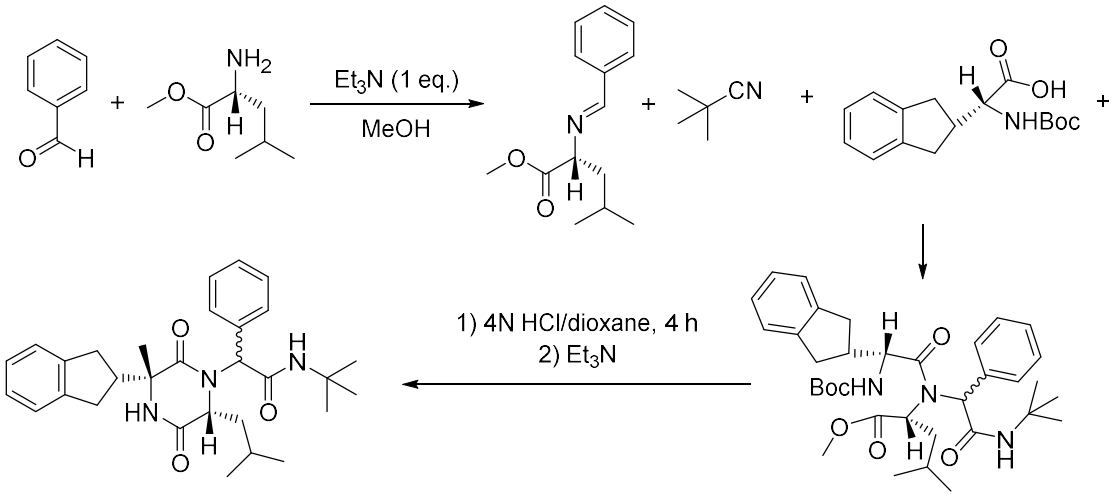

Scheme 2.3 – Example of Ugi-reaction type

The Ugi-type reaction approach has been used to synthesize pharmacological active DKP-containing compounds such as the Aplaviroc (Figure 2.19).[97d]

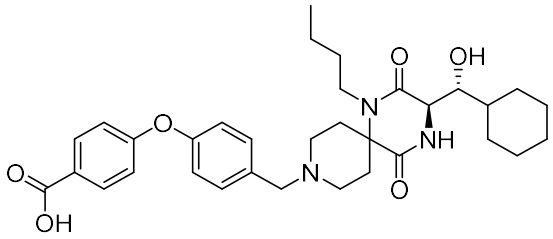

Figure 2.19 - Aplaviroc

A different protocol employs the Gly cyclic dipeptide as starting material for the synthesis of substituted DKPs in solution.[122a] A similar strategy allowed to generate olefin derivatives of *N*-acetylated DKPs with exocyclic double bonds,[128] as well as bis-epoxides. These molecules could serve as precursor to more complex DKPs.[129]

An innovating strategy envisages the use of microwaves to couple peptides intramolecularly thus obtaining the symmetrical DKP without epimerization in the α-position of the amino acids. An example of this application is depicted in Scheme 2.4 (synthesis of N^{α}-benzoyl-Arg(NO_2)-Leu-NH_2, a PAR-2 receptor antagonist): compared to conventional heating, the microwave synthesis produced the desired compounds in higher yields and shorter reaction times.[130] In this example a Gly residue was introduced at the C-terminal end of the pharmacophore and activated for auto-condensation thus obtaining a *cyclo*(Gly-Gly) DKP substituted on the nitrogen with the pharmacophore.

[128] Hayashi, Y.; Orisaka, S.; Tanaka, K.; Kanoh, K.; Kiso, Y., *J. Org. Chem.* **2000**, *65*, 8402-8405
[129] Ando, S.; Grote, A. L.; Koide, K., *J. Org. Chem.* **2011**, 1155-1158
[130] Santagada, V.; Fiorino, F.; Perissutti, E.; Severino, B.; Terracciano, S.; Cirino, G.; Caliendo, G., *Tetrahedron Letters* **2003**, *44*, 1145-1148

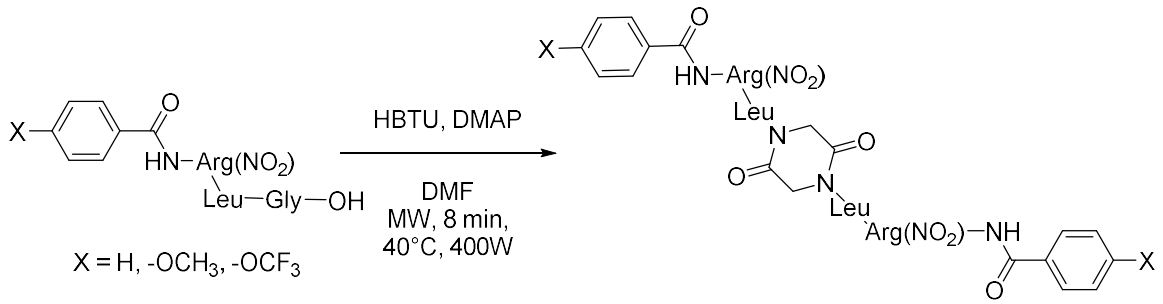

Scheme 2.4 – Synthesis of N^{α}-benzoyl-Arg(NO_2)-Leu-NH_2

However, symmetrical and unsymmetrical 2,5-DKPs can also be produced by a microwave-assisted stereoselective one-pot pathway starting from unprotected amino acids, through a phosphite-promoted one step coupling reaction (Scheme 2.5). Overall good yields, scalability (the reaction has been worked up simply by filtration through a pad of silica), and tolerance to several base-stable protecting groups have made this reaction an useful tool for DKPs synthesis.[131]

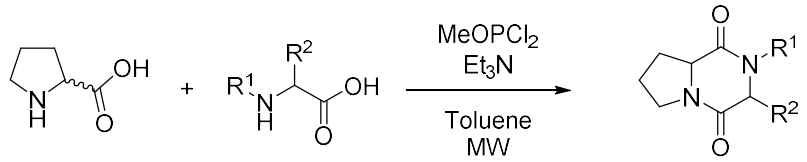

Scheme 2.5 – One-pot stereoselective microwave-assisted DKPs synthesis

Microwave irradiation has also been reported as a method to provide DKPs in excellent yields starting from the *N*-Boc-dipeptidyl-*tert*-butyl and -methyl esters through an aqueous *in situ* one-pot *N*-Boc-deprotection cyclization (Scheme 2.6).[132]

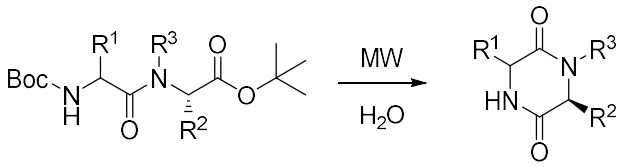

Scheme 2.6 – One-pot aqueous microwave-assisted DKPs synthesis

Phase-transfer catalysis has been suggested as another reliable method for the one-pot synthesis of symmetric 1,4-disubstituted-DKPs. The desired product is obtained through this strategy starting from a suitable amine and chloroacetyl chloride in presence of an aqueous base (example depicted in Scheme 2.7).[133]

[131] Jainta, M.; Nieger, M.; Bräse, S., *Eur. J. Org. Chem.* **2008**, 5418-5424
[132] Pérez-Picaso, L.; Escalante, J.; Olivo, H. F.; Rios, M. Y., *Molecules* **2009**, *14*, 2836-2849
[133] O'Reilly, E.; Pes, L.; Paradisi, F., *Tetrahedron Letters* **2010**, *51*, 1696-1697

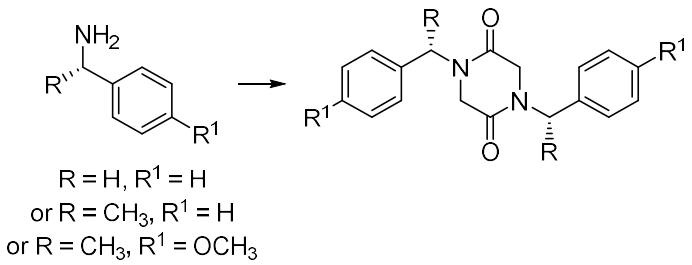

Scheme 2.7 – One-pot DKPs synthesis through phase-transfer catalysis

Another route that has to be mentioned is the *O,N*-acyl transfer, which is a valuable method for efficient synthesis of difficult peptide sequences with the advantage of allowing a racemization-free segment condensation. In this approach the first hindered amino acid, previously activated as ester, reacts with the free carboxylic acid of a second fragment. The generated mixed anhydride then undergoes spontaneous rearrangement and proceeds to the DKP product (Scheme 2.8). This approach is useful to produce oligomers and it was also employed in the synthesis of hexa- and pentasubstituted DKPs under mild conditions.[134]

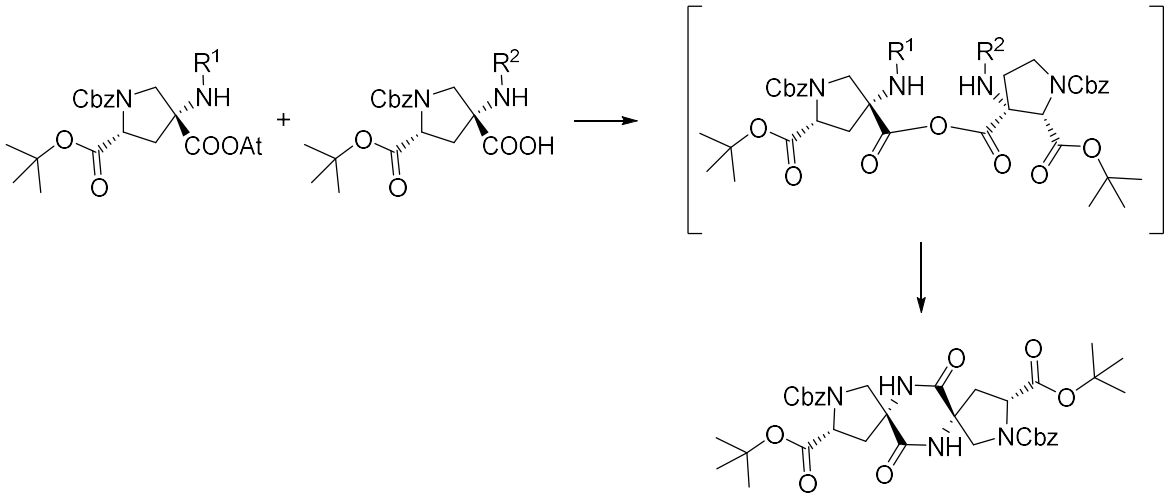

Scheme 2.8 – Synthesis of hexasubstituted DKPs *via O,N*-acyltransfer

The synthetic routes presented so far are solution-phase methods. These present the advantage of requiring a limited number of steps to produce the substituted DKPs. However, solid-phase synthesis has been mostly used to obtain these products. In solid phase synthesis resin type, PGs and cleavage systems can be varied thus allowing a wider spectrum of possibilities.

[134] Brown, Z. Z.; Schafmeister, C. E., *Org. Lett.* **2010**, *12*, 1436-1439

In scheme 2.9 a solid-phase protocol is depicted.[135] This synthetic route employs the phenacyl ester bond to attach the carboxylic amino acid terminal to the resin. The linear precursor is then obtained by Boc-deprotection and amino acid coupling of the second amino acid. The subsequent steps of deprotection, cleavage and cyclization are required to obtain the DKP. A side-chain PG is required because the bound resin-first amino acid is susceptible to nucleophilic attack.

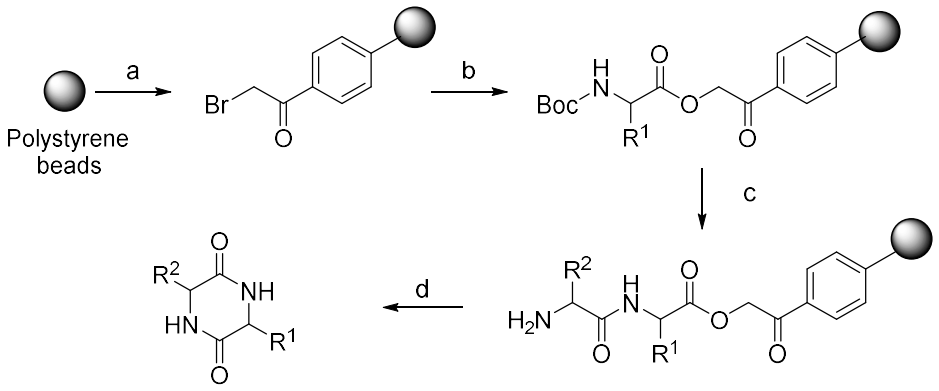

Scheme 2.9 – Generic protocol for the solid phase synthesis of DKPs

Reagent and conditions: a) $BrCH_2COBr$, $AlCl_3$, nitrobenzene/DCM (1:1); b) Boc-AA'-OH, Et_3N, DMF; c) 1) 3.5 N HCl/AcOH; 2) Boc-AA''-OH, HOBt, DCC, NMM, DMF; d) 1) 10% DIPEA/EtOAc; 2) 5% Et_3N/THF-H_2O (8:1).

To solve this problem, it has been suggested to attach the peptide to the resin *via* a safety-catch technique (Scheme 2.10). In this approach the stable resin-first AA bond is activated only after ending the peptide synthesis, allowing the cleavage and cyclization (usually a safety catch is an acyl sulfonamide that is easily hydrolyzed after methylation).

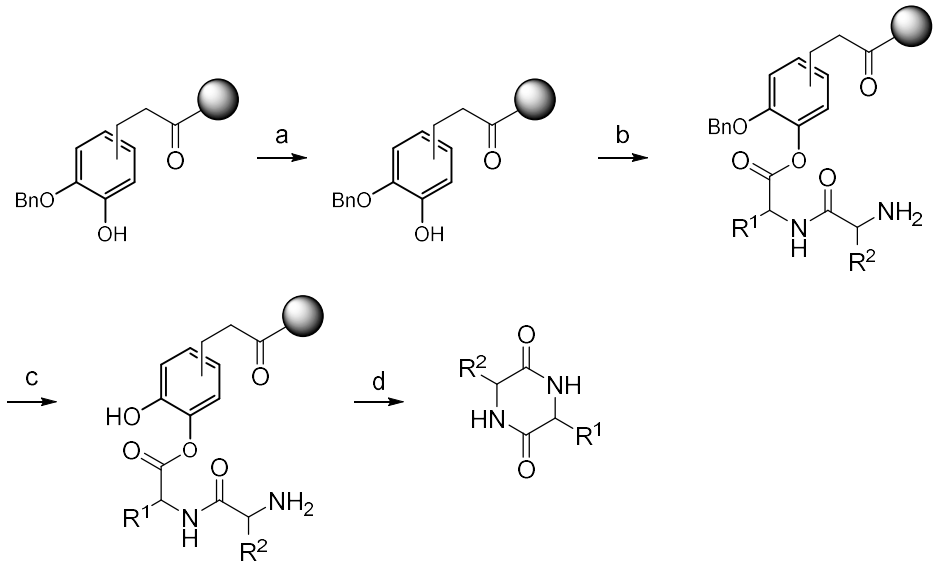

Scheme 2.10 – DKPs solid-phase synthesis by safety-catch approach

Reagents and conditions: a) Boc-AA'-OH, DIC, DIPEA; b) Boc-based solid-phase peptide synthesis; c) TFMSA, TFA; d) DIPEA.

[135] Wang, D.-X.; Liang, M.-T.; Tian, G.-J.; Lin, H.; Liu, H.-Q., *Tetrahedron Lett.* **2002**, *43*, 865-867

2.2.3.2 Synthesis via ester cyclization

This synthetic approach is widely used because it is effectively simple: dipeptide **2.15** is generated by the coupling between an α-amino acid protected at the amino group (**2.14**) and an a-amino ester (**2.13**). A large number of coupling reagents are suitable for that reaction. Lactamization of the resulting dipeptide **2.15** is spontaneous after deprotection of the terminal amine and generates the 2,5-DKP **2.16** (Scheme 2.11).[86]

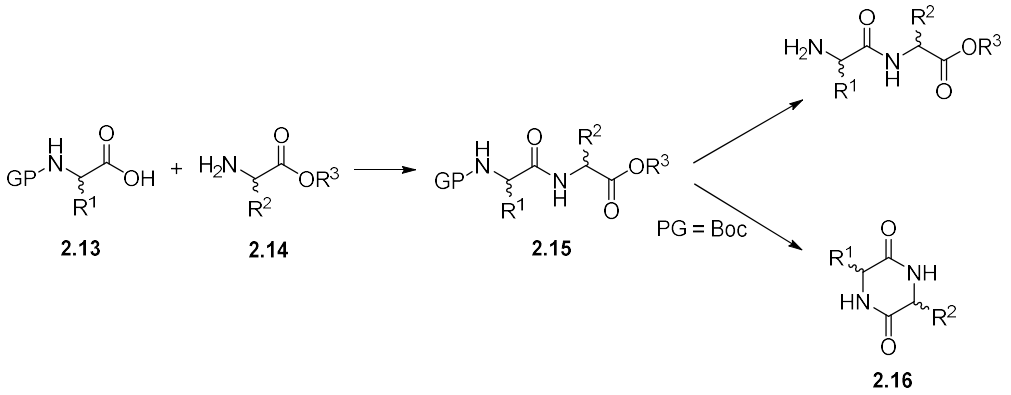

Scheme 2.11 - Dipeptide ester cyclization

The amide bond is known to be planar with a partial double bond character and in polypeptides it is generally present in the *trans*-conformation. *Trans*/*cis* isomerism activation barrier in the order of 15-20 kcal/mol) is relevant to DKP formation because the intramolecular attack of the amino group on the carboxylic group is possible only from a folded conformation containing a *cis* peptide bond. If the amide bond is not in *cis*-conformation (because of sterical hindrances or electronical interferences), the rate of cyclization is lower than when it is in a *cis*-conformation. When the cyclization is difficult, some expedients can be used (e.g., heating in acidic[136] or basic[137] medium, heating to reflux in high boiling solvents[138]) to improve the yield. Reactions conditions have to be carefully chosen to limit racemization.

Luthman et al. described a new general solution-phase synthesis using microwaves (heating for 10 min using water as solvent).[139] This new strategy is efficient, affording moderate to excellent yield (63%-97%), with no dependence on the amino acid sequence and no epimerization. Polysubstituted 2,5-piperazinedione derivatives[124a] and indolyl 2,5-DKP analogues[140] were synthesized directly by microwave irradiation of *N*-Boc dipeptide esters under solvent-free conditions in an efficient manner.

[136] Suzuki, K.; Sasaki, Y.; Endo, N.; Mihara, Y., *Chem. Pharm. Bull.* **1981**,*29*, 233
[137] Depew, K. M.; Marsden, S. P.; Zatorska, D.; Zatorski, A.; Bornmann, W.G.; Danishefsky, S. J., *J. Am. Chem. Soc.* **1999**, *121*, 11953-11963
[138] See, for instance: (a) Bull, S. D.; Davies, S. G.; Moss, W. O., *Tetrahedron: Asymmetry* **1998**, 9, 321-327; (b) Woodard, R. W., *J. Org. Chem.* **1985**, *50*, 4796-4799
[139] Tullberg, M.; Grotli, M.; Luthman, K., *Tetrahedron* **2006**, *62*, 7484-7491
[140] Pandey, S. K.; Awasthi, K. K.; Saxena, A. K., *Tetrahedron* **2001**, *57*, 4437-4442

2.2.3.3 Previous work in the group

Our research group has previously described the synthesis of a small library of bifunctional DKP scaffolds (Figure 2.20), formally derived from 2,3-diaminopropionic acid and aspartic acid or glutamic acid in the case of DKP8 (**2.23**, Figure 2.20).[65,120] These scaffolds could also be seen as formed by two β-amino acids (in particular a β^2- and a β^3-amino acids, following Seebach's nomenclature[141]). These DKPs, differing for the configuration of the two stereocenters and for the substitution at the endocyclic nitrogens, were synthesized using the ester cyclization pathway[86].[65] Depending on the relative configuration of the two stereocenters, the synthesized derivatives can be used as secondary structures inducers in linear or cyclic peptides.

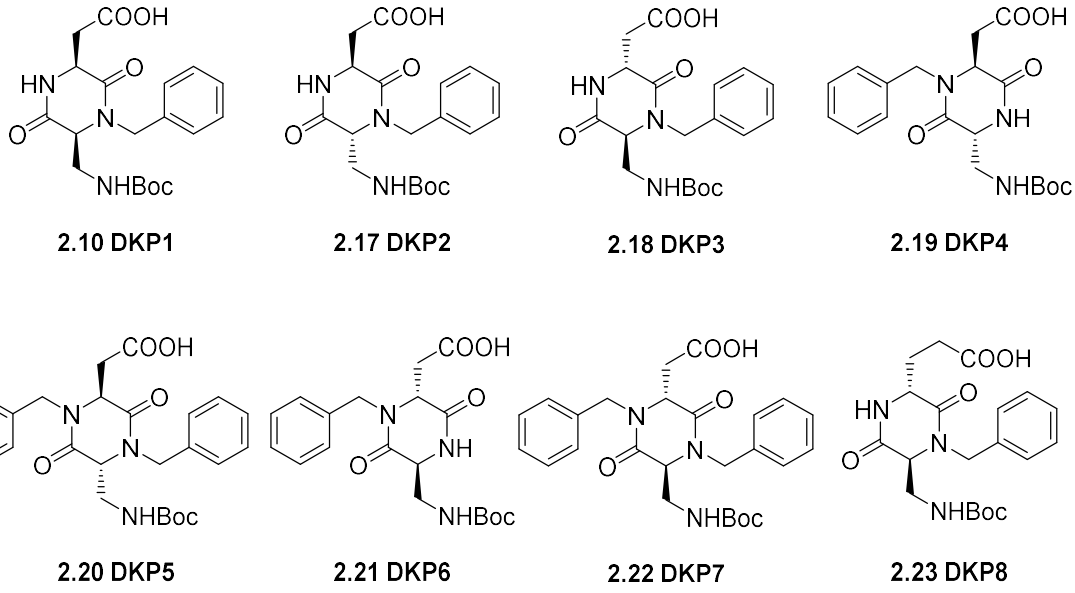

Figure 2.20 - DKPs library

For DKPs bearing a benzyl group at nitrogen N4 (DKP1 **2.10**, DKP2 **2.17** and DKP3 **2.18**) the serine ligation strategy (Scheme 2.12) was selected. Starting from either (*R*)- or (*S*)-Ser and (*S*)- or (*R*)-Asp, (*R*)- or (*S*)-*N*-benzylserine methyl ester **2.26** and (*R*)- or (*S*)-*N*-(*tert*-butoxycarbonyl)aspartic acid β-allyl ester **2.29** were easily prepared according to literature procedure[142]. The direct coupling of **2.26** and **2.29** generated the isopeptides **2.30** in high yield (72%). Among the various possibilities, the direct coupling of **2.26** and **2.29** was chosen in order to avoid the introduction of further protecting groups. After the Boc-deprotection of **2.30** and the cyclization, the introduction of the azide group was carried out through a Mitsunobu-type reaction. The azido derivative **2.32** was converted into the NHBoc-compound **2.33** in an one-pot Staudinger reduction-Boc protection followed by de-allylation (via a Pd(0) catalyzed Tsuji-Trost reaction) to give the final product **2.17** and

[141] The subscripted number after β specifies the position of the side chain on the corresponding β-amino acid, see: Hintermann, T.; Seebach, D., *Synlett* **1997**, 437-438

[142] For the benzyl-serine: Thompson, C. M.; Frick, J. A.; Green, D. L. C., *J. Org. Chem.* **1990**, *55*, 111-116; for he β-allyl ester: Webster, K. L.; Maude, A. B.; O'Donnell, M. E.; Mehrotra, A. P.; Gani, D., *J. Chem. Soc., Perkin Trans. 1* **2001**, 1673-1695

2.18. With the same procedure, allyl deprotection was performed directly on the azido derivative **2.32** to obtain the final scaffold **2.34** and **2.35** necessary for the Fmoc-SPPS, which does not allow the use of Boc-derivatives.

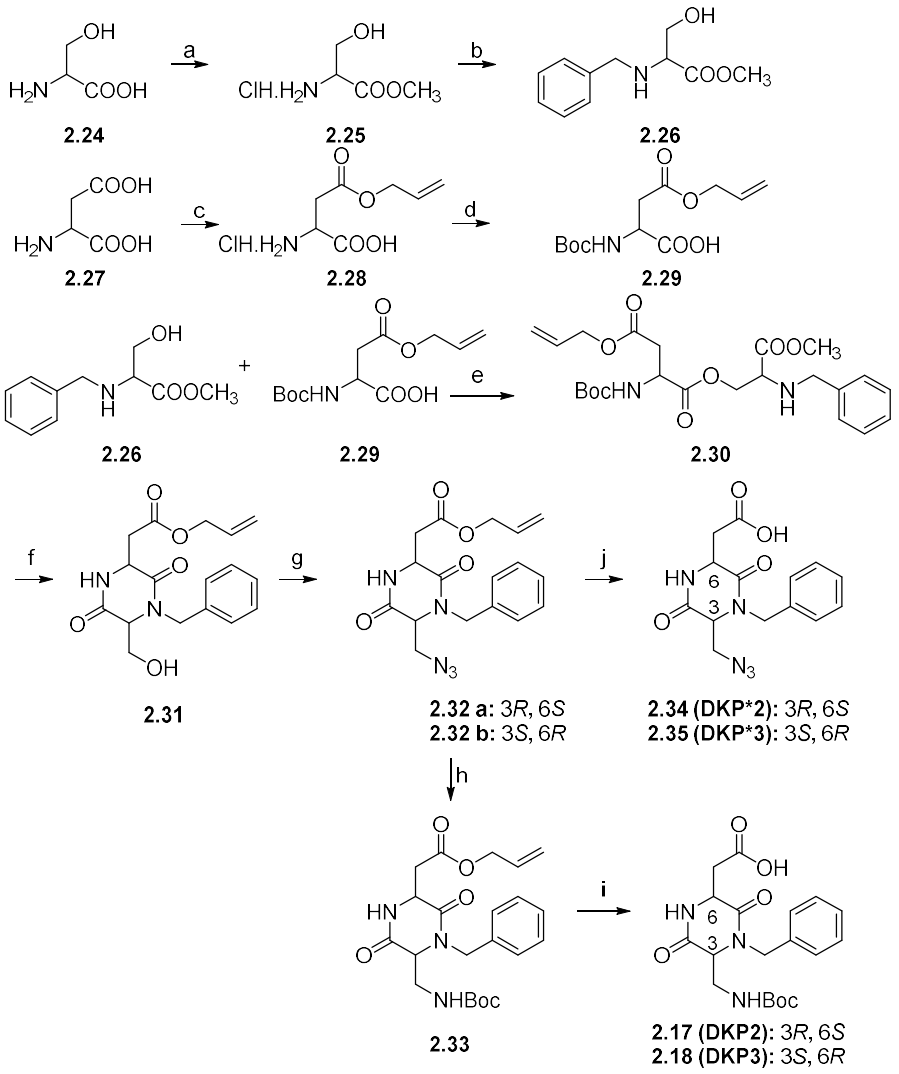

Scheme 2.12 - Synthesis of DKP1, DKP2/DKP*2 and DKP3/DKP*3

Reagents and conditions: a) CH_3COOH, CH_3OH, reflux; b) Et_3N, PhCHO, then $NaBH_4$, under N_2; c) CH_3COCl, Allyl alcohol, reflux; d) Et_3N, Boc_2O, 1:1 H_2O/THF, r.t.; e) EDC, DMAP cat., DCM, 0°C to r.t., under N_2; f) 1) TFA/DCM, 1:1; 2) DIPEA, *i*PrOH, r.t.; g) PPh_3, DIAD, H_3N.tol, -20°C, under N_2; h) PPh_3, BOC-ON, THF, -20°C to r.t., under N_2; i) $[Pd(PPh_3)_4]$, PPh_3, pyrrolidine, DCM, 0°C, under N_2; j) $[Pd(PPh_3)_4]$, PPh_3, pyrrolidine, DCM, 0°C, under N_2.

Isopetide **2.30** was detected instead of the expected dipeptide **2.36** the synthesis. The mechanism of this isopeptide formation was deeply studied in our research group (Scheme 2.13).[143] NMR spectra were measured (Figure 2.21) and confirmed the mechanism via *O*,*N*-acyl transfer[144] ("depsipepeptide technique"[145] or "*O*-acyl isopeptide methodology"[146]). The peptidic sequence is extended via functionalization of the β-hydroxy group of an *N*-protected Ser or Thr residue and the native peptide is restored after the final coupling and Ser/Thr deprotection thanks to the *O*,*N*-acyl transfer. As a matter of fact, selective *O*-acylation of the unprotected β-hydroxyl group of *N*-benzylserine methyl ester is preferred over the formation of the tertiary amide and the resulting ester bond is stable in solution to *O*,*N*-acyl transfer. Boc cleavage and base treatment trigger the *O*,*N*-acyl migration and promote the simultaneous cyclization.

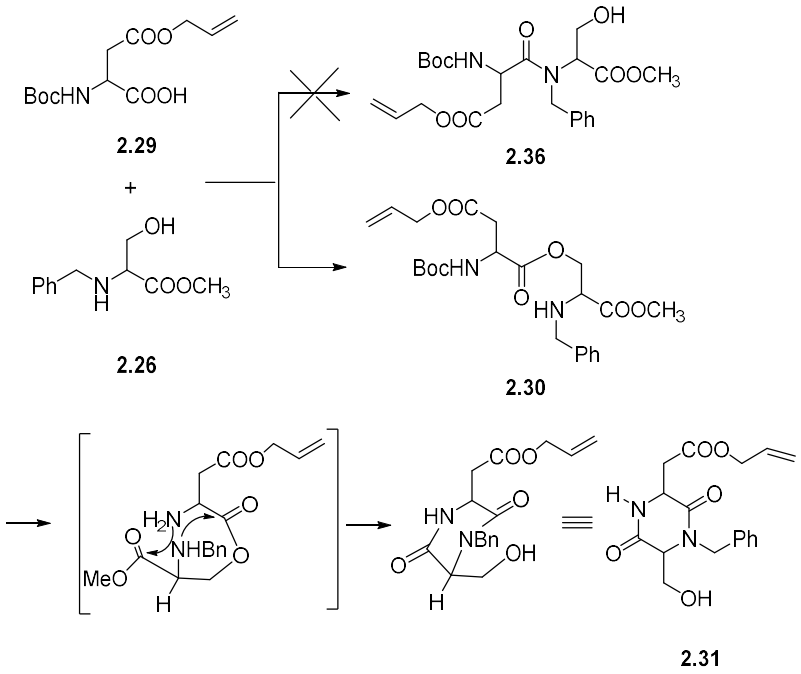

Scheme 2.13 – Isopeptide formation mechanism

[143] Marchini, M.; Mingozzi, M.; Colombo, R.; Gennari, C.; Durini, M.; Piarulli, U., *Tetrahedron* **2010**, *66*, 9528-9531
[144] Coin, I., *J. Pept. Sci.* **2010**, *16*, 223-230
[145] Carpino, L. A.; Krause, E.; Sferdean, C. D.; Schumann, M.; Fabian, H.; Bienert, M.; Beyermann, M., *Tetrahedron Lett.* **2004**, *45*, 7519-7523
[146] (a) Mutter, M.; Chandravarkar, A.; Boyat, C.; Lopez, J.; Dos Santos, S.; Mandal, B.; Mimna, R.; Murat, K.; Patiny, L.; Saucede, L.; Tuchscherer, G., *Angew. Chem. Int. Ed.* **2004**, *43*, 4172-4178; (b) Sohma, Y.; Sasaki, M.; Hayashi, Y.; Kimura, T.; Kiso, Y., *Chem. Commun.* **2004**, 124-125; (c) Kiewitz, S. D.; Kakizawa, T.; Kiso, Y.; Cabrele, C., *J. Pept. Sci.* **2008**, *14*, 1209-1215

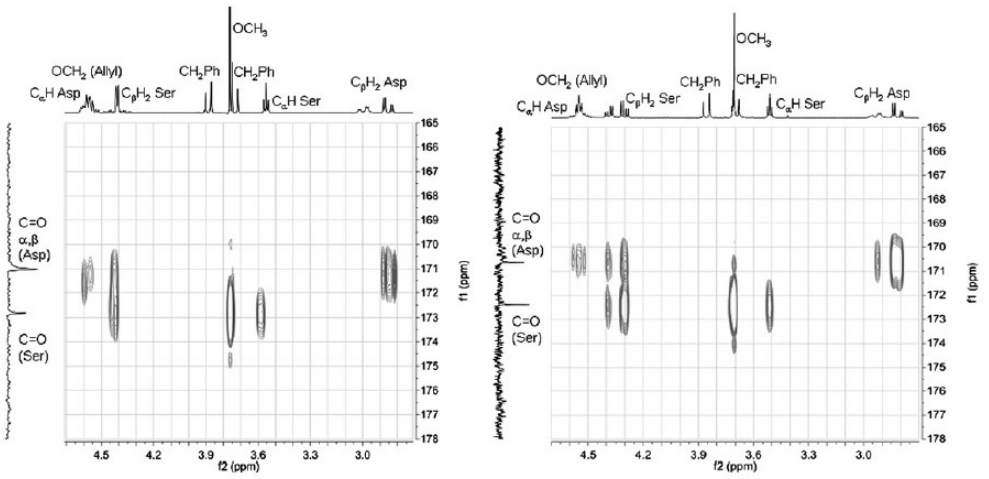

Figure 2.21 - NMR spectra of isopetides **2.30** (on the right isopeptide of *cis*-scaffold and on the left isopeptide of *trans*-scaffold)

The conversion of compound **2.31** into **2.32** was successfully achieved through a Mitsunobu reaction (Scheme 2.14). In the case of our DKPs, this resulted in a crucial reaction since the C6 acid proton could be easily extracted and then the activated hydroxyl functionality could undergo β-elimination before reacting with the hydrazoic acid (which acts as nucleophile). The β-elimination was particularly competitive in the case of the *cis*-derivative, which also required a more complex purification than the *trans* derivatives.

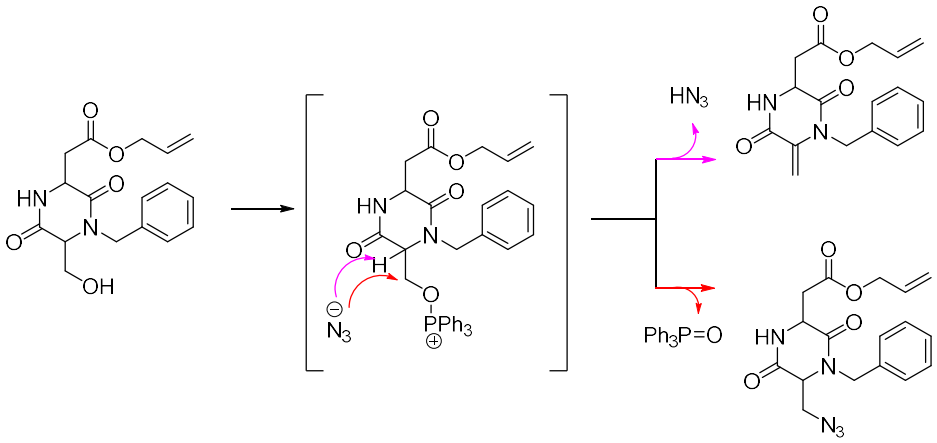

Scheme 2.14 – Mitsunobu-type reaction, mechanism

The following step (the conversion of **2.32** into **2.33**) involved a one-pot Staudinger-Boc protection. The mechanism is reported in Scheme 2.15: the azide reacts with a phosphine to generate phosphazide which then looses N_2 forming an iminophosphorane. In a classical Staudinger reaction, the hydrolysis of this last intermediate leads to the amine and the very stable phosphine oxide. However in this one-pot Staudinger-Boc protection, the iminophosphorane reacts directly with 2-(tert-butoxycarbonyloxyimino)-2-

phenylacetonitrile (Boc-ON) affording the desired Boc-protected amine in very good yield.

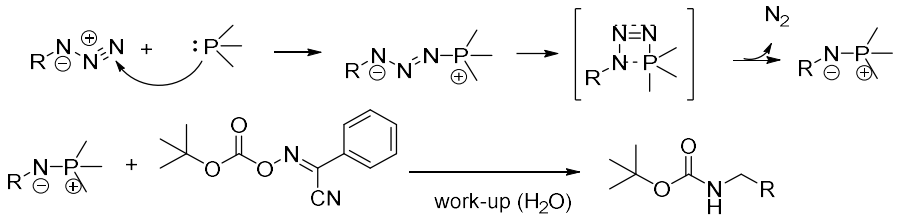

Scheme 2.15 – One-pot Staudinger-Boc protection reaction

The final deallylation on **2.32** or on **2.33** was performed in the presence of a catalytic amount of *Palladium tetrakis(triphenylphosphine)*, [$Pd(PPh_3)_4$], and pyrrolidine as nucleophile (which is necessary as allyl scavenger). Such methodology is of special interest for peptide synthesis because the deprotection conditions are usually mild enough to be compatible with the presence of labile *t*Bu and Boc protections.[147] The final amino acid derivatives have been obtained in good yields. The mechanism of this reaction is reported in Scheme 2.16.

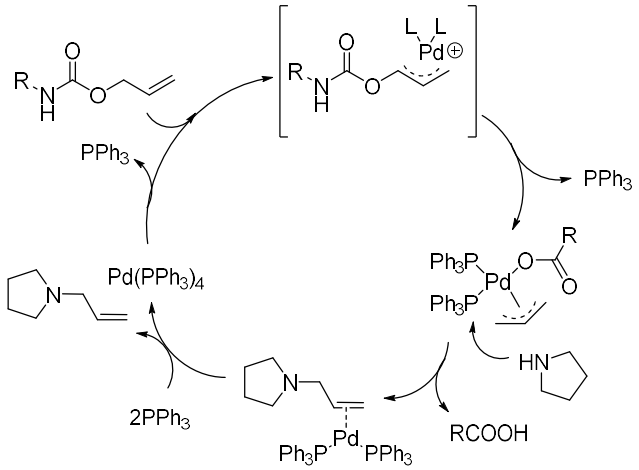

Scheme 2.16 – Deallylation mechanism

For DKPs benzylated on N4 (Figure 2.1 for numbering; **2.19** and **2.21**), a different synthetic pathway was developed (Scheme 2.17).[65b] The synthesis was accomplished starting from L- or D- Ser and D- or L-Asp. The aspartate residue was protected on both carboxylic groups as methyl ester and then coupled to the Boc-Ser-N_3 moiety, which was previously activated as symmetric anhydride. Notably, the Mitsunobu reaction was directly performed on the Boc-Ser-*O*-Mehydroxyl group, thus deleting the problem of β-elimination, avoiding the use of a further PG and allowing a scale-up of the synthesis. The coupling step (80% yield) has been followed by Boc-deprotection and cyclization (yield almost

[147] David, C.; Bischoff, L.; Meudal, H.; Mothé, A.; De Mota, N.; Da Nascimento, S.; Lorens-Cortes, C.; Fournié-Zaluski, M.-C.; Roques, B. P., *J. Med. Chem.* **1999**, *42*, 5197-5211

quantitative). The azide was then catalytically reduced and Boc protected. The methyl ester hydrolysis finally afforded the desired products.

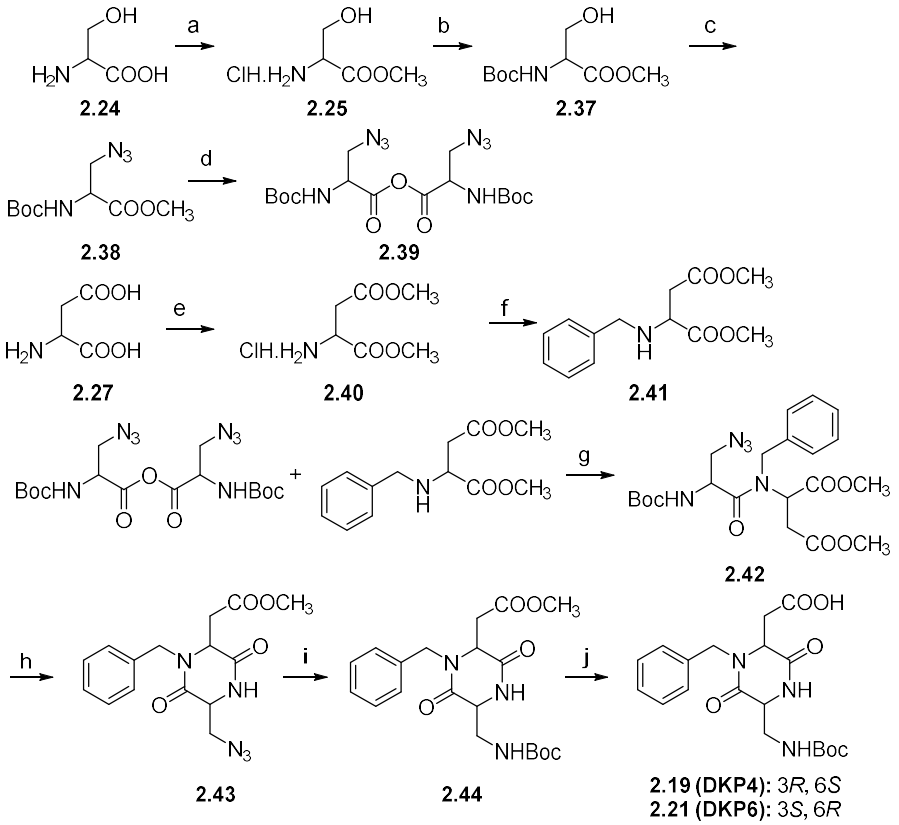

Scheme 2.17 – DKP4 and DKP6 synthesis

Reagents and conditions: a) CH_3COCl, CH_3OH, reflux; b) Boc_2O, H_2O/THF 1.1, r.t.; c) HN_3, DIAD, PPh_3, THF, -20°C, under N_2 d) 1) LiOH, H_2O/THF 1:1;2) DCC, DCM; e) CH_3COCl, MeOH, reflux; f) PhCHO, Et_3N, $NaBH(AcO)_3$, r.t, under N_2; g) DCC, rt; h) 1) TFA/DCM 1:2, Et_2SiH, r.t.; 2) DIPEA, *i*PrOH, r.t.; i) 1) H_2, Pd/C (10%), THF, r.t.;2) Boc_2O, THF, r.t.; j) LiOH, H_2O/THF 1:1, r.t..

For solid phase purposes with a Fmoc strategy the Boc-derivatives are not suitable, so a small library of azido-acid DKPs (DKPs*) was synthesized (Figure 2.22).[67,68]

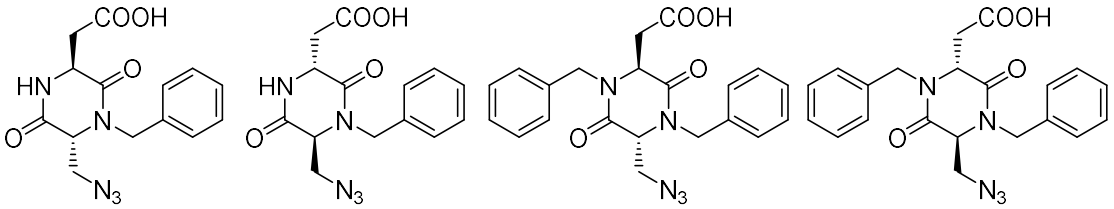

2.34 DKP*2 **2.35 DKP*3** **2.45 DKP*5** **2.46 DKP*7**

Figure 2.22 – DKP* library

The synthesis of scaffolds the **2.45** and **2.47** (as well as the synthesis of **2.20** and **2.22**) could be in principle performed starting from the benzylation of the second DKP nitrogen of the azide-intermediate in the synthesis of either DKP2 and DKP4 or, DKP3 and DKP6 respectively (Scheme 2.18). This strategy avoided the use of further protecting groups since the azide is stable in the reaction conditions thus behaving as PG.

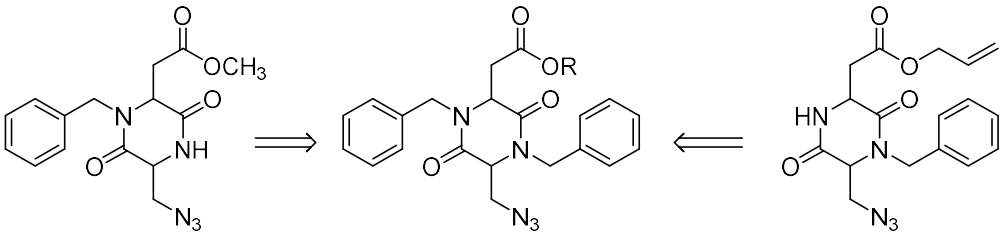

Scheme 2.18 – Possible retrosynthesis for DKP5 and DKP7

A previous synthesis performed in our group started from **2.43** (Scheme 2.19).[65b] The final compounds were obtained by deprotonation of the azido esters with KHMDS (which prevent elimination being an hindered base) followed by alkylation with benzyl bromide keeping the temperature between -70°C and -40°C. Conversion into the –NHBoc derivative and deprotection of the carboxylic acid were performed with the same procedure used for DKP4 and DKP6.

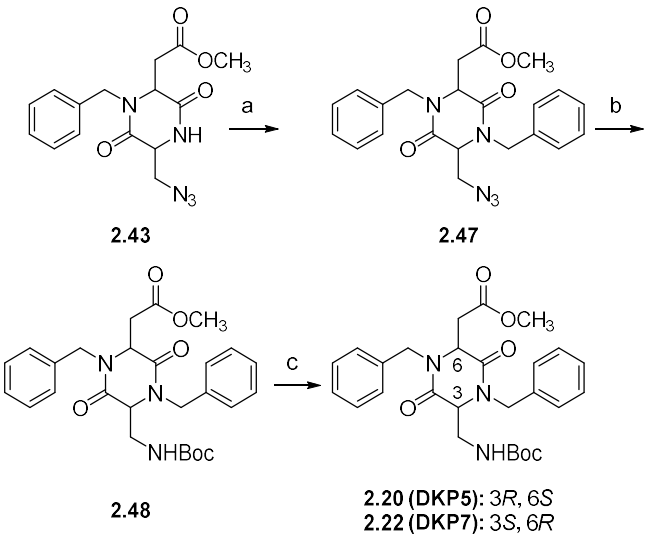

Scheme 2.19 – DKP5 and DKP7 synthesis starting from DKP4 and DKP6

Reagents and conditions: a) KHMDS, BnBr, THF/DMF 7:3, -70°C to -40°C, under N_2; b) PPh_3, Boc-ON, tol, -20°C to r.t., under N_2; c) LiOH, H_2O/THF 1:1, r.t..

In a subsequent synthetic approach, compounds **2.32**, intermediates in the synthesis of **2.34** and **2.35**, respectively, were used as starting materials for the preparation of **2.45** and **2.46** (Scheme 2.20).[68] Also in this case, the azido esters were synthesized with the same reactions used for derivatives DKP5 and DKP7 (Scheme 2.20). The only difference is in the last deprotection step since an allyl ester is present as PG in the carboxylic acid instead of a methylester. As a consequence, deprotection was accomplished by treatment with [$Pd(PPh_3)_4$] and *N*-methyl aniline.

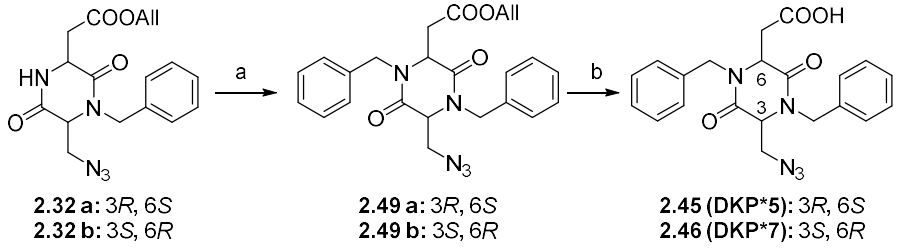

Scheme 2.20 – DKP5 and DKP7 synthesis

Reagents and conditions: a) KHMDS, BnBr, THF/DMF 7:3, -70°C to -40°C, under N_2; b) [$Pd(PPh_3)_4$], PPh_3, *N*-methyl aniline, DCM, under N_2,0°C to r.t., 1h (70%).

DPK8 (**2.23**, Figure 2.20) was synthesized using a mixed procedure starting from (*S*)-Ser and (*R*)-glutamic acid γ-methyl ester (Scheme 2.21).[65b] The synthetic pathway of DKP1-2-3 was followed to synthesize the –NHBoc methyl ester **2.50**, which was then deprotected as DKP4 and DKP6.

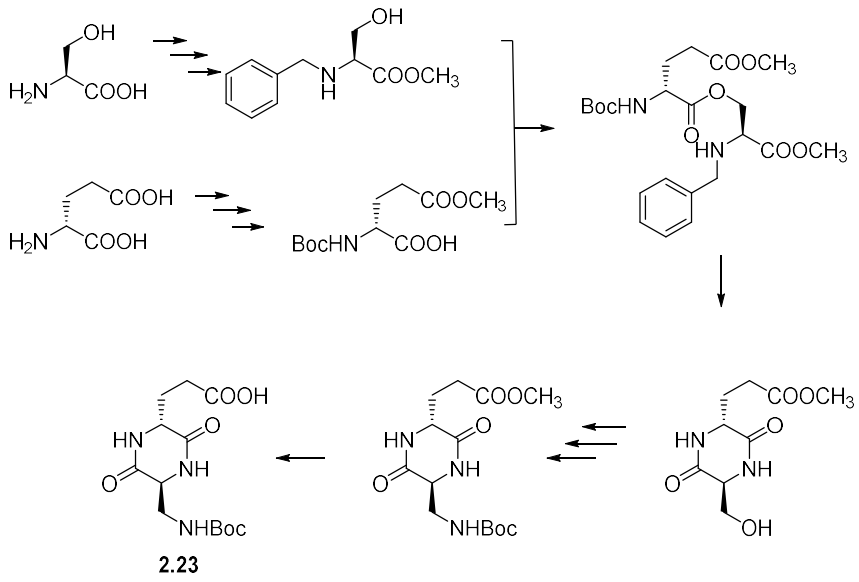

2.23

Scheme 2.21 – DKP8 (**2.23**) synthesis

In order to prepare cyclic RGD-peptidomimetics to be used in drug targeting, after conjugation with different payloads (e.g., cytotoxic agents[148], VEGFR ligands[149] and nanoparticles, see Chapter 3), four functionalized DKPs (DKP*f*) bearing a *p*-aminomethylenbenzyl substituent on N1 or N4 were synthesized as both stereoisomers at C3 and C6, namely: 3*R*,6*S* and 3*S*,6*R*[148] *Trans*-monobenzylated scaffolds were selected according to the binding data collected on unconjugated *Cyclo*[DKP-RGD] peptidomimetics (see paragraph 2.3). The selected linker for the DKP*f* bears two different functionalities: an aldehyde (for successive reductive amination) and an amino group (as moiety for the conjugation).

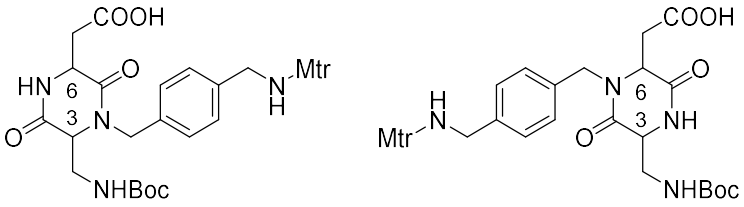

2.51 DKP*f*2: 3*R*, 6*S*
2.52 DKP*f*3: 3*S*, 6*R*

2.53 DKPf4: 3*R*, 6*S*
2.54 DKP6: 3*S*, 6*R*

Figure 2.23 – DKP*f* library

[148] Colombo, R.; Mingozzi, M.; Belvisi, L.; Arosio, D.; Piarulli, U.; Carenini, N.; Perego, P.; Zaffaroni, N.; De Cesare, M.; Castiglioni, V.; Scanziani, E.; Gennari, C., *J. Med. Chem.* **2012**, *55*, 10460−10474

[149] Zanella, S.; Mingozzi, M.; Dal Corso, A.; Fanelli, R.; Arosio, D.; Cosentino, M.; Schembri, L.; Marino, F.; De Zotti, M.; Formaggio, F.; Pignataro, L.; Belvisi, L.; Piarulli, U.; Gennari, C., *ChemistryOpen* **2015**, *4*, 633-641

The synthetic pathway depicted in Scheme 2.22 refers to DKP*f*2 (**2.51**) and DKP*f*3 (**2.52**) and was developed following the same approach of the unfunctionalized scaffolds. The only difference was the aldehyde used in the reductive amination step which bore the linker with the $–NH_2$ moiety suitable for further functionalization. According to the applications for which was developed the scaffold, Mtr was selected as PG on the amine functionality on the aldehyde. The overall yield (60%) is high and, thanks to the small number of chromatographic purifications, it is a suitable route for multi-gram scale synthesis.

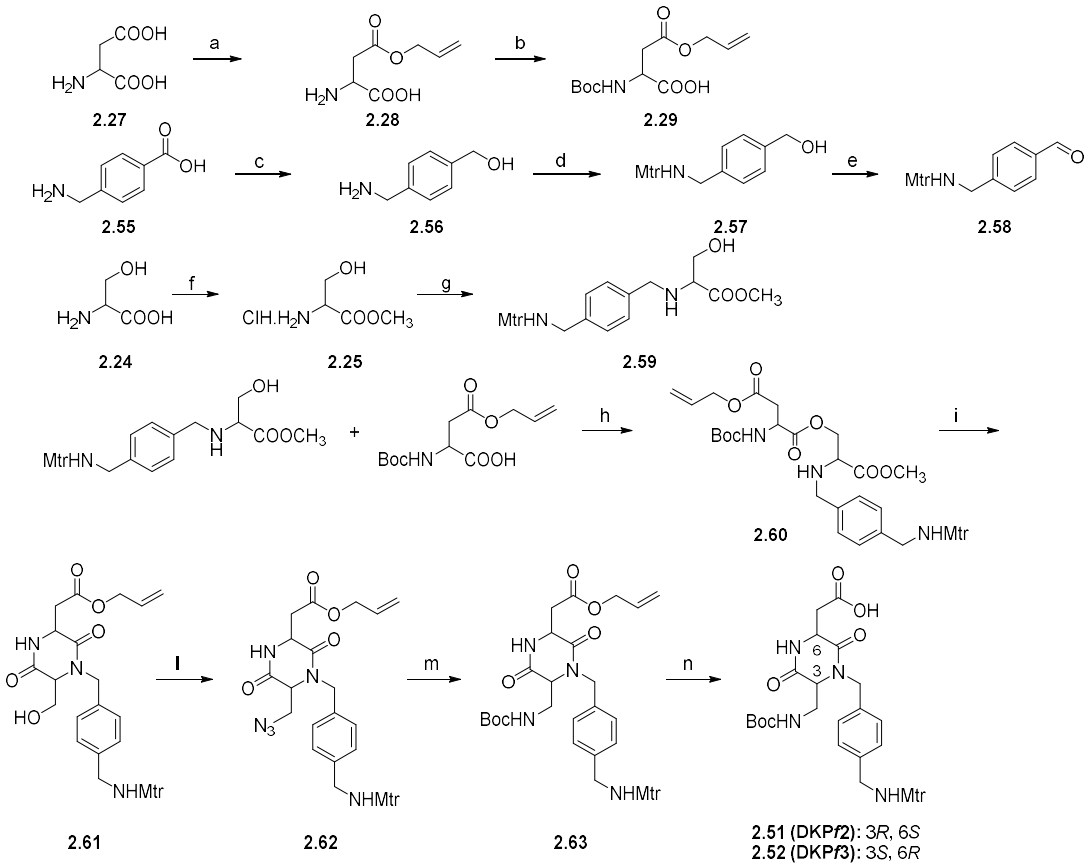

Scheme 2.22 – DKP*f*2 and DKP*f*3 synthesis

Reagents and conditions: a) CH_3COCl, Allyl alcohol, reflux; b) Boc_2O, TEA, dioxane/water 1:1, r.t.; c) $LiAlH_4$, dry THF, reflux, under N_2; d) Mtr-Cl, DIPEA, THF, r.t.; e) MnO_2, THF, r.t.; f) CH_3COCl, MeOH, reflux; g) (**2.58**), $NaBH(OAc)_3$, Et_3N, MeOH, r.t.; h) HATU, HOAt, DIPEA, DMF, 0°C to r.t.; i) 1) TFA/DCM (1:2), 0°C to rt 2) DIPEA, *i*PrOH, DMF, r.t., under N_2; l) H_3N in toluene, DIAD, Ph_3P, DCM/toluene 1:3, -20°C, under N_2; m) Me_3P, Boc-ON, THF, -20°C to rt; n) pyrrolidine, Ph_3P, $[Pd(Ph_3P)_4]$, DCM, r.t..

Also DKP*f*4 (**2.53**) and DKP*f*6 (**2.54**) were prepared following a synthetic pathway patterned after the corresponding DKP4/DKP6 synthetic route (Scheme 2.23)[65b,67,68] As for **2.51** and **2.52**, the aldehyde **2.58** was used instead of the benzyl aldehyde in the reductive amination to give the isopeptide **2.65**.

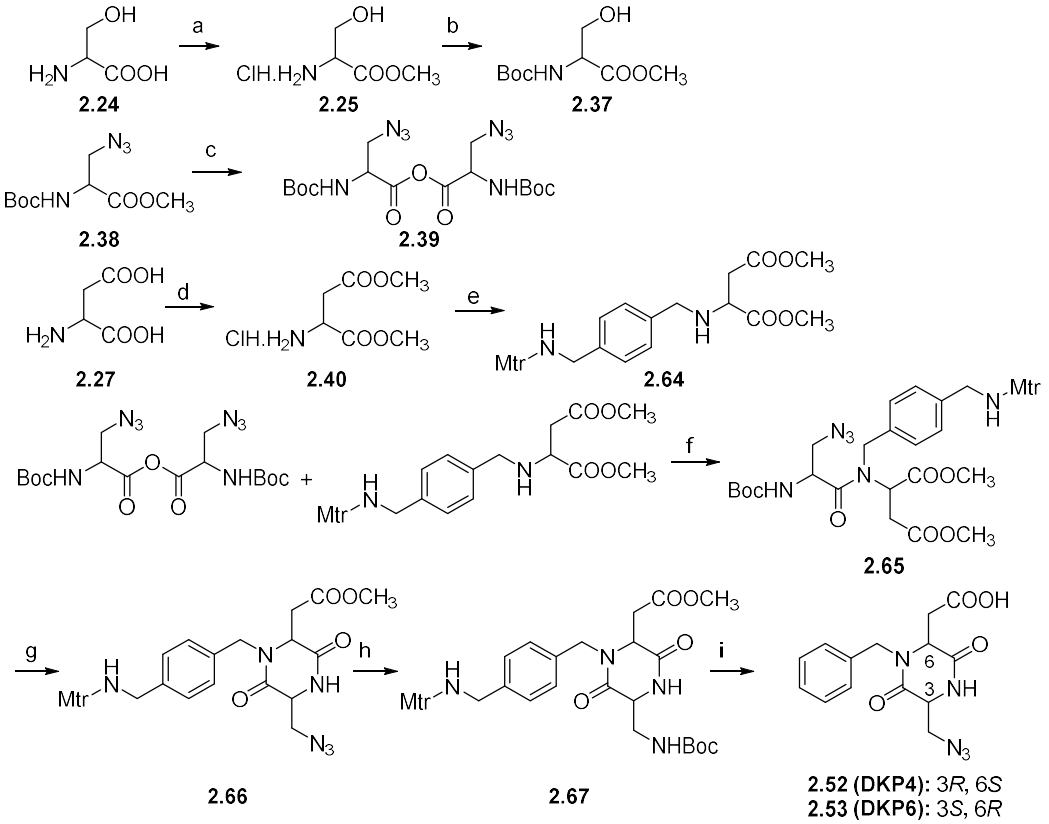

Scheme 2.23 – DKPf4 and DKPf6 synthesis

Reagents and conditions: a) CH_3COCl, MeOH, reflux; b) Boc_2O, TEA, dioxane-water, r.t.; c) HN_3.tol, DIAD, Ph_3P, dry THF -20 °C, under N_2; d) 1)LiOH, H_2O/THF 1:1, 0°C; 2) DCC, DCM, r.t., e) CH_3COCl, MeOH, reflux; f) **2.58**, $NaBH_3(CN)$, MeOH, r.t.; g) DCM, r.t.; h) 1) TFA, Et_3SiH, DCM, r.t.; 2) DIPEA, *i*PrOH, r.t.; i) 1) H_2, 10% Pd/C, THF, r.t.; 2) Boc_2O, DIPEA, DCM, r.t. i) LiOH, H_2O/THF 1:1, 0°C.

2.3 DKP integrin ligands

As already presented in Chapter 1, several RGD- and *iso*DGR integrin ligands have been synthesized and tested. Thanks to their conformational properties, DKPs are suitable scaffolds to build peptidomimetics with different conformational properties.

2.3.1 *Cyclo*[DKP-RGD] integrin ligands

The RGD sequence is a recognition motif for integrins widely used in peptidomimetics active as ligands for these receptors. The DKPs library synthesized in our group was then used for the synthesis of cyclic RGD-peptidomimetics (Figure 2.24).[65]

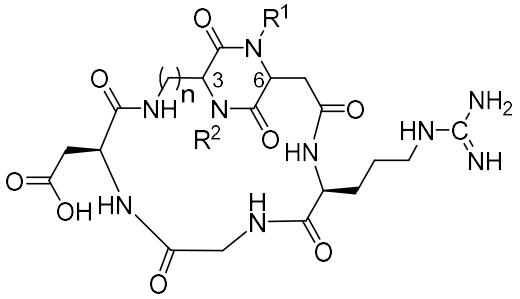

2.68 *Cyclo*[DKP1-RGD]: 3*S*, 6*S*; R^1=H, R^2=Bn, n =1
2.69 *Cyclo*[DKP2-RGD]: 3*R*, 6*S*; R^1=H, R^2=Bn, n =1
2.70 *Cyclo*[DKP3-RGD]: 3*S*, 6*R*; R^1=H, R^2=Bn, n =1
2.71 *Cyclo*[DKP4-RGD]: 3*R*, 6*S*; R^1=Bn, R^2=H, n =1
2.72 *Cyclo*[DKP5-RGD]: 3*R*, 6*S*; R^1=Bn, R^2=Bn, n =1
2.73 *Cyclo*[DKP6-RGD]: 3S, 6*R*; R^1=Bn, R^2=H, n =1
2.74 a *Cyclo*[DKP7-RGD]: 3*S*, 6*R*; R^1=Bn, R^2=Bn, n =1
2.74 b *Cyclo*[DKP7-RGD]: 3*S*, 6*R*; R^1=Bn, R^2=Bn, n =1
2.75 *Cyclo*[DKP-8-RGD]: 3*R*, 6*S*; R^1=H, R^2=Bn n =2

Figure 2.24 - Library of *Cyclo*[RGD-DKP] integrin ligands

2.3.1.1 Synthesis

A solution phase synthesis with Boc-protecting group strategy was adopted for the synthesis of the *Cyclo*[DKP-RGD] integrin ligands library (Scheme 2.24).[65b] The synthesis was accomplished starting from Boc-Arg(Mtr), Gly-OBn and Cbz-Asp(O*t*Bu)-OH. Each step consisted on the Boc- deprotection of the first moiety and the coupling to the second one, previously activated at the carboxylic acid group. Once the linear peptidomimetics Cbz-Asp(OtBu)-DKP-Arg(Mtr)-Gly-OBn (**2.76**) was obtained, it was deprotected by hydrogenolysis (Cbz and Bn). The linear deprotected derivative (**2.77**) was subjected to macrolactamization. Several methodologies were screened for the ring closure and the best yields were obtained by the literature procedure reported[61a,150] in Scheme 2.24. A final side-chain deprotection afforded the desired compounds that were purified by preparative HPLC.

[150] Luo, J.-M.; Dai, C.-F.; Lin, S.-Y.; Huang, P.-Q., *Chem. Asian. J.* **2009**, *4*, 328-335

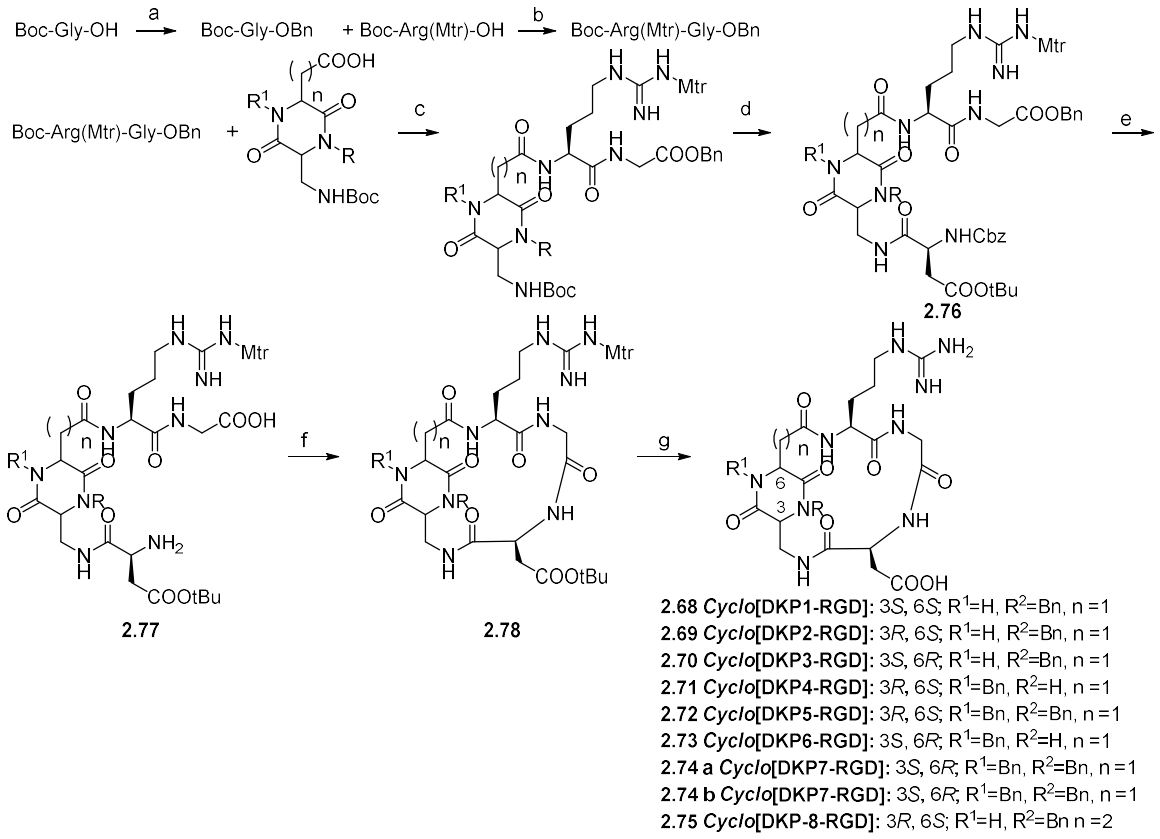

Scheme 2.24 - *Cyclo*[DKPs-RGD] ligands synthesis

Reagents and conditions: a) 1) $CsCO_3$, MeOH; 2) BnBr, DMF; b) 1) TFA/DCM 1:2; 2) HATU, HOAt, DIPEA, DMF, 0°C to r.t., under N_2; c) 1) TFA/DCM 1:2; 2) HATU, HOAt, DIPEA, DMF, 0°C to r.t., under N_2; d) 1) TFA/DCM 1:2; 2)Cbz-Asp(O*t*Bu)-OH, HATU, HOAt, DIPEA, DMF, 0°C to r.t., under N_2 e) 1) TFA/DCM 1:2; 2) H_2, Pd/C, THF/H_2O 1:1, r.t.; f) HATU, HOAt, DIPEA, DMF, 0°C to r.t., under N_2; g) TFA/thianisole/ethanedithiol/anisole 90:5:3:2.

Cyclic derivatives **2.72** and **2.74** containing the dibenzylated DKPs (DKP5 and DKP7) can exist as two different separable conformers (planar chirality) due to hindered rotation of one ring around the other. In the case of derivative **2.72** containing the DKP5 scaffold, only one diastereomer formed (either because it was formed exclusively/predominantly and the minor one was not detected/isolated). On the contrary, in the case of derivative **2.74**, containing DKP7, two diastereomers were detected. The two diastereomers were formed in the macrolactamization step, and, after side-chain deprotection, they could be separated, analyzed and tested separately (integrin affinity).

2.3.1.2 Biological evaluation

The library was examined *in vitro* for the ability to inhibit biotinylated vitronectin binding to the purified $\alpha_V\beta_3$ and $\alpha_V\beta_5$ receptors.[65] The *cis*-derivative (*Cyclo*[DKP-1-RGD] **2.68**) showed IC_{50} in a range of micromolar concentration, while *trans*-derivatives **2.69**-**2.75** ranged from submicro- to subnanomolar concentrations (Table 2.1), very similar to each other.

Structure	Compound number	$\alpha v\beta_3$ IC_{50} [nM]	$\alpha v\beta_5$ IC_{50} [nM]
***Cyclo*[DKP1-RGD]**	**2.68**	3898±418	$>10^4$
***Cyclo*[DKP2-RGD]**	**2.69**	3.2±2.7	114±99
***Cyclo*[DKP3-RGD]**	**2.70**	4.5±1.1	149±25
***Cyclo*[DKP4-RGD]**	**2.71**	7.6±4.3	216±5
***Cyclo*[DKP5-RGD]**	**2.72**	12.2±5.0	131±29
***Cyclo*[DKP6-RGD]**	**2.73**	2.1±0.6	79±3
***Cyclo*[DKP7-RGD]-major**	**2.74 a**	220.2±82.3	$>10^4$
***Cyclo*[DKP7-RGD]-minor**	**2.74 b**	0.2±0.09	109±15
Cyclo[DKP8-RGD]	**2.75**	7.5±0.6	$>10^3$
c(RGDfV)	/	3.2±1.3	7.5±4.8
ST1646	/	1.0±0.5	1.4±0.8

Table 2.1 – Inhibition of biotinylated vitronectin binding to $\alpha v\beta_3$ and $\alpha v\beta_5$ receptors

IC_{50} values were calculated as the concentration of compound required for 50% inhibition of biotinylated vitronectin binding as estimated by GraphPad Prism software; all values are the arithmetic mean ± SD of triplicate determination.

Moreover, the *trans*-compounds (except for **2.74 a**) showed a higher selectivity compared to the reference compounds. Interestingly, the behavior of **2.74 a** is peculiar taking into account that the diastereoisomer (**2.74 b**) is the most potent ligand if the series.

2.3.1.3 NMR characterization and conformational studies

^{1}H-NMR studies (in particular chemical shift dependence on temperature and concentration to detect intramolecular hydrogen bonds, as well as NOESY to investigate both sequential and long-range contacts),computational studies (MC/SD simulations[151], by using the implicit water GB/SA solvation model[152] and the OPLS_2001 force field[153]), and docking studies (starting from the representative conformations obtained from the MC/SD simulations) were performed with the aim of rationalizing the affinity of these compounds for the $\alpha v\beta_3$ receptor at a molecular level. Among the data collected, the ones regarding **2.70** will be deeply considered as this compound has been further investigated. This ligand is apparently characterized by conformational mobility, with a similarity to **2.68** for what concerns the NMR data and, consequently, of the detected conformation. Since these two ligands contain DKPs scaffolds with opposite configuration which should impart a different stereochemical orientation to the side arms, this similarity is quite surprising. This conformational similarity can be interpreted in terms of a quasienantiomeric structure

[151] Guarneri, F.; Still, W. C., *J. Comput. Chem.* **1994**, *15*, 1302-1310

[152] Still, W. C.; Tempczyk, A.; Hawley, R. C.; Hendrickson, T., *J. Am. Chem. Soc.***1990**, *112*, 6127-6129

[153] (a) Jorgensen, W. L.; Maxwell, D. S.; Tirado-Rives, J., *J. Am. Chem. Soc.***1996**, *118*, 11225-11236; (b) The OPLS_2001 force field, among several commonly used force fields, provided the highest correlation between calculated and experimental conformational preferences within the series of cyclic RGD peptidomimetics containing diketopiperazine scaffolds with different stereochemistry and substitution at the piperazinic nitrogen atoms.

(excluding the configuration of the remote RD amino acid side chains). In any case, the preferred conformation of **2.70** presents an extended arrangement of the RGD sequence with a distance of around 8.8 Å between the C^{β}(Arg) and the C^{β}(Asp) in the MC/SD simulation.[65]

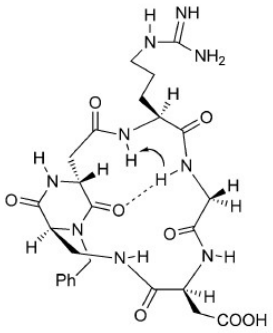

Figure 2.25 – Conformational analysis of **2.70**

Preferred intramolecular hydrogen-bonded pattern proposed on the basis of spectroscopic data (NOE contacts are indicated by an arrow).

Further docking studies on H-bonding patterns with a C^{β}(Arg)-C^{β}(Asp) distance ≥ 8.8 Å taking as a reference model the crystal structure of the extracellular segment of integrin $\alpha_V\beta_3$ complexed with the cyclic pentapeptide Cilengitide, showed top-ranked poses conserving all the important interactions of the X-ray complex (Figure 2.26).[65]

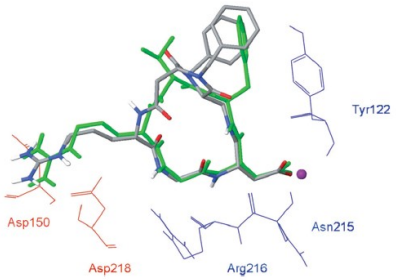

Figure 2.26 – Docking studies on 2.70

As an example is represented the best pose of **2.74 b** (atom color tube representation) into the crystal structure of the extracellular domain of $\alpha_V\beta_3$ integrin (a unit red and β unit blue wise representation) overlaid on the bound conformation of Cilengitide (green tube representation). Only selected integrin residues involved in the interaction with the ligand are shown. The metal ion in the MIDAS region is represented by a magenta sphere. Nonpolar hydrogen atoms were removed for clarity.

The micromolar affinity of RGD peptidomimetics **2.68** and **2.74 b** for $\alpha_V\beta_3$ can be explained in terms of their low pre-organization for binding. In fact, as determined by the computational and NMR spectroscopy studies, in solution these compounds mainly feature non-extended RGD conformations, which according to the docking results, are not able to properly fit into the $\alpha_V\beta_3$ receptor. On the contrary, the nanomolar affinity of **2.70** (and of all the other *trans*-RGD-ligands of the series) for $\alpha_V\beta_3$ can be attributed to their high structural pre-organization.

2.3.2 *Cyclo*[DKP-*iso*DGR] integrin ligands

The DKPs library synthesized in our group has later been used also as scaffold for cyclic *iso*DGR integrin ligands. For this, four derivatives, namely *Cyclo*[DKP2-*iso*DGR] **2.76,** *Cyclo*[DKP3-*iso*DGR] **2.77**, *Cyclo*[DKP5-*iso*DGR] **2.78** and *Cyclo*[DKP7-*iso*DGR] **2.78** (Figure 2.27) were prepared.[67,68] The conformational properties of the cyclic ligands **2.76** and **2.77** were investigated as well as their affinity to $\alpha v\beta_3$ and $\alpha v\beta_5$ integrin receptors.

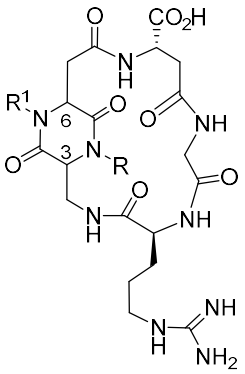

2.76 *Cyclo*[DKP2-*iso*DGR]: (3*R*,6*S*), R = Ph, R^1= H
2.77 *Cyclo*[DKP3-*iso*DGR]: (3*S*,6*R*), R = Ph, R^1= H
2.78 *Cyclo*[DKP5-*iso*DGR]: (3*R*,6*S*), R = R^1 = Ph
2.79 *Cyclo*[DKP7-*iso*DGR]: (3*S*,6*R*), R = R^1 = Ph

Figure 2.27 - *Cyclo*[DKP-*iso*DGR] integrin ligands

2.3.2.1 Synthesis

A SPPS protocol was used for the synthesis of these compounds, and it was carried out using Sasrin™ resin as solid support (Scheme 2.25).[67,68] The SPPS was chosen based on a successful synthesis of a DKP-containing decapeptide.[154]

Each coupling step consisted in:

i) activation of the Fmoc-protected amino acid,

ii) addition of the activated amino acid to the resin to effect the coupling reaction and, after the scaffold coupling, reduction of the azide

iii) capping and Fmoc-deprotection (except after the azide reduction and Cbz-Asp(O*t*Bu)-OH coupling).

Cleavage from the resin was accomplished in weakly acidic conditions. The linear cleaved precursor (**2.80**) was deprotected in presence of Pd/C 10% in THF. The linear deprotected precursor **2.81** was cyclized, deprotected and purified by semi-preparative HPLC. Fmoc-orthogonal PGs were selected for the lateral chains of the amino acids (Arg was protected as -Mtr and Asp as -*t*Bu).

[154] Marchini, M., PhD thesis, University of Milan

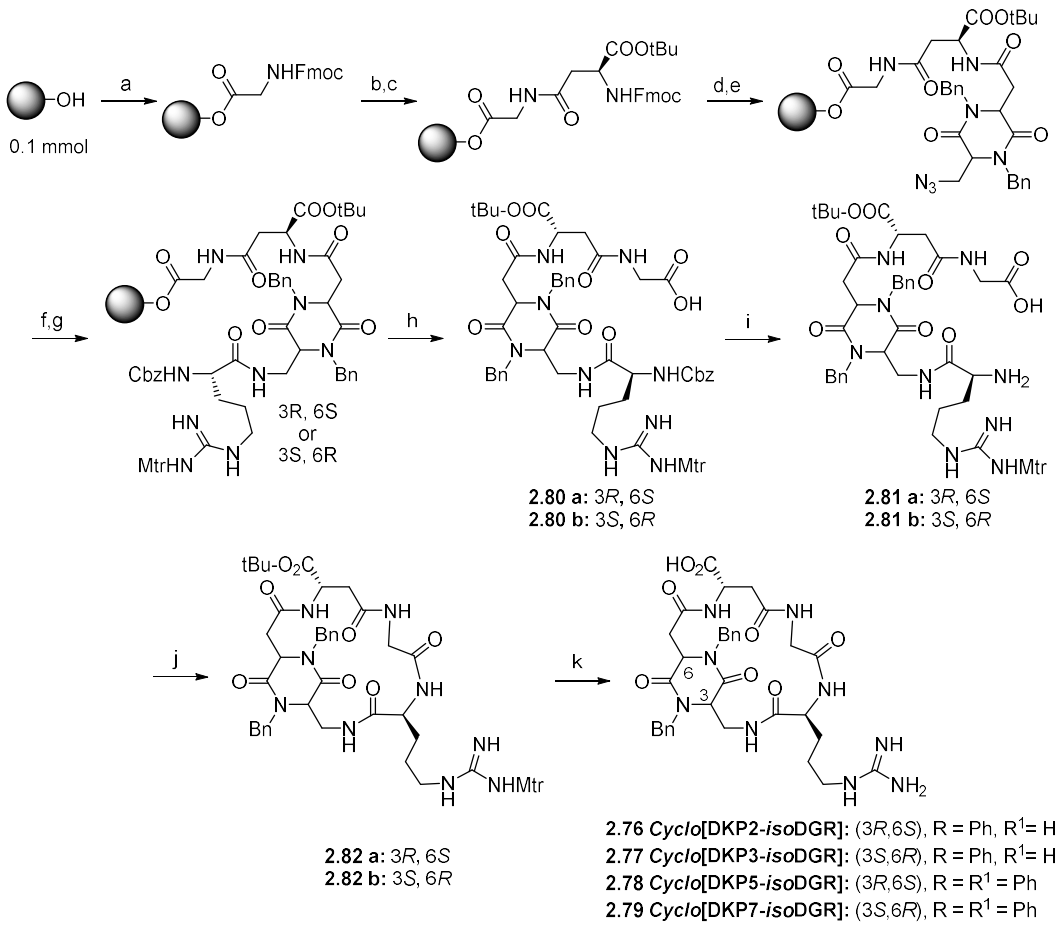

Scheme 2.25 - *Cyclo*[DKP-*iso*DGR] integrin ligands synthesis

Reagents and conditions: a)Fmoc-Gly-OH, DIC, DMAP cat., DMF; b) 25% piperidine in DMF or DBU 2% in DMF, piperidine 2% in DMF; c) Fmoc-Asp(O*t*Bu)-OH, DIC, HOAt, DMF; d) 25% piperidine in DMF or DBU 2% in DMF, piperidine 2% in DMF; e) DKP-N_3, HOAt, DIC, DMF; f) PMe_3, dioxane/water 4:1; g) Fmoc-Arg(Mtr)-OH, HOAt, DIC, DMF; h) 1% TFA in DCM; i) H_2, 10% Pd/C, THF/water 1:1; j) HATU, HOAt, DIPEA, 1.4 mM, DMF; k) TFA/thioanisole/ethanedithiol/anisole 90:5:3:2.

Interestingly and differently from the RGD series, in the case of compound **2.79**, containing the DKP7 scaffold, no trace of two diastereoismers was detected in the ^{1}H-NMR of the final cyclic compound.

2.3.2.2 Biological evaluation

Cyclo[DKP-*iso*DGR] peptidomimetics were examined *in vitro* in competitive binding assays with biotinylated vitronectin to purified $\alpha v\beta_3$ and $\alpha v\beta_5$ receptors (Table 2.2).[67,68] **2.77** showed a low nanomolar affinity for $\alpha v\beta_3$ integrins. These compounds compared well also with the corresponding RGD ligands[65] and much better than other *iso*DGR-ligands (Table 2.2)[155].

Structure	Compound number	$\alpha v\beta_3$ IC_{50} [nM]	$\alpha v\beta_5$ IC_{50} [nM]
***Cyclo*[DKP2-*iso*DGR]**	**2.76**	46.7±18.2	220±84
***Cyclo*[DKP3-*iso*DGR]**	**2.77**	9.2±1.1	312±21
***Cyclo*[DKP5-*iso*DGR]**	**2.78**	490±77	9100±800
***Cyclo*[DKP7-*iso*DGR]**	**2.79**	255±140	5100±400
***Cyclo*[DKP3-*RGD*]**	**2.70**	4.5±1.1	149±25
Cyclo[RGDfV]	/	3.2±1.3	7.5±4.8
***Cyclo*[*Giso*DGRphg]**	/	89 ± 19*	n.d.
Cilengitide	/	0.6±0.1**	11.7±1.5**

Table 2.2 – Inhibition of biotinylated vitronectin binding to $\alpha v\beta_3$ and $\alpha v\beta_5$ receptors

IC_{50} values were calculated as the concentration of compound required for 50% inhibition of biotinylated vitronectin binding. Screening assays were performed by incubating the immobilized integrins $\alpha v\beta_3$ and $\alpha v\beta_5$ with increasing concentrations (10^{-12}-10^{-15}M of the ligands in the presence of biotinylated vitronectin (1 mg/mL) and measuring the concentration of bound vitronectin in the presence of the competitive ligands[67]; * = determined by a solid phase binding assay by using supported vitronectin, soluble $\alpha v\beta_3$ integrin, specific primary and secondary antibodies[155e]; the IC_{50} value of this compound can be compared with the IC_{50} values of **2.76** and **2.77** notwithstanding that the binding assays were realized by using two different protocols. In fact, i) vitronectin is used as competitive natural ligand in both assays, and ii) Cilengitide gives the same IC_{50} value for $\alpha v\beta_3$ integrin with both assays, 155e and 55b respectively; ** = calculated as the concentration of compound required for 50% inhibition of biotinylated vitronectin binding[156]

In particular, **2.77** is the most potent ligand of the class. It is ten-times more potent in binding integrin $\alpha v\beta_3$ than *Cyclo*[*Giso*DGRphg],[155e] recently synthesized by Kessler and co-workers as part of a library of *iso*DGR-cyclopentapeptides. **2.77** is only 2–3-times less potent than the correspondent RGD ligands **2.70** and *Cyclo*[RGDfV], and fifteen-times less potent than the powerful RGD-ligand Cilengitide.

The *iso*DGR library showed very different IC_{50} values depending on the scaffold. Interestingly the RGD library differs under this aspect because all the IC_{50} values for peptidomimetics containing *trans*-scaffold are very similar (e.g., **2.70**: $\alpha v\beta_3$ = 4.5 ±1.1, $\alpha v\beta_5$ = 149 ±25; **2.72**: $\alpha v\beta_3$ = 12.2 ± 5.0, $\alpha v\beta_5$ = 131 ± 29).

[155] (a) Müller, G.; Gurrath, M.; Kessler, H., *J. Comput.-Aided Mol. Des.* **1994**, *8 (6)*, 709-730; (b) Haubner, R.; Gratias, R.; Diefenbach, B.; Goodman, S. L.; Jonczyk, A.; Kessler, H., *J. Am. Chem. Soc.* **1996**, *118*, 7461-7472

[156] Mas-Moruno, C.; Beck, J. G.; Doedens, L.; Frank, A. O.; Marinelli, L.; Cosconati, S.; Novellino, E.; Kessler, H., *Angew. Chem. Int. Ed.* **2011**, *50*, 9496–9500

2.3.2.3 NMR and conformational studies

As for the RGD library, the preferred conformations of **2.76** and **2.77** were investigated by ^{1}H-NMR spectroscopy (one dimensional ^{1}H-NMR to detect intramolecular hydrogen bonds, NOESY spectra to investigate both sequential and long-range NOE signals that provide evidences of preferred conformations), by computational methods (restrained mixed-mode Metropolis Monte Carlo/stochastic dynamics (MC/SD) simulations,[151] using the implicit water GB/SA solvation model[152]) and by docking analysis with the aim of rationalizing the affinity of these compounds for the $\alpha_v\beta_3$ receptor at a molecular level. All the collected data confirm that the *iso*DGR sequence of **2.77** can fit into the RGD binding pocket of $\alpha_v\beta_3$ integrin, establishing the same electrostatic clamp as well as additional key interactions. According to the collected data, compound **2.76** is characterized by a high conformational flexibility with approximately 50% of the conformations arrangement of the *iso*DGR sequence characterized by a pseudo-β-turn at DKP-*iso*Asp and a C^{β}(Arg)-C^{β}(Asp) average distance of 8.6 Å (Figure 2.28).

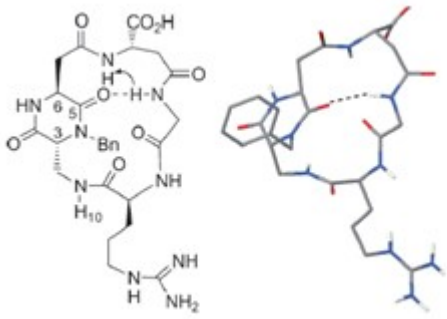

Figure 2.28 – Conformational studies on **2.76**

Left: preferred intramolecular hydrogen-bonded pattern proposed on the basis of spectroscopic data (NOE contacts are indicated by an arrow); right: MC/SD simulations based on experimental distance information after energy minimization (Pseudo-β-turn at DKP-Asp, C^{β}(Arg)-COO^{-}(Asp) distance = 8.8 Å).

On the other hand, **2.77** exists in two preferred conformations: a β-turn conformation and pseudo-β-turn motif similar to that observed for compound **2.76**. Approximately 80% of the conformations sampled during the simulations adopted an extended arrangement of the *iso*DGR sequence, characterized by a pseudo-β-turn at DKP-*iso*Asp with the formation of a distorted β-turn at Gly-Arg, was observed for 10% of the simulations. A C^{β}(Arg)-C^{β}(Asp) average distance of 10.8 Å was obtained during the MC/SD calculations for **2.77** (Figure 2.29 and 2.30).

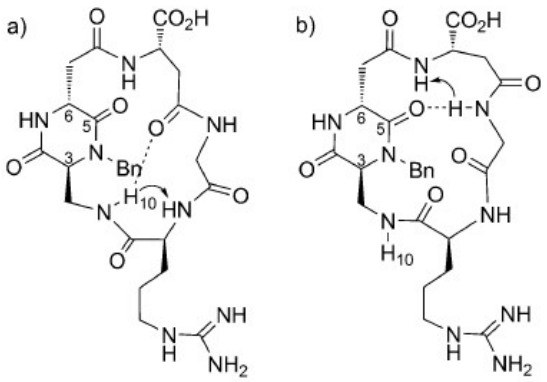

Figure 2.29 – NMR conformational studies on **2.77**

Preferred intramolecular hydrogen-bonded pattern proposed on the basis pf spectroscopic data. NOE contacts are indicated by an arrow. a) β-turn at Gly-Arg; b) pseudo-β-turn at DKP-*iso*Asp.

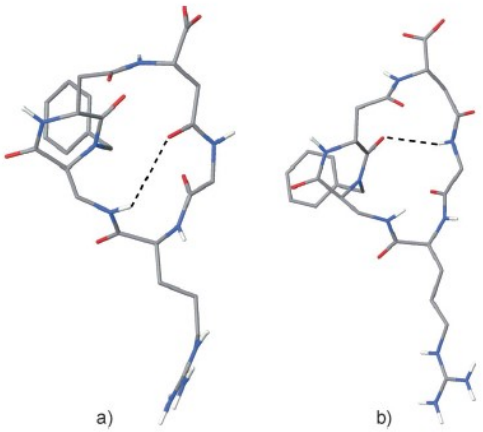

Figure 2.30 – MC/SD simulations based on experimental distance information after energy minimization

a) Distorted β-turn at Gly-Arg, populated for 10% of the simulations, C^{β}(Arg)-COO^{-}(Asp) distance = 10.7 Å; b) Pseudo-β-turn at DKP-Asp, populated for 80% of the simulations, C^{β}(Arg)-COO^{-}(Asp) distance = 10.8 Å.

The crystal structure of the extracellular segment of integrin $\alpha_v\beta_3$ complexed with Cilengitide was taken as a reference model.[33] Docking calculations were performed starting from the pseudo-β-turn DKP-*iso*Asp geometries of **2.76** and from the distorted β-turn Gly-Arg conformations of **2.77**. Calculations produced top-ranked poses conserving the key electrostatic interactions but lacking further stabilizing hydrogen bond interactions with the β-subunit for **2.76**. On the other hand, calculations for **2.77** produced top-ranked poses conserving all the important interactions of the X-ray complex Cilengitide-$\alpha_v\beta_3$ (Figure 2.31).

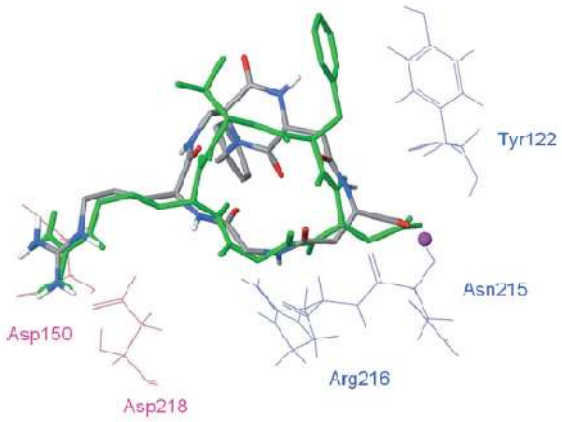

Figure 2.31 – Docking studies

Best pose of **2.77** (atom color tube representation, pseudo-β-turn at DKP-*iso*Asp) into the crystal structure of the extracellular domain of $\alpha v\beta_3$ integrin (a unit pink and β unit blue wise representation) overlaid on the bound conformation of Cilengitide (green tube representation). Only selected integrin residues involved in the interaction with the ligand are shown. The metal ion in the MIDAS region is represented by a magenta sphere. Nonpolar hydrogen atoms were removed for clarity.

2.4 Biological evaluation of *Cyclo*[DKP3-RGD] (2.70) and *Cyclo*[DKP3-*iso*DGR] (2.77) integrin ligands

2.4.1 *Cyclo*[DKP3-RGD] (2.70) as angiogenesis inhibitor

The activity of ligand **2.70** as an angiogenesis inhibitor has recently been investigated in HUVEC.[157] HUVEC have been chosen because they provides a valid model of the intracellular events leading to neovascularization in response to inflammation and hypoxia in cancer, ischemic events, and in embryogenesis.[158] HUVEC express integrins $\alpha_v\beta_3$ and $\alpha_v\beta_5$[159] and as a consequence these cells represent a suitable model to study agents acting on such targets. As already mentioned, competitive binding studies performed on **2.70** showed IC_{50} values of 4.5 ± 1.1 nM and 149 ± 25 nM to $\alpha_v\beta_3$ and $\alpha_v\beta_5$ integrins respectively[65] and it was chosen as reference compound of the RGD library because it is the easier to synthesize.

2.70 demonstrated an angiogenesis inhibition activity without affecting cell viability, apoptosis or proliferation. As a matter of facts, its antiangiogenic activity is independent from cytotoxicity, differently from the majority of anti-angiogenic compounds acting through the inhibition of integrin function (e.g. Cilengitide, Figure 1.2). Since the lack of cytotoxic effects of this integrin ligand has also been observed in several different cell-lines (ovarian carcinoma, IGROV-1 or SKOV3, human pancreatic carcinoma and MIA-PaCa2, human osteosarcoma U2-OS[148]), it can be considered a general feature of ligand **2.70**. Since neoangiogenesis is a key step also in other pathological conditions (e.g., atheromatous plaque vulnerability[160]) where cytotoxicity could represent a risk for adverse effects, these class of antagonists have a potential widespread applications. In any case, further studies are required to establish whether this lack of cytotoxicity is suggestive of reduced toxicity and increased tolerability *in vivo*. However, the data collected suggested a possible application of **2.70** as a candidate modulator of angiogenesis (not only in tumors), hopefully without the adverse effects of cytotoxic analogues (complete toxicological assessment are currently ongoing).

A deep investigation of the specific mechanisms of action of **2.70** has not still been performed but the compound has been shown not to affect the mRNA levels for the integrin subunits α_V, β_3 and β_5. However a significant inhibition of Akt phosphorylation was observed, as a consequence of disruption of endothelial cell−extracellular matrix

[157] Fanelli, R.; Schembri, U.; Piarulli, U.; Pinoli, M.; Rasini, E.; Paolillo, M.; Galiazzo, M. C.; Cosentino, M.; Marino, F., *Vascular Cell* **2014**, *6*, 11
[158] Xu, Y.; Zhou, Y.; Lin, H.; Hu, H.; Wang, Y.; Xu, G., *Int. J. Mol. Med. Mar.* **2013**, *31*, 555-560
[159] Baranska, P.; Jerczynska, H.; Pawlowska, Z.; Koziolkiewicz, W.; Cierniewski, C. S., *Cancer Genomics Proteomics* **2005**, *2*, 265-270
[160] Moreno, P. R.; Purushothaman, M.; Purushothaman, K. R., *Ann. NY Acad. Sci.* **2012**, *1254*, 7–17

attachment, due to integrin inhibition. Similarly, a marked inhibition of FAK phosphorylation has been reported[161] on glioblastoma cell lines.

Experiments on HUVEC were performed both in resting conditions (without any stimuli) and in stimulated conditions (in the presence of angiogenic growth factors or of the pro-inflammatory chemokine IL-8, key factor in pathological angiogenesis). Migration was evaluated by counting cells that had moved from the top compartment of a Boyen chamber to the bottom one. When **2.70** was added in the top compartment (together with cells), HUVEC migration increased in resting conditions and decreased in stimulated conditions. On the other hand, migration increased in both resting and stimulated conditions when the compound was added in the bottom compartment (Figure 2.33). It was hypothesized that the increased cell migration results from the direct inhibitory effect on integrins $\alpha_v\beta_3$ and $\alpha_v\beta_5$, which implicate a reduced cell anchorage to surfaces, while a slight chemoattractant effect of the compound on HUVEC cells could be the reason why there was a decrease of stimulated migration and a reduced increase of spontaneous migration when **2.70** has been added in the same compartment with the cells. This chemoattractant effect attracts the cells along its concentration and not only increases cell random migration through decreased integrin-mediated surface attachment gradient.[157] Anyway, the in vivo relevance of such effect is questionable because no concentration gradient is expected to occur in this situation. Further studies should be performed to understand whether these result simply different modes of action of **2.70** depending on the extension of integrin involvement. However, also Mrksich and co-workers have noticed a similar effect in promoting cell migration on self-assembled monolayers containing immobilized cyclic RGD by addition of exogenous linear RGD ligands.[162]

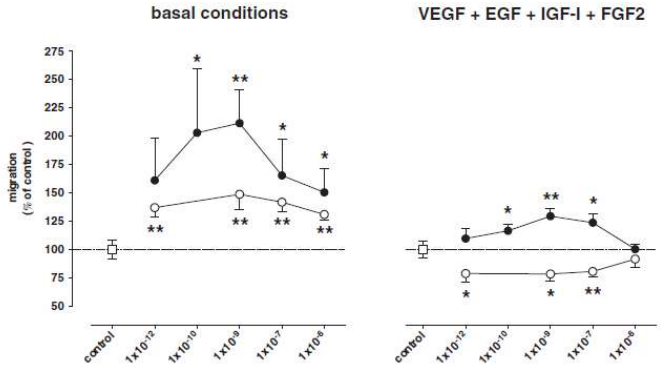

Figure 2.33 – Effect of **2.70** on HUVEC migration in the Boyden chamber assay

Empty circles = **2.70** in the top compartment; filled circles = **2.70** in the bottom compartment. Data are means ± SEM of 5-17 separate experiments; * = P<0.05, ** = P<0.01 vs respective control.

[161] Russo, M. A.; Paolillo, M.; Sanchez-Hernandez, Y.; Curti, D.; Ciusani, E.; Serra, M.; Colombo, L.; Schinelli, S., *Int. J. Oncol.* **2013**, *42*, 83-92
[162] Shabbir, S. H.; Eisenberg, J. L.; Mrksich, M., *Angew. Chem. Int. Ed.* **2010**, *49*, 7706-7709

In our experiments, **2.70** proved to be an inhibitor of angiogenesis induced by the growth factors VEGF, EGF, IGF-I and FGF2, as well as by IL-8 (Figure 2.34 and 2.35). **2.70** seems to block common mechanisms since all these proangiogenic agents act through distinct membrane receptors (the stimulated intracellular cascades finally activate common effector molecules, such as NF-κB or HIF-1[163]),[163,164]. A further confirmation is given by recent evidences indicating that direct interactions may occur between integrin activated pathways and VEGFr[165]/EGFr signaling[166].

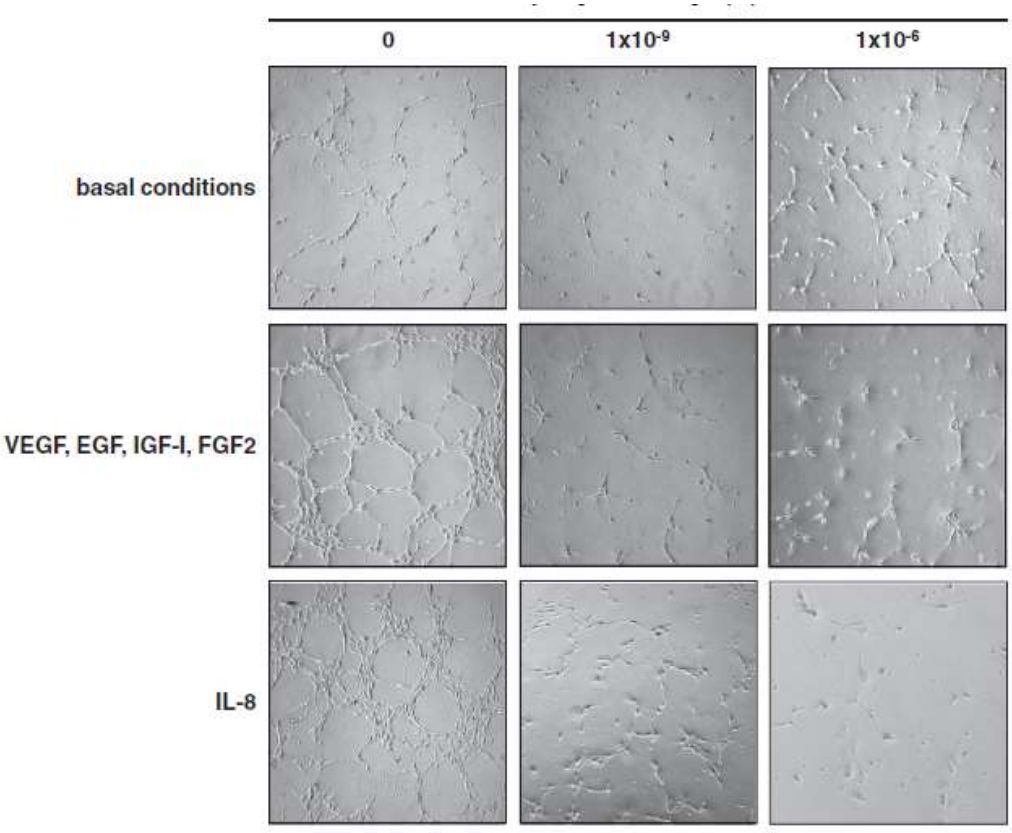

Figure 2.34 – Antiangiogenic effect of **2.70**

Phase contrast micrographs of HUVEC plated on Matrigel in basal conditions or in stimulated conditions with **2.70** at different concentration.

[163] Waugh, D. J. J.; Wilson, C., *Clin. Cancer Res.* **2008**, *14*, 6735–6741
[164] Brooks, A. N.; Kilgour, E.; Smith, P. D., *Clin.Cancer Res.* **2012**, *18*, 1855–1862
[165] Paesler, J.; Gehrke, I.; Poll-Wolbeck, S. J.; Kreuzer, K. A., Eur. *J. Haematol.* **2012**, *89*, 373–384
[166] Hu, B.; Wie, Y. Q.; Tian, L.; Zhao, X.; Lu, Y.; Wu, Y-; Yao. B.; Liu, J. Y.; Niu, T.; Wen, Y. J.; He, Q. M.; Su, J. M.; Huang, M. J.; Lou, Y. Y.; Luo, Y.; Kann, B., *J. Immunother.* **2005**, *28*, 236–244

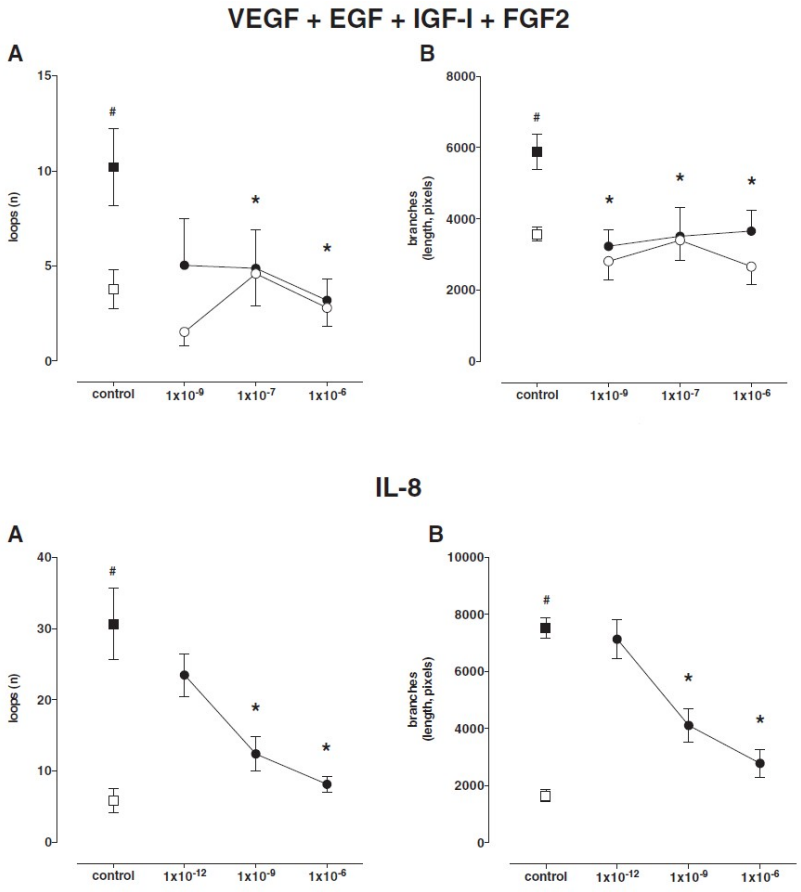

Figure 2.35 - Effect of **2.70** on HUVEC angiogenesis

Effect on HUVEC angiogenesis induced by VEGF, EGF, IGF-1 and FGF2 in the upper panels or by IL-8 in the lower panels. Angiogenesis has been evaluated as both number of loops (A) and length of branches (B). Empty symbols = basal conditions; filled symbols = stimulated conditions. Data are means ± SEM of 3-5 separate experiments; # = P<0.01 vs basal conditions, * = P<0.01 vs respective control.

2.4.2 Comparison between 2.70 and 2.77

Whether RGD ligands have an agonist/antagonist activity on integrins depending on the concentration is controversial. Taking into account that IC_{50} on $\alpha v\beta_3$ integrins of *Cyclo*[DKP3-*iso*DGR][67,68] is comparable to the value measured for *Cyclo*[DKPs-RGD] ligands,[65] *Cyclo*[1a-RGD][161] and considering biological data on HUVEC[157] and on glioblastoma cells[161] presented before, an interesting outlook for anticancer activity of these compounds has been disclosed.

Considering the structural correlation of **2.70** with **2.77** (the most potent *iso*DGR ligand of the library), it was selected for a comparison study. The aim of these experiments was the comprehension of the ligand-receptor interaction to see if one or both of these ligands act as pure antagonists on integrins.[68]

A series of cellular tests were performed on U373 human glioblastoma cells to evaluate if cell viability and infiltration was affected and to measure the effect of **2.70** and **2.77** on FAK and Akt phosphorylation. U373 cell line is useful for this kind of test because it expresses $\alpha_v\beta_3$, $\alpha_v\beta_5$,and $\alpha_5\beta_1$ integrins and the expression pattern of these receptors does not vary following treatment with integrin antagonists.[161]

First of all, an MTS preliminary cell viability assay (a colorimetric assay for assessing cell metabolic activity) was performed. Results confirmed known evidences concerning the lack of direct cytotoxic effects on cancer cell for RGD integrin antagonist.[148,157,161] As expected, MTS assay showed a decrease of cell viability only after 72h treatment. To confirm whether cell were undergoing apoptotic death, ELISA nucleosome assay was performed after treating the U373 cells with 1 μm and 25 μm concentrations of **2.70** and **2.77** for increasing times. After 72h of treatment with 25 μm the ligand (both **2.70** or **2.77**), the nucleosome contents increased significantly (Figure 2.36).[68] These data confirm that cell viability decrease was due to apoptotic cell death.

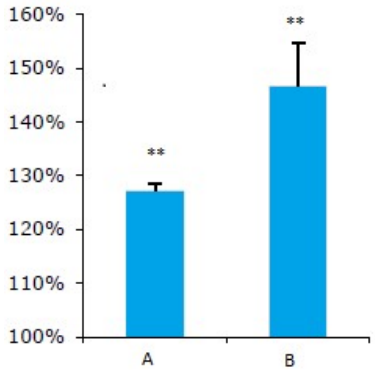

Figure 2.36 – ELISA assay, nucleosome content after 72h treatment

Data are expressed as percent of control (100%), in ordinate the nucleosome content (% of control); A = **2.70**, B = **2.77**; ** = calculated probability value P>0.005.

Inhibition of cell migration and cell infiltration processes is one the most interesting effects among the different ones exerted by RGD antagonists.[167] Infiltration assays on U373 were performed using FBS as chemo-attractant and treating cells with increasing concentrations of **2.70** and **2.77**. Experimental data shown a marked decrease of infiltrated cells for both compounds at 10 μm concentration (Figure 2.37). The value is substantially unchanged at 25 μm, as depicted in Figure 2.35.[68] The same experiment was reported for *cyclo*[1a-RGD]: data registered are consistent.

[167](a) Van der Horst, G.; Bos, L.; Van der Mark, M.; Cheung, H.; Heckmann, P.; Clément-Lacroix, P.; Lorenzon, G.; Pelger, R. C. M.; Bevers, R. F. M.; Van derPluijm, G., *PLoS ONE* **2014**, 9, e108464; (b) Paolillo, M.; Russo, M. A.; Serra, M.; Colombo, L.; Schinelli, S., *Mini Rev. Med. Chem.* **2009**, 9, 1439–1446

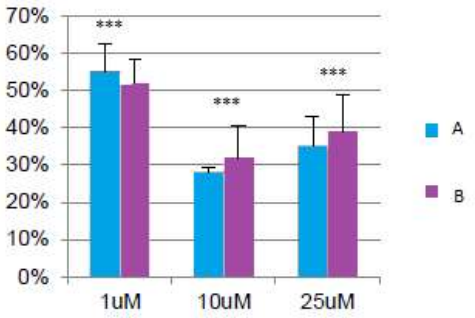

Figure 2.37 – Infiltration assay

Data are expressed as percent of control (100%), in ordinate the cell infiltration (% of control); A = **2.70**, B =**2.77**; *** = calculated probability value P>0.001.

Integrin-induced FAK cascade is an intracellular pathway involving the signaling between the ECM proteins and the cell. It involves FAK, a cytoplasmic tyrosine kinase, and Akt, an intracellular kinase. FAK is associated with protein complexes in the nucleus and receptors at the plasma membrane, promotes cell motility, survival, and proliferation through different mechanisms. This intracellular pathway appears to be the key step in tumor cell growth, tumor progression, and metastasis spreading. FAK-SRC complex, formed as a consequence of the FAK-clustering activation, directly activates the Akt signaling cascade. Akt is an intracellular integrin-linked effector suitable to evaluate the activation of RGD-binding integrin transduction pathway.[168] As mentioned before, a marked inhibition of FAK phosphorylation was reported in experiments with *cyclo*[1a-RGD] on glioblastoma cell lines.[161] In order to investigate if also the binding of **2.70** and/or **2.77** affected integrin-induced FAK and Akt phosphorylation, U373 cells have been incubated with the two ligands (at 25 μm concentration) for increasing times and cell extracts were monitored by western blot analysis (Figure 2.38).[68]

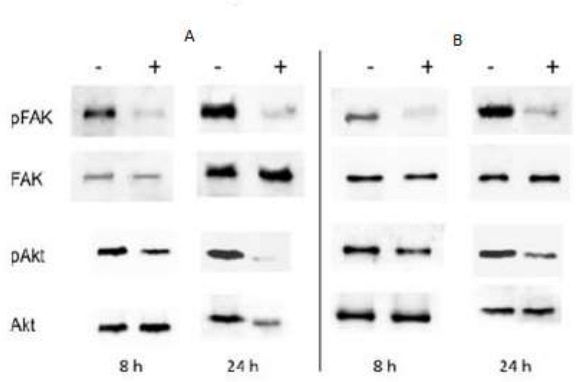

Figure 2.38 – FAk and Akt phosphorilation, western blot analysis (+ = treatment with the ligand; - = control)

[168] Sulzmaier, F. J.; Jean, C.; Schlaepfer, D. D., *Nat. Rev. Cancer* **2014**, *14*, 598–610

After treatment with both ligands a decrease of both FAK and Akt phosphorylation was observed and it was particularly evident after 24h treatment (Figure 2.39).[68]

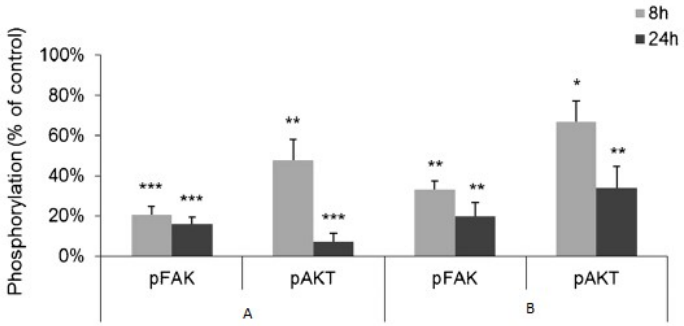

Figure 2.39 - FAK and Akt phosphorylation assays

A = **2.70**, B = **2.77**; Densiometric analysis, * = calculated probability value P>0.5, ** = calculated probability value P>0.005, *** = calculated probability value P>0.001.

From these data, it seems that **2.70** and **2.77** inhibit tumor cells infiltration processes and this process could be mediated by inhibition of the FAK and Akt signaling cascade.[68]

2.5 Conclusions and outlooks

Cyclo[DKP3-*iso*DGR] **2.77** is the first *iso*DGR ligand found to be active in the inhibition of FAK/Akt integrin activated transduction pathway and on integrin-mediated cell infiltration processes. From the collected data, consistent with other *iso*DGR-containing cyclopeptides results[47], an antagonist activity can be attributed to this compound.[68]

For what concerns **2.70**, results are consistent with literature data obtained for other RGD ligands at comparable concentrations (e.g., *cyclo*[1a-RGD][161]) and with data obtained for the same compound on human endothelial cells.[157] As a matter of facts, cellular effects of this ligand are consistent with an antagonist profile.[68]

Unfortunately the comparison with Cilengitide activity profile is not well defined. According to already presented analysis of literature data (Chapter 1), a comparison of these cyclic ligands with Cilengitide is not appropriate because of the different experimental settings and cell types.

Further *in vitro* and *in vivo* studies will be performed on **2.70** and on **2.77** to better understand their mechanism of action and to obtain a complete toxicity profile.

2.6 Experimental section

2.6.1 Materials and methods

All manipulations requiring anhydrous conditions were carried out in flame-dried glassware, with magnetic stirring and under a nitrogen atmosphere. All commercially available reagents were used as received. Anhydrous solvents were purchased from commercial sources and withdrawn from the container by syringe, under a slight positive pressure of nitrogen. The reactions were monitored by analytical TLC using silica gel 60 F_{254} pre-coated glass plates (0.25 mm thickness). Visualization was accomplished by irradiation with a UV lamp and/or staining with a potassium permanganate alkaline solution or ninhydrin. Flash column chromatography was performed according to the method of Still and co-workers[169] using Chromagel 60 ACC (40-63 μm) silica gel. Proton NMR spectra were recorded on a spectrometer operating at 400.16 MHz. Proton chemical shifts are reported in ppm (δ) with the solvent reference relative to TMS employed as the internal standard. The following abbreviations are used to describe spin multiplicity s = singlet, d = doublet, t = triplet, q = quartet, m = multiplet, bs = broad signal, dd = doublet of doublet, ddd = doublet of doublet of doublet, ddt = doublet of doublet of triplet. Carbon NMR spectra were recorded on a spectrometer operating at 100.63 MHz, with complete proton decoupling. Carbon chemical shifts are reported in ppm (δ) relative to TMS with the respective solvent resonance as the internal standard. ESI-MS spectra were recorded on the ion trap mass spectrometer Finnigan LCQ Advantage.

RP-HPLC purification

The HPLC purifications were performed on a Dionex Ultimate 3000 instrument equipped with a Dionex RS Variable Wavelenght Detector (column: Atlantis Prep T3 OBDTM 5 TM 19 x 100 mm).The crude reaction mixture was dissolved in water and the solution was filtered (polypropylene, 0.45 μm, 13 mm ø, PK/100) and injected in the HPLC, affording purified products.

RP-HPLC analysis

Purity analysis for each of the compounds was carried out on a Dionex Ultimate 3000 instrument equipped with a Dionex RS Variable Wavelenght Detector (column: Atlantis Prep T3 OBDTM 5TM 19 x 100 mm). 1 mg of purified product was dissolved in 1 mL of H_2O and was injected using the same gradient used in the purification step. The analysis of the integrals and the relative percentage of purity was performed with the software Cromeleon 6.80 SR11 Build 3161.

[169] Still, W. C.; Kahn, M.; Mitra, A., *J. Org. Chem.* **1978**, *43*, 2923-2925

Freeze-drying

The product was dissolved in water and frozen with dry ice: the freeze-drying was carried out at least for 48 h at -50 °C using the instrument 5Pascal Lio5P DGT.

2.6.2 General procedures for SPPS

The SPPS was accomplished using the semi-automatic synthesizer Biotage® Initiator™ assisted by microwaves. The programs "Tasks" used in the SPPS instrument are reported in the General Procedures. Each task can be modified in every parameter and it is performed under mechanical stirring at 1000 rpm. A Fmoc strategy was selected and the SASRIN™ Resin (200-400 mesh, loading: 1.02 mmol/g) were used.

Solutions and solvents

In order to execute the programs set, the synthesizer required two solutions and two solvents: 25% Ac_2O in DMF (v/v), 25% piperidine in DMF (v/v), MeOH and DMF. MeOH was used only as washing solvent, DMF was used for washes and reactions (coupling, capping and deprotection).

Resin preparation and storage

The resin was weighted in a 10 mL vial and processed with the swelling task (GP1). At the end of this operation the resin was ready for the SPPS. When necessary, beads were stored at 4 °C under nitrogen after being washed several times with DCM and dried at the high vacuum pump.

Kaiser test

GP0: Phenol (80% solution in ethanol), ninhydrin (6% solution in ethanol) and pyridine (two drops) were added to a small sample of the resin and then heated in a boiling water bath for 60 sec. If the colour of the solution maintained yellow, quantitative coupling was achieved. In the case of a slight blue colour, the coupling step was not fully completed and had to be repeated.

Swelling task

GP1: DMF (3.0 mL) was added to the resin: the swelling was accomplished at r.t. in 30 min. At the end of the swelling step, the vial was empty.

Activation, loading of the first amino acid and capping of the resin

GP2: To a solution of the first Fmoc-AA-OH in DMF, DIC and DMAP were added at 0 °C, under stirring and inert atmosphere. After 25 min, the reaction mixture was added to the resin at the synthesizer and a cycle of coupling (single or double-capping-deprotection-washing) was effected.

Activation of the Fmoc-AA-OH/DKP and coupling task

GP3: To a solution of the desired Fmoc-AA-OH or N_3-DKP-COOH in DMF, DIC, HOAt were added at 0 °C, under stirring and inert atmosphere. After 25 min, the reaction mixture was added to the resin at the synthesizer and a cycle of coupling (single or double-capping-deprotection-washing) was effected. The activated Fmoc-AA-OH/DKP scaffold was added to the beads and the coupling reaction assisted by microwaves started was carried out at 70 °C under inert atmosphere for 12 min. The beads were washed six times with DMF (2.5 mL × 20 s for every wash). Activation and coupling step involving commercial AA, were performed twice. At the end of the coupling task, a Kaiser test was performed. At the end of each step, the vial was empty.

Capping task

GP4: The solution 25% Ac_2O in DMF (3 mL) was added to the resin: the capping step was performed at r.t. under inert atmosphere for 15 min. The beads were washed six times with DMF (2.5 mL × 20 s for every wash). At the end of each step, the vial was empty.

Fmoc-deprotection task

GP5: Two deprotection steps were carried out adding the solution 25% piperidine in DMF (3.0 mL for each step) to the beads: the reaction was performed at r.t. under inert atmosphere for 5 min and 7 min for the first and the second deprotection step respectively. The beads were washed twice with DMF, MeOH, DMF, MeOH and DMF (3.0 mL × 20 s for every wash; 3.0 mL × 20 s for the last washes in MeOH and DMF). At the end of each step, the vial was empty.

Azide reduction on resin

GP6: Azidopeptidyl resin (1 eq.) was suspended in a 4:1 mixture of dioxane/water. Trimethylphosphine (1M solution in toluene, 6 eq.) was added and the reaction vessel was shaken for 40 min. The resin was then washed with dioxane (3 x) and the conversion was checked by Kaiser test.

Cleavage from the resin

GP7: The resin was thoroughly washed with DCM (10 x) and then treated with 1% TFA in DCM (2 mL) for 2-5 min. The mixture was filtered off with a N_2pressure into a vial containing 0.2 mL of 12% of Py in MeOH. The presence of the peptide was monitored by TLC (DCM/MeOH 9:1): after 5-8 cycles the peptide was completely cleaved from the resin. The fractions were collected and concentrated at reduced pressure. The mixture was then diluted with AcOEt and washed with 1 M $KHSO_4$ (4 x). The organic layer was dried over Na_2SO_4 and concentrated affording a white solid. The crude compounds were purified by flash chromatography on silica gel (gradient: DCM/MeOH 95:5 to 8:2) to give the desired products.

2.6.3 General procedures for solution-phase synthesis

Cbz hydrogenolytic cleavage

GP8: Protected compound (1 eq.) was dissolved in a mixture of THF/H_2O (1:1) and Pd/C 10% (0.1 eq.) was added. The reaction mixtures were subjected to three vacuum/hydrogen cycles and then left stirring overnight at room temperature under 1 bar of hydrogen. The mixture was filtered through Celite, and the cake was washed thoroughly with THF/H_2O (1:1). The filtrate was concentrated and dried.

Macrolactamization

GP9: HATU (4 eq.), HOAt (4 eq.) and DIPEA (6 eq.) were added successively to a solution of deprotected linear compound (1.4 mm; 1 eq.) in DMF, under a nitrogen atmosphere at 0°C. After stirring the reaction mixture at 0°C for 1 h, it was allowed to reach room temperature and stirred overnight. DMF was then removed under reduced pressure.

Mtr AND O*t*Bu ester removal

GP10: Protected macrolactam was treated for 2h with TFA, in the presence of ion scavengers: thioanisole (5%), EDT (3%), anisole (2%). After TFA removal under reduced pressure, the residue was dissolved in a 1:1 mixture of diisopropyl ether/water. Phases were separated and the aqueous layer was washed several times with diisopropyl ether. The aqueous phase was concentrated under reduced pressure to give the crude product, which was purified by HPLC.

2.6.4 Synthesis

N_3-(3*R*,6*S*)-DKP-COOAllyl **2.32 a**, N_3-(3*S*,6*R*)-DKP-COOAllyl **2.32 b**, N_3-(3*R*,6*S*)-DKP-COOAllyl **2.34** (DKP*2), N_3-(3*S*,6*R*)-DKP-COOAllyl **2.35** (DKP*3), *Cyclo*[DKP2-*iso*DGR] **2.76** and *Cyclo*[DKP3-*iso*DGR] **2.77** were synthesized according to literature procedure (Mingozzi, M.; Dal Corso, A.; Marchini, M.; Guzzetti, I.; Civera, M.; Piarulli, U.; Arosio, D.; Belvisi, L.; Potenza, D.; Pignataro, L.; Gennari, C., *Chem. Eur. J.* **2013**, *19*, 3563-3567) and their analytical data were in agreement with those already published.

N_3-(3*R*,6*S*)-DKP-COOAll (2.49 a) and N_3-(3*S*,6*R*)-DKP-COOAll (2.49 b)

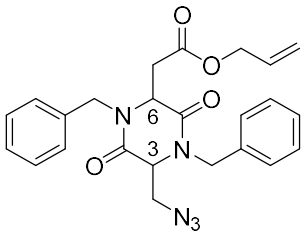

The reaction was performed in a flame-dried flask under nitrogen atmosphere. KHMDS (111 mg, 0.55 mmol, 1.1 eq.) was dissolved in dry toluene to give a 0.5 M solution. The solution was cooled to -70°C and **2.32 a** or **2.32 b** (180 mg, 0.5 mmol, 1 eq.), previously dissolved in dry THF (9.9 mL), was added drop wise. The mixture was stirred under these conditions for 30 minutes, then benzyl bromide (0.30 μl, 2.5 mmol, 5 eq.) and DMF (4.2 mL) were sequentially added under these conditions. The reaction was allowed to reach -40°C and it was stirred under these conditions for 5 hours. After this time, a saturated solution of NH_4Cl was added and the mixture was extracted three times with EtOAc (3 x 40 mL). Organic layers were reunited, washed with brine and dried over Na_2SO_4 anhydrous. Volatiles were removed under reduced pressure then the crude was purified by flash chromatography on silica gel eluting hexane: EtOAc (from 7:3 to 6:4). The product was recovered as a transparent oil (134 mg, 66%).

*R*f=0.4 (Hexane/AcOEt 6:4); ^{1}H-NMR (400 MHz, $CDCl_3$, T = 298K) δ 7.37 – 7.27 (10 H, m), 5.87-5.77 (1H, m), 5.36 (2 H, dd, *J* 16, 8), 5.29 (3H, s), 5.23 (1H, d, *J* 12), 4.50 (2H, dq, *J* 44, 12, 8), 4.24 (1H, s), 4.18– 4.15 (2 H, m), 4.09 (2 H, d, *J* 12), 3.74 (1 H, dd, *J* 12, 4), 3.30 (1 H, dd, *J* 16, 4), 2.92 (1 H, dd, *J* 20, 8); ^{13}C-NMR (101MHz, CD_2Cl_2, T = 298K) δ 169.5, 166.1, 164.9, 135.3, 131.8, 128.8, 128.8, 128.6, 128.1, 128.0, 127.9, 127.8, 127.8, 127.3, 126.6, 118.4, 103.7, 65.6, 58.4, 55.0, 51.4, 47.1, 47.0, 34.8; MS (ESI) *m*/z calcd. for $[C_{24}H_{24}N_5O_4Na]^+$: 447.19; $[M+Na]^+$; found: 470.4.

N_3-(3*R*,6*S*)-DKP-COOH 2.45 (DKP*5) and N_3-(3*S*,6*R*)-DKP-COOH 2.46 (DKP*7)

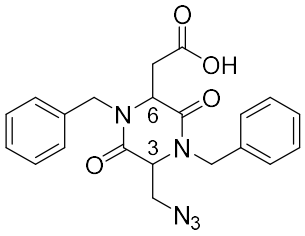

N_3-(3*R*,6*S*)-DKP-COOAll (**2.49 a**) or N_3-(3*S*,6*R*)-DKP-COOAll (**2.49 b**) (120 mg, 0.27 mmol, 1 eq.) was dissolved in DCM (2.7 mL) under a nitrogen atmosphere, and the mixture was cooled to 0°C. [$Pd(PPh_3)_4$] (94 mg, 0.08 mmol, 0.3 eq.) and freshly distilled N-methyl aniline (35 µl, 0.32 mmol, 1.2 eq.) were added successively. The mixture was then allowed to reach room temperature. After 1 h of stirring, the mixture was diluted with EtOAc (40 mL) and extracted with aqueous $NaHCO_3$ (4 x 20 mL). The combined aqueous phases were acidified to pH 2 by adding $KHSO_4$ (1M solution) and then extracted with DCM (4 x 20 mL). The resulting organic phase was dried over Na_2SO_4 and the solvent was evaporated to afford the desired product as a slightly yellow solid (77 mg, 70%) which was used without further purification.

*R*f=0.20 (Hexane/AcOEt 1:1); ^{1}H-NMR (400 MHz, $CDCl_3$, T = 298K) δ 7.41 – 7.25 (10 H, m), 5.47 (2 H, dd, *J* 48, 16), 4.25 (1H, s), 4.14 – 4.06 (3H, m), 4.02 (1 H, d, *J* 16), 3.77 (1 H, dd, *J* 12, 2), 3.37 (1 H, dd, *J* 20, 4), 2.97 (1 H, dd, *J* 20, 4); ^{13}C-NMR (101MHz, $CDCl_3$, T = 298K) δ 173.8, 166.1, 165.3, 134.8, 134.4, 129.1, 129.0, 128.2, 128.1, 127.9, 127.8, 58.2, 54.3, 51.4, 47.1, 46.9, 34.2; MS (ESI) *m/z* calcd for $[C_{21}H_{20}N_5O_4Na]^+$: 429.40 $[M+Na]^+$; found: 430.1020.

Cbz-Arg(Mtr)-(3*R*,6*S*)-DKP-*iso*Asp(O*t*Bu)-Gly-OH (2.80 a) and Cbz-Arg(Mtr)-(3*S*,6*R*)-DKP-*iso*Asp(O*t*Bu)-Gly-OH (2.80 b)

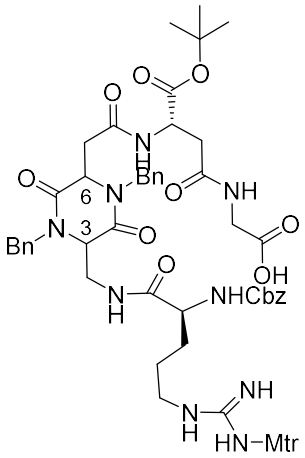

The resin was prepared and swelled (**GP1**). Fmoc-Gly-OH was activated and coupled to the resin (**GP2**). After a capping step (**GP4**) and a Fmoc deprotection step (**GP5**), Fmoc-L-Asp(OH)-O*t*Bu was activated and coupled (**GP3**). Then a capping step (**GP4**) and a Fmoc deprotection step (**GP5**) were performed. DKP-N_3 scaffold was activated and coupled to the resin (**GP3**); the coupling was followed by the azide reduction (**GP6**). Fmoc-Asp(O*t*Bu)-OH was activated and coupled (**GP3**). After the Fmoc deprotection step (**GP5**), the linear precursor was cleaved from the resin (**GP7**). The desired products were obtained as white foams (**2.80 a**: 157 mg, 71%; **2.80 b**: 90 mg, 81%).

Compound 2.80 a:

*R*f=0.15 (9:1 DCM/MeOH); ^{1}H-NMR (400 MHz, CD_3OD) δ 7.43-7.20 (m, 15H), 6.63 (s, 1H), 5.39 (d, *J* = 15.4 Hz, 1H), 5.14-4.99 (m, 3H), 4.57 (t, *J* = 6.2 Hz, 1H), 4.38 (s, 1H), 4.32 (dd, *J* =15.5, 6.9 Hz, 2H), 4.09 (s, 1H), 4.03 (s, 1H), 3.80 (s, 5H), 3.74 (s, 2H), 3.19-3.04 (m, 3H), 2.90 (dd, *J* = 16.9, 4.5 Hz, 1H), 2.72-2.64 (m, 5H), 2.59 (s, 3H), 2.10 (s, 3H), 1.68 (s, 1H), 1.58-1.38 (m,12H). ^{13}C-NMR (101 MHz, CD_3OD) δ 178.2, 175.4, 172.1, 171.5, 171.1, 168.7, 167.8, 159.9,158.4, 158.2, 139.5, 138.1, 137.9, 137.1, 136.8, 134.8, 130.0, 130.0, 129.5, 129.4, 129.0, 128.9,125.7, 112.8, 83.2, 67.9, 59.8, 56.8, 56.3, 56.0, 51.6, 44.5, 40.5, 38.6, 36.4, 30.1, 28.3, 24.4, 18.9,12.1.; MS (ESI) *m*/*z* calcd. for $[C_{55}H_{70}N_9O_{14}S]^+$: 1112.5 $[M+H]^+$; found: 1112.5.

Compound 2.80 b:

*R*f=0.15 (9:1 DCM/MeOH); MS (ESI) *m*/*z* calcd. for $[C_{55}H_{70}N_9O_{14}S]^+$: 1156.4 $[M+2Na-H]^+$;found: 1156.6.

Exact amounts of the AA and coupling reagents used for SPPS are reported in Table 2.3 for *Cyclo*[*iso*DGR-3*R*,6*S*)-DKP] (**2.76**) and in Table 2.4 for *Cyclo*[*iso*DGR-3*S*,6*R*)-DKP] (**2.77**).

Table 2.3

Reagents	Eq. or concentration	mmol	Amounts
SASRIN™ resin	1 eq.	0.2	200 mg
Fmoc-Gly-OH*	4 eq.	0.8	238 mg
DIC	4 eq.	0.8	124 µL
DMAP	0.1 eq.	0.02	2.4 mg
DMF	0.27 M	/	3 mL
Fmoc-L-Asp(OH)-O*t*Bu*	3 eq.	0.6	247 mg
DIC	3 eq.	0.6	93 µL
HOAT	3 eq.	0.6	82 mg
DMF	0.20 M	/	3 mL
N_3-(3*R*,6*S*)-DKP-COOH 2.45	2.3 eq.	0.46	185 mg
DIC	2.3 eq.	0.46	71 µL
HOAT	2.3 eq.	0.46	63 mg
DMF	0.15 M	/	3 mL
Cbz-L-Arg(Mtr)-OH . CHA*	2.5 eq.	0.5	310 mg
DIC	2.5 eq.	0.5	77 µL
HOAT	2.5 eq.	0.5	68 mg
DMF	0.17 M	/	3 mL

* a double coupling step is performed.

Table 2.4

Reagents	Eq. or concentration	mmol	Amounts
SASRIN™ resin	1 eq.	0.1	100 mg
Fmoc-Gly-OH*	4 eq.	0.4	119 mg
DIC	4 eq.	0.4	62 µL
DMAP	0.1 eq.	0.01	1.2 mg
DMF	0.27 M	/	1.5 mL
Fmoc-L-Asp(OH)-O*t*Bu*	3 eq.	0.3	124 mg
DIC	3 eq.	0.3	47 µL
HOAT	3 eq.	0.3	41 mg
DMF/DCM	0.20 M	/	1.5 mL
N_3-(3*S*,6*R*)-DKP-COOH 2.46	2.3 eq.	0.23	93 mg
DIC	2.3 eq.	0.23	36 µL
HOAT	2.3 eq.	0.23	32 mg
DMF/DCM	0.15 M	/	1.5 mL
Cbz-L-Arg(Mtr)-OH ·CHA*	2.5 eq.	0.25	155 mg
DIC	2.5 eq.	0.25	39 µL
HOAT	2.5 eq.	0.25	34 mg
DMF	0.17 M	/	1.5 mL

* a double coupling step was performed.

H-Arg(Mtr)-(3*R*,6*S*)-DKP-*iso*Asp(O*t*Bu)-Gly-OH (2.81 a) and H-Arg(Mtr)-(3*S*,6*R*)-DKP-*iso*Asp(O*t*Bu)-Gly-OH (2.81 b)

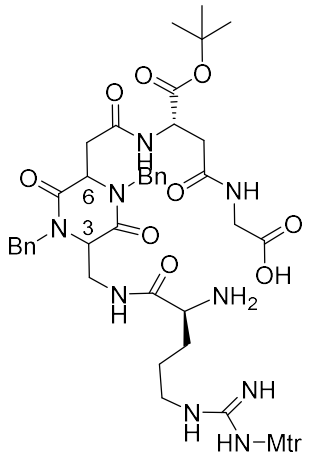

Compound **2.80 a** or **2.80 b** (**2.80 a**: 145 mg, 0.14 mmol, 1 eq; **2.80 b**: 90 mg, 0.08 mmol, 1 eq) was treated with10% Pd/C (**2.80 a**: 14 mg, 0.014 mmol, 0.1 eq; **2.80 b**: 8 mg, 0.008 mmol, 0.1 eq) under the conditions described in **GP8**. The product was obtained as a white solid (**2.81 a**: 134 mg, 98%; **2.81 b**: 80 mg, quantitative yield) and it was used without further purification.

Compound 2.81 a:

^{1}H-NMR (400 MHz, CD_3OD) δ 7.44-7.15 (m, 10H), 6.64 (s, 1H), 5.45 (d, *J* = 15.4 Hz, 1H), 4.58 (bt, *J* = 4.9 Hz, 1H), 4.43 (d, *J* = 15.4 Hz, 1H), 4.34 (bs, 1H), 4.24 (d, *J* = 15.7 Hz, 1H), 4.11 (bs,1H), 3.90 (s, 3H), 3.79 (s, 3H), 3.71 (dd, *J* = 14.2, 5.9 Hz, 1H), 3.24-3.10 (m, 2H), 3.06 (d, *J* = 15.2Hz, 1H), 2.92 (dd, *J* = 16.8, 4.9 Hz, 1H), 2.72 (d, *J* = 6.0 Hz, 2H), 2.66 (s, 3H), 2.59 (s, 3H), 2.10 (s,3H), 1.88-1.75 (m, *J* = 14.3, 7.1 Hz, 2H), 1.61-1.49 (m, 2H), 1.43 (s, 9H), 1.46-1.35 (m, 2H). ^{13}C-NMR (101 MHz, CD_3OD) δ 172.4, 171.3, 171.0, 170.8, 168.7, 167.8, 163.0, 162.7, 159.9, 158.1, 139.4, 137.9, 137.3, 136.6, 134.5, 129.9, 129.8, 129.4, 129.1, 128.8, 128.1, 126.1, 125.7, 112.8, 83.2, 59.2, 57.7, 56.9, 56.0, 53.9, 51.3, 50.4, 49.8, 48.0, 41.9, 40.7, 38.3, 36.4, 35.8, 30.8, 30.7, 30.5, 29.6, 28.2, 24.3, 18.8, 12.1; MS (ESI) *m*/z calcd. for $[C_{47}H_{64}N_9O_{12}S]^+$: 978.4 $[M+H]^+$; found:978.7.

Compound 2.81 b:

MS (ESI) *m*/z calcd. for $[C_{47}H_{63}N_9O_{12}SNa]^+$: 1000.4 $[M+Na]^+$; found: 1000.5.

***Cyclo*[(3*R*,6*S*)-DKP-*iso*Asp(O*t*Bu)-Gly-Arg(Mtr)] (2.82 a) and *Cyclo*[(3*S*,6*R*)-DKP-*iso*Asp(O*t*Bu)-Gly-Arg(Mtr)] (2.82 b)**

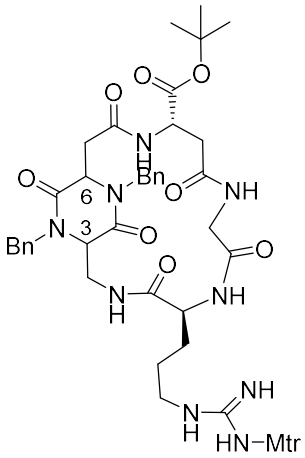

Compound **2.81 a** (127 mg, 0.13 mmol, 1 eq) was cyclized in the presence of HATU (198 g, 0.52mmol, 4 eq), HOAt (71 mg, 0.52 mmol, 4 eq) and DIPEA (136 μL, 0.78 mmol, 6 eq) under the conditions described in **GP9**. The crude product was purified by RP-HPLC [gradient: 90% H_2O + 0.1% CF_3COOH / 10% CH_3CN + 0.1% CF_3COOH to 100% CH_3CN + 0.1% CF_3COOH in 10 min; flow: 15 mL/min, *t*R (product) = 7 min ca.] to afford the desired product **2.82 a** as a white foam (39 mg, 32%).

Compound 2.82 a:

^{1}H-NMR (400 MHz, CD_3OD) δ 7.44-7.15 (m, 10H), 6.68 (s, 1H), 5.37 (d, *J* = 15.1 Hz, 1H), 5.26 (d, *J* = 16.0 Hz, 1H), 5.15 (d, *J* = 8.0 Hz, 1H), 4.73-4.62 (m, *J* = 5.4 Hz, 1H), 4.40 (d, *J* = 16.1 Hz,1H), 4.29-4.07 (m, 4H), 3.99 (s, 1H), 3.83 (s, 3H), 3.68 (d, *J* = 16.5 Hz, 1H), 3.47 (d, *J* = 13.5 Hz,1H), 3.37 (s, 1H), 3.28-3.15 (m, 2H), 2.86 (dd, *J* = 14.6, 3.3 Hz, 1H), 2.77 (d, *J* = 6.6 Hz, 2H), 2.70(s, 3H), 2.64 (s, 3H), 2.34-2.23 (m, 1H), 2.15 (s, 3H), 1.80-1.55 (m, *J* = 18.4, 14.0, 5.9 Hz, 3H),1.49 (s, 9H). ^{13}C-NMR (101 MHz, CD_3OD) δ 175.4, 172.2, 171.7, 171.2, 171.1, 167.8, 167.1, 160.0, 157.9, 139.5, 138.8, 136.8, 130.1, 129.8, 129.5, 129.2, 128.9, 128.4, 128.1 , 125.8, 112.9, 83.4, 60.0, 59.4, 56.0, 55.0, 51.8, 51.3, 49.9, 47.7, 42.8, 40.5, 38.8, 29.0, 28.2, 24.3, 18.8, 12.1; MS(ESI) *m*/z calcd. for $[C_{47}H_{62}N_9O_{11}S]^+$: 960.4 $[M+H]^+$; found: 960.6.

Compound **2.81 b** (40 mg, 0.04 mmol, 1 eq) was cyclized in the presence of HATU (60 mg, 0.16 mmol,4 eq), HOAt (22 mg, 0.16 mmol, 4 eq) and DIPEA (62 μL, 0.24 mmol, 6 eq) under the conditions described in **GP4**. The residue was purified over flash column eluting DCM/MeOH (from 97:3 to 9:1) to afford the crude product **2.82 b** as a pale yellow foam.

Compound 2.82 b: *R*f = 0.16 (9:1 DCM/MeOH); MS (ESI) *m*/z calcd. for $[C_{47}H_{62}N_9O_{11}S]^+$: 960.4$[M+H]^+$; found: 960.6 $[M+H]^+$.

***Cyclo*[(3*R*,6*S*)-DKP-*iso*DGR] (2.76) and *Cyclo*[(3*S*,6*R*)-DKP-*iso*DGR] (2.77)**

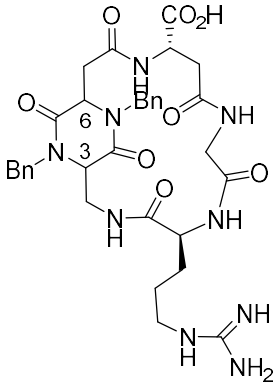

Compound **2.82 a** (40 mg, 0.04 mmol, 1 eq) or **2.82 b**(15 mg, 0.015 mmol, 1 eq) was deprotected under the conditions described in **GP10**. The crude product was purified by RP-HPLC [compound **2.76**= gradient: 90% H_2O + 0.1% CF_3COOH / 10% CH_3CN + 0.1% CF_3COOH to 100% CH_3CN + 0.1% CF_3COOH in 10 min; flow: 15 mL/min, *t*R (product) = 4.7 min; compound **2.77** = gradient: 100% H_2O + 0.1% CF_3COOH to 50% H_2O + 0.1% CF_3COOH / 50% CH_3CN + 0.1% CF_3COOH in 11 min; flow: 15 mL/min, *t*R (product) = 9.6 min]. The pure fractions were concentrated and freeze-dried, affording **2.76** or **2.77**as a white solid (**2.76**: 12.5 mg, 37%; **2.77**: 3.0 mg, 25%).

Compound 2.76:

^{1}H-NMR (400 MHz, D_2O) δ 7.54-7.31 (m, 10H), 5.26 (d, *J* = 15.3 Hz, 1H), 5.09-5.00 (m, 2H), 4.79(d , 1H), 4.67 (d, *J* = 16.4 Hz, 1H), 4.33-4.30 (m, 1H), 4.29-4.17 (m, 3H), 4.11 (dd, *J* = 14.7, 3.6Hz, 1H), 3.91 (d, *J* = 16.8 Hz, 1H), 3.68 (dd, *J* = 14.6, 1.6 Hz, 1H), 3.25 (t, *J* = 6.8 Hz, 2H), 3.02 (dd, *J* = 14.8, 3.9 Hz, 1H), 2.90 (d, *J* = 5.9 Hz, 2H), 2.45 (dd, *J* = 14.8, 11.2 Hz, 1H), 1.88-1.55 (m, 4H).^{13}C-NMR (101 MHz, D_2O) δ 175.3, 174.2, 172.1, 171.5, 170.5, 156.8, 135.8, 135.1, 129.2,128.9, 128.3 128.1, 127.7, 126.8, 66.6, 59.1, 57.7, 54.2, 50.1, 49.7, 47.2, 41.6, 40.7, 40.4, 39.8, 37.3, 27.5, 24.4

Compound 2.77:

^{1}H-NMR (400 MHz, CD_3OD) δ 7.48-7.15 (m, 10H), 5.20 (d, *J* = 15.4 Hz, 1H), 4.68-4.56 (m, 2H),4.50 (dd, *J* = 9.4, 2.4 Hz, 1H), 4.43-4.37 (m, 1H), 4.27 (d, *J* = 5.4 Hz, 1H), 4.19 (d, *J* = 15.4 Hz,1H), 4.07 (d, *J* = 8.8 Hz, 1H), 4.03 (d, *J* = 5.4 Hz, 1H), 3.75-3.65 (m, 2H), 3.13 (dd, *J* = 11.7, 6.5Hz, 2H), 2.96 (dd, *J* = 15.3, 8.6 Hz, 1H), 2.83 (dd, *J* = 14.5, 2.4 Hz, 1H), 2.67 (dd, *J* = 15.3, 3.8 Hz,1H), 2.55 (dd, *J* = 14.5, 9.5 Hz, 1H), 1.94-1.83 (m, 1H), 1.62-1.48 (m, 3H), 1.32-1.20 (m, 2H); ^{13}C-NMR (101 MHz, CD_3OD, HSQC projection) δ 135.2, 129.2, 129.0, 128.3, 127.7, 126.7, 59.7, 56.3, 53.2, 52.2, 47.8, 40.5, 39.4, 36.5, 26.9, 24.4

HPLC TRACE OF THE FINAL PRODUCT 2.76

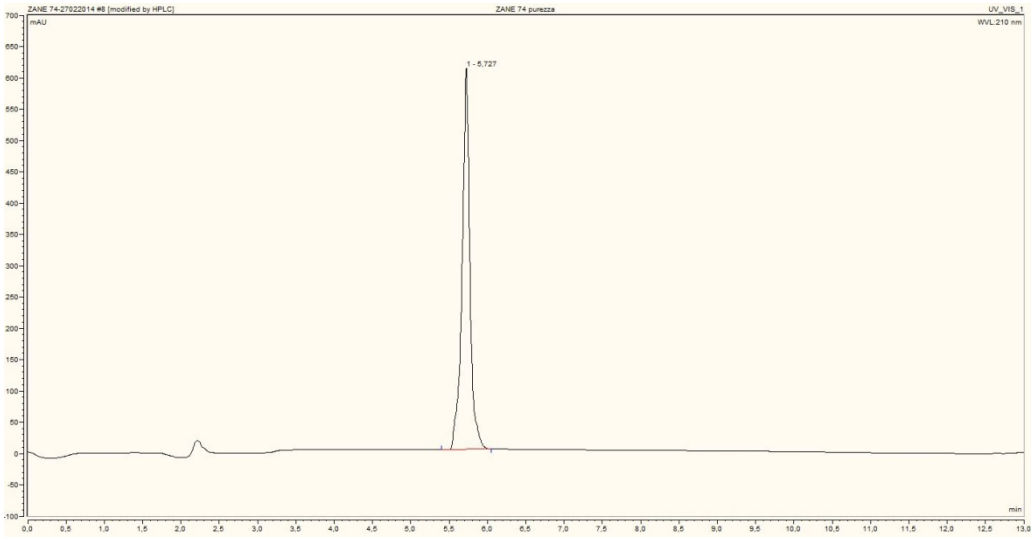

Purity: ≥99%

HPLC TRACE OF THE FINAL PRODUCT 2.77

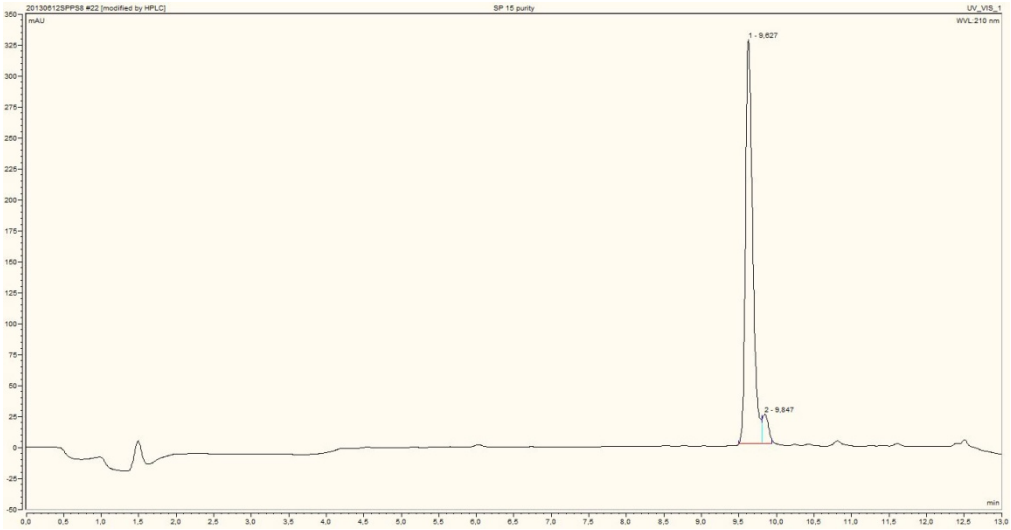

Purity: 94%

CHAPTER 3

DKP-RGD MAGNETIC NANOPARTICLES CONJUGATES

3.1 Aim of the project

The aim of this part of the work was the "active targeting" of MNPs to specific type of cells in order to allow hyperthermia therapy. The strategy of "active targeting" consists in adding to the surface of MNPs ligands such as small molecules, peptides, antibodies or antibodies fragments, and nucleic acids to activate the molecular recognition of the cells through the ligand-receptor binding. In particular, we were interested in obtaining bioconjugates between MNPs and *cyclo*-RGD integrin ligand peptidomimetics to target $\alpha_v\beta_3$ overexpressing cells. We planned to obtain the bioconjugation by a Cu(I)-catalyzed Azide-Alkyne Click chemistry (CuAAC) reaction between the azide component containing the *cyclo*-RGD integrin ligand peptidomimetics and the alkyne component linked to the MNPs.

3.2 Hyperthermia and magnetic nanoparticles

3.2.1 Hyperthermia

Hyperthermia (also named thermal therapy or thermotherapy) is a cancer treatment in which a tissue is exposed to high temperatures (up to 45°C). The use of increased temperature for therapeutical purposes has been reported for many centuries: a first evidence could be found in the Egyptian Edwin Smith surgical papyrus (dated around 3000BC). Later (19th and 20th centuries) radiofrequency techniques have been investigated as a method to produce heating, as well as fever therapy [170]. High temperatures can damage and kill cancer cells without affecting in a relevant manner normal tissues.[171] The *in vivo* moderate selectivity for tumor tissues (achieved between 40°C and 44°C) is reached thanks to a characteristic difference between normal and tumor physiology which is present in tumor regions with hypoxia and low pH, while it cannot be found in normal healthy tissues.[172] These regions are more sensitive to high temperatures. Cell death occurs probably by protein denaturation and consequent cytoskeleton and membranes alterations. Moreover, changes in enzyme complexes for DNA synthesis and repair occur. [173] Hyperthermia has been used as monotherapy treatment or, almost always, in association with radiation therapy and chemotherapy.[174]

Heating tissues causes an increase blood flow, and a consequent higher sensitivity to radiotherapy (because of the improved tissue oxygenation [175]) or to chemotherapy (because of the major amount of cytotoxic agent that reaches the tumor). The supra-additive effect of the combination hyperthermia-radiotherapy is mediated both by a direct action on cells that cannot be damaged by radiations and sensitizing cancer cells to radiations.[176] In addition, hyperthermia is also able to potentiate radiations effects because it interferes with the cellular repair of radiation-induced DNA damage, probably acting on cellular proteins.[177]

Hyperthermia has also been studied in association with chemotherapy and various examples can be found in the literature proving that hyperthermia is able to enhance the effects of certain anticancer drugs (if given in close sequence to the drug treatment).[178] A deep analysis of this application is beyond the scope of this thesis, however an extensive

[170] Seegenschmiedt, M. H.; Veron, C.C. in "Thermoradiotherapy and Thermochemotherapy", *1*, (Berlin: Springer Verlag), **1995**, 3-4
[171] Van der Zee, J., *Annals of Oncology* **2002**, *13*, 1173-1184
[172] Reinhold, H. S.; Endrich, B., *Int. J. Hyperthermia* **1986**, *2*, 111-137
[173] (a) Streffer, C. in "Thermoradiotherapy and Thermochemioterapy ", *1* (Berlin: Springer Verlag), **1995**, 47-74; (b) Hildebrandt, B.; Wust, P.; Ahlers, O.; Dieing, A.; Sreenivasa, G.; Kerner, T.; Felix, R.; Riess, H., *Critical Reviews in Oncology/Hematology* **2002**, *43(1)*, 33–56
[174] Wust, P.; Hildebrandt, B.; Sreenivasa, G.; Rau, B.; Gellermann, J.; Riess, H.; Felix, R.; Schlang, P. M., *The Lancet Oncology* **2002**, *3(8)*, 487–497
[175] Song, C. W. M.; Shakil, A.; Griffin, R. J.; Okajima, K., *Semin. Oncol.* **1997**, *24*, 626-632
[176] Raaphorst, G. P. in "An Introduction to the Practical Aspects of Clinical Hyperthermia (London: Taylor and Francis), **1990**, 10-54
[177] Kampinga, H. H.; Dikomey, E., *Int. J. Radiat. Biol.* **2001**, *77*, 399-408
[178] For example see: (a) Engelhard, R., *Recent Results Cancer Res.* **1987**, *104*, 136-203, (b) Hanhn, G. M., *Cancer Res.* **1979**, *39*, 2264-2268; (c) Dahl, O.; Mella, O., *Anticancer Res.***1982**, *2*, 359-364

review on the combination of hyperthermia with chemotherapy was published in 1995.[179] In addition to the enhanced tissue perfusion, guarantee by the increased blood flow, it was shown a reduction of the drug resistance and an increase of the intracellular drug uptake.[171]

3.2.2 Magnetic nanoparticles

Magnetic nanoparticles (MNPs) are interesting in various research fields: magnetic fluid, [180] catalysis, [181] biotechnology/biomedicine, [182] data storage, [183] environmental remediation.[184] The synthesis of MNPs could be performed according to many different procedures, however the stability of the particles over a range of different conditions is one big limitation to their applications.

3.2.2.1 Application of MNPs in hyperthermia

MNPs offer some attractive possibilities in biomedicine because of their peculiar properties. First, the controllable size. Since the size is ranging from a few nanometers up to tens of nanometers, it is smaller than or comparable to cells (10-100 μm), viruses (20-450 nm), proteins (5-50 nm) or genes (2nm wide and 10-100 nm long) size. Because of this, MNPs can interact with or bind to a biological entity that can be targeted or addressed in such a way. Second, particles can be manipulated by an external magnetic field gradient delivering anticancer drugs, or radionuclide atoms, to a targeted region of the body. Third, MNPs are responsive to a time-varying magnetic field and for example they can be made to heat up thus delivering heat to the surrounding areas.[185] As a result, MNPs find applications as hyperthermia agents[186], drug delivery carriers[187], and as MRI contrast enhancement agents[182,188]. Among all these applications, hyperthermia will be deepened as it was hypothesized as application for *Cyclo*[RGD-DKP*f*3]-MNPs conjugates.

---

[179] Dahl, O. in "Thermoradiotherapy and Termochemoterapy", *1* (Berlin: Springer Verlag) **1995**, 103-121

[180] Chikazumi, S.; Taketomi, S.; Ukita, M.; Mizukami, M.; Miyajima, H.; Setogawa, M.; Kurihara, M., *J. Magn. Mater.* **1987**, *65*, 245-251

[181] (a) Lu, A.-H.; Schmidt, W.; Matoussevitch, N.; Bönnermann, H.; Spliethoff, B.; Tesche, B.; Bill, E.; Kiefer, W.; Schüt, F., *Angew. Chem. Int. Ed.* **2004**, *43*, 4303-4306; (b) Tsang, S. C.; Caps, V.; Paraskevas, I.; Chadwick, D.; Thompsett, D., *Angew. Chem. Int. Ed.* **2004**, *43*, 5645-5649

[182] (a) Gupta, A. K.; Gupta, M., *Biomaterials* **2005**, *26*, 3995-4021; (b) Mornet, S.; Vasseur, S.; Grasset, F.; Verveka, P.; Goglio, G.; Demourgues, A.; Portier, J.; Pollert, E.; Duguet, E., *Prog. Solid State Chem.* **2006**, *34*, 237; (c) Li, Z.; Wei, L.; Gao, M. Y.; Lei, H., *Adv. Mater.* **2005**, *17*, 1001-1005

[183] Hyeon, T., *Chem. Commun.* **2003**, 927-934

[184] (a) Elliott, D. W.; Zhang, W.-X., *Environ. Sci. Technol.* **2001**, *35*, 4922-4926; (b) Takafuji, M.; Ide, S.; Ihara, H.; Xu, Z., *Chem. Mater.* **2004**, *16*, 1977-1983

[185] Pankhurst, Q. A.; Connolly, J.; Jones, S. K.; Dobson, J., *J. Phys. D: Appl. Phys.* **2003**, *36*, R167-R181

[186] See references in paragraph 3.1.2.1

[187] For example see: (a) Widder, K. J.; Senyei, A. E.; Scarpelli, D. G., *Proc. Soc. Exp. Biol. Med.* **1987**, *58*, 141-146; (b) Senyei, A.; Widder, K.; Czerlinski, C., *J. Appl. Phys.* **1987**, *49*, 3578-3583; (c) Mosbach, K.; Schröder, U., *FEBS Lett.* **1979**, *102*, 112-116; (d) Alexiou, C.; Arnold, W.; Klein R. J.; Parak, F. G.; Hulin, P.; Bergemann, C.; Erhardt, W.; Wagenpfeil, S.; Lübbe, A. S., *Cancer Res.* **2000**, *60*, 6641-6648; (e) Lübbe, A. S.; Bergemann, C.; Huhnt, W.; Fricke, T.; Reiss, H.; Brock, J. W.; Huhnt, D., *Cancer Res.* **1996**, *56*, 4694-4701; (f) Lübbe, A. S.; Bergemann, C.; Riess, H.; Schriever, F.; Reichardt, P.; Possinger, K.; Matthias, M.; Doerken, B.; Herrmann, F.; Guertler, R., *Cancer Res.* **1996**, *56*, 4686-4693 (g) Häfeli, U. O.; Casillas, S.; Dietz, D. W.; Pauer, G. J.; Rybiki, L. A.; Conzone, S. D.; Day, D. E., *Int. J. Radiat. Oncol. Biol. Phys.* **1999**, *44*, 189-200; (h) Häfeli, U.; Pauer G.; Failing, F.; Tapolsky, G., *J. Magn Mater.* **2001**, *225*, 73-78

[188] For example see: (a) Lawaczeck, R.; Bauer, H.; Frenzel, T.; Hasegawa, M.; Ito, Y.; Kito, K.; Miwa, N.; Tsutsui, H.; Vogler, H.; Weinmann, H. *J., Acta Radiol.* **1997**, *38*, 584-597; (b) Weissleder, R.; Elizondo, G.; Wittenburg, J.; Rabito, C. A.; Bengele, H. H.; Josephson, L., *Radiol.* **1990**, *175*, 489-493; (c) Ruehm, S. G.; Corot, C.; Vogt, P.; Kolb, S.; Debatin, J. F., *Circulation* **2001**, *103*, 415-422; (d) Wacker, F. K.; Reither, K.; Ebert, W.; Wendt, M.; Lewin, J. S.; Wolf, K. J.,

Ferromagnetic material (FM) are magnetic even without an applied field, while superparamgnetic material (SPM) exhibit a magnetic behavior only when inserted into a magnetic field. These second class of material has emerged as the best one for hyperthermia because it requires lower magnetic field strengths to produce an useful amount of heating. The challenge in humans is to generate enough heat using clinical safe field conditions (high magnetic fields can have dangerous effects[189]). When a magnetic field is applied, there is a constant flow of energy into the magnetic material and this energy will be transferred into thermal energy. This is the physical basis of magnetic hyperthermia. Therapeutic efficacy of magnetically mediated hyperthermia was proved in animals model[190] and different devices were developed to heat selectively malignant cells.[171,174,191] The first evidences regarding the use of magnetic materials in hyperthermia date back to 1957[192] and since then many different publications concerning that topic have been written.[193] Since most of the hyperthermia devices cannot avoid the heating of healthy tissues, magnetic particles hyperthermia offers a way to heat only the targeted tissue(s) by selective delivery of MNPs.

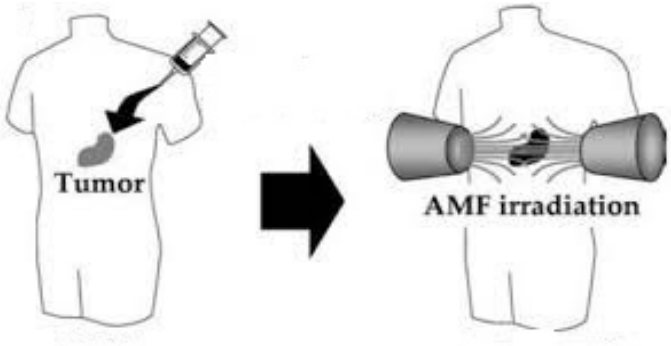

Figure 3.1 – Magnetic hyperthermia: MNPs are selectively delivered to the tumor tissues and then heated up through the application of an external magnetic field

Radiology, **2003**, *226*, 459-464; (e) Dosset, V.; Gomez, C.; Petry, K. G.; Delalande, C.; Caille, J.-M., *Magn. Res. Mater. Phys. Biol. Med.***1999**, *8*, 185-189; (f) Michel, S. C. A.; Keller, T. M.; Frohlich, J. M.; Fink, D.; Caduff, R.; Seifert, B.; Marincek, B.; Kubik-Huch, R. A., *Radiology*, **2002**, *225*, 527-536; (g) Semelka, R. C.; Helmberger, T. K. G., *Radiology* **2001**, *218*, 27-38; (h) Enochs, W. S.; Harsh, G.; Hochberg, F.; Weissleder, R., *J. Magn. Res. Imag.* **1999**, *9*, 228-232; (i) Bulte, J.; De Cuyper, M.; Despres, D.; Frank, J., *J. Magn. Res. Imag.* **1999**, *9*, 329-335; (j) Weissleder, R.; Moore, A.; Mahmood, U.; Bhorade R.; Benveniste, H.; Chiocca, E. A.; Basilion, J. P., *Nature Med.* **2000**, *6*, 351-354; (k) Zhao, M.; Beauregard, D.; Loizou, L.; Davletov, B.; Brindle, K., *Nature Med.* **2001**, *7*, 1241-1244

[189] (a) Oleson, J. R.; Cetas, T. C.; Corry, P. M., *Radiat. Res.* **1983**, *95*, 175-186; (b) Reilly, J. P., *Ann. New York Acad. Sci.*, **1992**, *649*, 96-117

[190] Moroz, P.; Jones, S. K.; Gray, B. N., *Int. J. Hyperthermia* **2002**, *18*, 267-284

[191] Moroz, P.; Jones, S. K.; Gray, B. N., *J. Surg. Oncol.* **2001**, *77*, 259-269

[192] Gilchrist, R. K.; Medal, R.; Shorey, W. D.; Hanselman, R. C.; Parrott, J. C.; Taylor, C. B., *Ann. Surg.* **1957**, *146*, 596-606

[193] For example see: (a) Gordon, R. T.; Hines, J. R.; Gordon, D., *Med. Hypotheses* **1979**, *5*, 83-102; (b) Borrelli, N. F.; Luderer, A. A.; Panzarino, J. N., *Phys. Med. Biol.* **1984**, *29*, 487-494; (c) Suzuki, S.; Arai, K.; Koike, T.; Oguchi, K., *J. Japan. Soc. Cancer Therapy* **1990**, *25*, 2649-2658; (d) Chan, D. C. F.; Kirpotin, D. B.; Bunn, P. A. Jr., *J. Magn. Magn. Mater.* **1993**, *122*, 374-378; (e) Mitsumori, M.; Hiraoka, M.; Shibata, T.; Okuno, Y.; Nagata, Y.; Nishimura, Y.; Abe, M.; Hasegawa, M.; Nagae, H.; Ebisawa, Y., *Hepato-gastroenterology* **1996**, *43*, 1431-1437; (f) Shinkai, M.; Yanase, M.; Suzuki, M.; Honda, H.; Wakabayashi, T.; Yoshida, J.; Kobayashi, T., *J. Magn. Magn. Mater.* **1999**, *194*, 176-184; (g) Hilger, I.; Fruhauf, K.; Andra, W.; Hiergeist, R.; Hergt, R.; Kaiser, W. A., *Acad. Radiol.* **2002**, *9*, 198-202

3.2.2.2 Synthesis and coating of MNPs: general methods

MNPs of different compositions are reported in the literature: oxides (such as Fe_3O_4 and γ-Fe_2O_3)[194], pure metals (such as Fe and Co)[195], spinel-type ferromagnets (such as $MgFe_2O_4$, $MnFe_2O_3$, and $CoFe_2O_4$)[196], alloys (such as $CoPt_3$ and FePt)[197]. Several methods directed to the synthesis of high-quality MNPs are reported. Since comprehensiveness is not the purpose of this work, only some examples will be taken into account.

Co-precipitation is an useful protocol to prepare Fe_3O_4 and γ-Fe_2O_3 MNPs starting from aqueous Fe^{2+}/Fe^{3+} salt solutions by addition of a base under inert atmosphere at room temperature or at elevated temperature. Depending on the type of salt, the Fe^{2+}/Fe^{3+} ratio, the reaction temperature, the pH value and the ionic strength of the media, MNPs with different sizes, shapes and compositions can be produced. However once the reaction conditions are set, the quality of MNPs is reproducible even if the particle size distribution is not narrow. The resulting MNPs are stabilized by repulsive electrostatic forces because of the positive charge.[198] The effects of several organic anions were extensively studied[199]: chelation of the metal ions and adsorption of additives on the nuclei act in an opposite way. As a matter of facts, chelation leads to the formation of a small number of nuclei that then grow up while absorption of additives may inhibit the growth of the particles, which favors the formation of small units. A proper organic additive acting as stabilizer and reducing agents are useful tools to produce monodisperse Fe_3O_4 MNPs. The best one resulted the oleic acid.[200]

Thermal decomposition in non-aqueous media was developed as a method to synthesize high quality semiconductor nanocrystals.[201] Also MNPs could be obtained by thermal decomposition of organometallic compound in high-boiling organic solvents containing stabilizing surfactants.[196b,202] The ratios of all the starting materials, the reaction temperature, and the reaction time are crucial parameters to control the size and the morphology of the MNPs. A zerovalent metal in the precursor lead to oxide MNPs but there are two-step procedures that give oxide MNPs.[201a,203] For example Peng and co-workers

---

[194] (a) Neveu, S.; Bee, A.; Robineau, M.; Talbot, D.; *J. Colloid Interface Sci.* **2002**, *255*, 293-298; (b) Grasset, F.; Labhsetwar, N.; Li, D.; Park, D. C.; Saito, N.; Haneda, H.; Cador, O.; Roisnal, T.; Mornet, S.; Duguet, E.; Portier, J.; Etourneau, J., *Langmuir* **2002**, *18*, 8209-8216; (c) Sun, S.; Zeng, H., *J. Am. Chem. Soc.* **2002**, *124*, 8204-8205; (d) Ge, J.; Hu, Y.; Biasini, M.; Dong, C.; Guo, J.; Beyermann, W. P.; Yin, Y., *Chem. Eur. J.***2007**, *13*, 7153-7161

[195] (a) Park, S.-J.; Kim, S.; Lee, S.; Khim, Z.; Char, K.; Heyeon, T., *J. Am. Chem. Soc.* **2000**, *122*, 8581-8582; (b) Puntes, V. F.; Krishan, K. M.; Alivisatos, A. P., *Science* **2001**, *291*, 2115-2117

[196] (a) Chen, Q.; Rondinone, A. J.; Chakoumakos, B. C.; Zhang, Z. J., *J. Magn. Magn. Mater* **1999**, *194*, 1; (b) Park, J.; An, K.; Hwang, Y.; Park, J.-G.; Noh, H.-J.; Kim, J.-Y.; Park, J.-H.; Hwang, N.-M.; Heyeon, T., *Nat. Mater.* **2004**, *3*, 891-895

[197] (a) Sun, S.; Murray, C. B.; Weller, D.; Folks, L.; Moser, A., *Science* **2000**, *287*, 1989-1992; (b) Shevchenko, E. V.; Talapin, D. V.; Rogach, A. L.; Kornowski, A.; Haase, M.; Weller, H., *J. Am. Chem. Soc.* **2002**, *124*, 11480-11485

[198] Bee, A.; Massart, R.; Neveu, S., *J. Magn. Magn. Mater.***1995**, *149*, 6-9

[199] (a) Ishikawa, T.; Kataoka, S.; Kandori, K., *J. Mater. Sci.* **1993**, *28*, 2693-2698; (b) Ishikawa, T.; Takeda, T.; Kandori, K., *J. Mater. Sci.* **1992**, *27*, 4531-4535; (c) Kandori, K.; Kawashima, Y.; Ishikawa, T., *J. Colloid Interface Sci.* **1992**, *152*, 284-288

[200] (a) Willis, A. L.; Turro, J. N.; O'Brien, S., *Chem. Mater.* **2005**, *17*, 5970-5975; (b) Cushing, B. L.; Kolesnichenko, V. L.; O'Connor, C. J., *Chem. Rev.* **2004**, *104*, 3893-3946

[201] (a) Murray, C. B.; Norris, D. J.; Bawendi, M. G., *J. Am. Chem. Soc.* **1993**, *115*, 3893; (b) Peng, X.; Wickham, J.; Alivisatos, A. P., *J. Am. Chem. Soc.* **1998**, *120*, 5343-5344; (c) O'Brien, S.; Brus, L.; Murray, C. B., *J. Am. Chem. Soc.* **2001**, *123*, 12085-12086

[202] (a) Sun, S.; Zeng, H.; Robinson, D. B.; Raoux, S.; Rice, P. M.; Wang, S. X.; Li, G., *J. Am. Chem. Soc.* **2004**, *126*, 273-279; (b) Redl, F. X.; Black, C. T.; Papaefthymiou, G. C.; Sandstorm, R. L.; Yin, M.; Zeng, M.; Murray, C. B.; O'Brien, S. B., *J. Am. Chem. Soc.* **2004**, *126*, 14583-14599

[203] For example see: (a) Heyeon, T.; Lee, S. S.; Park, J.; Chung, Y.; Na, H. B., *J. Am. Chem. Soc.* **2001**, *123*, 12798-12801

developed a general decomposition approach for the synthesis of Fe_3O_4 nanocrystals[204] that was later generalized to other metal oxides (Cr_2O_3, MnO, Co_3O_4, NiO). A similar protocol was also used by Hyeon and co-workers to prepare Fe_3O_4 MNPs with size depending on the decomposition temperature and on the aging period. The obtained MNPs are dispersible in organic solvent.[202] This method was also used to prepare metal MNPs, for example Co MNPs[205] or nanodisks[195,206] or nanorods[207].

A microemulsion is a thermodynamically stable isotropic dispersion of two immiscible liquids stabilized by an interfacial film of surfactants molecules.[208] The size of the reverse micelle is determined by the molar ratio of the co-solvent and surfactants.[209] For example metallic cobalt, cobalt/platinum alloys, and gold-coated cobalt/platinum nanoparticles were synthesized in reverse micelles.[210] Also $MnFe_2O_4$ MNPs with controllable sizes (depending on the ratio solvent/co-solvent) were synthesized through the formation of water-in-toluene inverse micelles with sodium dodecylbenzensulfonate as surfactant.[211] This techniques allows to obtain spheroids or particles with an oblong cross section.[212] However, the particle size is varying over a relative wide range, yields are lower than with other methods and large amounts of solvents are required.

Li and co-workers reported a general hydrothermal methods which allows the synthesis of a various range of nanostructured materials.[213] At the interfaces of the solid, liquid, and solution phases in the reaction mixture, phase transfer and separation mechanisms occur. These events are at the basis of the hydrothermal method.

[204] Jana, R. L.; Chen, Y.; Peng, X., *Chem. Mater.* **2004**, *16*, 3931-3935
[205] Song, Q.; Zhang, Z. J., *J. Am. Chem. Soc.* **2004**, *126*, 6164-6168; (b) Bönnemann, H.; Brijoux, W.; Brinkmann, R.; Matoussevitch, N.; Waldoefner, N.; Palina, N.; Modrow, H., *Inorg. Chim. Acta* **2003**, *350*, 617-6124
[206] Puntes, V. F.; Zanchet, D.; Erdonmez, C. K.; Alivisatos, A. P., *J. Am. Chem. Soc.* **2002**, *124*, 12874-12880
[207] (a) Cordente, N.; Respaud, M.; Senocq, F.; Casanove, M.-J.; Amiens, C.; Chaudret, B., *Nano Lett.* **2001**, *1*, 565-568; (b) Dumestre, F.; Chaudret, B.; Amiens, C.; Fromen, M.-C.; Casanove, M.-J.; Respaud, P.; Zurcher, P., *Angew. Chem. Int. Ed.* **2002**, *41*, 4286-4289; (c) Dumestre, F.; Chaudret, B.; Amiens, C.; Respaud, M.; Fejes, P.; Renaud, P.; Zurcher, P., *Angew. Chem. Int. Ed.* **2003**, *42*, 5213-5216
[208] Langevin, D., *Annu. Rev. Phys. Chem.* **1992**, *43*, 341-369
[209] Paul, B. K.; Moulik, S. P., *Curr. Sci.* **2001**, *80*, 990-1001
[210] Carpenter, E. E.; Seip, C. T.; O'Connor, C. J., *J. Appl. Phys.* **1999**, *85*, 5184-5186
[211] Liu, C.; Zou, B.; Rondinone, A. J.; Zhang, Z., *J. Phys. Chem. B* **2000**, *104*, 1141-1145
[212] Tan, W.; Santra, S.; Zhang, P.; Tapec, R.; Dobson, J., US Patent 6548264, **2003**
[213] Wang, X.; Zhuang, J.; Peng, Q.; Li, Y., *Nature*, **2005**, *437* 121-124

In table 3.1 is reported a short summary on the different synthetic techniques.

Method	Synthesis	Reaction T (°C)	Reaction time	Sol.	Size distribution	Shape control	Yield
Co-precipitation	Very simple, ambient conditions	20-90	Minutes	Water	Relatively narrow	Not good	High/ scalable
Thermal decomposition	Complicated, inert atmosphere	100-320	Hours-days	Organic	Very narrow	Very good	High/ scalable
Microemulsion	Complicated, ambient conditions	20-50	Hours	Organic	Relatively narrow	Good	Low
Hydrothermal synthesis	Simple, high pressure	220	Hours ca. days	Water-ethanol	Very narrow	Very good	Medium

Table 3.1 – Summary comparison on the synthetic methods

Underlined the best advantage of each technique: co-precipitation is the preferred route in terms of synthesis simplicity, thermal decomposition is the best one in terms of size and morphology and hydrothermal synthesis allows to obtain a very narrow size distribution range.

Long time stability and suspendibility in solvents without agglomeration of these particle are an important requirements for almost any application. Pure metals and their alloys are instable towards oxidation in air and this susceptibility becomes higher the smaller the particles are. Two main solutions were developed: synthesize nanoparticles with a core-shell structure (that means naked magnetic nanoparticles as a core and an isolating shell coating), or synthesize MNPs dispersed in a solid matrix (that means embedded MNPs, fixed in space relative to each other)[214]. In this latter approach MNPs can be dispersed in a continuous matrix, or they can be dispersed in coating/larger particles, or they can agglomerate of individual nanoparticles which are connected through their protective shells. For what concerns MNPs coating, there are three main options: oxides (created by mild oxidation of the MNPs surface[205b,215] or additionally deposited[216]) or organic shell (surfactant and polymers[217]) or inorganic components (mainly silica,[218] carbon,[219] precious metals such as Ag,[220] Au[221]). Moreover, further modifications of the MNPs surface can be achieved by anchoring molecules to the shell of the MNPs, creating new materials with specific functions.[222]

[214] (a) Stoeva, S. I.; Huo, F.; Lee J.-S.; Mirkin, C. A., *J. Am. Chem. Soc.* **2005**, *127*, 15362-15363; (b) Yi, D. K.; Selvan, S. T.; Lee, S. S.; Papaefthymiou, G. C.; Kundaliya; Ying, J. Y., *J. Am. Chem. Soc.* **2005**, *127*, 4990-4991; (c) Caruso, F.; Spasova, M.; Susha, A.; Giersig, M.; Caruso, R. A., *Chem. Mater.* **2001**, *13*, 109-116

[215] (a) Peng, D. L.; Sumiyama, K.; Hihara, T.; Yamamuro, S.; Konno, T. J., *Phys. Rev. B* **2000**, *61*, 3103

[216] Nunez, N. O.; Tartaj, P.; Morales, M. P.; Bonville, P.; Serna, C. J., *Chem. Mater.* **2004**, *16*, 3119-3124

[217] (a) Euliss, L. E.; Grancharov, S. G.; O'Brien, S.; Deming, T. J.; Stucky, G. D.; Murray, C. B.; Held, G. A., *Nano Lett.* **2003**, *3*, 1489-1493; (b) Liu, X.; Guan, Y.; Ma, Z.; Liu, H., *Langmuir* **2004**, *20*, 10278-10282; (c) Hong, R.; Fischer, N. O.; Emrik, T.; Rotello, V. M., *Chem. Mater.* **2005**, *17*, 4617-4621; (d) Sahoo, Y.; Pizem, H.; Fried, T.; Golodnitsky, D.; Burstein, L.; Sikenik, C. N.; Markovich, G., *Langmuir* **2001**, *17*, 7907-7911; (e) Kim, M.; Chen, Y.; Liu, Y.; Peng, X., *Adv. Mater.* **2005**, *17*, 1429-1432

[218] For example see: Kobayashi, Y.; Horie, M.; Konno, M.; Rodriguez-Gonzalez, B.; Liz-Marzan, L. M., *J. Phys. Chem. B.* **2003**, *107*, 7420-7425

[219] Lu, H.-A.; Li, W.; Matoussevitch, N.; Spliethoff, B.; Bönnemann, H.; Schüth, F., *Chem. Comm.* **2005**, 98-100

[220] Sobal, N. S.; Hilgendorff, M.; Moehwald, H.; Giersig, M.; Spasova, M.; Radetic, T.; Farle, M., *Nano Lett.* **2002**, *2*, 62

[221] (a) Liu, Q.; Xu, Z.; Finch, J. A.; Egerton, R., *Chem. Mater.***1998**, *10*, 3936-3940; (b) Lin, J.; Zhou, W.; Kumbhar, A.; Wiemann, J.; Fang, J.; Carpenter, E. E.; O'Connor, C. J., *J. Solid State Chem.* **2001**, *159*, 26-31

[222] (a) Kainz, Q. M.; Fernandes, S.; Eichenseer, C. M.; Besostri, F.; Körner, H.; Müller, R.; Reiser, O., *Faraday Discuss.* **2014**, *175*, 27-39; (b) Salgueiriño-Maceira, V.; Correa-Duarte, M. A.; Farle, M.; López-Quintela, A.; Sieradzki, K.; Diaz, R., *Chem. Mater.* **2006**, *18*, 2701-2706; (c) Deng, Y.; Yang, W.; Wang, C.; Fu, S., *Adv. Mater.* **2003**, *15*, 1729-1732; (d) Frankamp, B. L.; Fischer, N. O.; Hong, R.; Srivastava, S.; Rotello, V. M., *Chem. Mater.* **2006**, *18*, 956-959

Since a comprehensive treatment of the topic is beyond the purpose of this thesis, only the techniques involved in the *Cyclo*[DKP*f*3-RGD] conjugates preparation will be considered in the corresponding paragraph.

3.3 Polyethylenimine magnetic nanoparticles (PEI MNPs)

PEI MNPs (Figure 3.2) have a cobalt core, a protective carbon shell and a further polyethylenimine coating which confers water dispersibility and the chance of a further functionalization.

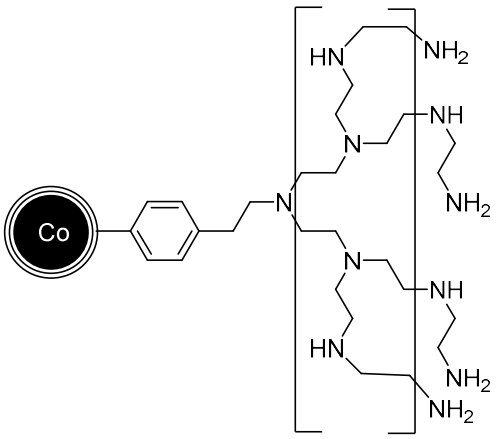

3.1

Figure 3.2 – Co/C PEI MNPs

Co/C MNPs (Figure 3.3) were successfully produced by Stark and co-workers through a flame-spray procedure.[223] The addition of acetylene to the Co-MNPs-forming process resulted in the deposition of carbon on the particles.

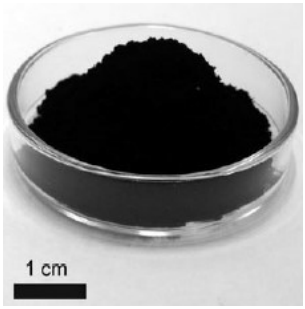

Figure 3.3 – Co/C MNPs

TEM pictures revealed that several carbon layers coated the particles in an onion-type arrangement. The produced MNPs exhibited excellent magnetic properties with a saturation magnetization of 158 Am^2/Kg. As a consequence, recovery from a suspension is fast and complete (Figure 3.4).

[223] Grass, R. N.; Stark, W. J., *J. Mater. Chem.* **2006**, *16*, 1825-1830

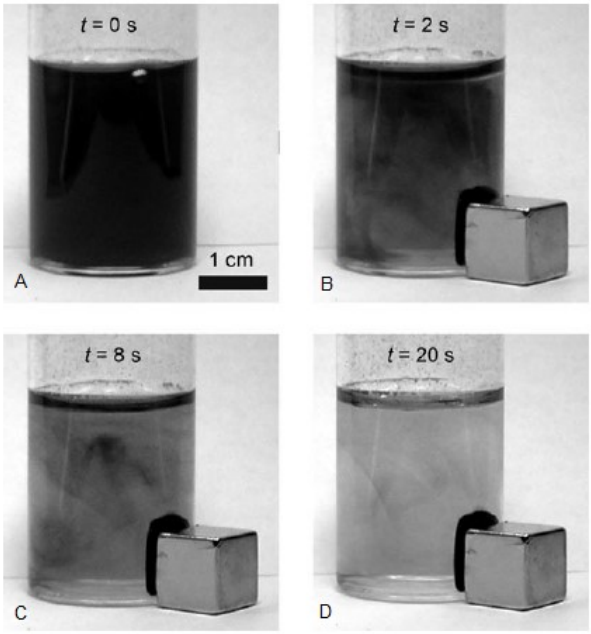

Figure 3.4 – Co/c MNPs recovery through an external magnet

These functionalized MNPs were selected to produce the bioconjugates with the cyclic RGD-peptidomimetic because carbon-based materials have many advantages over polymer or silica, such as much higher chemical and thermal stability as well as biocompatibility. Carbon-coated nanoparticles are usually in the metallic state, and thus have a higher magnetic moment than the corresponding oxides. The graphitic carbon layers provide an effective barrier against acid leaching and oxidation.[224] The main problem of carbon-coated MNPs is related to their synthesis: the formation mechanism is usually quite not understood and it often leads to agglomerated clusters instead of single units. Various synthetic strategies were developed to lay down the protective shell around nanoparticles: for example carbon-encapsulated metal or metal carbide nanocrystallites can be generated by the Krätschmer arc-discharge process[225] or under laser ablation, and electron irradiation. [226] Gedanken and co-workers reported a sonochemical procedure that leads to air-stable cobalt nanoparticles in which the high stability arises from the formation of the carbon shell. However, MNPs produced in this way are rather polydispersed.[227] As further example can be mentioned the work of Johnson et al., that described the synthesis of Fe and Fe_3C nanoparticles by direct pyrolisis of iron stearate at 900°C under an argon atmosphere[228], and the Co/C MNPs of Lu et al.[219]

[224] Chan, H. B. S.; Ellis, B. L.; Sharma, H. L.; Frist, W.; Caps, V.; Shields, S. C.; Tsang, S. C:, *Adv. Mater.* **2004**, *16*, 144-149
[225] Scott, J. H. J.; Majetich, S. A., *Phys. Rev. B* **1995**, *52*, 12564
[226] (a) Ang, K. H.; Alexandrou, I.; Mathur, N. D.; Amaratunga, G. A. J.; Haq, S., *Nanotechnology* **2004**, *15*, 520; (b) Teunissen, W.; De Grot, F. M. F.; Geus, J.; Stephan, O.; Tence, M.; Colliex, C., *J. Catal.* **2001**, *204*, 169-174; (c) Hayashi, T.; Hirono, S.; Tomita, M.; Umemura, S., *Nature* **1996**, *381*, 772-774; (d) Nesper, R.; Ivantchenko, A.; Krumeich, F., *Adv. Funct. Mater.* **2006**, *16*, 296-305
[227] Nikitenko, S. I.; Koltypin, Y.; Palchin, O.; Felner, I.; Xu, X. N.; Gedanken, A., *Angew. Chem. Int. Ed.* **2001**, *40*, 4447-4449
[228] Geng, J.; Jefferson, D. A.; Johnson, B. F. G., *Chem. Commun.* **2004**, 2442-2443

3.3.1 Co/C MNPs

The diazonium chemistry was used to covalently functionalize graphene coated MNPs.[229] The mechanism (Scheme 3.1) involves an electron transfer reaction. A graphene electron is transferred to the adsorbed diazonium ion, generated by the thermal decomposition of the diazonium salt, and nitrogen is released. As a consequence, a phenil radical, more reactive, is formed. This radical reacts with the carbon surface[230], even if the reaction is rather unspecific (simultaneous polymerization can occur).

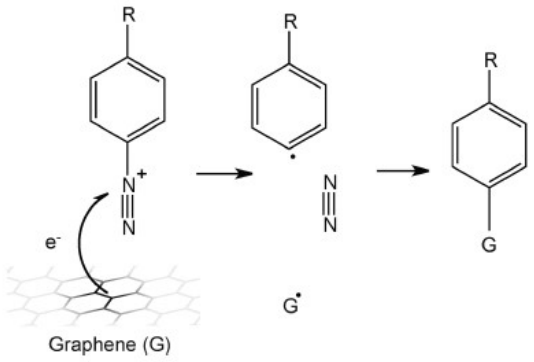

Scheme 3.1 – Mechanism for the diazonium reaction with the graphene surface

Organic chemistry on metal nanoparticles bound graphene has yielded a broad range of accessible structures (Figure 3.5).

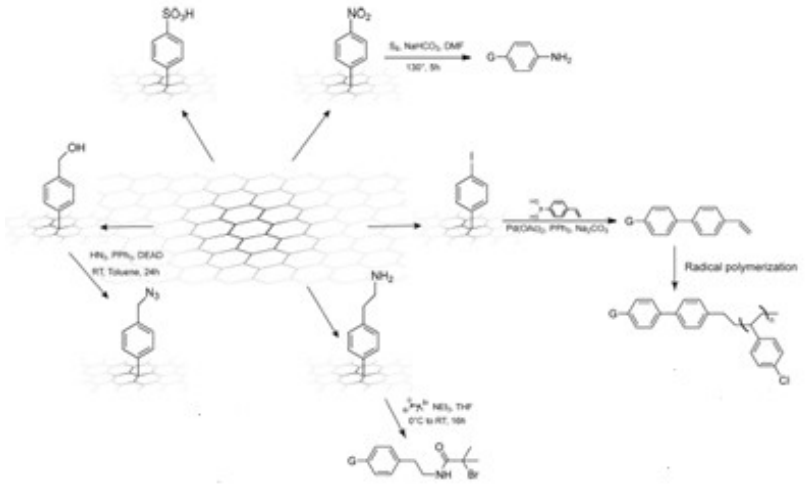

Figure 3.5 – Diazonium salt chemistry on graphene: accessible structures

[229] Koehler, F. M.; Stark, W. J., *Acc. Chem. Res.*, **2013**, *46 (10)*, 2297–2306
[230] Usrey, M. L.; Lippmann, E. S.; Strano, M. S., *J. Am. Chem. Soc.* **2005**, *127*, 16129-16135

Co/C MNPs were functionalized by Stark and co-workers with highly charged polymers thus obtaining stable suspension in water.[231] Reiser's research group developed also different procedures: a covalent ligation strategy and a non-covalent ligation strategy were developed for the functionalization of the Co/C MNPs (Scheme 3.2).[222a] In the covalent method the $-NO_2$ intermediate, generated through the diazonium chemistry, was converted into an amine and then into the corresponding azide.[232] The azide is a suitable moiety to insert further functionalization through an azide-alkyne cycloaddition.[233] On the other hand, polyarenes could be connected to the carbon shell by attractive π-stacking interactions with the graphene-like layers of the MNPs surface.[222a] In water, hydrophobic effects have resulted useful for this approach, as demonstrated by the successful immobilization on MNPs of metal complexes.[234]

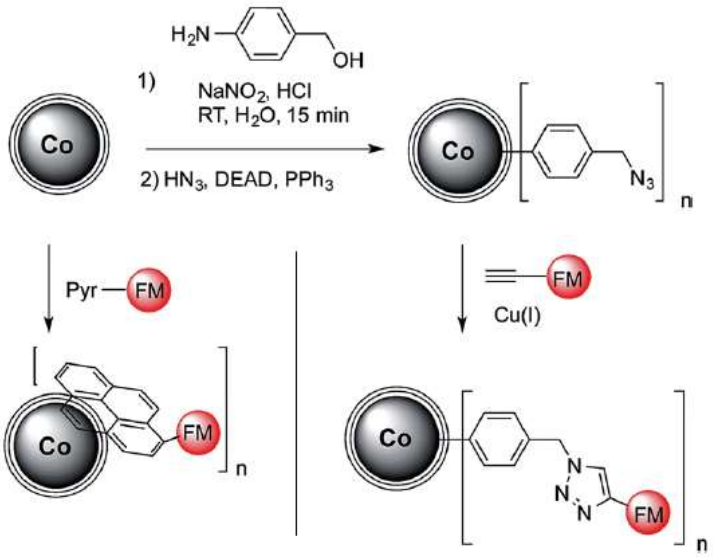

Scheme 3.2 – Principal strategies for covalent and non-covalent functionalization of Co/C MNPs (FM = functional molecule)

All these modified MNPs were tested for the dispersibility in water: positively charged ammonium groups confer somehow higher dispersibility than hydroxy groups. Also the use of the covalent ligation strategy increases the dispersibility in water. In any case, the best water-dispersible particles showed only a 60 min stable dispersion.[222a] It was hypothesized that a high loading of polar functional groups is a requirement to obtain stable water-suspensions of the functionalized MNPs.

[231] Zeltner, M.; Grass, R. N.; Schaetz, A.; Bubenhofer, S. B.; Luechinger, N. A.; Stark, W. J., *J. Mater. Chem.* **2012**, *22*, 12064-12071
[232] Mclaughlin, M. A.; Barnes, D. M., *Tetrahedron Lett.* **2006**, *47*, 9095-9097
[233] (a) Schätz, A.; Grass, R. N.; Stark, W. J.; Reiser, O., *Chem. Eur. J.* **2008**, *14*, 8262-8266; (b) Kainz, M. Q.; Schätz, A.; Zopfl, A.; Stark, W. J.; Reiser, O., *Chem. Mater.* **2011**, *23*, 3606-3613; (c) Sun, X.-L.; Haller, C.; Wu, X.; Conticello, V. P.; Chaikof, E. L., *J. Proteome Res.* **2005**, *4*, 2355-2359
[234] (a) Wittmann, S.; Schätz, A.; Grass, R. N.; Stark, W. J.; Reiser, O., *Angew. Chem. Int. Ed.* **2010**, *49*, 1867-1870; (b) Keller, M.; Collière, V.; Reiser, O.; Caminade, A.-M.; Majoral, J.-P.; Ouali, A., *Angew. Chem. Int. Ed.* **2013**, *52*, 3626-3629

3.3.2 Co/C PEI synthesis and characterization

Reiser's research group developed highly amine-loaded Co/C nanoparticles (**3.1**) grafting a polyethyleneimine (PEI) onto the MNPs (Scheme 3.3) with the aim of producing highly water-dispersible MNPs. Aziridine (**3.5**) was polymerized with the phenylethyleneamine-functionalized particles (**3.4**). These functionalized particles were produced through the reaction of Co/C MNPs (**3.2**) with the diazonium salt generated from the aniline **3.3**.

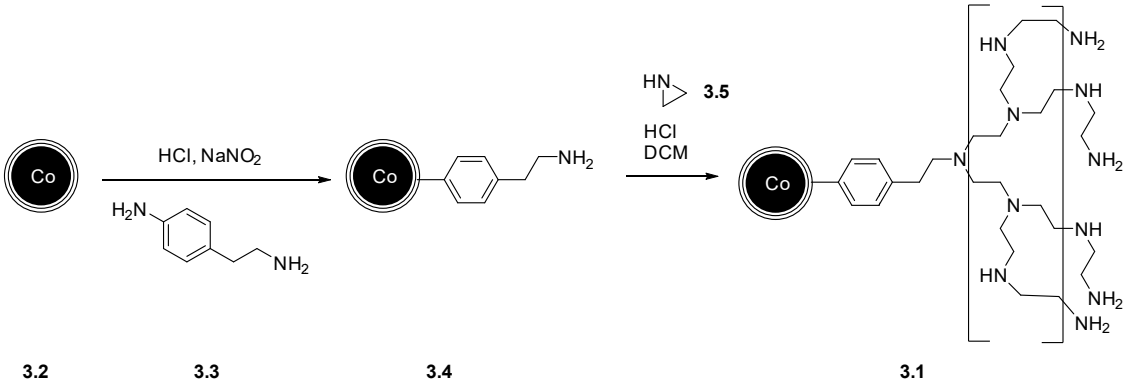

Scheme 3.3 – PEI MNPs synthesis

The loading of amino functionalities was evaluated by elemental analysis (on nitrogen) and by TGA. The nitrogen loading was calculated: 10-14mmol/g. Since the shell is a polymeric coating, it is not possible to describe the exact structure. Statistically, ¼ of the nitrogen groups are primary amines, half are secondary amines and ¼ are tertiary amines. Co/C. PEI MNPs **3.1** were characterized by IR (Figure 3.6) and by TEM (Figure 3.7): they are discrete particles and no cross-links are present.

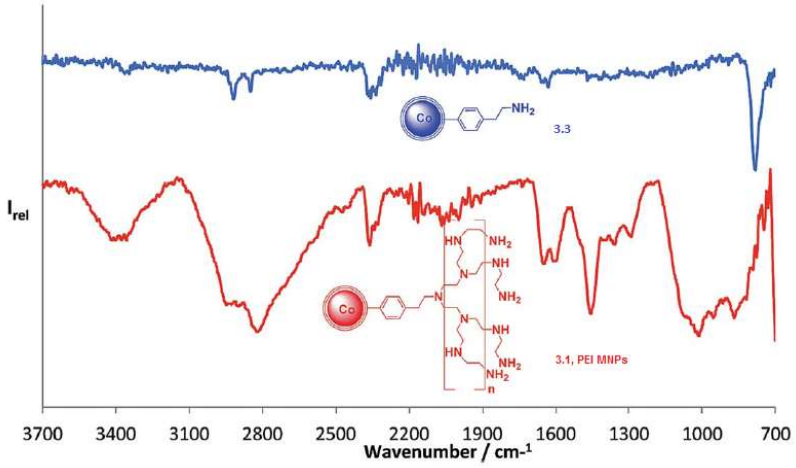

Figure 3.6 – IR spectra of phenylethyleneamine-functionalized particles (**3.3**) and of PEI MNPs (**3.1**)

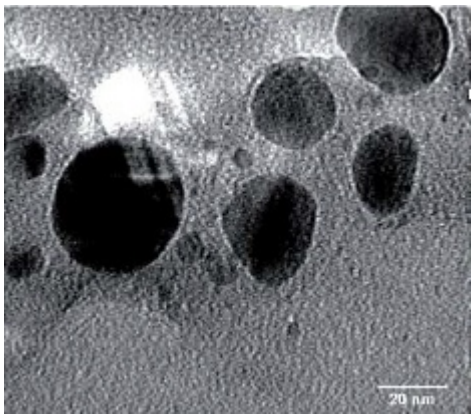

Figure 3.7 – TEM picture of PEI MNPs (**3.1**)

The superconducting quantum interference device (SQUID) measurements confirmed the high mass proportion of PEI polymer (60% wt by TGA): the magnetic saturation value was reduced from 128 emu/g (value for Co/C naked MNPs) to 39 emu/g (value for PEI MNPs)(Figure 3.8).

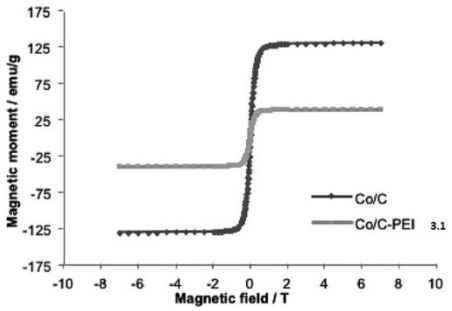

Figure 3.8 – SQUID measurements for naked Co/C MNPs and PEI MNPs (**3.1**)

This system proved to form water dispersions stable over days (stability test reported in the same paper[222a]) without any sedimentation or agglomeration even in a biphasic system with DCM (Figure 3.9). Because of all their properties, MNPs **3.1** are suitable candidates as carrier for bioactive compounds.

Figure 3.9 – PEI MNPs (**3.1**) dispersibility between water and DCM

3.3.3 Co/CPEI further functionalization

As mentioned in the introduction of this chapter, we planned to obtain the MNPs functionalized as alkynes and the biological active compound linked to an azide moiety. Different strategies were explored to introduce the alkyne (Scheme 3.4). In table 3.2 is presented a brief summary.

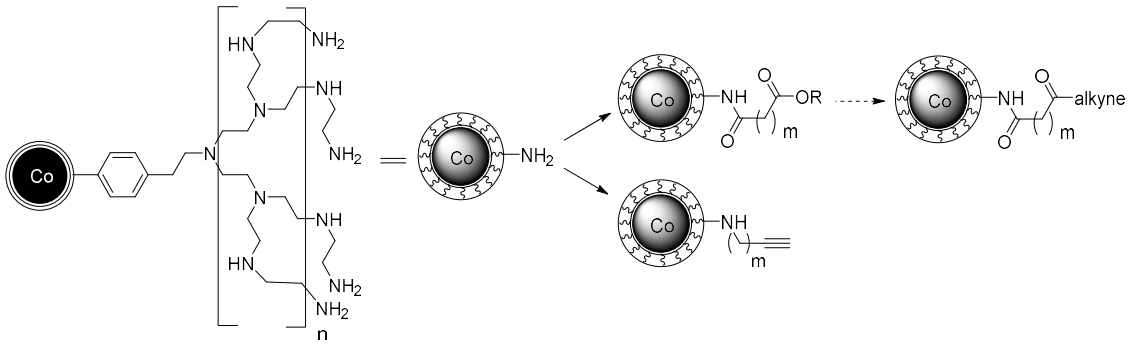

Scheme 3.4 – PEI MNPs functionalization, general scheme

Entry	Ligand	Reactant(s)	Solvent	Temperature	Reaction time	Loading
1	Succinic anhydride	/	DCM	r.t.	24 h	0.01 mmol/g[a]
2	Glutaric acid	HATU, HOAt, DIPEA	DMF	r.t.	15 h	0.003 mmol/g[a]
3	Mono-methyl glutarate	HATU, HOAt, DIPEA	DMF	r.t.	15 h	0.160 mmol/g[a]
4	4-pentenoic acid	NHS, DIC	DMF	r.t.	15 h	<0.01 mmol/g[b]
5	3-bromopropionic acid	K_2CO_3	DMF	80°C	24 h	0.376 mmol/g[a]
6	Propargyl bromide	K_2CO_3	DMF	80°C	24 h	1.542 mmol/g[a]

Table 3.2 – Functionalization strategies on Co/C MNPS ([a] = Initial loading 8.53 mmol N/g; [b] Initial loading 7.28 mmol N/g)

All these attempts could be divided into two main classes: direct insertion of the alkyne (entry 4 and 6) or insertion of a linker on which a further functionalization would allow to put the desired alkyne moiety (entries 1 to 3 and 5). The second strategy gave low loadings of the linker, especially taking into account that the first strategy does not require a further step. The letter synthetic procedure is represented in Scheme 3.5. Between entry 4 and 6, the difference is marked: coupling reagents, used to form an amide bond, are absolutely less efficient than the bromide. The alkyne functionality was introduced by a nucleophilic substitution.[235]

[235] Levy, D. E.; Marlowe, C.; Kane-Mauire, K.; Bao, M.; Cherbavaz, D. B.; Tomlison, J. E.; Sedlock, D. M.; Scarborough, R. M., *Bioorg. Med. Chem. Lett.* **2002**, *12*, 3085-3088

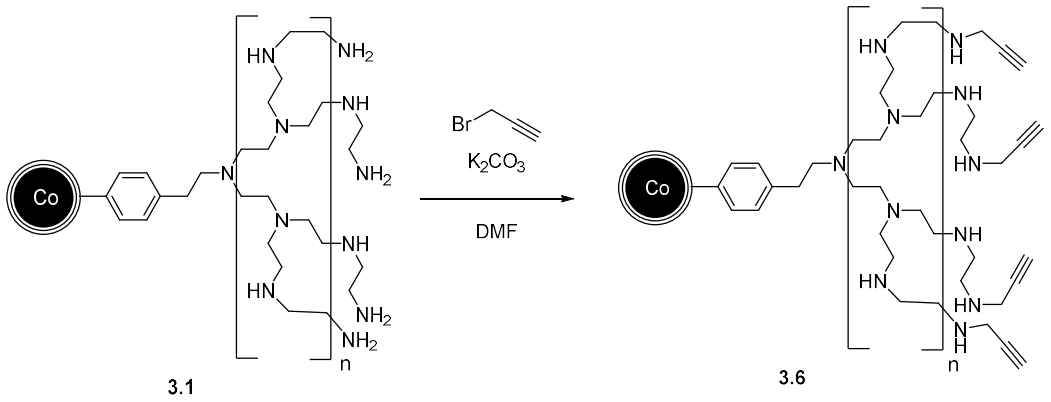

Scheme 3.5 – Synthesis of alkyne-PEI MNPs (**3.6**)

MNPs **3.6** were characterized by elemental analysis (alkyne loading of 1.542 mmol/g) and by SQUID measurements. SQUID measurements afforded a saturation magnetization value of 70.57 emu/g. Interestingly, these MNPs **3.6** are not suspensible in water, thus the alkyne functionalization cancels the high water suspendibility of PEI MNPs.

3.4 Iron oxide silica coated magnetic nanoparticles (Fe_3O_4@silica MNPs)

Fe_3O_4 is an iron oxide that has a cubic inverse spinel structure with oxygen forming a fcc closed packing and Fe cations occupying interstitial tetrahedral sites and octahedral sites.[236] With proper surface coating, these magnetic nanoparticles can be dispersed into water.[237] The use of Fe_3O_4 MNPs (with various coatings) for biological purposes is consolidated and a lot of examples are present in the literature.[238] In particular Fe_3O_4 and γ-Fe_2O_4 MNPs have appropriate magnetic properties and biological compatibility[239]. Naked Fe_3O_4 MNPs usually have a magnetic saturation values in the range of 30-50 emu/g but unfortunately they are not very stable under ambient conditions: they are easily oxidized to maghemite (that, luckily, is still ferrimagnetic) or dissolved in acid media.

Fe_3O_4 MNPs are commonly produced *via* co-precipitation of ferrous (Fe^{2+}) and ferric (Fe^{3+}) ions by a base in aqueous solution,[240] or by thermal decomposition of alkaline solutions of Fe^{3+} chelate in presence of hydrazine,[241] or by sonochemical decomposition of hydrolyzed Fe^{2+} salts followed by thermal treatment.[242] As an alternative, also the microemulsion method has been reported.[243]

Among the most used surface coating materials, silica and alkoxysilanes are the preferred ones, especially for iron oxide MNPs.[244] Silica has the advantage of being biocompatible, hydrophilic[244h,l], stabile under aqueous conditions (if the pH value is not extremely basic), chemically inert and physically stable.[245] The silica shell exercises two main functions: the magnetic core protection and the prevention of the contact between the MNPs core and additional agents linked to the silica, thus avoiding unwanted reactions.[246] In addition, silica prevents the aggregation of particles.[244h,l] Furthermore, the silica coating can react with various agents to covalently attach specific ligands allowing

[236] Cornell, R. M.; Schwertmann, U. in " The Iron Oxides: Structure, Properties, Reactions, Occurrence and Uses" (VHC: New York) **1996**, 28-29
[237] Fu, L.; Dravid, V. P.; Johnson, D. L., *Appl. Surf. Sci.* **2001**, *181*, 173-178
[238] For example see: (a) Lin, R.-Y.; Dayananda, K.; Chen, T.-Y.; Chen, C.-Y.; Liu, G.-C.; Lin, K.-L.-; Wang, Y.-M., *Contrast Media Mol. Imaging* **2012**, *7*, 7-18; (b) Zheng, S. W.; Huang, M.; Hong, R. Y.; Deng, S. M.; Cheng, L. F.; Gao, B.; Badami, D., *Journal of Biomaterials Applications* **2014**, *28 (7)*, 1051-1059; (c) Deng, S.; Zhang, W.; Zhang, B.; Hong, R.; Chen, Q.; Dong, J.; Chen, Y.; Wu, Y., *J. Nanopart. Res.* **2015**, *17*, 19; (d) Xie, J.; Chen, K.; Lee, H.-Y.; Xu, C.; Hsu, A. R.; Peng, S.; Chen, X.; Sun, S., *J. Am. Chem. Soc.* **2008**, *130*, 7542-7543
[239] (a) Weissleder, R.; Cheng, H. C.; Bogdavova, A.; Bogdanov A., *J. Magn. Reson. Imaging* **1997**, *7*, 258-263; (b) Cengelli, F.; Maysinger, D.; Tschudi-Monnet, F.; Montet, X.; Corot, C.; Petri-Fink, A.; Hofmann, H.; Juillerat-Jeanneret, L., *J. Pharmacol. Exp. Ther.* **2006**, *318*, 108-116; (c) Brigger, I.; Dubernet, C.; Couvreur, P., *Adv. Drug Delivery Rev.* **2002**, *54*, 631-651; (d) Wang, L.; Bao, J.; Wang, L.; Zhang, F.; Li, Y., *Chem. Eur. J.* **2006**, *12*, 6341-6347
[240] (a) Kang, Y. S.; Risbud, S.; Rabolt, J. F.; Stroeve, P., *Chem. Mater.* **1996**, *8*, 2209-2211; (b) Hong, C.-Y.; Jang, L. J.; Horng, H. E.; Hsu, C. J.; Yao, Y. D.; Yang, H. C., *J. Appl. Phys.* **1997**, *81*, 4275-4277; (c) Fried, T.; Shemer, G.; Markovic, G., *Adv. Mater.* **2001**, *13*, 1158-1161
[241] Sapieszko, R. S.; Matijevic, E., *J. Colloid Interface Sci.* **1980**, *74*, 405-422
[242] Vijayakumar, R.; Koltypin, Y.; Felner, I.; Gedanken, A., *Mater. Sci. Eng.* **2000**, *A286*, 101-105
[243] Santra, S.; Tapec, R.; Theodoropoulou, N.; Dobson, J.; Hebrad, A.; Tan, W., *Langmuir* **2001**, *17*, 2900-2906
[244] (a) Philipse, A. P.; Van Bruggen, M. P.; Pathmamanoharan, C., *Langmuir* **1994**, *10*, 92-99; (b) Yang, H. H.; Zhang, S. Q.; Chen, X. L.; Zhuang, Z. X.; Xu, J. G.; Wang, X. R., *Anal. Chem.* **2004**, *76*, 1316-1321; (c) Bruce, I. J.; Sen, T., *Langmuir* **2005**, *21*, 7029-7035; (d) Kohler, N.; Fryxell, G. E.; Zhang, M., *J. Am. Chem. Soc.* **2004**, *126*, 7206-7211; (e) Mikhaylova, M.; Kim, D. K.; Berry, C. C.; Zagorodni, A.; Toprak, M.; Curits, A. S.; Muhammed, M., *Chem. Mater.* **2004**, *16*, 2344-2345; (f) Fan, H.; Chen, Z.; Brinker, C. J.; Clawson, J.; Alam, T., *J. Am. Chem. Soc.* **2005**, *127*, 13746-13747; (g) Donselaar, L. N.; Philipse, A. P.; Suurmond, J., *Langmuir* **1997**, *13*, 6018; (h) Liu, Q.; Xu, Z.; Finch, J. A.; Egerton, R., *Chem. Mater.* **1998**, *10*, 3936-3940; (i) Correa-Duarte, M. A.; Giersig, M.; Kotov, N. A.; Liz-Marzan, L. M., *Langmuir* **1998**, *14*, 6430-6435
[245] Smith, J. E.; Wang, L.; Tan, W., *Trends Anal. Chem.* **2006**, *25*, 848-855
[246] Lu, A.-H; Salabas, E. L.; Schüth, F., *Angew. Chem. Int. Ed.* **2007**, *46*, 1222-1244

the insertion of various functionalities on the MNPs.[247] Alkoxysilanes are bifunctional molecules with the general formula $[X(CH_2)_n]_mSiR(OR')_{3-m}$, where X represents the headgroup functionality, $(CH_2)_n$ a flexible spacer, and Si(OR')the anchor groups by which they can attach to free SiOH or FeOH surface groups after hydrolysis of the alkoxy group.[244c] These molecules can be used to directly connect functional groups or bioactive molecules on the MNPs. However, silica as two main disadvantages: it is not stable under basic conditions and it may contain pores through which oxygen or other species could diffuse affecting the core. The silica coating is usually deposited on the MNPs through the Stöber method[248] or through sol-gel processes.[249] The coating thickness can be tuned by varying the concentrations of ammonium and the ratio of tetraethoxysilane (TEOS) to H_2O. Since the iron oxide surface has a strong affinity towards silica, no primer is required to promote the deposition and adhesion of silica.[249c]

In the case of the iron oxide MNPs used for our purposes, their synthesis is depicted in Scheme 3.6. Alkyne-Fe_3O_4@silica MNPs **3.7** were conveniently silica coated and functionalized with an alkyne in an one-step reaction. In order to introduce the alkyne group, reagent **3.8** was synthesized by reaction of equimolar amounts of TEOS and 4-pentyn-1-ol in dry toluene. The resulting solution was directly used to coat the MNPs.[250]

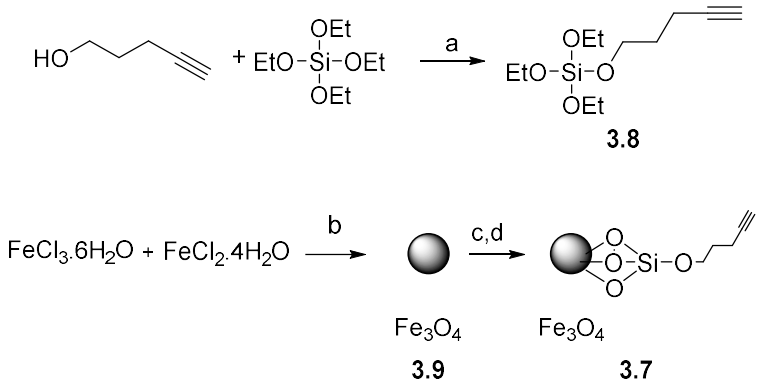

Scheme 3.6 - Alkyne-Fe_3O_4@silica MNPs

Reagents and conditions: a) dry toluene, 90°C, under N_2; b) Na_2CO_3, H_2O, 90°C; c) ultrapure water, citric acid, ultrasonic bath for 1 h, T< 40°C; d) **3.8**, acetic acid cat., ultrapure water cat., dry toluene, reflux.

MNPs **3.7** were analyzed by elemental analysis: the alkyne loading was evaluated 0.519 mmol/g. The SQUID measurement gave a saturation magnetization value of 52.41 emu/g (Figure 3.10).

[247] Ulman, A., *Chem. Rev.***1996**, 96, 1533-1554

[248] Stöber, M.; Fink, A.; Bohn, E. J., *J. Colloid Interface Sci.* **1968**, *26*, 62-69

[249] (a) Tago, T.; Hatsuta, T.; Miyajima, K.; Kishida, M.; Tashiro, S.; Wakabayashi, K., *J. Am. Ceram. Soc.* **2002**, *85*, 2188-2194; (b) Lu, Y.; Yin, Y.; Mayers, B. T.; Xia, Y., *Nano Lett.* **2002**, *2*, 183-186; (c) Graf, C.; Vossen, D. L. J.; Imhof, A.; Van Blaaderen, A., *Langmuir* **2003**, *19*, 6693-6700; (d) Philipse, A. P.; Van Bruggen, M. P. B.; Pathmamanoharan, C., *Langmuir*, **1994**, *10*, 92-99; (e) Zhao, W.; Gu, J.; Zhang, L.; Chen, H.; Shi, J., *J. Am. Chem. Soc.* **2005**, *127*, 8916-8917

[250] Mader, H.; Li, X.; Saleh, S.; Link, M.; Kele, P.; Wolfbeis, O. S., *Ann. N. Y. Acad. Sci.* **2008**, *1130*, 218-223

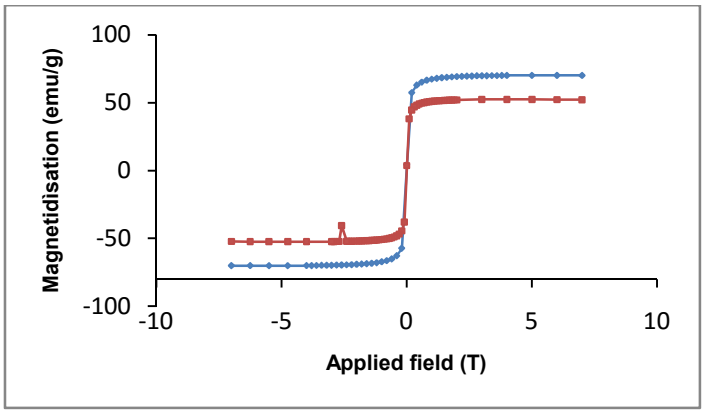

Figure 3.10 – SQUID measurements for Fe_3O_4 MNPs and alkyne-Fe_3O_4@silica MNPs (light blue: Fe_3O_4 MNPs **3.9**; red: alkyne-Fe_3O_4@silica MNPs **3.7**)

Since the alkyne loading was low, a different strategy was explored. MNPs were functionalized with different commercially available silane-derivatives **3.10** (Figure 3.13), bearing a terminal amino group, and **3.11**, bearing a terminal chlorine (Figure 3.11) to obtain a starting material for a further functionalization.

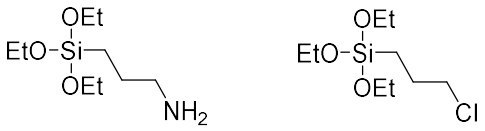

3.10 **3.11**

Figure 3.11 – Silane-derivatives used for MNPs functionalization

Amino- and chloro-functionalized MNPs were prepared with the same protocol used for MNPs **3.7**, differing only for the silane used (Scheme 3.7).[250] The loading for **3.12** and **3.13** MNPs are reported in Table 3.3, and compared with MNPs **3.7**.

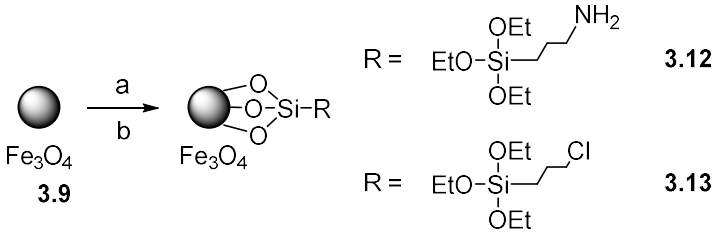

Scheme 3.7 – Coating of Fe_3O_4 MNPs **3.9** with silane-derivatives **3.10** and **3.11**

Reagents and conditions: a) dry toluene, 90°C, under N_2; b) ultrapure water, citric acid, ultrasonic bath for 1 h, T< 40°C; c) **3.10** or **3.11**, acetic acid cat., ultrapure water cat., dry toluene, reflux.

Ligand	Functionlized MNPs	Loading (evaluated by EA)
/	**3.7**	0.51mmol alkyne/g
3.10	**3.12**	1.76 mmol N/g
3.11	**3.13**	1.71 mmol Cl/g

Table 3.3 – Loading values of different functionalities on Fe_3O_4 (**3.9**) MNPs

Luckily, these loadings resulted quite high. The best value was obtained with the aminosilane. Therefore MNPs **3.12** were deemed the best starting material to insert the alkyne. The reaction protocol reproduced the one used on PEI MNPs (Scheme 3.8).[235] The final compound, MNPs **3.14**, has an alkyne loading of 1.54 mmol/g (according to EA).

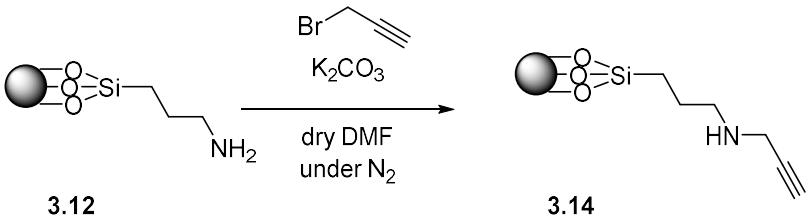

Scheme 3.8 – Fe_3O_4@silica-NH-alkyne MNPs synthesis

3.5 Iron oxide poly(acrylic acid) coated magnetic nanoparticles (Fe_3O_4@PAA-COOH MNPs)

These MNPs have a Fe_3O_4 core and a poly(acrylic) acid coating with free carboxylic acid groups on the surface (Figure 3.12).

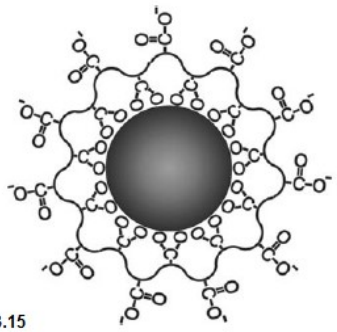

Figure 3.12 – Schematic illustration of the Fe_3O_4@PAA-COOH nanocrystals

A ferrofluid is a liquid that becomes strongly magnetized in the presence of a magnetic field.[251] In the case of ferrofluids, surface charge is very important for their stabilization. For example, the MNPs obtained through co-precipitation (starting from Fe^{2+} and Fe^{3+}) of Fe_3O_4 MNPs in ammonia or NaOH solution are usually negatively charged. This surface charge causes agglomeration. Thus, to obtain stable colloids, MNPs have to be treated with aqueous tetramethylammonium hydroxide or with aqueous perchloric acid.[252] Surfactants or polymers can be chemically anchored or physically adsorbed on MNPs to form a single or a double layer[253] to passivate the surface of MNPs during or after the synthesis. These agents create repulsive (mainly as steric repulsion) forces to balance the magnetic and the van der Waals attractive forces acting on the nanoparticles thus avoiding agglomeration and keeping MNPs in a stable colloidal state. Examples of biocompatible polymers-coated MNPs can be found in the literature and they have a widespread use.[254] The main disadvantage of surfactants/polymer coating is related to metallic MNPs: even if they are stabilized by single or double layers of surfactant or polymer, they are not air stable and they are easily leached by acidic solution,[255] resulting in the loss of magnetization.

[251] Papell, S. S., US Patent 3215572, **1965**
[252] Massart, R., *IEEE Trans. Magn.* **1981**, *MAG-17*, 1247
[253] (a) Shen, L.; Laibinis, P. E.; Hatton, T. A., *Langmuir* **1999**, *83*, 217; (b) Sousa, M. H.; Tourinho, F. A.; Depeyrot, J.; Da Silva, G. J.; Lara, M. C. F. L., *J. Phys. Chem. B* **2001**, *105*, 1168-1175
[254] (a) Harris, L. A.; Goff, J. D.; Carmichael, A. Y.; Riffle, J. S.; Harburn, J. J.; St. Pierre, T. G.; Saunders, M., *Chem. Mater.* **2003**, *15*, 1367-1377; (b) Thunemann, A. F.; Schutt, D.; Kaufner, L.; Pison, U.; Möhwald, H., *Langmuir* **2006**, *22*, 2351-2357
[255] Farrell, D.; Majetich, S. A.; Wilcoxon, J. P., *J. Phys, Chem. B* **2003**, *107*, 11022-11030

3.5.1 Fe_3O_4@PAA-COOH MNPs synthesis

Yin and co-workers synthesized high quality water-soluble, uniform size nanocrystals with a poly(acrylic acid) (PAA) as capping agent.[194d] These MNPs are highly soluble in water and their solutions show a ferrofluidic behavior when subjected to an external magnetic field. It was shown that a low reaction temperature causes a low degree of control over the size, the distribution, the crystallinity and a narrow size distribution of the coated MNPs.[256] Not all the capping agents are stable at high temperatures and are able to maintain hydrophilicity after binding to electron-poor Fe atoms. Short-chain PAA satisfies both these requirements.[194d] MNPs were prepared through the hydrolysis of Fe_3Cl with NaOH solution at temperature higher than 200°C in diethylene glycol in the presence of PAA. The reaction proceeds through hydrolysis (favored by the NaOH addition which increases the alkalinity) under reductive atmosphere (provided by DEG) at high temperature.[257] Under these conditions, $Fe(OH)_3$ partially transforms to $Fe(OH)_2$, finally leading to the formation of Fe_3O_4 particles through dehydratation. For these MNPs, the solubility in water is guaranteed by the large number of uncoordinated carboxylate groups on the polymer chains that extend into the aqueous solution. These same groups could also be employed to link biomolecules or for further electrostatic functionalization. The other carboxylate groups on PAA chains strongly coordinate the Fe cations on the surface of MNPs forming a robust coating. Every polymer chain has multiple anchor points. These MNPs are soluble in water at basic and neutral pH values. As the pH decreases, also the solubility of the nanocrystal decreases because the carboxylate groups are progressively less ionized. At pH values < 4, the carboxylate groups are protonated and so less hydrophilic thus creating aggregates and precipitating out from the solution. On the other hand, the higher is the pH, the higher is the solubility (Figure 3.13).

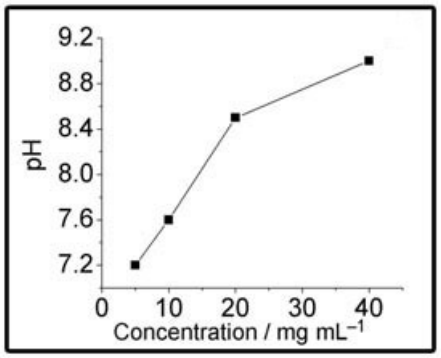

Figure 3.13 – Water solubility of Fe_3O_4@PAA-COOH at different pH

[256] (a) Babes, L.; Denizot, B.; Tanguy, G.; Le Jeune, J. J.; Jallet, P., *J. Colloid Interface Sci.* **1999**, *212*, 474; (b) Jeong, J.-R.; Shin, S.-C.; Lee, S.-J.; Kim, J.-D., *J. Magn. Magn. Mater.* **2005**, *286*, 5; (c) Pileni, M. P., *J. Phys. Chem. B* **2001**, *105*, 3358

[257] (a) Sun, Y.; Xia, Y., *Science* **2002**, *298*, 2176-2179; (b) Deng, H.; Li, X. L.; Peng, Q.; Wang, X.; Chen, J. P.; Li, Y. D., *Angew. Chem. Int. Ed.* **2005**, *44*, 2782-2785

These magnetic nanocrystals resulted superparamagnetic, biocompatible, with small and uniform particle size (Figure 3.14). Thanks to the high temperature annealing that occurs during the synthesis, particles have an high crystalline character and each particles is a well-ordered single crystal.[194d]

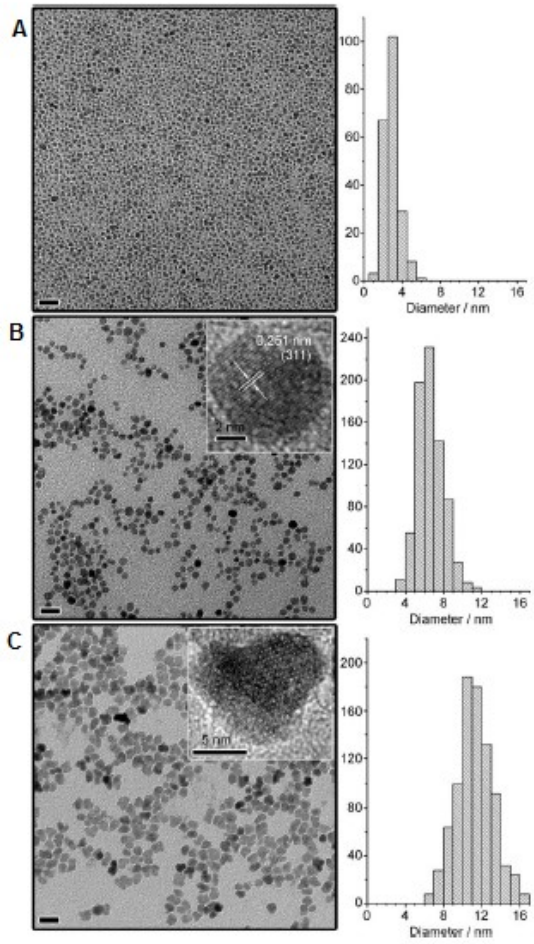

Figure 3.14 – TEM images and corresponding measured size distributions of Fe_3O_4@PAA nanocrystals

A) Average diameter of 2.9 Å; B) Average diameter of 6.6 nm, individual nanocrystal shown in the insert (HRTEM picture); C) Average diameter of 11.3 nm, individual nanocrystal shown in the insert (HRTEM picture).

The amount of NaOH added allows the control of the nanocrystal size if all the other parameters are fixed: the larger is the amount of NaOH, the bigger are the crystals. Probably this happens because of the alkalinity variation and the difference in H_2O concentration. As a matter of fact, only when Fe^{3+} is fully hydrolyzed both nucleation and growth can be relatively quick, otherwise the crystal growth is very slow. The full hydrolysis of Fe^{3+} can take place when the amount of H_2O, the alkalinity and the NaOH are sufficient. Thanks to the high reaction temperature, a relatively rapid nucleation occurs shortly after the injection of NaOH, leading to magnetite nanocrystals with narrow size distribution.[258]

[258] Yin, Y.; Alivisators, A. P., *Nature* **2005**, *437*, 664-670

3.5.2 Fe_3O_4@PAA-COOH functionalization

PAA-capped nanocrystals can be conveniently conjugated to biological molecules through an appropriate bifunctional linker and one of the well-established techniques.[259] An alkyne functionality is required to click **3.25** on them. As first attempt, a classical protocol for esterification was employed (Scheme 3.9). The C_5-alkyne was selected in analogy to the alkyne used for MNPs **3.7**. and the loading, evaluated by elemental analysis, was 0.115 mmol/g. These particles resulted extremely dispersible in water and their suspension is stable over weeks (dispersibility test according to procedure in the reference 222a).

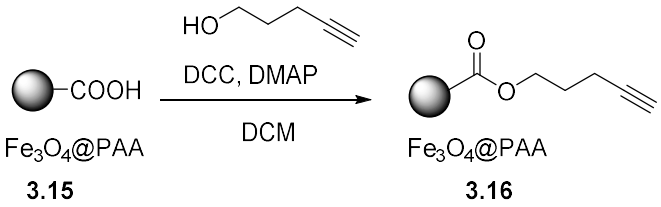

Scheme 3.9 – Functionalization of Fe_3O_4-@PAA MNPs with 4-pentyn-1-ol

However the alkyne loading was not really satisfying. Looking deeply in the literature, a protocol for the alkyne functionalization of the very same **3.15** MNPs had already been developed.[260] Thus alkyne-Fe_3O_4@PAA-COOH MNPs **3.17** were synthesized following the exact reported procedure (Scheme 3.10) with the same C_3-alkyne. Unfortunately, it was impossible to reproduce this procedures and according to the elemental analysis nitrogen was present in the final product even after various washing steps with water and with organic solvents.

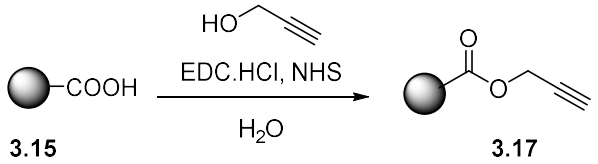

Scheme 3.10 – Functionalization of Fe_3O_4-@PAA MNPs with propargyl alcohol, 1st procedure

Since alkyne-MNPs **3.16** had been successfully obtained with a different protocol, I applied the same procedure[261] changing only the alkyne (propargyl bromide instead of 4-penty-1-ol) to prepare the same MNPs of reference 260 (Scheme 3.11). Fe_3O_4@PAA-alkyne **3.18** were successfully obtained and the alkyne loading evaluated by elemental analysis was 3.8 mmol/g, higher than the literature value of reference 260. These particles resulted

[259] Hermanson, G. T., *Bioconjugate Techniques*, Academic Press, **1996**
[260] He, H.; Zhang, Y.; Gao, C.; Wu, J., *Chem. Commun.* **2009**, 1655-1657
[261] Wang, H.; Negretti, S.; Knauff, A. R.; Montgomery, J., *Org. Lett.* **2015**, *17*, 1493-1496

extremely dispersible in water and their suspension is stable over weeks (dispersibility test according to procedure in the reference 222a).

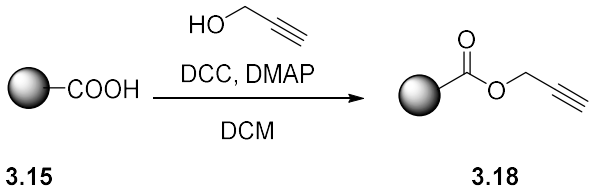

3.15 **3.18**

Scheme 3.11 – Functionalization of Fe_3O_4-@PAA MNPs with propargyl alcohol, 2nd procedure

SQUID (Figure 3.15) confirmed the MNPs functionalization. A magnetization saturation value of 17.89 emu/g was measured for **3.18** while the value for naked MNPs was 37.93 emu/g.

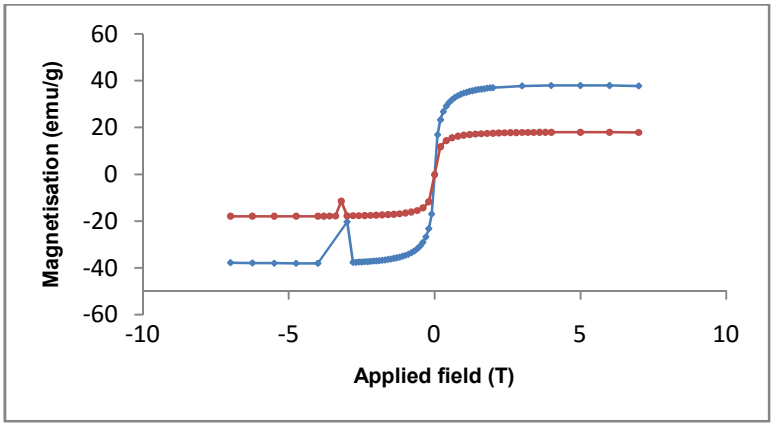

Figure 3.15 – SQUID measurements for Fe_3O_4@PAA MNPs and alkyne-Fe_3O_4@PAA MNPs (light blue: Fe_3O_4@PAA MNPs **3.15**; red: alkyne-Fe_3O_4@PAA MNPs **3.18**)

3.6 [DKP*f*3-RGD]-MNPs conjugates

A huge number of RGD-containing-MNPs conjugates has been developed for cancer-cell targeting and therapy.[238b,238c,262] For example, USPIOs (ultrasmall iron oxide magnetic nanoparticles) coated with different RGD-peptides were used as MRI and/or PET or SPECT contrast agents.[263] The physiochemical properties of the core provide the therapeutic effect and, in addition, passive targeting while the compound on the MNPs surface offers an higher level of specific targeting (active cell targeting).

3.6.1 *Cyclo*[DKP*f*3-RGD]-PEG

3.6.1.1 *Cyclo*[DKP*f*-RGD] library: short overview and synthesis

Our group has already synthesized a small collection of *Cyclo*[DKP*sf*-RGD]-Paclitaxel conjugates (Figure 3.16) containing the DKP*f* library (Figure 2.23, Chapter 2) as scaffolds.[148]

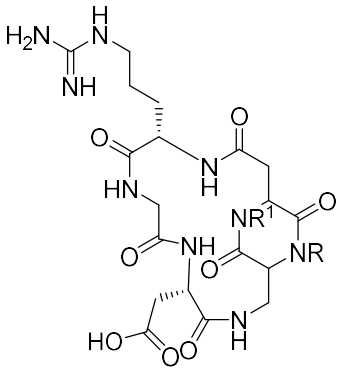

3.19 *Cyclo*[DKP*f*2-RGD]: 3*R*, 6*S*; R^1=H, R= *p*-Bn-CH_2-NH_2
3.20 *Cyclo*[DKP*f*3-RGD]: 3*S*, 6*R*; R^1=H, R= *p*-Bn-CH_2-NH_2
3.21 *Cyclo*[DKP*f*4-RGD]: 3*R*, 6*S*; R^1= *p*-Bn-CH_2-NH_2, R =H
3.22 *Cyclo*[DKP*f*6-RGD]: 3S, 6*R*; R^1= *p*-Bn-CH_2-NH_2, R =H

Figure 3.16 – *Cyclo*[DKP*f*-RGD] library

[262] For example see: (a) Xie, J.; Chen, K.; Lee, H.-Y.; Xu, C.; Hsu, A. R.; Peng, S.; Chen, X.; Sun, S., *J. Am. Chem. Soc.* **2008**, *130*, 7542-7543; (b) Lin, R.-Y.; Dayananda, K.; Chen, T.-J.; Chen, C.-Y.; Liu, G.-C.; Lin, K.-L.; Wang, Y.-M., *Contrast Media Mol. Imaging* **2012**, *7*, 7-18

[263] For example see: (a) Bouziotis, P.; Psimadas, D.; Tsotakos, T.; Stamopoulos, D.; Tsoukalas, C., *Curr. Top Med. Chem.* **2012**, *12*, 2694-2702; (b) Lee, H. Y.; Li, Z.; Chen, K.; Hsu, A. R.; Xu, C.; Xie, J.; Sun, S.; Chen, X., *J. Nucl. Med.* **2008**, *49*, 1371-1379; (c) Zhang, C.; Jugold, M.; Woenne, E. C.; Lammers, T.; Morgenstern, B.; Mueller, M. M.; Zentgraf, H.; Bock, M.; Eisenhut, M.; Semmler, W.; Kiessling, F., *Cancer Res.* **2007**, *67*, 1555-1562; (d) Zhang, F.; Huang, X.; Zhu, L.; Guo, N.; Niu, G.; Swierczewska, M.; Lee, S.; Xu, H.; Wang, A. Y.; Mohamedali, K. A.; Rosenblum, M. G.; Lu, G.; Chen, X., *Biomaterials* **2012**, *33*, 5414-5422

Among these, the derivative containing the DKP*f*3 (**3.20**), was already conjugated also to a peptidic sequence to produce a dual-action ligand targeting $\alpha_v\beta_3$ integrin and VEGF receptors[149] and, through lysosomally cleavable linkers, again to Paclitaxel[264]. **3.20** seemed also suitable for the link to MNPs both Co/C and Fe_3O_4. The solution synthesis pathway employed to prepare the library, is the same that was used for the *Cyclo*[DKPs-RGD]ligands, differing only for the DKP scaffolds (Scheme 3.12).

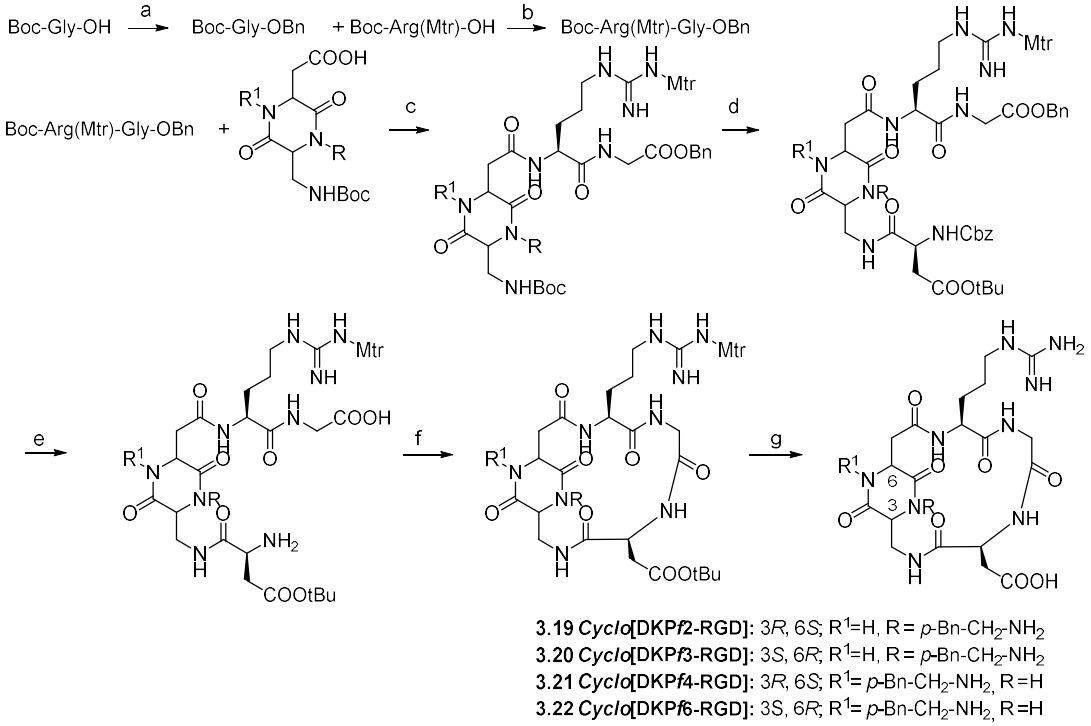

Scheme 3.12 - *Cyclo*[DKP*f*-RGD] ligands synthesis

Reagents and conditions: a) 1) $CsCO_3$, MeOH; 2) BnBr, DMF; b) 1) TFA/DCM 1:2; 2) HATU, HOAt, DIPEA, DMF, 0°C to r.t., under N_2; c) 1) TFA/DCM 1:2; 2) HATU, HOAt, DIPEA, DMF, 0°C to r.t., under N_2; d) 1) TFA/DCM 1:2; 2)Cbz-Asp(O*t*Bu)-OH, HATU, HOAt, DIPEA, DMF, 0°C to r.t., under N_2 e) 1) TFA/DCM 1:2; 2) H_2, Pd/C, THF/H_2O 1:1, r.t.; f) HATU, HOAt, DIPEA, DMF, 0°C to r.t., under N_2; g) TFA/thianisole/ethanedithiol/anisole 90:5:3:2.

[264] Dal Corso, A.; Caruso, M.; Belvisi, L.; Arosio, D.; Piarulli, U.; Albanese, C.; Gasparri, F.; Marsiglio, A.; Sola, F.; Troiani, S.; Valsasina, B.; Pignataro, L.; Donati, D.; Gennari, C., *Chem. Eur. J.* **2015**, *21*, 6921-6929

3.6.1.2 *Cyclo*[DKP*f*3-RGD]-(PEG)$_8$-N$_3$

A bifunctional linker is necessary to connect the biological active compound and the functionalized MNPs. Poly(ethylene glycol) (PEG) is a highly hydrophilic, biocompatible, non-toxic and non-immunogenic polymer.[265] Pegylation is known in the literature as a method to increase functionality, biocompatibility and water solubility.[266] Moreover, also the blood circulation times of pegylated compounds is increased compared to the non-pegylated ones, because pegylation reduces clearance *via* reticuloendothelial system (RES)[267], protein adsorption, platelet adhesion, and cell adhesion.[268] An average molecular weight of 2000 g/mol is enough for this cell repellent effect[269].

Because of these properties, a commercially available PEG-linker was considered the best choice for our purposes. The commercial available compound N_3-(PEG)$_8$-NH_2 (**3.23**) bears an amino functionality thus it is unsuitable to be directly connected to **3.20**. Since in our group a PEG-linker had already successfully been conjugated to **3.20**,[149] a similar approach was followed (Scheme 3.13). **3.24** was synthesized through the direct opening of the succinic anhydride. This derivative is suitable for the further coupling with **3.20** on the amino-moiety. The final compound **3.25** has an azido moiety appropriate for a conjugation to MNPs *via* click chemistry reaction.

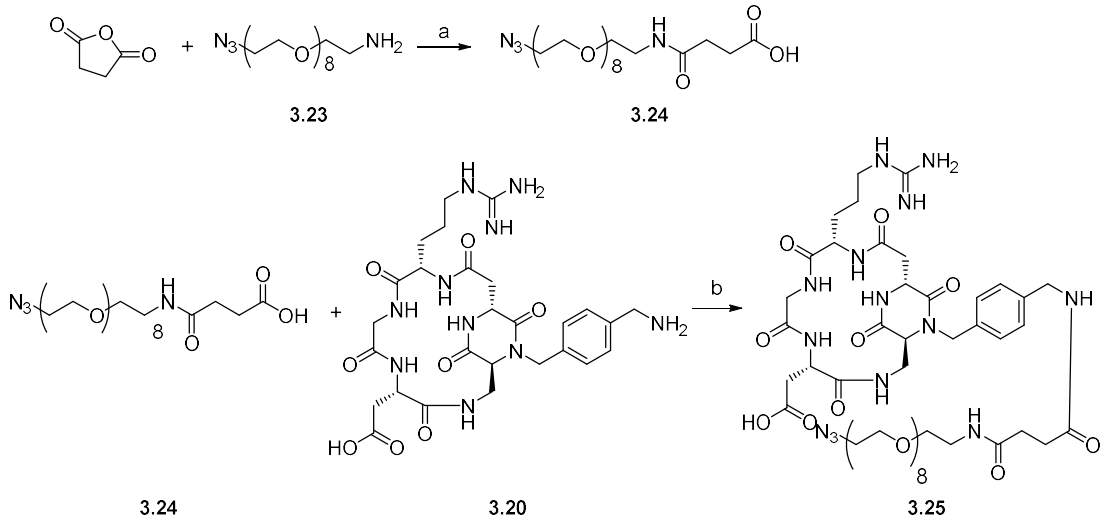

Scheme 3.13 – *Cyclo*[DKP*f*3-RGD]-(PEG)$_8$ (**3.25**) synthesis

Reagents and conditions: a) dry DCM, under N_2, r.t.; b) NHS, DIC, DCM, under N_2, r.t.; c) buffer (pH=7), CH_3CN.

[265] (a) Amiji, M.; Park, K., *J. Biomater. Sci., Polym. Ed.* **1993**, *4*, 217-234; (b) Fuerteges, F.; Abuchowski, A., *J. Controlled Release* **1990**, *11*, 139

[266] (a) Adams, M. L.; Lavasanifar, A.; Kwon, G. S., *J. Pharm. Sci.* **2003**, *92 (7)*, 1343-1355; (b) Yang, S. T.; Fernando, K. A. S.; Liu, J. H.; Wang, J.; Sun, H. F.; Liu, Y. F.; Chen, M.; Huang, Y. P.; Wang, X.; Wang, H. F.; Sun, Y. P., *Small* **2008**, *4 (7)*, 940-944; (c) Xiaoming Sun, Z. L.; Welsher, K.; Robinson, J. T.; Goodwin, A.; Zaric, S.; Dai, A. H., *Nano Res.* **2008**, *1*, 203-212; (d) Lin Wang, W. Z., *Nano Res.* **2008**, *1*, 99-115

[267] (a) Xie, J.; Huang, J.; Li, X.; Sun, S.; Chen, X., *Curr. Med. Chem.* **2009**, *16 (10)*, 1278-1294; (b) Chen, K.; Xie, J.; Xu, H.; Behera, D.; Michalski, M. H.; Biswal, S.; Wang, A.; Chen, X., *Biomaterials* **2009**, *30 (36)*, 6912-6919; (c) Sunderland, C. J.; Steiert, M.; Talmadge, J. E.; Derfus, A. M.; Barry, S. E., *Drug Dev. Res.* **2006**, *67 (1)*, 70-93; (d) Veiseh, O.; Sun, C.; Gunn, J.; Kohler, N.; Gabikian, P.; Lee, D.; Bhattarai, N.; Ellenbogen, R.; Sze, R.; Hallahan, A.; Olson, J.; Zhang, M., *Nano Lett.* **2005**, *5 (6)*, 1003-1008

[268] (a) Shin, H.-S.; Park, K.; Kim, J. H.; Kim, J.-J.; Han, D. K., *J. Bioact. Compat. Polym.*, **2009**, *24*, 316-328; (b) Zhang, F.; Kang, E. T.; Neoh, K. G.; Huang, W., J. *Biomater. Sci., Polym. Ed.* **2001**, *12*, 515-531; (c) Han D. K.; Hubbell, J. A., *Macromolecules*, **1997**, *30*, 6077-6083

[269] Bozukova, D.; Pagnoulle, C.; De Pauw-Gillet, M.-C.; Desbief, S.; Lazzaroni, R.; Ruth, N.; Jérôme R.; Jérôme, C., *Biomacromolecules* **2007**, *8*, 2379-2387

3.6.2 *Cyclo*[DKP*f*3-RGD]-$(PEG)_8$-MNPs conjugates

Cu(I)-catalyzed Azide-Alkyne Click chemistry (CuAAC) reaction was selected since it is a well-known versatile and highly selective reaction that tolerates a wide spectrum of experimental conditions. The discovery that the Huisgen 1,3-dipolar cycloaddition[270] of an alkyne and an azide can be catalyzed by Cu(I) species under mild conditions dates back to 2002, when the groups of Sharpless[271] and Meldal[272] discovered it independently. The azide-functionalized molecule reacts with a terminal alkyne-functionalized molecule forming regioselectivelya stable 1,4-disubstituted 1,2,3-triazoles (Figure 3.17).

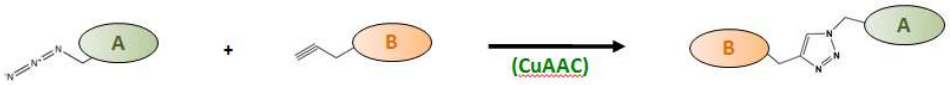

Figure 3.17 – General reaction scheme for a Cu(I)-catalyzed Azide-Alkyne Click Chemistry reaction

This click chemistry reaction has been widely applied in organic synthesis as well as in medicinal and materials research. Since biomolecule conjugations require reaction procedures that could be performed under mild and physiological conditions (neutral pH, aqueous solution, ambient temperature), the CuAAC is a first-choice reaction in medicinal chemistry.

In the past years, great progress were made in the development of the efficient catalytic procedures for CuAAC and a large amount of similar protocols is present in the literature.[149, 273] To conjugate **3.25** to the alkyne functionalized MNPs, a procedure developed for solid phase reactions was used as first approach.[274] This protocol seemed the most appropriate since MNPs could be compared to a solid support on which the bioactive compound is linked. First attempts were performed only with the purpose of identify the most promising conjugate among the Co/C PEI MNPs conjugate (Scheme 3.14), the Fe_3O_4@silica MNPs conjugate (Scheme 3.15), and the Fe_3O_4@PAA MNPs conjugate (Scheme 3.16).

[270] Huisgen, R. in: "1,3-Dipolar Cycloaddition Chemistry" (New York: Wiley) **1984**, 1 – 176
[271] Rostovtsev, V. V.; Green, L. G.; Fokin, V. V.; Sharpless, K. B., *Angew. Chem. Int. Ed.* **2002**, *41*, 2596 – 2599
[272] Tornøe, C.; Christensen, C.; Meldal, M., *J. Org. Chem.* **2002**, *67(9)*, 3057 – 3064
[273] For example see: (a) Shao, C.; Cheng, G.; Su, D.; Xu, J.; Wang, X.; Hu, Y., *Adv. Synth. Catal.* **2010**, *352*, 1587-1592; (b) Presolsky, S. I.; Hong, V.; Cho, S.-H.; Finn, M. G., *J. Am. Chem. Soc.* **2010**, *132*, 14570-14576; (c) Hein, C. D.; Liu, X.-M.; Wang, D., *Pharm Res.* **2008**, *25 (10)*, 2216-2230

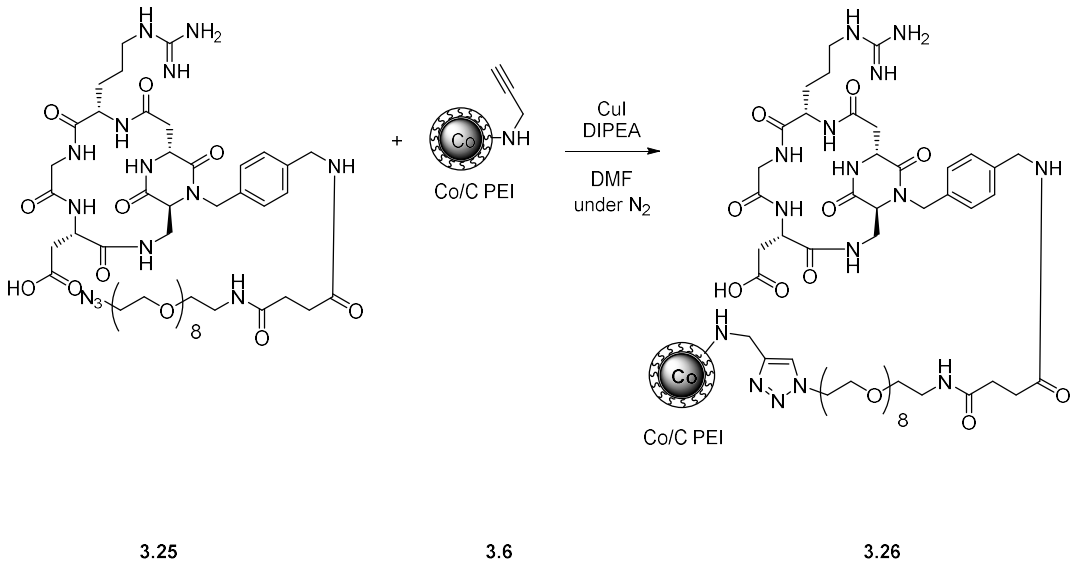

3.25 3.6 3.26

Scheme 3.14 – Synthesis of the conjugate with Co/C PEI MNPs **3.26**

The conjugate **3.26** (Scheme 3.14) was characterized through elemental analysis and SQUID measurement (Figure 3.18). The magnetization saturation value of the conjugate is 50.83 emu/g, as expected lower than the value of the MNPs **3.6** (70.57 emu/g).

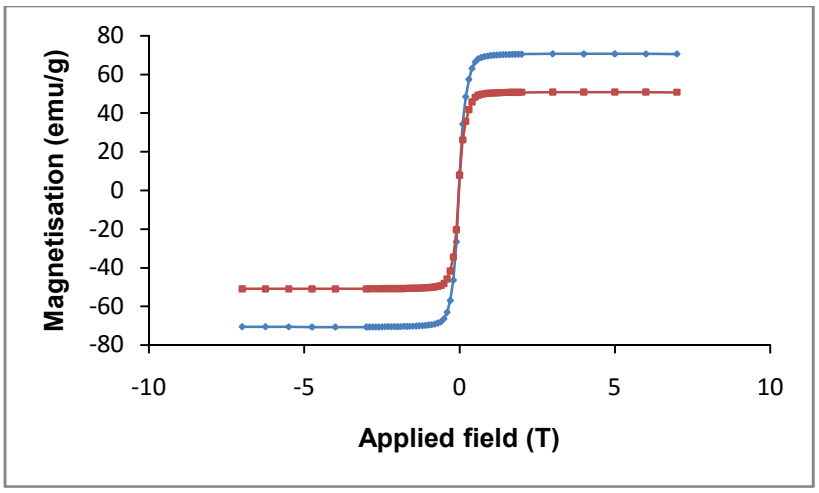

Figure 3.18 – SQUID measurements for alkyne-Co/C PEI MNPs and the for the conjugate (light blue: alkyne-Co/C PEI MNPs **3.6**; red: conjugate **3.26**)

The loading of **3.25** resulted very low (0.054 mmol/g). In any case it was enough to evaluate if the conjugation of an hydrophilic moiety changed the water dispersibility of MNPs **3.6**. The same test was performed in water at different pH values (pH = 8.0, pH = 6.9, pH = 7.4, pH = 6.0) following the procedure reported in reference 222a. The lightly basic pH was chosen to see if avoiding the protonation of the free amino groups on the MNPs surface would favor the dispersibility. The lightly acid pH (pH = 8.0) was selected to see the effect on the protonation of the free amino groups on the MNPs surface. Finally the physiological pH was selected because it is a common pH in a biological environment. Unfortunately, as presented in the pictures (Figure 3.19), the conjugate did not give a

stable suspension in water at the three pH values, thus preventing the conjugate to be biologically tested.

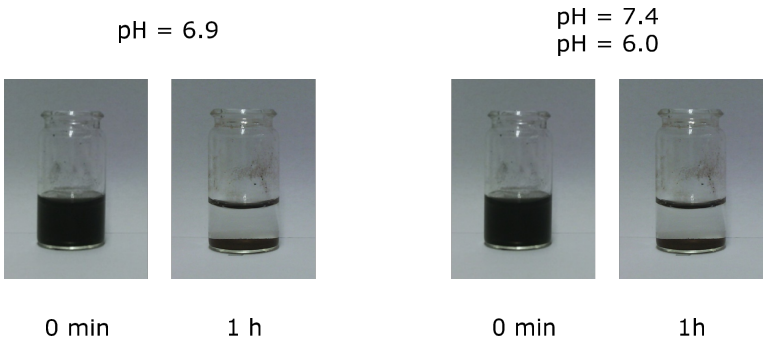

Figure 3.19 – Dispersibility test on the Co/C PEI MNPs conjugate **3.26**

3.26 (pH = 6.0, pH = 6.9, pH = 7.4): 0 min: dispersion; 15 min: precipitation ongoing (large amount already on the bottom of the flask); 30 min: almost everything precipitated; water almost limpid; 1h: everything precipitated and limpid water; 3 h: everything precipitated and limpid water. pH was adjusted with drops of NaOH 0.2 M or with drops of concentrated HNO_3.

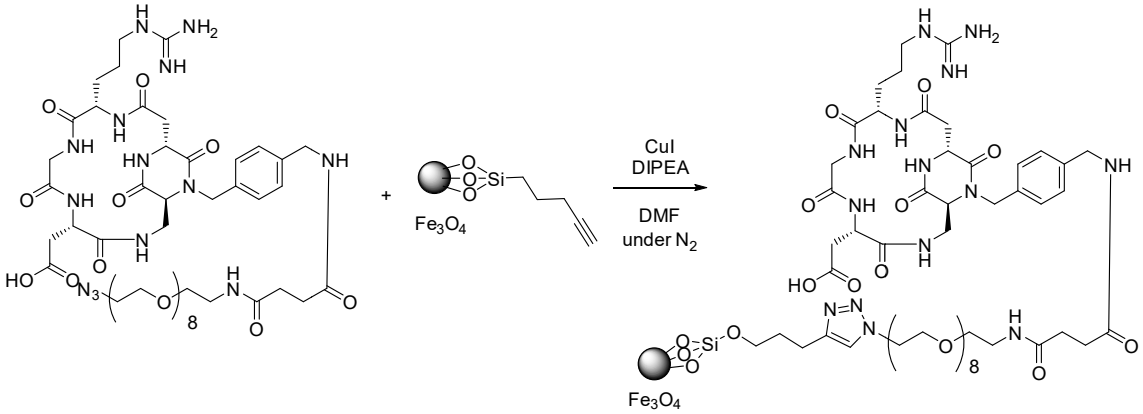

3.25 **3.7** **3.27**

Scheme 3.15 – Synthesis of the conjugate with Fe_3O_4@silica MNPs **3.27**

The conjugate **3.27** (Scheme 3.15) was characterized through the elemental analysis and the SQUID measurement (Figure 3.20). The saturation magnetization value measured is 43.59 emu/g, lower than the measured value for both naked MNPs (70.09 emu/g) and alkyne-silica coated MNPs (52.41 emu/g).

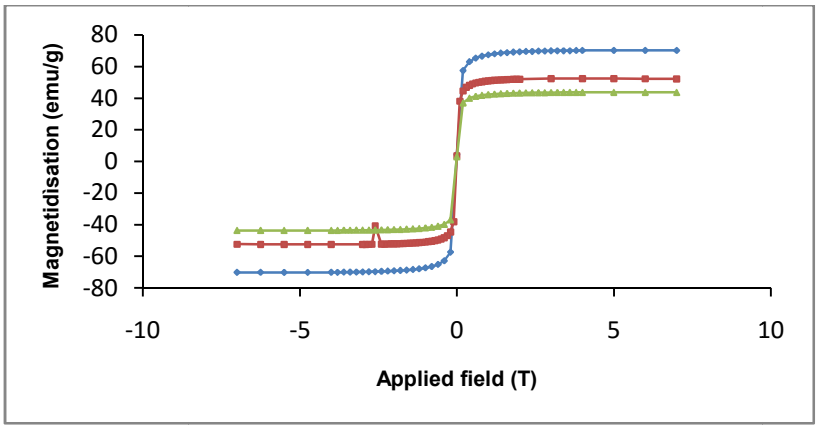

Figure 3.20 – SQUID measurements for Fe_3O_4 MNPs and alkyne-Fe_3O_4@silica (light blue: Fe_3O_4 MNPs **3.9**; green: alkyne-Fe_3O_4@silica **3.7**; red: conjugate **3.27**)

The loading of **3.25** resulted very low (0.041 mmol/g), in any case it was enough to evaluate the dispersibility in water of the conjugate (according to the procedure in reference 222a). The same test was performed at different pH values (pH = 8.0, pH = 6.9, pH = 7.4, pH = 6.0), to evaluate a possible effect on the silica shell. Finally the physiological pH was selected because it is a common pH in a biological environment. As presented in the pictures (Figure 3.21), the water dispersion at the three different pH values is not stable more than 3 h, thus preventing the conjugate to be biologically tested.

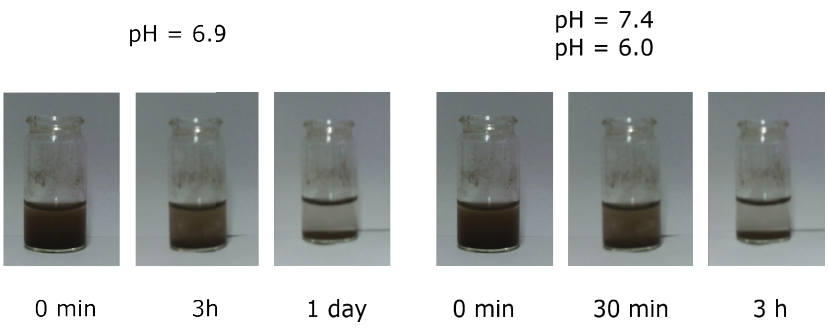

Figure 3.21 – Dispersibility test on the Fe_3O_4@silica MNPs conjugate **3.27**

3.27 (pH = 6.9): 0 min: dispersion; 15 min: dispersion but the precipitation was starting; 30 min: precipitation ongoing, water brown; 3 h: almost everything precipitated, water still brown; 5 h: everything precipitated and water still brown; 1day: everything precipitated and water still brown; 1 week: everything precipitated and limpid water. **3.27** (pH = 6.0, pH = 7.4): 0 min: dispersion; 15 min: dispersion but the precipitation was starting; 30 min: precipitation ongoing, water brown; 3 h: everything precipitated and limpid water. pH was adjusted with drops of NaOH 0.2 M or with drops of concentrated HNO_3.

Since the conjugate **3.27** was not dispersible in water as well as MNPs **3.14**, the conjugation with **3.25** was not performed.

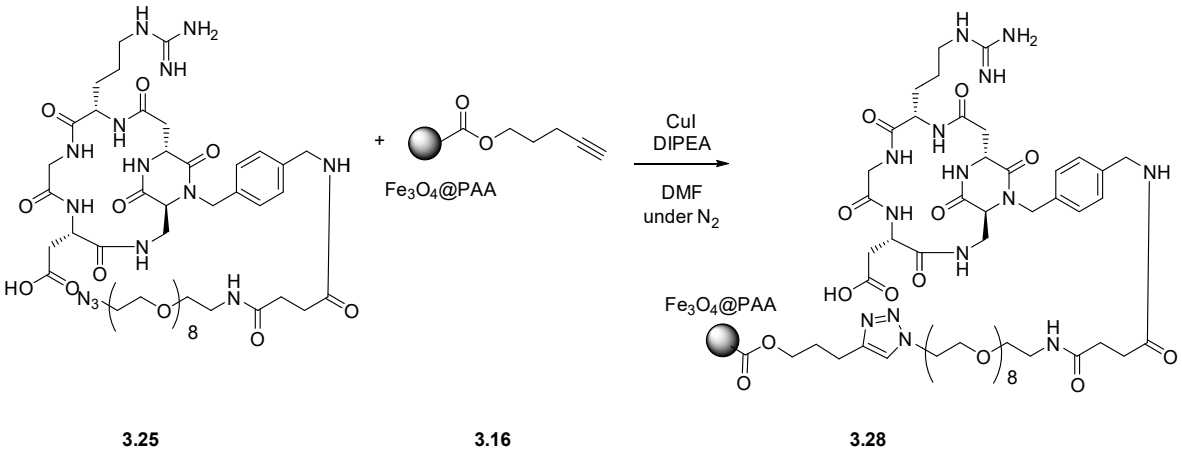

3.25 **3.16** **3.28**

Scheme 3.16 – Synthesis of the conjugate with Fe_3O_4@PAA MNPs

The conjugate **3.28** (Scheme 3.16) was characterized through the elemental analysis while further analysis are ongoing. The loading of **3.25** has resulted extremely low (0.00257 mmol/g), in any case it was enough to evaluate the dispersibility in water of the conjugate. The test was also performed at physiological pH (pH = 7.4) and in water (pH = 6.9) according to the procedure in reference 222a. The dispersibility test was not run at acid pH values because the carboxylic group would be obviously protonated as in MNPs **3.15** reducing the MNPs dispersibility (as on the naked MNPs)[194d]. As presented in the pictures, this conjugate is the only one that gave a suspension extremely stable both in water and in water with the pH adjusted to 7.4. (Figure 3.22).

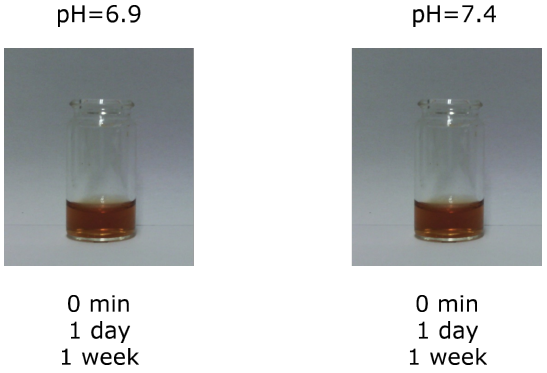

Figure 3.22 – Dispersibility test on the Fe_3O_4@silica MNPs conjugate **3.25**

3.28 (pH = 6.9 and pH = 7.4): 0 min -15 min – 30 min -1 h -3h -5h -1 day - 1 week: brown suspension stable over weeks. pH was adjusted with drops of NaOH 0.2 M.

3.7 Conclusions and outlooks

MNPs **3.1** were generated for biological purposes,[222a] but unfortunately the alkyne functionalization prevented their dispersion in water. As a matter of facts, different conjugations strategies directly performed on the $-NH_2$ group, might afford a conjugate able to produce stabile suspensions in water.

For what concerns the Fe_3O_4@silica MNPs, the most promising derivative is compound **3.14** which presents a good alkyne loading. Unfortunately, they do not produce stable suspensions in water so a different functionalization has to be developed to guarantee water-stable suspensions of the MNPs.

Since MNPs **3.16** and **3.18** are very similar and they generate extremely stable water suspensions, they are both suitable substrate for the conjugation with **3.25**. Up to now, only MNPs **3.16** were conjugated to **3.25**.

Among the three different kind of conjugates synthesized, only the conjugate **3.28** resulted appropriate for biological tests because of the water dispersibility. Unfortunately, the loading value of the bioactive compound **3.25** is extremely low. However, in all the conjugation reactions the yield was very low.

Since in the literature there are a lot of different protocols to perform click reactions and since in CuAAC the optimal conditions are known to be strictly depending on the substrates, the best strategy has to be selected according to the **3.25** and to the alkyne-MNPs. The conditions have to be optimize thus leading to higher loading value for the biological active compound. As an alternative, different synthetic conjugation methodologies, not considering CuAAC reactions, could be explored.

The final conjugated hopefully would show enhanced ability to inhibit the binding of biotinylated vitronectin to immobilized $\alpha_v\beta_3$ integrin if compared with unconjugated compound because of the contemporary presentation of several ligands on the MNPs (displaying a cooperative effect).

Since preliminary studies performed on the Fe_3O_4@PAA-COOH MNPs[194d] suggested a possible application in hyperthermia, the conjugate would be a candidate to be tested for selective hyperthermia therapy thanks to its ability of targeted delivery of MNPs to cell overexpressing the integrin $\alpha_v\beta_3$.

3.8 Experimental section

3.8.1 Materials and methods

All manipulations requiring anhydrous conditions were carried out in flame-dried glassware, with magnetic stirring and under a nitrogen atmosphere. All commercially available reagents were used as received. Carbon coated cobalt nanoparticles (Co/C, 20.5 m^2/g, mean particle size ≈ 25 nm) were obtained from Turbobeads Llc, Switzerland. Anhydrous solvents were purchased from commercial sources and withdrawn from the container by syringe, under a slight positive pressure of nitrogen. The reactions were monitored by analytical TLC using silica gel 60 F_{254} pre-coated glass plates (0.25 mm thickness). Visualization was accomplished by irradiation with a UV lamp and/or staining with a potassium permanganate alkaline solution or ninhydrin. Proton NMR spectra of compound **3.20** (and of all the intermediates in its synthetic pathway) were recorded on a spectrometer operating at 400.16 MHz while NMR spectra of compound **3.8**, **3.24**, **3.25** were recorded on a spectrometer operating at 300 MHz. Proton chemical shifts are reported in ppm (δ) with the solvent reference relative to TMS. The following abbreviations are used to describe spin multiplicity s = singlet, d = doublet, t = triplet, q = quartet, m = multiplet, bs = broad signal, dd = doublet of doublet, ddd = doublet of doublet of doublet, ddt = doublet of doublet of triplet. Carbon NMR spectra were recorded on a spectrometer operating at 100.63 MHz, with complete proton decoupling. Carbon chemical shifts are reported in ppm (δ) relative to TMS. ESI-MS spectra were recorded on the ion trap mass spectrometer Finnigan LCQ Advantage.

3.8.2 Synthesis

Co/C PEI MNPs (**3.1**) were synthesized according to literature procedure (Kainz, Q. M.; Fernandes, S.; Eichenseer, C. M.; Besostri, F.; Körner, H.; Müller, R.; Reiser, O., *Faraday Discuss.* **2014**, *175*, 27-39); EA: N loading = 7.28 mmol N/g

3.8 was synthesized according to literature procedure (Mader, H.; Li, X.; Saleh, S.; Link, M.; Kele, P.; Wolfbeis, O. S., *Ann. N. Y. Acad. Sci.* **2008**, *1130*, 218-223) and its analytical data were in agreement with those already published.

Fe_3O_4 @PAA-COOH MNPs (**3.15**) were synthesized according to literature procedure (Ge, J.; Hu, Y.; Biasini, M.; Dong, C.; Guo, J.; Beyermann, W. P.; Yin, Y., *Chem. Eur. J.* **2007**, *13*, 7153-7161)

3.20 was synthesized according to literature procedure (Wang, H.; Negretti, S.; Knauff, A. R.; Montgomery J., *Org. Lett.* **2015**, *17*, 1493-1496) and its analytical data were in agreement with those already published.

Co/C PEI-alkyne MNPs 3.6

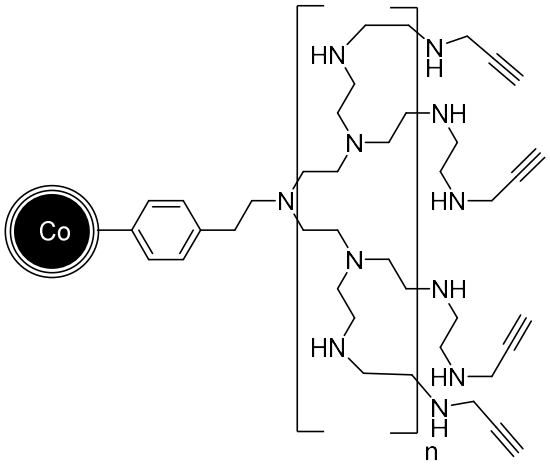

MNPs **3.1** (loading 7.28 mmol N/g-statistically 1.82 mmol NH_2/g, 100 mg) were suspended in dry DMF (3.0 mL) at room temperature under N_2. K_2CO_3 (0.728 mmol, 4.0 eq), previously milled, and propargyl bromide (80% in toluene, 3.640 mmol, 20.0 eq.) were sequentially added in one portion. The mixture was stirred heating at 80°C under N_2 for 24 hours, then it was allowed to reach rt. MNPs were collected thanks to an external magnetic field and liquids were removed. MNPs were sequentially washed with DCM (3 x 2 mL), water (3 x 2 mL), acetone (3 x 2 mL) and dried under vacuum. 95 mg of alkyne-MNPs **3.6** were recovered.

EA: alkyne loading = 1.542 mmol/g

Fe_3O_4 MNPs (3.9)

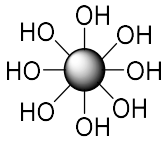

Fe_3O_4

Na_2CO_3 (5.29 g) was dissolved in water (200 mL) and the mixture was heated up to 90°C under argon atmosphere. In a second flask, $FeCl_3.6H_2O$ (6.75 g) and $FeCl_2.4H_2O$ (2.485 g) were dissolved in 50 mL of water; the mixture was added drop wise in the first flask when the temperature reached 90°C. The mixture was stirred for 1h under these conditions and then it was allowed to reach r.t.. MNPs were washed three times with water and then dried under vacuum.

Fe_3O_4@silica-alkyne MNPs (3.7)

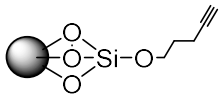

Fe_3O_4 MNPs (100 mg) were suspended in ultrapure water (44 mL) and sonicated for 10 min. Citric acid (244 mg) in ultrapure water (44 mL) was added to the suspension and the mixture was sonicated for 1 h keeping the temperature under 40°C. Particles were collected and liquids were eliminated. Particles were washed with ultrapure water (1 x 30 mL). A small portion of MNPs was dried under high vacuum and submitted to EA (%C = 0.895%); the remaining particles were stored in ethanol solution. MNPs were collected and EtOH was removed; MNPs were washed with toluene (to eliminate completely EtOH) and toluene was removed. MNPs were transferred into a flame-dried flask under N_2. **3.8** (1.13 mmol, directly used in toluene solution), acetic acid (24 μL) and ultrapure water (33 μL) were sequentially added at r.t. under N_2. The mixture was stirred heating to reflux for 24h, then it was allowed to reach r.t.. MNPs were collected thanks to an external magnetic field and liquids were removed. MNPs were sequentially washed with methanol (3 x 3 mL), hexane (3 x 3 mL) and acetone (3 x 3 mL); then they were dried under vacuum. 115 mg of alkyne-MNPs **3.7** were recovered.

EA: alkyne loading = 0.519 mmol/g

Fe_3O_4@silica-NH_2 MNPs (3.12)

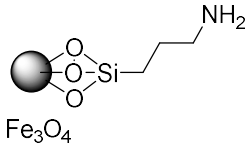

Fe_3O_4 MNPs (100 mg) were suspended in ultrapure water (44 mL) and sonicated for 10 min. Citric acid (244 mg) in ultrapure water (44 mL) was added to the suspension and the mixture was sonicated for 1 h keeping the temperature under 40°C. Particles were collected and liquids were eliminated. Particles were washed with ultrapure water (1 x 30 mL). MNPs were transferred into a flame-dried flask under N_2 and suspended in dry toluene (2 mL). **3.10** (1.76 mmol, 412 μL), acetic acid (24 μL) and ultrapure water (33 μL) were sequentially added at r.t. under N_2. The mixture was stirred heating to reflux for 24h, then it was allowed to reach r.t.. MNPs were collected and liquids were removed. MNPs were sequentially washed with methanol (3 x 3 mL), hexane (3 x 3 mL) and acetone (3 x 3 mL); then they were dried under vacuum. 95 mg of MNPs **3.12** were recovered.

EA: **3.10** loading = 1.76 mmol N/g

Fe_3O_4@silica-Cl MNPs (3.13)

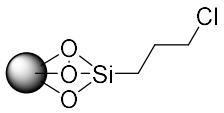

Fe_3O_4 MNPs (100 mg) were suspended in ultrapure water (44 mL) and sonicated for 10 min. Citric acid (244 mg) in ultrapure water (44 mL) was added to the suspension and the mixture was sonicated for 1 h keeping the temperature under 40°C. Particles were collected thanks to an external magnetic field and liquids were eliminated. Particles were washed with ultrapure water (1 x 30 mL). MNPs were transferred into a flame-dried flask under N_2 and suspended in dry toluene (2 mL). **3.11** (1.76 mmol, 424 μL), acetic acid (24 μL) and ultrapure water (33 μL) were sequentially added at r.t. under N_2. The mixture was stirred heating to reflux for 24h, then it was allowed to reach r.t.. MNPs were collected thanks to an external magnetic field and liquids were removed. MNPs were sequentially washed with methanol (3 x 3 mL), hexane (3 x 3 mL) and acetone (3 x 3 mL); then they were dried under vacuum. 90 mg of MNPs **3.13** were recovered.

EA: **3.11** loading = 1.71 mmol/g

Fe_3O_4@silica-NH-alkyne MNPs (3.14)

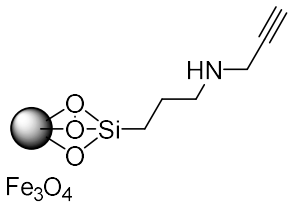

MNPs **3.12** (loading 1.76 mmol N/g, 77 mg) were suspended in dry DMF (3.0 mL) at room temperature under N_2. K_2CO_3 (0.135 mmol, 1.0 eq), previously milled, and propargyl bromide (80% in toluene, 0.675 mmol, 5.0 eq.) were sequentially added in one portion. The mixture was stirred heating at 80°C under N_2 for 24 hours, then it was allowed to reach rt. MNPs were collected thanks to an external magnetic field and liquids were removed. MNPs were sequentially washed with DCM (3 x 2 mL), water (3 x 2 mL), aceton (3 x 2 mL) and dried under vacuum. 83 mg of alkyne-MNPs **3.14** were recovered.

EA: alkyne loading = 1.54 mmol/g

Fe_3O_4@PAA-alkyne MNPs (3.16)

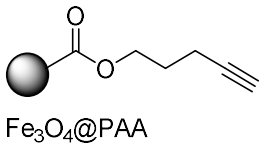

MNPs **3.15** (100 mg) were suspended in DCM (2 mL) at r.t. under N_2. 4-pentyn-1-ol (4.5 eq., 3.00 mmol), DCC (1.0 eq., 0.67 mmol) and DMAP (0.18 eq., 0.12 mmol), previously dissolved in DCM (1.5 mL and 0.5 mL respectively), were sequentially added. The mixture was stirred under these conditions for 24 h, then MNPs were collected thanks to an external magnetic field and liquids were removed. MNPs were washed with DCM (6 x 3 mL), then dried under vacuum and submitted to EA. 98 mg of alkyne-MNPs **3.16** were recovered.

EA: alkyne loading = 0.115 mmol/g

Fe_3O_4@PAA-alkyne MNPs (3.18)

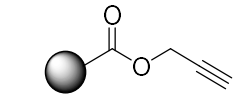

Fe_3O_4@PAA

MNPs **3.15** (700 mg) were suspended in DCM (50.0 mL) at r.t. under N_2. propargyl alcohol (1.8 eq., 21.04 mmol), DCC (1.0 eq., 11.69 mmol) and DMAP (0.2 eq., 21.04 mmol), were sequentially added. The mixture was stirred under these conditions for 24 h, then MNPs were collected thanks to an external magnetic field and liquids were removed. MNPs were washed with DCM (6 x 3 mL), then dried under vacuum and submitted to EA. 517 mg of alkyne-MNPs **3.18** were recovered.

EA: alkyne loading = 3.8 mmol/g

N_3-$(PEG)_8$-$(CH_2)_2$-COOH (3.24)

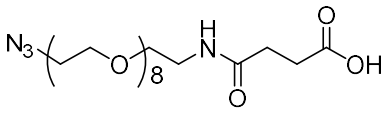

The reaction was performed in a flame-dried flask. N_3-$(PEG)_8$- NH_2 **3.23**(0.11 mmol, 50 mg) was dissolved in dry DCM (1.1 mL) at r.t. under N_2. Succinic anhydride (5.0 eq., 0.55 mmol) was added in one portion and the mixture was stirred over night under these conditions. In the morning the reaction was complete. The excess of succinic anhydride was eliminated by sublimation at 30°C and 0.1mbar. The final compound **3.24** was used without further purification.

Compound 3.24:

^{1}H-NMR (300 MHz, $CDCl_3$) δ 6.78 (s, 1H), 3.88 – 3.79 (m, 1H), 3.60 (dt, J = 4.9, 3.8 Hz, 32H), 3.53 – 3.46 (m, 2H), 3.41 – 3.36 (m, 2H), 3.35 – 3.29 (m, 2H), 2.59 (dd, J = 12.6, 6.2 Hz, 2H), 2.52 – 2.45 (m, 1H); ^{13}C-NMR (151 MHz, $CDCl_3$) δ 172.97, 70.73 – 69.33, 69.42 – 69.33, 52.79 – 50.57, 39.52, 30.95, 30.52; MS (ESI) *m/z* calcd. for $[C_{22}H_{41}N_4O_{11}]^-$: 537.2777 [M-H]$^-$; found: 537.2788; IR 2870 cm^{-1}, 2102 cm^{-1}, 1729 cm^{-1}, 1651cm^{-1}

***Cyclo*[DKP*f*3-RGD]-(PEG)$_8$-(CH$_2$)$_2$-COOH (3.25)**

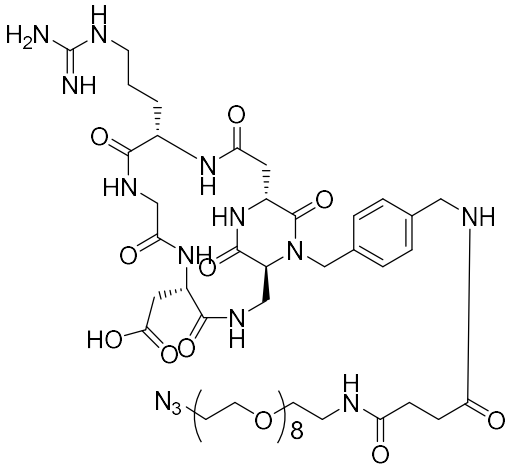

3.24 (1.25 eq., 39.6 μmol) was dissolved under N_2 in dry DCM (1.4 mL) at room temperature. NHS (1.8 eq., 57.1 μmol) and DIC (2.42 eq., 76.7 μmol) were added in one portion under these conditions. The solution was stirred for 2 h then the solvent was removed under reduced pressure and the resulting solid was taken-up with acetonitrile (1.4 mL). **3.20** (20 mg, 31.7 μmol), previously dissolved in a pH 7 buffer (0.7 mL), was cooled to 0°C and added in one portion to the mixture. The mixture was stirred overnight under these conditions. The pH was monitored for the first 2 h and it was kept between 7.3 and 7.6 by correction with a 0.2 M aqueous NaOH solution. In the morning volatiles were removed under reduced pressure and then dried under high vacuum. The crude, 80 mg, was checked by LR-Mass [$(M + 2H)^{2+}$ = 576.28] and used as crude in the following step.

***Cyclo*[DKP*f*3-RGD]-(PEG)$_8$-(CH$_2$)$_2$-COOH-Co/C PEI MNPs (3.26)**

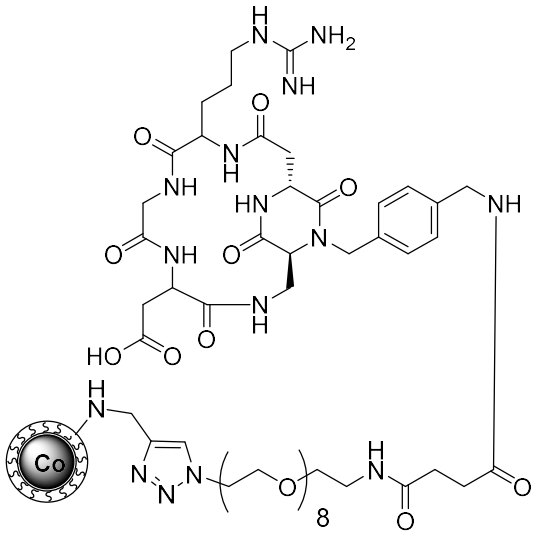

3.5 (18 μmol, 1.25 eq., crude*) was dissolved in DMF under N_2 at room temperature and the mixture was added to **3.6** (alkyne loading 1.542 mmol/g, 14 μmol of alkyne, 50 mg) at r.t. under N_2. CuI (18 μmol, 1.25 eq) and DIPEA (180 μmol, 12.5 eq) were added in one portion. The mixture was stirred at r.t. under N_2 over weekend. MNPs were collected, liquids were removed and MNPs were sequentially washed with DMF (3 x 3 mL) and DCM (3 x 3 mL). MNPs were dried under vacuum. 10 mg of MNPs were recovered and a portion was submitted to EA.

* calculation done considering a reaction yield of 50%

EA: **3.25** loading = 0.054 mmol/g; SQUID = 50.72 emu/g

***Cyclo*[DKP*f*3-RGD]-(PEG)$_8$-(CH$_2$)$_2$-COOH-Fe$_3$O$_4$@silica MNPs (3.27)**

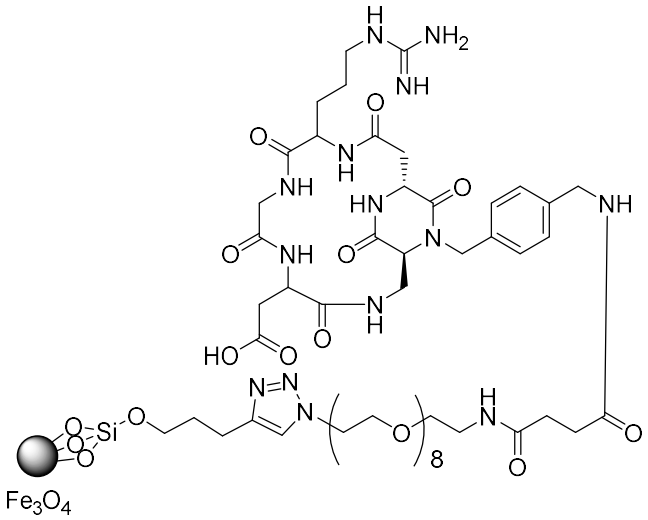

3.5 (3.13 μmol, 1.25 eq., crude*) was dissolved in DMF under N_2 at r.t. and the mixture was added to **3.7** (alkyne loading 0.519 mmol/g, 2.5 μmol of alkyne, 50 mg) at r.t. under N_2. CuI (13.25 μmol, 5.3 eq) and DIPEA (132.5 μmol, 53 eq) were added in one portion. The mixture was stirred at room temperature under N_2 over weekend. MNPs were collected, liquids were removed and MNPs were sequentially washed with DMF (3 x 3 mL) and DCM (3 x 3 mL). MNPs were dried under vacuum and a portion was submitted to EA.

* calculation done considering a reaction yield of 50%

EA: **3.25** loading = 0.04 mmol/g

***Cyclo*[DKP*f*3-RGD]-(PEG)$_8$-(CH$_2$)$_2$-COOH-Fe$_3$O$_4$@PAA MNPs (3.28)**

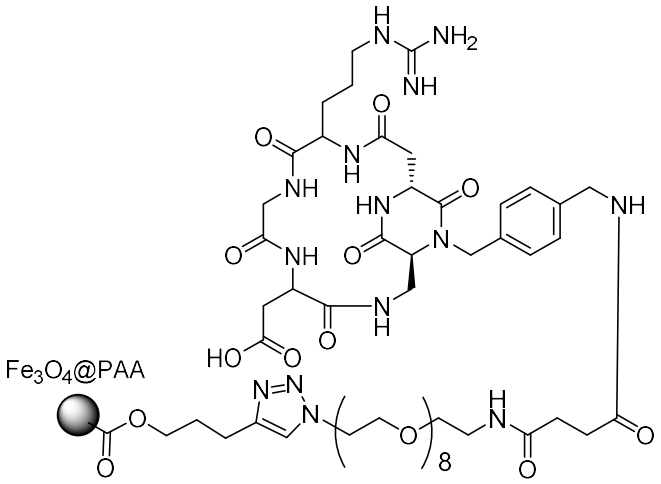

3.25 (μmol, 1.25 eq., crude*) was dissolved in DMF under N_2 at r.t. and the mixture was added to **3.16** (alkyne loading 0.115 mmol/g, 2.5 μmol of alkyne, 50 mg) at r.t. under N_2. CuI (μmol, 5.3 eq) and DIPEA (μmol, 53 eq) were added in one portion. The mixture was stirred at room temperature under N_2 over weekend. MNPs were collected, liquids were removed and MNPs were sequentially washed with DMF (3 x 3 mL) and DCM (3 x 3 mL). MNPs were dried under vacuum and a portion was submitted to EA.

* calculation done considering a reaction yield of 50%

EA: **3.25** loading = 0.00257 mmol/g

CHAPTER 4

RGD- AND *iso*DGR-β-ACPC INTEGRIN LIGANDS

4.1 Aim of the project

The aim of this project was the synthesis of a small collection of RGD- and *iso*DGR-containing peptidomimetics constrained by a five member ring scaffold. The cyclic derivatives obtained should be tested for activity and selectivity on integrins. The synthesis was planned in a mixed solid phase/solution phase approach.

4.2 β-ACC-containing peptidomimetics

4.2.1 β-amino acids

Four β-aminocarboxylic acids naturally occur in mammals: β-Alanine (**a**), (*S*)-β^2-aminoisobutyrate (**b**), (*R*)-β^2-aminoisobutyrate (**c**), and β^3-Leucine (**d**) (Figure 4.1). β-amino acids do not generally occur in mammalian proteins.[274] On the other hand many β-amino acids were isolated from plants and microorganisms as free molecules and components of peptides and antibiotics.[275]

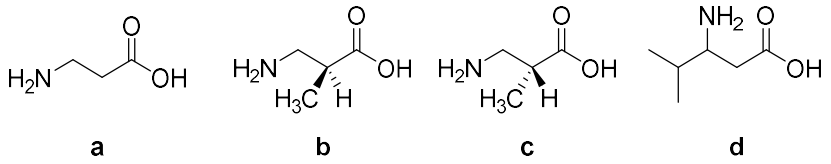

Figure 4.1 – β-amino acids occurring in mammals

β-amino acids received considerable attention as constituents of β-peptides[276], as analogues of the common protein amino acids and they were used as alternative substrates, to probe the structural specificity of α-amino acid binding-sites or as inhibitors of enzymes, or they were incorporated into synthetic peptides in combination with α-amino acids[277]. In addition, their incorporation into peptides of pharmacological interest was sometimes advantageous in terms of biological activity, metabolic stability or both because of their limited normal metabolism (and consequently, extended biological half-lives compared to the correspondent α-amino acid-containing peptides).[274] Early studies by Abderhalden[278], tempered by later studies[279] on enzymatic hydrolysis stability of peptide bonds involving β-amino acids, arose interest in their synthesis, hydrolytic stability, and conformational characteristics. β-amino acids stabilize distinct overall conformations of cyclopeptides and they act as γ-turn mimetics: if a single β-amino acid is incorporated into a cyclic pentapeptide, it preferably occupies the central position of a γ-turn. As a

[274] Griffith, O. W., *Ann. Rev. Biochem.* **1986**, *55*, 855-878

[275] For reviews see: (a) Dery, C. N. C in "The Chemistry and Biochemistry of Amino Acids" (ed. B Weinstein, New York: Dekker), **1976**, *4*, 241-299; (b) Dery, C. N. C in "The Chemistry and Biochemistry of Amino Acids" (ed. G. C. Barrett, London: Chapman & Hall) **1976**, 25-54

[276] Leading reviews: (a) Seebach, D.; Matthews, J. L., *Chem. Commun.***1997**, 2015-2022; (b) Gellman, S. H., *Acc. Chem. Res.***1998**, *31*, 173-180

[277] (a) Juaristi, E. in "Synthesis of β-amino acids" (Wiley-VHC: New York), **1997**; (b) Cole, D. C., *Tetrahedron* **1994**, *50*, 9517-9582; (c) Palomo, C.; Oiarbide, M.; González-Rego, M. C.; Sharma, A. K.; Garcia, J. M.; González, A.; Landa, C.; Linden, A., *Angew. Chem.* **2000**, *112*, 1105-1107; (d) Tang, T. P.; Ellman, J. A., *J. Org. Chem.* **1999**, *64*, 12-13, (e) Miyabe, H.; Fujii, K.; Naito, T., *Org. Lett.* **1999**, *1*, 569-572; (f) Marcotte, S.; Pannecoucke, X.; Feasson, C.; Quiron, J.-C.; *J. Org. Chem.* **1999**, *64*, 8461-8464; (g) Nocioni, A., M.; Papa, C.; Tomasini, C., *Tetrahedron Lett.* **1999**, *40*, 8453-8456; (h) Davies, S. G.; Ichihara, O., *Tetrahedron Lett.* **1999**, *40*, 9313-9316; (i) Enders, D.; Wahl, H.; Bettray, W., *Angew. Chem.* **1995**, *107*, 527-529; (j) Es-Sayed, M.; Gratkowski, C.; Krass, N.; Meyers, A. I.; De Meijere, A., *Tetrahedron Lett.* **1993**, *34*, 289-292; (k) Jefford, C. W.; Wang, J., *Tetrahedron Lett.* **1993**, *34*, 1111-1114; (l) Juaristi, E.; Quintana, D.; Escalante, J., *Aldrichimica Acta* **1994**, *27*, 3-11; (m) Burgess, K.; Liu, L. T.; Pal, B., *J. Org. Chem.* **1993**, *58*, 4758-4763; (n) Lombardi, A.; Saviano, M.; Nastri, F.; Maglio, O.; Mazzeo, M.; Isernia, C.; Paolillo, L.; Pavone, V., *Biopolymers* **1996**, *38*, 693-703; (o) Pavone, V.; Lombardi, A.; Yang, X.; Pedone, C.; Blasio, B. D., *Biopolymers* **1990**, *30*, 189-196; (p) Blasio, B. D.; Lombardi, A.; Yang, X.; Pedone, C.; Pavone, V., *Biopolymers* **1991**, *31*, 1181-1188; (q) Pavone, V.; Lombardi, A.; D'Auria, G.; Saviano, M.; Nastri F.; Paolillo, L.; Blasio, B. D.; Pedone, C., *Biopolymers* **1992**, *32*, 173-183; (r) Pavone, V.; Lombardi, A.; Maggi, C. A.; Quartara, L.; Pedone, C. J., *J, Pept. Sci.* **1995**, *1*, 236-240; (s) Dado, G. P.; Gellman, S. H., *J. Am. Chem. Soc.* **1994**, *116*, 1054-1062

[278] (a) Abderhalden, E.; Reich, F., *Fermentforschung*, **1928**, *10*, 173-194; (b) Adberhalden, E.; Fleischmann, R., *Fermenforschung* **1928**, *10*, 195-206

[279] Hanson, H. T.; Smith, E. L., *J. Biol. Chem.* **1948**, *175*, 833-848

consequence, the turn is extended by one CH_2 group and hence it is called a pseudo-γ-turn (Ψγ).[64]

Since only β-alanine and a few racemic β-aminocarboxylic acids are available commercially, most β-amino acids (both racemic and pure) must be synthesized or isolated from natural sources. A review on these aspect was written by Balenovic[280] and Drey and procedures of general utility are described in Griffith review[281]. However, β-amino acids synthesis is a research field always in evolution. β-amino acid racemates are generally resolved by the same methods used with α-amino acids[282] even if less easily by HPLC chiral solvent systems (presumably because of the increased separation between the amino and the carboxyl groups that allows greater flexibility in the complex with the solvent component).

4.2.2 *Cyclo*[β-ACC-RGD] peptidomimetics

4.2.2.1 β-ACC scaffolds

The use of rigid amino acids is a powerful tool to investigate the bioactive structure of peptides[283] and to build constrained peptides. Among the various rigid amino acids, in this paragraph β-aminocyclopropane carboxylic acids (β-ACCs, Figure 4.2)[284] will be treated in particular for what concerns the synthesis of cyclic peptides.[285] These cyclic β-amino acids are among the most restricted β-alanine derivatives. The rigidity is conferred by the bridging of the carbons bearing the amino and the carboxylic acid functionality by a methylene group.[286]

---

[280] Balenovic, K. in "CibaFound. Symp. Amino Acids and Peptides with Antimetabolic Activity" (ed. G. E. W. Wolstenholme, Boston: Little Brown), **1958**, 5-16

[281] (a) Kupiecki, F. P.; Coon, M. J., *J. Biol. Chem.* **1957**, *229*, 743-754; (b) Kakimoto, Y.; Armstrong, M. D., *J. Biol. Chem.* **1961**, *236*, 3283-3286; (c) Bohme, H.; Broese, R.; Eiden, F., *Chem. Ber.* **1959**, 92, 1258-1262; (d) Bauce, L. G.; Goren, H. J., *Int. J. Peptide Protein Res.* **1979**, *14*, 216-226; (e) Sekura, R.; Hochreiter, M.; Meister A., *J. Biol. Chem.* **1976**, *251*, 2263-2270; (f) Birkofer, L.; Storch, I., *Chem. Ber.* **1953**, *86*, 529-534; (g) Dietriche, R. F.; Sakurai, T.; Kenyon, G. L., *J. Org. Chem.* **1979**, *44*, 1894-1895; (h) Shimohigashi, Y.; Waki, M.; Izumiya, N., *Mem. Fac. Sci. Kyushu, Univ., Ser. C* **1979**, *11*, 217-224; (i) Shimohigashi, Y.; Waki, M.; Izumiya, N., *Bull. Chem. Soc. Jpn.* **1979**, *52*, 949-950; (j) Wingo, W. J.; Lewis, H. B., *J. Biol. Chem.* **1946**, *165*, 339-346; (k) Gundermann, K. D., *Ann. Chem.* **1954**, *588*, 167-181

[282] For example see: (a) Rossi, D.; Lucente, G.; Romeo, A., *Experientia*, **33**, 1557-1559; (b) Khedouri, E.; Meister, A., *J. Biol. Chem.* **1965**, *240*, 3357-3360; (c) Cohen, S. G.; Khedouri, E., *J. Am. Chem. Soc.* **1961**, *83*, 1093-1096; (d) Kotani, H.; Kuze, Y.; Uchida, S.; Miyabe, T.; Iimori, T.; Okano, K., Kobayashi, S.; Ohno, M., *Agric. Biol. Chem.* **1983**, *47*, 1363-1365; (e) Winnacker, E. L.; Herbst, M. M.; Barker, H. A., *Biochim. Biophys. Acta* **1971**, *237*, 280-283; (f) Pollock, G., *Anal. Biochem.* **1974**, *57*, 82-88; (g) Solem, E., *Clin. Chim. Acta* **1974**, *53*, 183-190; chiral solvents: (h) Gil-Av, E.; Tishbee, A.; Hare, P. E., *J. Am. Chem. Soc.* **1980**, *102*, 5115-5117; (i) Lam, S. K., *J. Chromatogr.* **1982**, *234*, 485-488; (j) Gilon, C.; Leshem, R.; Grushka, E., *Anal. Chem.* **1980**, *52*, 1206-1209; (d) Weinstein, S.; Engel, M. H.; Hare, P. E., *Anal. Biochem.* **1982**, *121*, 370-377; chiral stationary phase: (k) Pirkle, W. H.; Hyun, M. H.; Tsipouras, A. Hamper, B. C.; Banks, B., *J. Pharmacol. Biomed. Anal.* **1984**, 2, 173-181; (l) Gubitz, G.; Jellenz, W.; Santi, W., *J. Chromatogr.* **1981**, *203*, 377-384; (m) Pirkle, W. H.; Finn, J. M.; Schreiner, J. L.; Hamper, B. C., *J. Am. Chem. Soc.* **1981**, *103*, 3964-3966

[283] (a) Jakubke, H.-D. in "Peptide" (Spektrum: Heidelberg), **1996**; (b) Jones, J. in "Amino Acid and Peptide Synthesis" (Oxford University Press: Oxford, UK,) **1992**

[284] For a review see: Gnad, F.; Reiser, O., *Chem. Rev.* **2003**, *103*, 1603-1624

[285] (a) Paulini, K.; Reissing, H.-U., *Liebigs Ann. Chem.* **1994**, 549-554; (b) Beck-Sickinger, A. G.; Hoffmann, E.; Paulini, K.; Reissing, H.-U.; Willim, K.-D.; Wieland, H. A.; Jung, G., *Biochem. Soc. Trans.* **1994**, 22, 145-149; (c) Hibbs, D. E.; Hursthouse, M. B.; Jones, I. G.; Jones, W.; Malik, K. M. A.; North, M., *Tetrahedron* **1997**, *53*, 17417-17424; (d) North, M., *J. Pept. Sci.* **2000**, *6*, 301-313; (e) Voigt, J.; Noltemeyer, M.; Reiser, O., *Synlett* **1997**, 202-204; (f) Bubert, C.; Cabrele, C.; Reiser, O., *Synlett* **1997**, 827-829

[286] Beumer, R.; Reiser, O., *Tetrahedron* **2001**, *57*, 6497-6503

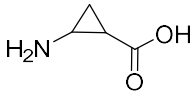

Figure 4.2 – β-aminocylopropanecarboxylic acid

Reiser and co-workers synthesized short α/β peptides alternating α-amino acids (L-Ala residues) with 3-substituted-*cis*-β-ACCs. The product (Figure 4.3) showed a high affinity to the Y_1 receptor of neuropeptide Y.[287] In addition, β-ACCs improved the stabilization of the secondary structure of peptides[288] and have been embedded into cyclic RGD peptides as constraining scaffolds (as presented in paragraph 4.2.2.2).[289]

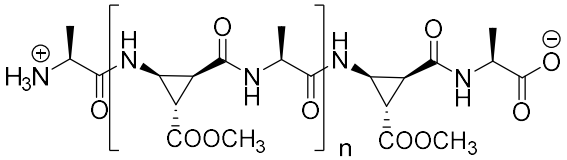

Figure 4.3 - α/β peptides alternating α-amino acids (L-Ala residues) with 3-substituted-*cis*-β-ACCs

However their synthesis and utilization as building blocks in peptide synthesis is not simple because the two new stereocenters created require a control of diastereoselectivity (*cis*- or *trans*-β-ACC) and enantioselectivity.[286] A further problem is related to the β-ACCs nature of vicinally donor-acceptor 1,2-substituted cyclopropanes, which are extremely prone to ring opening.[290] These aspect could be useful for some synthetic applications but on the other hand it means that these derivatives are only stable if the amino group is protected by at least one electron withdrawing group.[291] However a lot of effort was done to improve their synthesis and a number of different approaches towards the synthesis[292] of β-ACCs and their incorporation into peptides[285] are present in the literature. An efficient synthesis of both *cis*- and *trans*-β-ACC (**4.1** and **4.2** respectively, Figure 4.4) diastereo- and enantiomerically pure was developed.[285f,286,292f]

[287] Koglin, N.; Zorn, C.; Beumer, R.; Cabrele, C.; Bubert, C.; Sewald, N.; Reiser, O.; Beck-Sickinger, A. G., *Angew. Chem. Int. Ed.* **2003**, *42*, 202-205
[288] De Pol, S.; Zorn, C.; Zerbe, O.; Reiser, O., *Angew. Chem. Int. Ed.* **2004**, *43*, 511-514
[289] Urman, S.; Gaus, K.; Yang, Y.; Strijowski, U.; Sewald, N.; De Pol, S.; Reiser, O., *Angew. Chem. Int. Ed.* **2007**, *46*, 3976-3978
[290] For a review see: (a) Ressing, H. U., *Top Curr. Chem.* **1988**, *144*, 73; for an examples see: (b) Patra, P. K.; Reissing, H.-U., *Synlett* **2001**, 33-36; (c) Böhm, C.; Reiser, O., *Organic Lett.* **2001**, *3*, 1315-1318
[291] For an exception see: Kraus, G. A.; Kim, H.; Thomas, P. J.; Metzler, D. E.; Metzler, C. M.; Taylor, J. E., *Synth. Commun.* **1990**, *20*, 2667-2673
[292] (a) Cannon, J. G.; Garst, J. E., *J. Org. Chem.* **1975**, *40*, 182-184; (b) Shroff, C. C.; Stewart, W. S.; Uhm, S. J.; Wheeler, J. W., *J. Org, Chem.* **1971**, *22*, 3356-3361; (c) Paulini, K.; Reissing, H.-U., *Liebigs Ann. Chem.* **1991**, 455-461; (d) Vilsmaier, E. in "The Chemistry of the Cyclopropyl Group" (ed.; VHC-Wiley: New-York), **1987**, 1341; (e) Martin-Vila, M.; Murray, E.; Aguada, G. P.; Alvarez-Larena, A.; Branchadell, V.; Minguillon, C. G. E.; Ortuno, R. M., *Tetrahedron: Asymmetry* **2000**, *11*, 3569-3584; (f) Beumer, R.; Bubert, C.; Cabrele, C.; Vielhauer, O.; Pietzsch, M.; Reiser, O., *J. Org. Chem.* **2000**, *65*, 8960-8969; (g) Bubert, C.; Voigt, J.; Biasetton, S.; Reiser, O., *Synlett* **1994**, 675-677

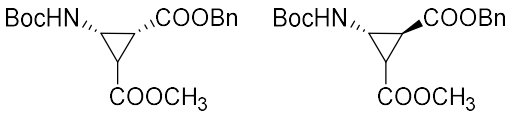

4.1 **4.2**

Figure 4.4 - **4.1** and **4.2**

Since these constrained molecules are often difficult to prepare as amine-free or they are unstable in the unprotected form, coupling through the classical carboxylic acid activation pathway could be difficult. Reiser and co-workers developed a procedure for a one-pot amine deprotection-coupling of a Boc-β-ACC[285f] or an Alloc-β-ACC[293] with an amine-protected amino acid. Thus, (+)-β-ACC **4.1 a** and (-)-β-ACC **4.1 b** were introduced into the cyclic peptides already coupled to Fmoc-Asp(O*t*Bu)-OH (respectively **4.2** and **4.3**, Figure 4.5).

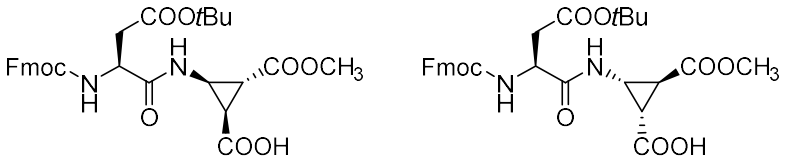

4.2 **4.3**

Figure 4.5 – Dipeptide building blocks containing the β-ACC scaffold and Fmoc-Asp(O*t*Bu)-OH

4.2.2.2 Conformational and biological evaluation of the cyclic peptidomimetics

The chemistry and biology of RGD-containing peptides were already illustrated in Chapter 1. The conformation has an important role in this class of peptides, thus β-ACCs-seemed interesting constraining moieties to produce cyclic RGD-containing peptides. Reiser group synthesized *Cyclo*-[Arg-Gly-Asp-(+)-β-ACC-Val] **4.4** and *Cyclo*[Arg-Gly-Asp-(-)-β-ACC-Val] **4.5** containing enantiomeric (+)- or (-)- β-ACC adjacent to the RGD sequence (Figure 4.6).

[293] Zorn, C.; Gnad, F.; Salmen, S.; Herpin, T.; Reiser, O., *Tetrahedron Lett.* **2001**, *42*, 7049-7053

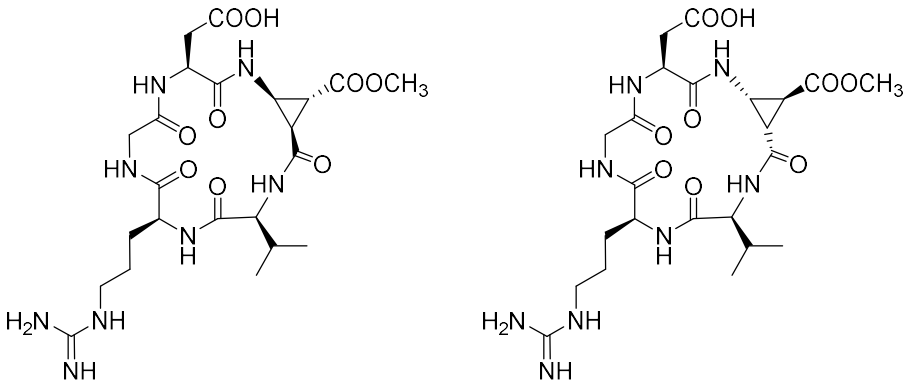

4.4 **4.5**

Figure 4.6 – Cyclic peptides containing the β-ACC scaffolds

The biological activity of peptides **4.4** and **4.5** was evaluated and compared to *Cyclo*[Arg-Gly-Asp-D-Phe-Val] **4.6**[54,294] and *Cyclo*[Arg-Gly-Asp-D-Phe-Val-β-Ala] **4.7**[295] in cell-adhesion assays on K562 and WM115. K562 is a myelogenous leukemia cell line in which adhesion to ECM proteins is mediated predominantly by integrin $\alpha_5\beta_1$ while WM115 is a human skin melanoma cell line in which adhesion to ECM proteins is mediated predominantly by integrin $\alpha_v\beta_3$. The inhibition of the adhesion of the cells was evaluated establishing the IC_{50} value of the various compounds (Table 4.1).

Compound	WM115, $\alpha_v\beta_3$ IC_{50} μM	K562, $\alpha_5\beta_1$ IC_{50} μM	Ratio IC_{50} K562/WM115
4.6	0.2 ± 0.06	18.5 ± 6.4	92.5
4.7	1.4 ± 0.40	9.1 ± 5.3	6.5
4.4	0.02 ± 0.002	1.5 ± 0.5	75.0
4.5	0.6 ± 0.23	1.8 ± 0.7	3.0

Table 4.1 – IC_{50} values of the cyclic peptides as determined by cell-adhesion assays

The value measured on WM115 cells for the reference compound **4.6**[294b] (IC_{50} = 0.2 μM) is in good agreement with literature data as estimated by Aumailley et al.[54]. Peptide **4.4**, (containing the (+)-β-ACC), displayed a tenfold higher affinity (IC_{50} = 20 nM) than **4.6**. Peptides **4.4** and **4.5** were proved to nearly equally inhibit integrin $\alpha_5\beta_1$ mediated adhesion of K562 cells to fibronectin with IC_{50} values of 1.5 μM and 1.8 μM respectively. This means that they are five- to sixfold more active than **4.7**, which was twice as active as peptide **4.6**. Peptides **4.4** and **4.5** had a larger influence on the interaction between vitronectin and integrin $\alpha_v\beta_3$ than on the interaction between fibronectin and integrin $\alpha_5\beta_1$. As shown in Table 4.1, peptides **4.6**[296] and **4.4** showed a higher selectivity towards integrins $\alpha_v\beta_3$.

[294] (a) Gurrath, M.; Müller, G.; Kessler, H.; Aumailley, M.; Timpl, R., *Eur. J. Biochem.* **1992**, *210*, 911-921; (b) Haubner, R.; Finsinger, D.; Kessler, H., *Angew. Chem. Int. Ed. Engl.* **1997**, 36, 1374-1389

[295] Zimmermann, D.; Guthöhrlein E.; Malešević, M.; Sewald, K.; Wobbe, L.; Heggemann, C.; Sewald, N., *ChemBioChem* **2005**, 6, 272-276

Distance geometry calculations were performed applying the distance restrains derived from the NOESY spectra. For both peptides, one major cluster (comprising more than 95% of the structures) was obtained and used as starting structure for restrained molecular dynamics calculations (Figure 4.7). For peptide **4.4** only one major torsion-angle cluster was observed (more than 87% of the observed conformation were contained) while for peptide **4.5** two clusters were observed (the major one was populated during the 80% of the trajectories).

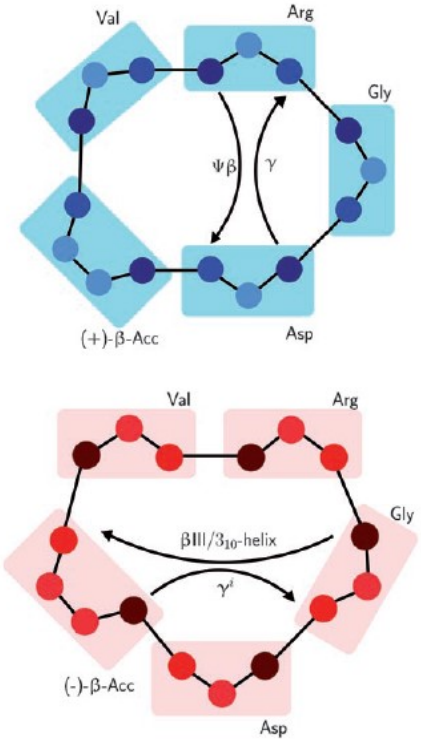

Figure 4.7 – Schematic representation of the structure of peptides **4.4** and **4.5**

The representations were obtained by restrained MD calculations based on experimental distance information. Ψβ indicates a pseudo-β-turn and the arrows indicate the hydrogen bonds.

In both peptides, the backbone remained rigid around the β-ACC residue. However a high dynamics in the RGD sequence was observed, as known for RGD peptides[296]. According to Kessler and co-workers, the RGD motif should adopt a non-stretched conformation to interact with $\alpha_v\beta_3$ integrins, whit a C^{β}(Arg)-C^{β}(Asp) distance of about 650 pm.[57c] For example, reference compound **4.7**, presents an elongated conformation of the RGD motif with a C^{β}(Arg)-C^{β}(Asp) distance of 930 pm which correlates well with the lower affinity toward integrin $\alpha_v\beta_3$[57c]. According to the torsion angles, the Gly residue in peptide **4.4** is in the central position of a γ-turn while (+)-β-ACC occupies the *i*+1 position of a pseudo-β-turn and the C^{β}(Arg)-C^{β}(Asp) distance lies between 600 pm and 800 pm for the majority of the structures (706 pm in the central structure of the major cluster). For peptide

[296] Chatterjee, J.; Mierke, D.; Kessler, H., *J. A. Chem. Soc.* **2006**, *128*, 15164-15172

4.5 this distance is between 700 pm and 900 pm for the majority of the structures (although it fluctuates during the trajectory). These data indicate a more stretched conformation of the RGD sequence for peptide **4.5** than for peptide **4.4**, as confirmed also by the C^{α}(Arg)-C^{α}(Asp) distance. In **4.4** the β and γ turns are at the same positions as in **4.6** (even if the type of β-turn is different) while **4.5** displays a more stretched RGD sequence like **4.7**. All these data in combination with the biological results indicates that the more active cyclic β-ACC-RGD-containing $\alpha_V\beta_3$ integrin ligand is **4.4**, which showed a bent RGD sequence.

4.2.2.3 Synthesis of the cyclic ligands

Reiser and co-workers were able to couple Boc-β-ACC with amino acids via their ammonium chloride salt through a protocol which employs saturated HCl gas ethyl acetate.[294a] The procedure was employed to synthesize the building blocks **4.8** and **4.9** (Scheme 4.1).

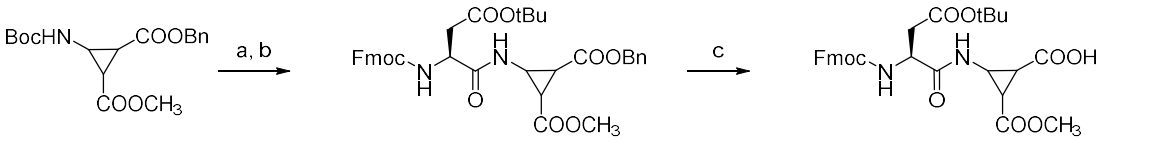

4.1 a: (+)-beta-ACC
4.1 b: (-)-beta-ACC

4.2: Fmoc-Asp(O*t*Bu)-(+)-beta-ACC
4.3: Fmoc-Asp(O*t*Bu)-(-)-beta-ACC

4.8: Fmoc-Asp(O*t*Bu)-(+)-beta-ACC-COOH
4.9: Fmoc-Asp(O*t*Bu)-(+)-beta-ACC-COOH

Scheme 4.1 – Synthesis of **4.2** and **4.3**

Reagents and conditions: a) HCl/Ethyl acetate, under N_2, 0°C; b) Fmoc-Asp(O*t*Bu)-OH, EDC, HOBt, Py DCM, r.t.; c) 1,4-cyclohexadiene in pentane, Pd/C 5%, MeOH, r.t., under N_2.

The linear precursors **4.10** and **4.11** were assembled by SPPS with a Fmoc/*t*Bu protection protocol (Scheme 4.2). *O*-chlorotritylchloride resin (loading: 1.51 mmol/g) was selected as solid support. Each coupling step consisted in:

i) activation of the Fmoc-protected amino acid,
ii) addition of the activated amino acid to the resin to effect the coupling reaction,
iii) capping and Fmoc- deprotection

The cleavage of the linear precursor from the resin was accomplished in weakly acidic conditions.

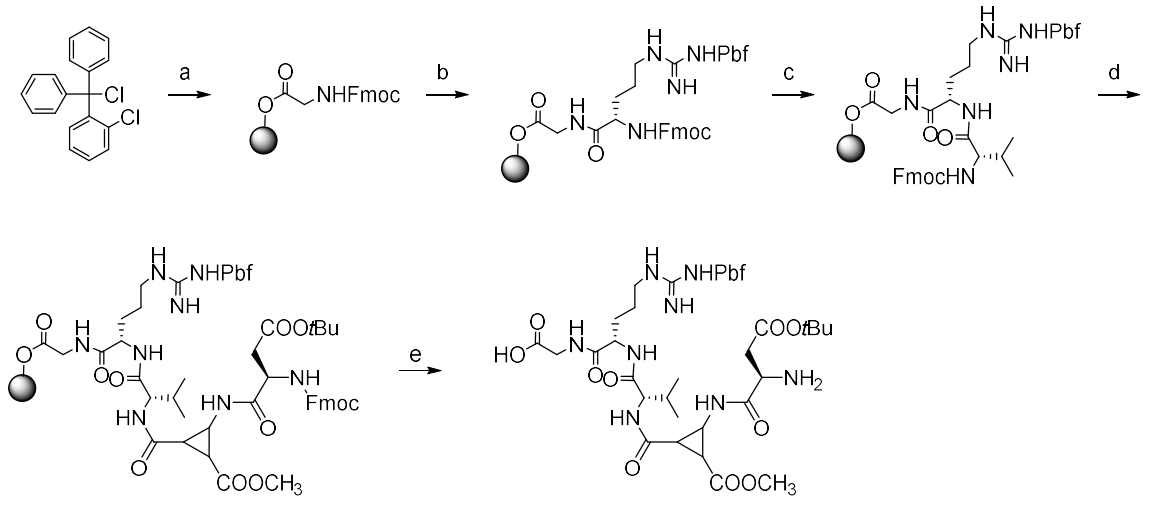

4.10
4.11

Scheme 4.2 – Linear precursors (**4.10** and **4.11**) synthesis

Reagents and conditions: a) Fmoc-Gly-OH, DIPEA, DCM; b) 1) 2%DBU in DMF, 2% piperidine DMF; 2) Fmoc-Arg(Pbf)-OH, TBTU, DIPEA; c) 1) 2% DBU in DMF, 2% piperidine DMF; 2) Fmoc-Val-OH, DIPEA, DCM; d) 1) 2% DBU in DMF, 2% piperidine DMF; 2) **4.2** or **4.3** HATU, DIPEA; e) 1) 2% DBU in DMF, 2% piperidine DMF; 2) TFA/DCM.

The linear cleaved precursors (**4.10** and **4.11**) were cyclised under pseudo-high dilution conditions to give derivatives **4.12** and **4.13**.[297] Fmoc-ortogonal PGs were selected for the lateral chains of the amino acids (Pbf for Arg and *t*Bu for Asp). The cyclic derivatives **4.12** and **4.13** were deprotected (by treatment with TFA/Et_3SiH/water, 95%/2.5%/2.5%) and purified by preparative HPLC (Scheme 4.2) to give the final peptidomimetics **4.14** and **4.15**.

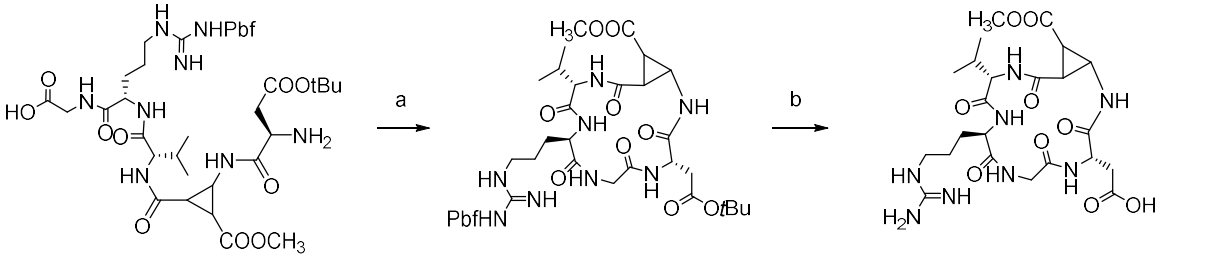

4.10
4.11

4.12
4.13

4.14: Cyclo[Arg-Gly-Asp-(+)-beta-ACC-Val]
4.15: Cyclo[Arg-Gly-Asp-(-)-beta-ACC-Val]

Scheme 4.3 – Cyclic derivatives synthesis

Reagents and conditions: a) HATU, DIPEA, r.t.; b) TFA/Et_3SiH/water 95%/2.5%/2.5%

[297] Malešević, M.; Strijowski, U.; Bächle, D.; Sewald, N., *J. Biotechnol.* **2004**, *112*, 73-77

4.3 β-ACPC-containing peptidomimetics

4.3.1 β-ACPC scaffolds

A wide variety of natural products contain α-alkyl-β-amino acids,[274a,298] many of which exhibit interesting biological properties. For example, *cis*-(1*R*,2*S*)-2-aminocyclopentane-1-carboxylate **4.16** (Cispentacin, Figure 4.8) is a potent antifungal agent.[299] However, the incorporation of an oxygen or a sulfur heteroatom within the carbocyclic skeleton, generates heterocyclic β-amino acid derivatives **4.17** (Figure 4.8) and **4.18** (Figure 4.8) with a significant reduced biological activity.[300] The *cis*-*N*-heterocyclic compound **4.19** (Figure 4.8) and its Boc-protected derivative **4.20** (Figure 4.8) has also found application in medicinal chemistry as probe to test the structure of the GABA receptor[301] and as bioactive compound respectively. **4.20** has resulted a modestly active influenza neuramidase inhibitor.[302]

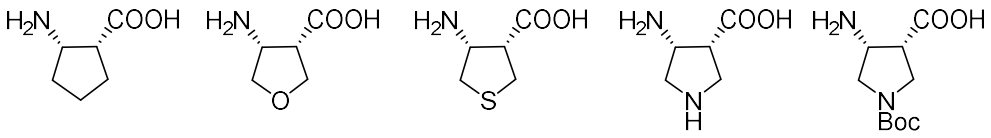

4.16 **4.17** **4.18** **4.19** **4.20**

Figure 4.8 – Cispentacin and its heterocyclic analogues

Furthermore these kind of derivatives were embedded also in longer structures, such as the water soluble short chain peptides **4.22** (Figure 4.9) containing both transpentacin and the *trans*-derivative **4.21** residues (Figure 4.9). It adopted a distinct helical secondary structures in solution.[303]

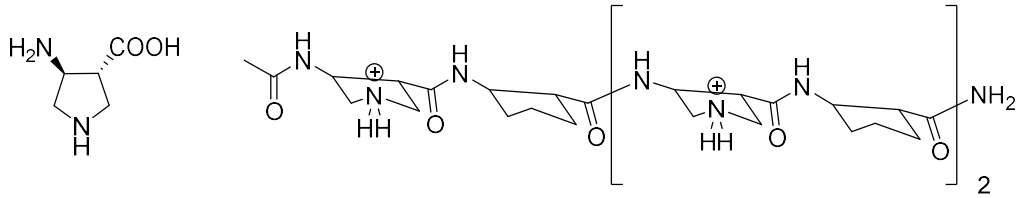

4.21 **4.22**

Figure 4.9 – Derivatives **4.21** and **4.22**

[298] (a) Dery, C. N. C. in "The Chemistry and Biochemistry of Amino Acids" (ed. G. C. Barrett, Chapman & Hall: London), **1984**, *4*, 25
[299] (a) Konishi, M.; Nishio, M.; Saitoh, K.; Miyaki, T.; Oki, T.; Kawaguchi, H., *J. Antibiot.* **1989**, *42*, 1749-1755; (b) Oki, T.; Hirano, M.; Tomatsu, K.; Numata, K.; Kamei, H., *J. Antibiot.* **1989**, *42*, 1756-1762; (c) Iwamoto, T.; Tsujii, E.; Ezaki, M.; Fujie, A.; Hashimoto, S.; Okuhara, M.; Kohsaka, M.; Imanaka, H., *J. Antibiot.* **1990**, *43*, 1-7; (d) Kawabata, K.; Inamoto Y.; Sakane, K.; *J. Antibiot.* **1990**, *43*, 513-518; (e) Ohki, H.; Inamoto, Y.; Kawabata, K.; Kamimura, T.; Sakane, K., *J. Antibiot.* **1991**, *44*, 546-549
[300] Mittendrof, J.; Kunish, F.; Matzke, M.; Militzer, H.-C.; Schmidt, A.; Schönfeld, W., *Biorg. Med. Chem. Lett.* **2003**, *13*, 433-436
[301] Thorbeck, P.; Hjeds, H.; Schaumburg, K., *Acta Chem. Scand.* **1981**, *B35*, 473-478
[302] Bunnage, M. E.; Davies, S. G.; Roberts, P. M.; Smith A. D.; Withey J. M., *Biomol. Chem.* **2004**, *2*, 2763-2776
[303] Wang, X.; Espinosa, J. F.; Gellman, S. H., *J. Am. Chem. Soc.* **2000**, *122*, 4821-4822

Also 2:1 and 1:2 α/β-backbone patterns (Figure 4.10) were found to promote helix formation in short oligomers.[304]

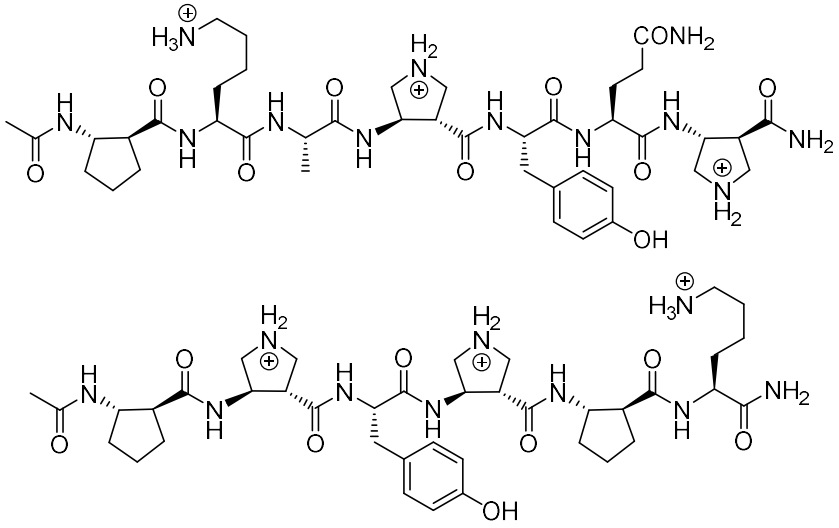

Figure 4.10 – Short oligomers containing 2:1 and 1:2 α/β-backbone patterns

Reiser and co-workers presented helical peptides foldamers (Figure 4.11) containing β-*cis*-aminocyclopentanecarboxylic (β-*cis*-ACPC, **4.16** and **4.23**, Figure 4.12) acids.[305] These molecules have been combined following the stereochemical patterning approach by Fülöp and co-workers.[306] They have shown a defined spatial distributions of their functional groups in polar solvents including water.

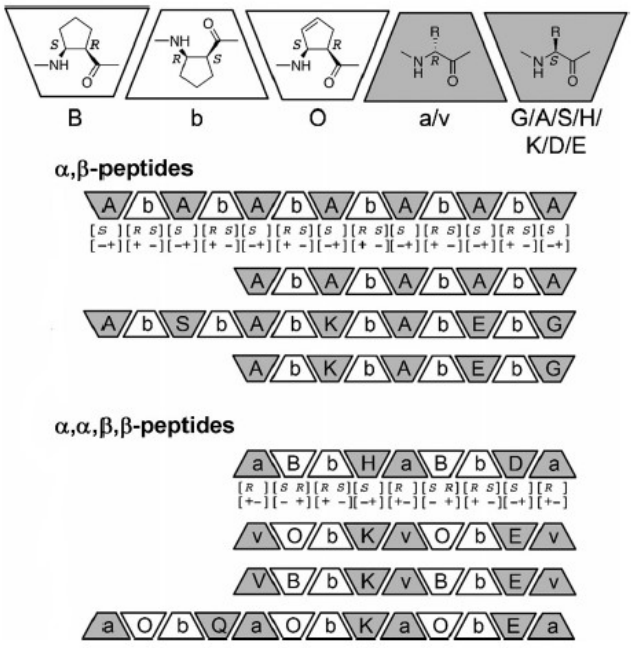

Figure 4.11 – Reiser's foldamers

[304] Schmidt, M. A.; Choi, S. H.; Guzzi, I. A.; Gellmann, S. H., *J. Am. Chem. Soc.* **2006**, *128*, 4538-4539
[305] Berlicki, Ł.; Pilsl, L.; Wéber, E.; Mándity, I.; Cabrele, C.; Martinek, T. A.; Fülöp, F.; Reiser, O., *Angew. Chem. Int. Ed.* **2012**, *51*, 2208-2212
[306] Mándity, I. M.; Wéber, E.; Martinek, T. A.; Olajos, G.; Tóth, G. K.; Vass, E.; Fülöp, F., *Angew. Chem. Int. Ed.* **2009**, *48*, 2171-2175

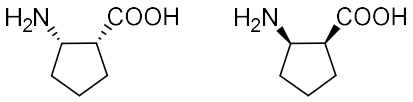

4.16 **4.23**

Figure 4.12 - β-ACPC scaffolds **4.16** and **4.23**

All the foldamers were successfully obtained by SPPS using the Fmoc-chemistry. As a consequence, the correspondent Fmoc-protected **4.24** (Figure 4.13) and **4.25** (Figure 4.13) derivatives were synthesized. Differing from the 3-membered rings, these derivatives are stable and they can be used as this in the SPPS, the one-pot deprotection-coupling procedure is not required.

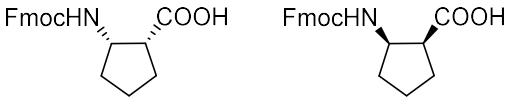

4.24 **4.25**

Figure 4.13 - β-ACPC scaffolds **4.24** and **4.25**

4.3.2 *Cyclo* RGD- and *iso*DGR-peptidomimetics

The work carried out has at the moment produced four compounds containing the β-ACPC scaffold, two RGD-peptidomimetics (**4.26** and **4.27**, Figure 4.14), one *iso*DGR-peptidomimetic (**4.28**, Figure 4.14), and the compound **4.29** (characterization ongoing at the moment, Figure 4.14). Since the *iso*DGR-peptidomimetics contain the *iso*Asp instead of the Asp, the RGD-peptidomimetics are 17-membered ring cyclic compounds while the *iso*DGR feature16-membered rings having one more carbon in the *iso*Asp amino acid skeleton (which is a β-amino acid as well).

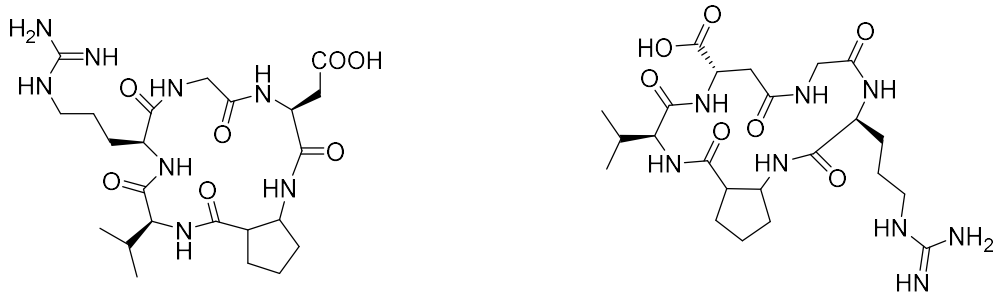

4.26: *Cyclo*[Arg-Gly-Asp-(1*R*,2*S*)-beta-ACPC-Val]
4.27: *Cyclo*[Arg-Gly-Asp-(1*S*,2*R*)-beta-ACPC-Val]
4.28: *Cyclo*[*iso*Asp-Gly-Arg-(1*R*,2*S*)-beta-ACPC-Val]
4.29: *Cyclo*[*iso*Asp-Gly-Arg-(1*S*,2*R*)-beta-ACPC-Val]

Figure 4.14 - β-ACPC-containing peptides **4.26**, **4.27**, **4.28** and **4.29**

This small collection of molecules is under investigation as integrin ligand class to evaluate whether the 5-membered ring scaffold changes preferred conformations of the cyclic peptidomimetics, affinity and/or selectivity against $\alpha_v\beta_3$, $\alpha_v\beta_5$, and $\alpha_5\beta_1$ compared to the 3-membered ring scaffolds. In order to evaluate these aspects, the synthesized compounds will be tested for the ability to inhibit biotinylated vitronectin binding to the purified $\alpha_v\beta_3$ and $\alpha_v\beta_5$ receptors. Biological tests on **4.26**, **4.27**, **4.28** and **4.29** are ongoing as well as their conformational analysis.

4.3.3 Synthesis

Only a limited number of methods for the asymmetric synthesis of these heterocyclic β-amino acid derivatives in enantiomerically pure form exist. However Cispentacin was isolated from *Streptomyces setonii*[299c] and *Bacillus cereus*[299a] or, in the homochiral form, it was prepared by classical[299a,d] and kinetic[307] resolution methods. However, for instance, *cis*-4-amino-pyrrolidine-3-carboxylic acid was diastereoselectively synthesized *via* enantioselective hydrogenation[308] and 1,3-dipolar cycloaddition of nitrones[309]. On the other hand, *trans*-4-aminoppyrrolidine-3-carboxylic acid was diastereoselectively obtained through radical addition[310] and through reductive amination.[311] However, there is no single methodology that allows the selective asymmetric synthesis of both *cis*- and *trans*-diastereoisomers.

In Davies' work it was shown that conjugate addition of homochiral lithium **4.30** to compound **4.31** and subsequent *N*-deprotection and ester hydrolysis allows an efficient synthesis of Cispentacin **4.16** (Scheme 4.4).[312] An extension of this methodology envisaged that the conjugate addition of homochiral lithium (*S*)-*N*-benzyl-*N*-α-methylbenzylamide **4.30** to a range of dihydrofuran-, *N*-protected dihydropyrrole-and dihydrothiophene-α,β-unsaturated esters would facilitate the asymmetric synthesis of both *cis*- and *trans*-stereoisomers of the corresponding β-amino acid derivatives.[303]

[307] (a) Konosu, T.; Oida, S., *Chem. Pharm. Bull.* **1993**, *42*, 1012; (b) Evans, C.; McCague, R.; Roberts, S. M.; Sutherland, A. G.; Wisdom, R., *J. Chem. Soc., Perkin Trans. 1* **1991**, 2276-2277

[308] Tang, W.; Wu, S.; Zhang, X., *J. Am. Chem. Soc.* **2003**, *125*, 9570-9571

[309] (a) Hanselmann, R.; Zhou, J.; Ma, P.; Confalone, P. N., *J. Org. Chem.* **2003**, *68*, 8739-8741; (b) Aggareal, V. K.; Roseblade, S.; Alexander, R., *Org. Biomol. Chem.* **2003**, *1*, 684-691

[310] Miyata, O.; Muroya, K.; Kobayashi, T.; Yamanaka, R.; Kajisa, S.; Koide, J.; Naito, T., *Tetrahedron* **2002**, *58*, 4459-4479

[311] Lee, H.-S.; LePlae, P. R.; Porter, E. A.; Gellman, S. H., *J. Org. Chem.* **2001**, *66*, 3597-3599

[312] (a) Davies, S. G.; Ichihara, O.; Walters, A. S., *Synlett* **1993**, 461-462; (b) Davies, S. G.; Ichihara, O.; Lenoir, I.; Walters, A. S., *J. Chem. Soc. Perkin Trans. 1* **1994**, 1411-1415; for the asymmetric synthesis of derivatives of Cispentacin using kinetic resolution methodology see: (c) Bailey, S.; Davies, S. G.; Smith, A. D.; Withey, J. M., *Chem. Commun.* **2002**, 2910-2911; (d) Davies, S. G.; Diez, D.; El Hammouni, M. M.; Garrido, N. M.; Garner, A. C.; Long, M. J. C.; Morrison, R. M.; Smith, A. D.; Sweet, M. J.; Withey, J. M., *Chem. Commun.* **2003**, 2410-2411

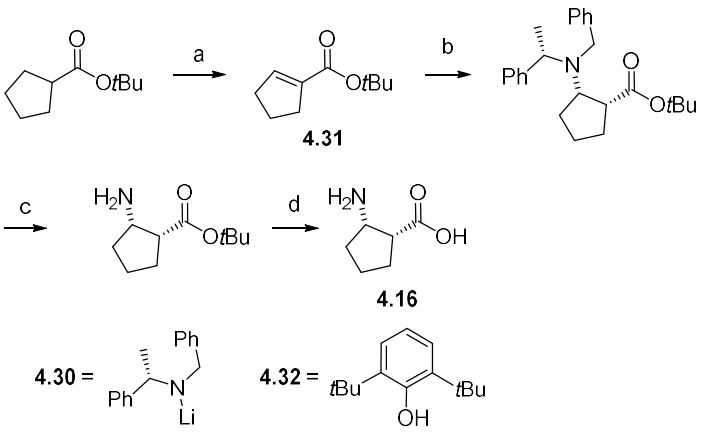

Scheme 4.4 – Synthesis of Cispentacin

Reagents and conditions: a) 1) 2-methylpropene, H_2SO_4; 2) LDA, I_2; 3) DBU; b) 1) **4.30** in THF, 2) **4.32**; c) H_2, Pd/C; d) TFA then Dowex 50X8-200.

The scaffold **4.24** was synthesized according to this procedure (Scheme 4.5) and the derivative **4.16** was converted in the building block **4.24** *via* Fmoc-protection of the amino group. In analogy to the scaffold **4.24**, the synthesis of scaffold **4.25** was accomplished through the synthetic pathway represented in Scheme 4.5 using the correspondent (*R*)-litum derivative.

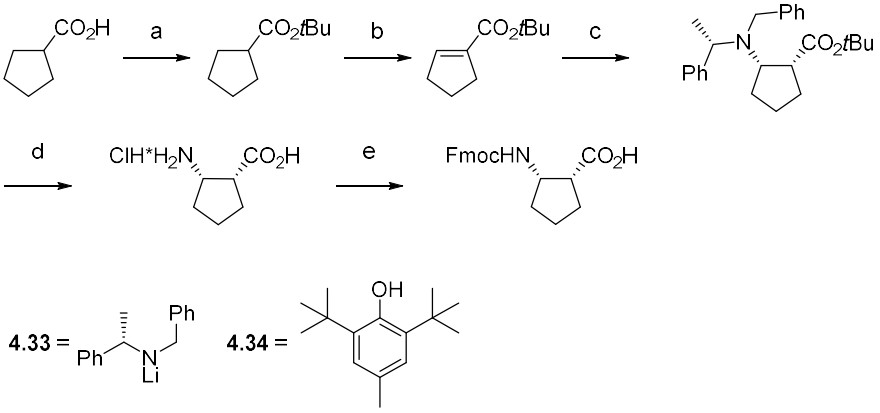

Scheme 4.5 – Synthesis of scaffolds **4.24** and **4.25**

Reagents and conditions: a) Isobutylene, conc. H_2SO_4, DCM, -78°C to r.t.; b) 1) LDA, THF, -78°C; 2) I_2, THF, -78°C; 3) DBU, THF, -78°C; c) 1) **4.33**, THF, -95°C to -78°C; 2) **4.34**, THF, -95°C; d) 1) H_2 (20 atm), $Pd(OH)_2$ (20%), AcOH, MeOH, r.t.; 2) TFA, DCM; e) FmocOSu, $NaHCO_3$, 1,4-dioxane:water (1:1), 0°C to r.t..

Cyclic peptidomimetics were synthesized through a mixed solid-phase/solution-phase approach (Scheme 4.6) following the example of cyclic compounds **4.14** and **4.15** (presented in chapter 4.2). The linear precursors **4.32** and **4.33** were assembled by SPPS on *O*-chlorotritylchloride resin as solid support using a Fmoc/*t*Bu protection strategy. The linear cleaved precursors (**4.32** and **4.33**) were cyclised under pseudo-high dilution conditions[297] to give derivatives **4.34** and **4.35**. Referring to the synthesis of **4.14** and **4.15**, the same Fmoc-ortogonal PGs were selected for the lateral chains of the amino acids. The cyclic

derivatives **4.34** and **4.35** were deprotected and purified by preparative HPLC (Scheme 4.2) to give the final peptidomimetics **4.26** and **4.27**.

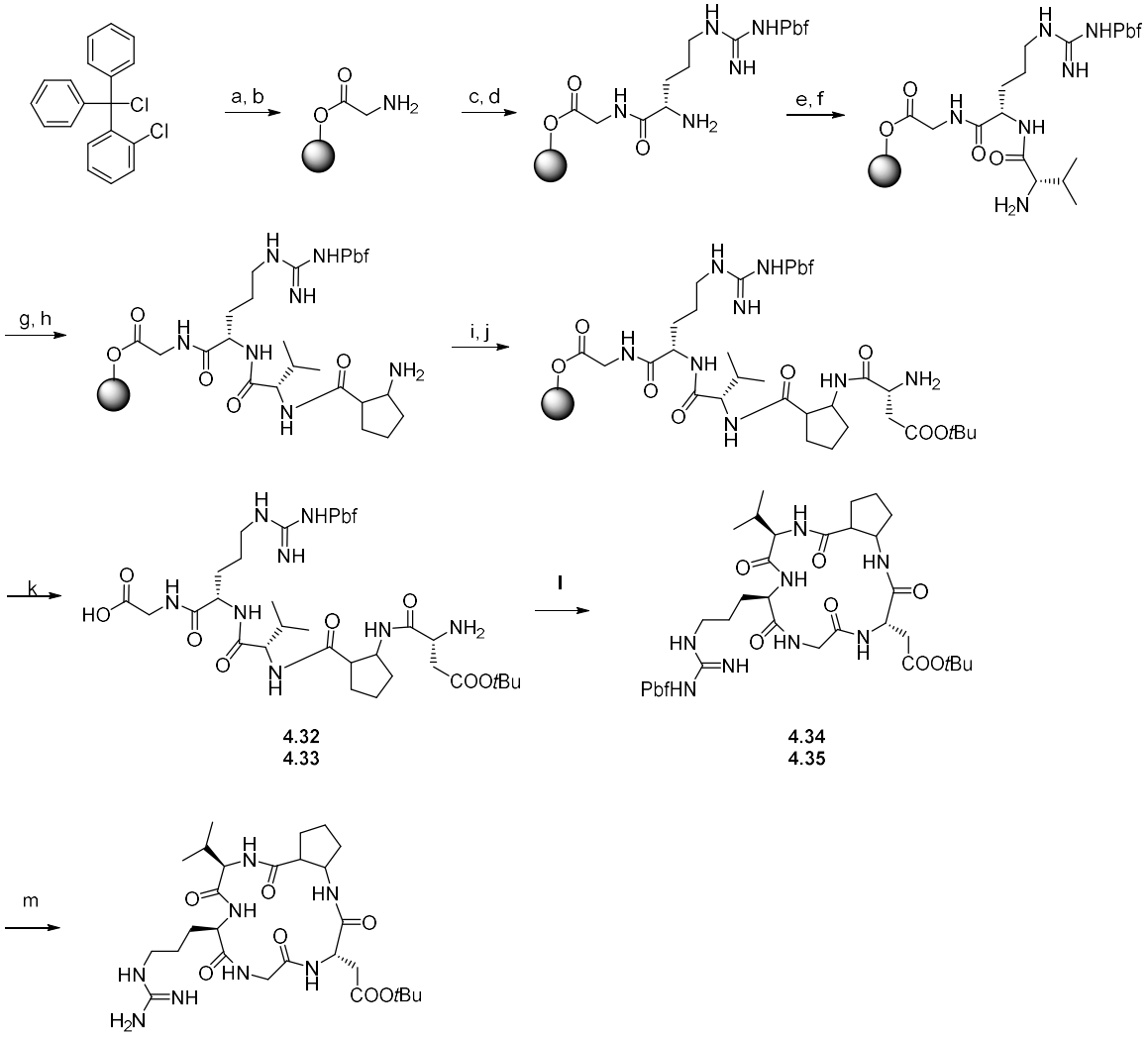

Scheme 4.6 – Synthesis of RGD-containing peptidomimetics **4.26** and **4.27**

Reagents and conditions: a) Fmoc-Gly-OH, DIPEA, DCM; b) 2% DBU, 2% piperidine, DMF; c) Fmoc-Arg(Pbf)-OH, TBTU, DIPEA, DMF; d) 2% DBU, 2% piperidine, DMF; e) Fmoc-Val-OH, TBTU, DIPEA, DMF; f) 2% DBU, 2% piperidine, DMF; g) **4.24** or **4.25**, HATU, DIPEA, DMF; h) 2% DBU, 2% piperidine, DMF; i) Fmoc-Asp(O*t*Bu)-OH, DIPEA, DCM; j) 2% DBU, 2% piperidine, DMF; k) TFA in DCM; l) TFA/Et_3SiH/H_2O (95%:2.5%:2.5%).

The attributions of ^{1}H-NMR and ^{13}C-NMR signals for **4.26** are reported in Table 4.2.

	^{1}H (δ ppm)	^{13}C (δ ppm)
NH1	7.59	
2	4.21	53.4
3	2.09 -1.98	27.1
4	1.80 – 1.69	21.4
5	1.88 – 1.83	27.4
6	2.92	47.4
NH Val	7.59	
Hα Val	3.80	61.8
Hβ Val	2.08	28.9
Hγ Val	0.94	19.0
NH Arg	8.31	
Hα Arg	4.22	53.4
Hβ Arg	1.86 – 1.80	31.1
Hγ Arg	1.60	25.1
Hδ Arg	3.18	40.8
NHε Arg	7.18	
NH Gly	8.62	
Hα Gly	3.86 – 3.78	44.1
NH Asp	8.38	
Hα Asp	4.59	50.7
Hβ Asp	2.93 – 2.86	35.4

Table 4.2

The attributions of ^{1}H-NMR and ^{13}C-NMR signals for **4.27** are reported in Table 4.3.

	^{1}H (δ ppm)	^{13}C (δ ppm)
NH1	7.33	
2	4.29	53.4
3	1.91 – 1.60	31.3
4	1.78 – 1.56	22.1
5	1.90 – 1.85	27.4
6	3.08	46.7
NH Val	7.92	
Hα Val	4.12	59.2
Hβ Val	2.05	30.4
Hγ Val	0.91	18.1
NH Arg	9.11	
Hα Arg	3.86	54.4
Hβ Arg	1.98 – 1.81	26.4
Hγ Arg	1.79 – 1.58	25.9
Hδ Arg	3.23 – 3.17	40.6
NHε Arg	7.21	
NH Gly	8.37	
Hα Gly	4.14 – 3.68	43.1
NH Asp	7.73	
Hα Asp	4.89	49.6
Hβ Asp	2.91 – 2.58	36.3

Table 4.3

Also the *iso*DGR-containing peptidomimetics **4.28** and **4.29** were synthesized *via* a similar synthetic pathway (Scheme 4.7). Obviously, the *iso*DGR derivatives present some differences compared to the RGD-containing ones because of the use of *iso*Asp and because of the different order of linking the amino acids. The linear precursors **4.36** and **4.37** were cyclized to give derivatives **4.38** and **4.39** and then deprotected on the lateral chains. Final HPLC purification gave the compounds **4.28** and **4.29** (the characterization of **4.29** is ongoing at the moment).

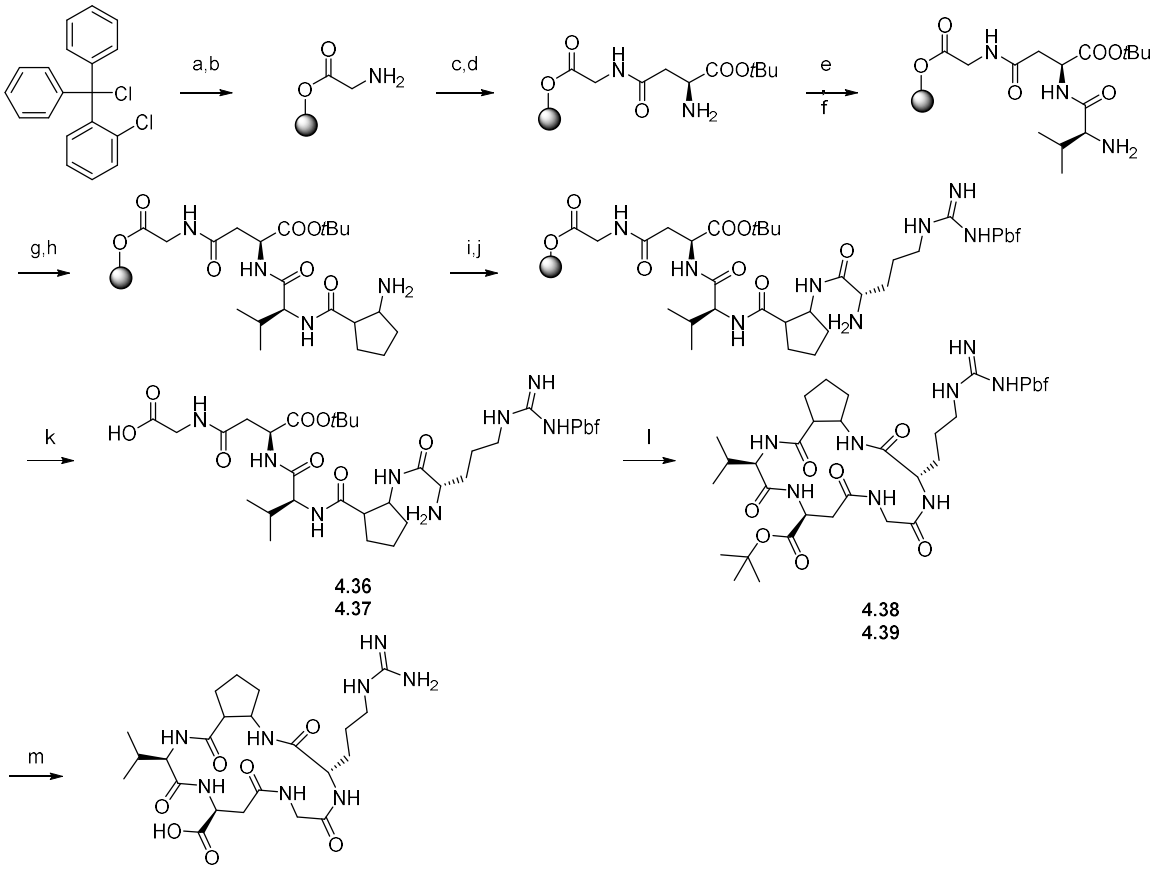

Scheme 4.7 – Synthesis of RGD-containing peptidomimetics **4.28** and **4.29**

Reagents and conditions: a) Fmoc-Gly-OH, DIPEA, DCM; b) 2% DBU, 2% piperidine, DMF; c) Fmoc-*iso*Asp(OH)-O*t*Bu, TBTU, DIPEA, DMF; d) 2% DBU, 2% piperidine, DMF; e) Fmoc-Val-OH, TBTU, DIPEA, DMF; f) 2% DBU, 2% piperidine, DMF; g) **4.24** or **4.25**, HATU, DIPEA, DMF; h) 2% DBU, 2% piperidine, DMF; i) Fmoc-Arg(Pbf)-OH, DIPEA, DCM; j) 2% DBU, 2% piperidine, DMF; k) TFA in DCM; l) TFA/Et_3SiH/H_2O (95% : 2.5% : 2.5%).

The attributions of ^{1}H-NMR and ^{13}C-NMR signals for **4.28** are reported in Table 4.4.

	^{1}H (d ppm)	^{13}C (d ppm)
NH1	7.92	
2	4.22	53.5
3	1.93 – 1.82	27.1
4	1.72 – 1.63	21.9
5	1.72 – 1.67	27.5
6	2.87	46.9
NH Val	7.74	
Hα Val	3.75	60.7
Hβ Val	1.94	29.4
Hγ Val	0.96 – 0.91	18.9
NH Arg	8.44	
Hα Arg	4.19	53.8
Hβ Arg	1.88	27.3
Hγ Arg	1.66 – 1.58	24.7
Hδ Arg	3.15	40.2
NHε Arg	7.14	
NH Gly	8.04	
Ha Gly	4.13 – 3.98	42.7
NH isoAsp	8.42	
Hβ isoAsp	4.74	50.2
Hγ isoAsp	2.85 – 2.73	37.7

Table 4.4

4.4 Conclusions and outlooks

According to the biological tests, the activity and selectivity on integrins $\alpha v\beta_3$, $\alpha v\beta_5$ and $\alpha v\beta_1$ of **4.26**, **4.27**, **4.28** and **4.29** will be evaluated. A further conformational analysis will allow to better understand these binding data and, possibly, the disposition of the compound in the integrin binding pocket. With all these data in our hands, a comparison will be done with the two β-ACC-RGD-containing compounds. If the results will be interesting, *in cell* studies could be performed to evaluate the agonist/antagonist activity of these molecule. Since the scaffold has no points suitable for a further functionalization, a correspondent moiety containing a *N*-protected group (Figure 4.15) could be inserted to get a cyclic peptide suitable for a conjugation step.

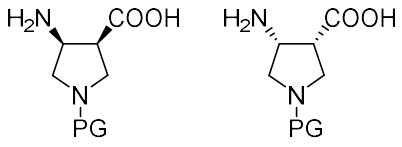

Figure 4.15 – *Cis*-scaffold containing a N-protected moiety

4.5 Experimental section

4.5.1 Materials and methods

All commercially available reagents were used as received; DMF was anhydrify according to GP0. Non solid-phase reactions were monitored by analytical thin layer chromatography (TLC) using silica gel 60 F_{254} pre-coated glass plates (0.20 mm thickness). Visualization was accomplished by irradiation with a UV lamp and/or staining with a ninhydrin; solid phase steps was followed by LR-Mass. Visualization was accomplished by irradiation with a UV lamp and/or staining with a potassium permanganate alkaline solution or ninhydrin. Flash column chromatography was performed according to the method of Still and co-workers[169] using Chromagel 60 ACC (40-63 μm) silica gel. Proton NMR spectra were recorded on a spectrometer operating at 500 MHz. Carbon NMR spectra were recorded on a spectrometer operating at 125 MHz, with complete proton decoupling. The following abbreviations are used to describe spin multiplicity s = singlet, d = doublet, t = triplet, q = quartet, m = multiplet, bs = broad signal, dd = doublet of doublet, ddd = doublet of doublet of doublet, ddt = doublet of doublet of triplet. Carbon chemical shifts are reported in ppm (δ) relative to TMS with the respective solvent resonance as the internal standard. ESI-MS spectra were recorded on the ion trap mass spectrometer Finnigan LCQ Advantage.

RP-HPLC purification

HPLC purifications were performed on a Dionex Ultimate 3000 instrument equipped with a Dionex RS Variable Wavelenght Detector (column: Atlantis Prep T3 OBDTM 5 TM 19 x 100 mm). The crude reaction mixture was dissolved in water and the solution was filtered (polypropylene, 0.45 μm, 13 mm ø, PK/100) and injected in the HPLC, affording purified products.

RP-HPLC analysis

Purity analysis for each of the compounds was carried out on a Dionex Ultimate 3000 instrument equipped with a Dionex RS Variable Wavelenght Detector (column: Atlantis Prep T3 OBDTM 5 TM 19 x 100 mm). 0.8 mg of purified product was dissolved in 0.5 mL of H_2O and 0.3 mL of acetonitrile and was injected using gradient: 100% H_2O + 0.1% CF_3COOH/0% CH_3CN + 0.1% CF_3COOH to 50% H_2O + 0.1% CF_3COOH/50% CH_3CN + 0.1% CF_3COOH in 11 min. The analysis of the integrals and the relative percentage of purity was performed with the software Cromeleon 6.80 SR11 Build 3161.

Freeze-drying

The product was dissolved in water and frozen with dry ice: the freeze-drying was carried out at least for 48 h at -50 °C using the instrument 5Pascal Lio5P DGT.

4.5.2 General procedures for SPPS

DMF anhydrification

GP0: A flask was charged with CaH_2 (around 5g/L) and DMF. The mixture was stirred at r.t. over night. DMF was subsequently transferred into a flask under N_2 and distilled under reduced pressure (around 20 mBar). DMF was stored under N_2 in a dark brown flask over molecular sieves (3Å).

SPPS was manually accomplished using a shaker. Fmoc strategy and 2-chlorotritylchloride resin (100-200 mesh, 1% DVB; loading: 1.51 mmol/g resin) were used. Each coupling step consisted in:

i) activation of the Fmoc-protected amino acid,

ii) addition of the activated amino acid to the resin at the shaker to effect the coupling reaction;

iii) following steps of capping, deprotection and washing.

Resin preparation and storage

The resin was weighted in a 10 mL vial and swelled (**GP1**); at the end of this operation the resin was ready for the SPPS. When necessary, beads were stored at 4 °C under nitrogen after being washed several times with DCM and dried at the high vacuum pump.

Swelling of the resin

GP1: The resin was weighted in a vial, suspended in DCM (approximately 10 mL per gram of resin) and shaken for 30 minutes. The solvent was dried from the resin and, at the end of this operation, the resin was ready for the SPPS. This step is repeated every times before starting procedures on the resin if it was previously dried under vacuum and stored at 4°C.

Loading of the first amino acid and capping of the resin

GP2: The resin was suspended in DCM (approximately 14 mL per gram of resin); Fmoc-AA-OH (2.0 eq.) and DIPEA (0.3 eq.) were sequentially added. The resin was shaken for 10 minutes then DIPEA (0.5 eq.) was added and the resin was shaken for 1h 30min; after this time the solvent was removed. The resin was washed with DCM (3 x 2 mL), then methanol was added (approximately 1.5 mL per gram of resin) and the resin was shaken for 15

minutes. The solvent was removed and the resin was washed with DCM (3 x 2 mL), DMF (3 x 2 mL), DCM again (3 x 2 mL), and methanol (1 x 2 mL).

Amino acid activation and coupling

GP3: To a 0.14 M solution of the amino acid (1.5 eq.) in dry DMF under N_2 at 0°C, TBTU (1.5 eq. in DMF) and DIPEA (3.0 eq. in DMF) were added. The mixture was stirred under these conditions for 30-40 minutes and then the solution was added to the resin. The resin was shaken at r.t. for 3 hours then the solvent was removed. Each coupling step was performed twice times. After the second coupling, the resin was washed with DCM (3 x 2 mL), DMF (3 x 2 mL), and DCM again (3 x 2 mL).

Scaffold activation and coupling

GP4: To a solution of the scaffold (1.5 eq.) in dry DMF (solution 0.14 M) under N_2 at 0°C, HATU (1.5 eq. in DMF) and DIPEA (3.0 eq. in DMF) were added. The mixture was stirred under these conditions for 45 minutes and then the solution was added to the resin. The resin was shaken at r.t. for 7 hours then the solvent was removed. After the coupling, the resin was washed with DCM (3 x 2 mL), DMF (3 x 2 mL), and DCM again (3 x 2 mL).

Capping procedure

GP5: A 1M solution of Ac_2O (50 eq.) and pyridine (50 eq.) in DMF (approximately 30 mL per gram of unsubstituted resin) was added to the resin. The mixture was shaken at r.t. for 40 minutes then solution was removed and beads were washed with DMF (3 x 2 mL).

Fmoc removal procedure

GP6: Deprotection of the N-terminal Fmoc group was achieved using a solution of 2% DBU and 2% piperidine (v/v) in DMF (approximately 30 mL per gram of the unsusbstituted resin). The solution was added to the resin which was shaken for 15 minutes then the solution was removed. Two deprotection steps were carried out. At the end of each step, the solvent was removed. At the end of the second step, beads were sequentially washed with DMF (6 x 2 mL) and DCM (3 x 2 mL).

Peptide cleavage:

GP7: The resin was washed with DCM (3 x 2 mL) and then treated with 1% TFA in DCM (15.0 mL for gram of the not substituted resin) for 5 minutes each time. Treatment was repeated as long as the peptide was cleaved from the resin (approximately 10 times), checking by TLC. Combined solutions were evaporated under reduced pressure and then in vacuum. The crude obtained was used without purification in the macrolactamization step.

4.5.3 General procedures for solution-phase synthesis

Macrolactamization

GP8: The linear precursor (1 eq.) was dissolved in dry DMF (5 mM solution) and transferred into a syringe. HATU (3.0 eq.) was dissolved in the same volume of dry DMF and transferred into a second syringe. These two solutions were added slowly using two syringe pumps to a stirred solution of DIPEA (6.0 eq.) and HATU (0.1 eq.) in half of the previous volume of dry DMF at a rate of 0.7mL/h. Once the addition was complete, the mixture was stirred for another 30 minutes. The solvent was evaporated under reduced pressure at a temperature lower than 35°C. Crude was taken up with ethyl acetate (25 mL), sequentially washed with a solution 1M of $KHSO_4$, a saturated solution of $NaHCO_3$ and brine. The organic layer was dried over Na_2SO_4 anhydrous and volatiles were removed under reduced pressure. The mixture was taken-up dissolved in DCM:MeOH (9:1) and filtered over silica gel.

Side chain deprotection

GP9: Crude fully protected macrolactam was treated for 8 h with a solution (around 21 mL/mg of protected peptide) of TFA (95%) at room temperature in the presence of water (2.5%) and triisopropylsilane (2.5%). After TFA removal under reduced pressure, the residue was taken up with a 1:1 mixture of diethyl ether/water. Phases were separated and the aqueous layer was washed several times with diethyl ether. The aqueous phase was concentrated under reduced pressure and then the solution was freeze-dried. The crude was purified by preparative HPLC.

4.5.4 Synthesis

4.24 and **4.25** were synthesized according to literature procedure ((a) Bunnage, M. E.; Davies, S. G.; Roberts, P. M.; Smith, A. D.; Withey, J. M. *Org. Biomol. Chem.* **2004**, *2*, 2763; (b) Davies, S. G.; Ichihara, O.; Lenoir, I.; Walters, I. A. S. *J. Chem. Soc., Perkin Trans. 1* **1994**, *11*, 1411) and their analytical data were in agreement with those already published.

Asp(O*t*Bu)-(1*R*,2*S*)-β-ACPC-Val-Arg(Pbf)-Gly-OH (4.32) and Asp(O*t*Bu)-(1*S*,2*R*)-β-ACPC-Val-Arg(Pbf)-Gly-OH (4.33)

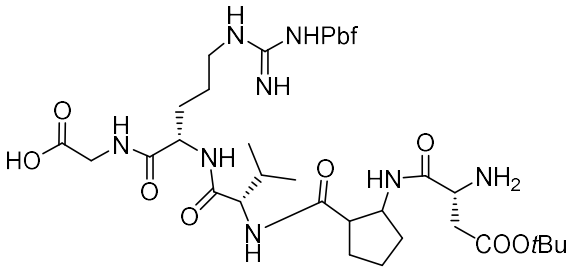

The resin was weighed in a solid phase syringe and swelled (**GP1**) and Fmoc-Gly-OH was activated and coupled to the resin (**GP2**). After a capping step (**GP5**) and a Fmoc deprotection step (**GP6**), Fmoc-Arg(Pbf)-OH was activated and coupled to the Gly-resin (**GP3**). Then a capping a capping step (**GP5**) and a Fmoc deprotection step (**GP6**) were performed. Fmoc-Val-OH was activated and coupled to the Arg(Pbf)-Gly-resin (**GP3**); the coupling was followed by a capping step (**GP5**) and a Fmoc deprotection step (**GP6**). **4.24** and **4.25** were activated and coupled to the Val-Arg(Pbf)-Gly-resin (**GP4**), then a capping step (**GP5**) and a Fmoc deprotection step (**GP6**) were performed. Fmoc-Asp(O*t*Bu)-OH was activated and coupled to the **4.24**-Val-Arg(Pbf)-Gly-resin (**GP3**) and **4.25**-Val-Arg(Pbf)-Gly-resin (**GP3**), then Fmoc deprotection step (**GP6**) was performed. The linear precursor was cleaved from the resin (**GP7**), checked by LR-Mass and used in the following steps as crude. The crude **4.32** (140 mg) and **4.33** (185 mg) were obtained as brown oils.

Exact amounts of the amino acids and coupling reagents used for SPPS are reported in Table 4.5 for **4.32** and in Table 4.6 for **4.33**.

Table 4.5

Reagents	Eq. or concentration	mmol	Amounts
Chlorotritylchloride resin (1.51 mmol/g)	1.0 eq	0.190	130 mg
Fmoc-Gly-OH*	2.0 eq	0.380	113 mg
DIPEA	0.3 eq	0.057	10 µL
DIPEA	0.5 eq	0.095	17 µL
DCM	/	/	2.0 mL
Fmoc-Arg(Pbf)-OH*	1.5 eq	0.285	185 mg
TBTU	1.5 eq	0.285	92 mg
DIPEA	3.0 eq	0.570	99 µL
DMF	0.14 M	/	2 mL
Fmoc-Val-OH*	1.5 eq	0.285	97 mg
TBTU	1.5 eq	0.285	92 mg
DIPEA	3.0 eq	0.570	99 µL
DMF	0.14 M	/	2 mL
4.24	1.5 eq	0.285	100
HATU	1.5 eq	0.285	108
DIPEA	4.0 eq	0.760	132 µL
DMF	0.14 M	/	2 mL
Fmoc-Asp(OtBu)-OH*	1.5 eq	0.285	117 mg
TBTU	1.5 eq	0.285	92 mg
DIPEA	3.0 eq	0.570	99 µL
DMF	0.14 M	/	2 mL

* a double coupling step is performed.

Table 4.6

Reagents	Eq. or concentration	mmol	Amounts
Chlorotritylchloride resin (1.51 mmol/g)	1.0 eq	0.190	130 mg
Fmoc-Gly-OH*	2.0 eq	0.380	113 mg
DIPEA	0.3 eq	0.057	10 µL
DIPEA	0.5 eq	0.095	17 µL
DCM	/	/	2.0 mL
Fmoc-Arg(Pbf)-OH*	1.5 eq	0.285	185 mg
TBTU	1.5 eq	0.285	92 mg
DIPEA	3.0 eq	0.570	99 µL
DMF	0.14 M	/	2 mL
Fmoc-Val-OH*	1.5 eq	0.285	97 mg
TBTU	1.5 eq	0.285	92 mg
DIPEA	3.0 eq	0.570	99 µL
DMF	0.14 M	/	2 mL
4.25	1.5 eq	0.285	100 mg
HATU	1.5 eq	0.285	108 mg
DIPEA	4.0 eq	0.760	132 µL
DMF	0.14 M	/	2 mL
Fmoc-Asp(O*t*Bu)-OH*	1.5 eq	0.285	117 mg
TBTU	1.5 eq	0.285	92 mg
DIPEA	3.0 eq	0.570	99 µL
DMF	0.14 M	/	2 mL

* a double coupling step was performed.

Cyclo[Asp(O*t*Bu)-(1*R*,2*S*)-β-ACPC-Val-Arg(Pbf)-Gly] (4.34) and _Cyclo_[Asp(O*t*Bu)-(1*S*,2*R*)-β-ACPC-Val-Arg(Pbf)-Gly] (4.35)

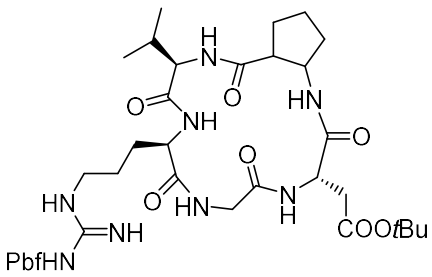

Compound **4.32** or **4.33** (**4.32**: 140 mg crude, 0.163 mmol, considered 1.0 eq for stoichiometric calculations; **4.33**: 185 mg crude, 0.217 mmol, considered 1.0 eq for stoichiometric calculations) was treated with HATU (**4.32**: 193, 0.489 mmol, 3.1 eq; **4.33**: 252 mg, 0.662 mmol, 3.1 eq) and DIPEA (**4.32**: 170 µL, 0.979 mmol, 6.0 eq; **4.33**: 226 µL, 1.299 mmol, 6.0 eq) under the conditions described in **GP8**. The product was obtained as pale yellow solid (**4.34**: 61 mg, crude; **4.35**: 94 mg, crude).

***Cyclo*[Asp-(1*R*,2*S*)-β-ACPC-Val-Arg-Gly] (4.26) and *Cyclo*[Asp-(1*S*,2*R*)-β-ACPC-Val-Arg-Gly] (4.27)**

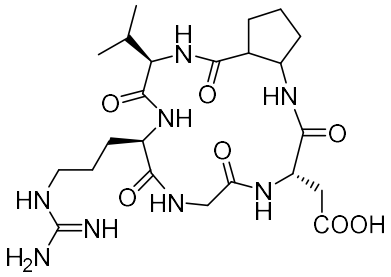

Compound **4.34** (61 mg, crude) or **4.35** (94 mg, crude) was deprotected under the conditions described in **GP9**. The crude product was purified by RP-HPLC [compound **4.26** = gradient: 100% H_2O + 0.1% CF_3COOH/0% CH_3CN + 0.1% CF_3COOH to 50% H_2O + 0.1% CF_3COOH/50% CH_3CN + 0.1% CF_3COOH in 11 min; flow: 15 mL/min; compound **4.27** = gradient: 100% H_2O + 0.1% CF_3COOH/0% CH_3CN + 0.1% CF_3COOH to 50% H_2O + 0.1% CF_3COOH/50% CH_3CN + 0.1% CF_3COOH in 11 min; flow: 15 mL/min]. Pure fractions were concentrated and freeze-dried, affording **4.26** or **4.27** as a white solid (**4.26**: 11 mg, 0.017 mmol, overall yield 9%; **4.27**: 13 mg, 0.020 mmol, overall yield 10%).

Compound 4.26:

^{1}H-NMR (500 MHz, D_2O) δ 8.62 (1H), 8.38 (1H), 8.31 (1H), 7.59 (2H), 7.18 (4H), 4.59 (1H), 4.22 (1H), 4.21 (1H), 3.86-3.78 (2H), 3.80 (1H), 3.18 (2H), 2.93-2.86 (2H), 2.92 (1H), 2.09-1.98 (2H), 2.08 (1H), 1.88-1.83 (2H), 1.86-1.80 (2H), 1.80-1.69 (2H), 1.60 (2H), 0.94 (6H). ^{13}C-NMR (125 MHz, D_2O) δ 61.8, 53.4, 53.4, 50.7, 47.4, 44.1, 40.8, 35.4, 31.1, 28.9, 27.4, 27.1, 25.1, 21.4, 19.0; MS (ESI) m/z calcd. for $[C_{38}H_{38}N_8O_7]^+$: 538.2863 $[M+H]^+$; found: 539.2944.

Compound 4.27:

^{1}H-NMR (500 MHz, D_2O) δ 9.11 (1H), 8.37 (1H), 7.92 (1H), 7.73 (1H), 7.33 (1H), 7.21 (4H), 4.89 (1H), 4.29 (1H), 4.14-3.68 (2H), 4.12 (1H), 3.86 (1H), 3.23-3.17 (2H), 3.08 (1H), 2.91-2.58 (2H), 2.05 (1H), 1.98-1.81 (2H), 1.91-1.60 (2H), 1.90-1.85 (2H), 1.79-1.58 (2H), 1.78-1.56 (2H), 0.91 (6H). ^{13}C-NMR (125 MHz, D_2O) δ 59.2, 54.4, 53.4, 49.6, 46.7, 43.1, 40.6, 36.3, 31.3, 30.4, 27.4, 26.4, 25.9, 22.1, 18.1; MS (ESI) m/z calcd. for $[C_{38}H_{38}N_8O_7]^+$: 538.2863 $[M+H]^+$; found: 539.2935.

HPLC trace of compound 4.26

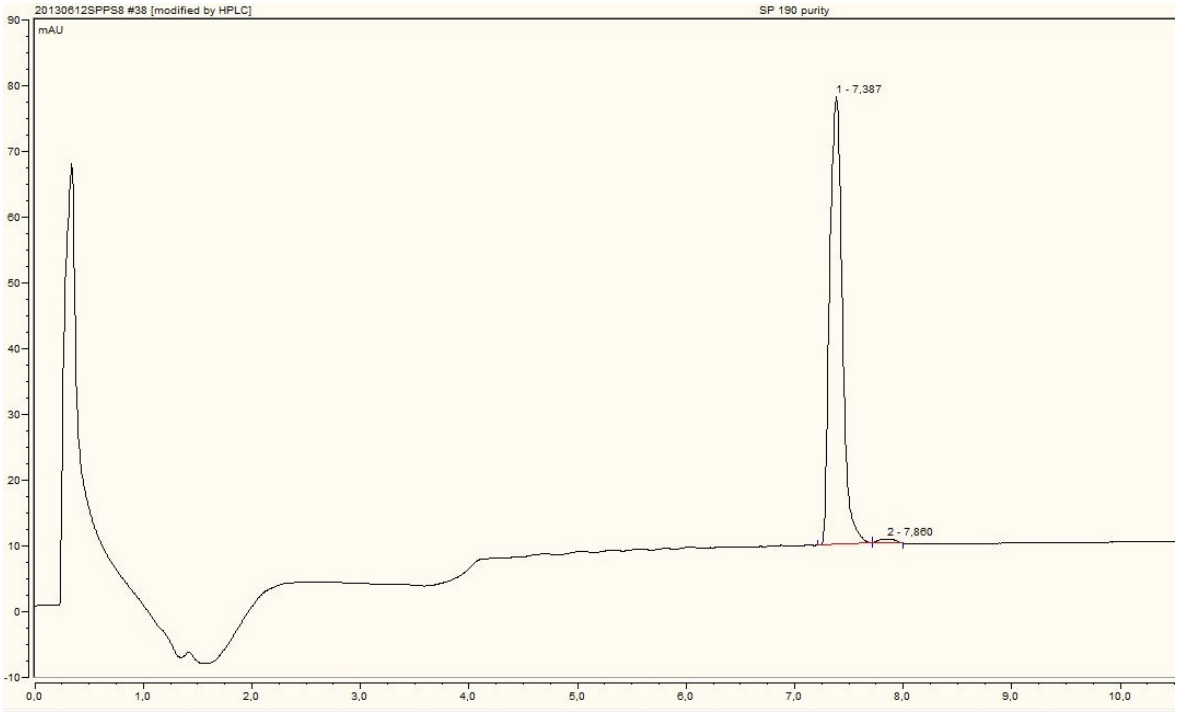

HPLC purity = 99%

HPLC trace of compound 4.27

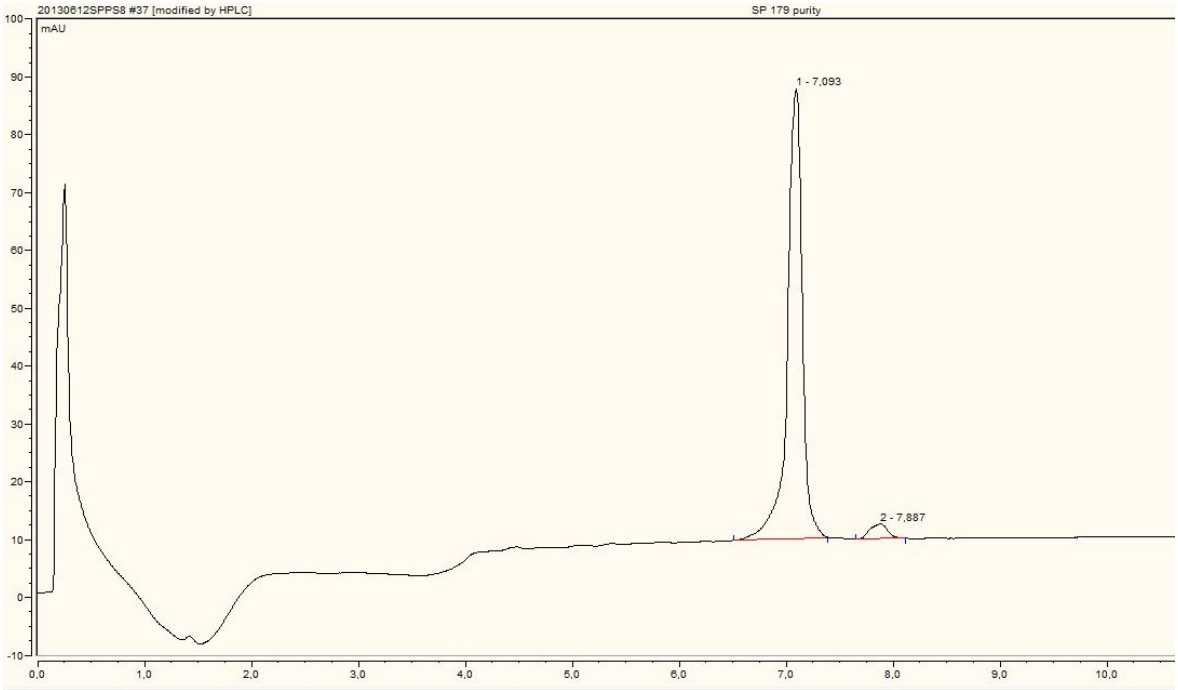

HPLC purity = 96%

Arg(Pbf)-(1*R*,2*S*)-β-ACPC-Val-*iso*Asp(O*t*Bu)-Gly-OH (4.36) and Arg(Pbf)-(1*S*,2*R*)-β-ACPC-Val-*iso*Asp(O*t*Bu)-Gly-OH (4.37)

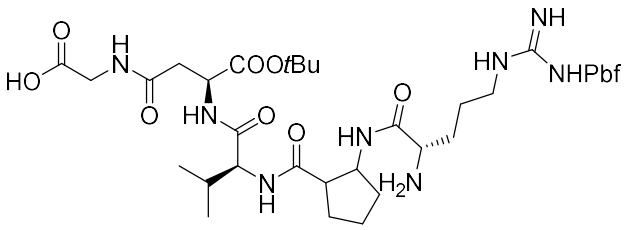

The resin was weighed in a solid phase syringe and swelled (**GP1**) and Fmoc-Gly-OH was activated and coupled to the resin (**GP2**). After a capping step (**GP5**) and a Fmoc deprotection step (**GP6**), Fmoc-Asp(OH)-O*t*Bu was activated and coupled to the Gly-resin (**GP3**). Then a capping step (**GP5**) and a Fmoc deprotection step (**GP6**) were performed. Fmoc-Val-OH was activated and coupled to the Asp(O*t*Bu)-Gly-resin (**GP3**); the coupling was followed by a capping step (**GP5**) and a Fmoc deprotection step (**GP6**). **4.24** and **4.25** were activated and coupled to Val-Asp(O*t*Bu)-Gly-resin (**GP4**), then a capping step (**GP5**) and a Fmoc deprotection step (**GP6**) were performed. Fmoc-Arg(Pbf)-OH was activated and coupled to **4.24**-Val-Asp(O*t*Bu)-Gly-resin (**GP3**) and to **4.25**-Val-Asp(O*t*Bu)-Gly-resin (**GP3**), then Fmoc deprotection step (**GP6**) was performed. The linear precursor was cleaved from the resin (**GP7**), checked by LR-Mass and used in the following steps as crude. The crude **4.36** (114 mg) and **4.37** (80 mg) was obtained as a yellow solid.

Exact amounts of the amino acids and coupling reagents used for SPPS are reported in Table 4.7 for **4.36** and in Table 4.8 for **4.37**.

Table 4.7

Reagents	Eq. or concentration	mmol	Amounts
Chlorotritylchloride resin (1.51 mmol/g)	1.0 eq	0.095	65 mg
Fmoc-Gly-OH*	2.0 eq	0.190	56 mg
DIPEA	0.3 eq	0.029	5 µL
DIPEA	0.5 eq	0.048	8 µL
DCM	/	/	1.0 mL
Fmoc-Asp(OH)-O*t*Bu*	1.5 eq	0.142	58 mg
TBTU	1.5 eq	0.142	46 mg
DIPEA	3.0 eq	0.285	50 µL
DMF	0.14 M	/	1.0 mL
Fmoc-Val-OH*	1.5	0.142	48 mg
TBTU	1.5	0.142	46 mg
DIPEA	3.0	0.142	50 µL
DMF	/	/	1.0 mL
4.24	1.5 eq	0.142	50 mg
HATU	1.5 eq	0.142	54 mg
DIPEA	4.0 eq	0.380	66 µL
DMF	0.14 M	/	1.0 mL
Fmoc-Arg(Pbf)-OH*	1.5	0.142	92 mg
TBTU	1.5	0.142	46 mg
DIPEA	3.0	0.285	50 µL
DMF	/	/	1.0 mL

* a double coupling step is performed.

Table 4.8

Reagents	Eq. or concentration	mmol	Amounts
Chlorotritylchloride resin (1.51 mmol/g)	1.0 eq	0.095	65 mg
Fmoc-Gly-OH*	2.0 eq	0.190	56 mg
DIPEA	0.3 eq	0.029	5 µL
DIPEA	0.5 eq	0.048	8 µL
DCM	/	/	1.0 mL
Fmoc-Asp(OH)-O*t*Bu*	1.5 eq	0.142	58 mg
TBTU	1.5 eq	0.142	46 mg
DIPEA	3.0 eq	0.285	50 µL
DMF	0.14 M	/	1.0 mL
Fmoc-Val-OH*	1.5 eq	0.142	48 mg
TBTU	1.5 eq	0.142	46 mg
DIPEA	3.0 eq	0.285	50 µL
DMF	0.14 M	/	1.0 mL
4.25	1.5 eq	0.142	50 mg
HATU	1.5 eq	0.142	54 mg
DIPEA	4.0 eq	0.380	66 µL
DMF	0.14 M	/	1.0 mL
Fmoc-Arg(Pbf)-OH*	1.5	0.142	92 mg
TBTU	1.5	0.142	46 mg
DIPEA	3.0	0.285	50 µL
DMF	0.14 M	/	1.0 mL

* a double coupling step was performed.

Cyclo[Arg(Pbf)-(1*R*,2*S*)-β-ACPC-Val-_iso_Asp(O*t*Bu)-Gly] (4.38) and _Cyclo_[Arg(Pbf)-(1*S*,2*R*)-β-ACPC-Val-_iso_Asp(O*t*Bu)-Gly] (4.39)

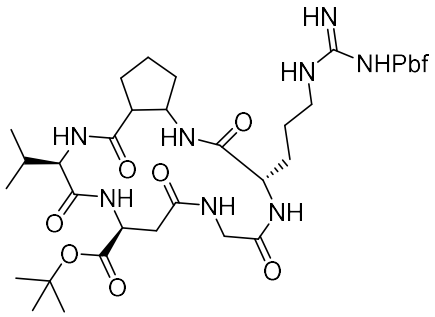

Compound **4.36** and **4.37** (**4.36**: 114 mg, 0.13 mmol, considered 1.0 eq for stoichiometric calculations; **4.37**: 80 mg, 0.093 mmol, considered 1.0 eq for stoichiometric calculations) were treated with HATU (**4.36**: 154 mg, 0.41 mmol, 3.1 eq; **4.37**: 110 mg, 0.29 mmol, 3.1 eq) and DIPEA (**4.36**: 136 µL, 0.78 mmol, 6.0 eq; **4.37**: 98 µL, 0.55 mmol, 6.0 eq) under the conditions described in **GP8**. The product was obtained as pale yellow solid (**4.38**: 70 mg, 0.08 mmol, 0.1 eq; **4.39**: 73 mg, 0.09 mmol) and it was used without purification.

***Cyclo*[Arg-(1*R*,2*S*)-β-ACPC-Val-*iso*Asp-Gly] (4.28)**

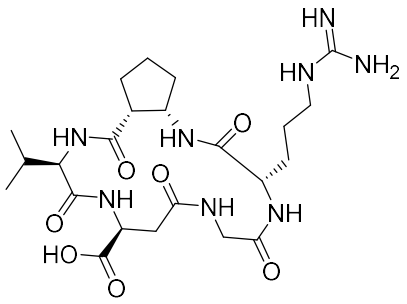

Compound **4.38** (70 mg, crude) was deprotected under the conditions described in **GP9**. The crude product was purified by RP-HPLC [gradient: 100% H_2O + 0.1% CF_3COOH/0% CH_3CN + 0.1% CF_3COOH to 50% H_2O + 0.1% CF_3COOH/50% CH_3CN + 0.1% CF_3COOH in 11 min; flow: 15 mL/min]. Pure fractions were concentrated and freeze-dried, affording **4.28** as a white solid (9.97 mg, 0.015 mmol, 16% overall yield).

Compound 4.28:

^{1}H-NMR (500 MHz, D_2O) δ 8.44 (1H), 8.42 (1H), 8.04 (1H), 7.92 (1H), 7.74 (1H), 7.14 (4H), 4.74 (1H), 4.22 (1H), 4.19 (1H), 4.13-3.98 (2H), 3.75 (1H), 3.15 (2H), 2.87 (1H), 2.85-2.73 (2H), 1.94 (1H), 1.93-1.82 (2H), 1.88 (2H), 1.72-1.67 (2H), 1.72-1.63 (2H), 1.66-1.58 (2H), 0.96-0.91 (6H). ^{13}C-NMR (125 MHz, D_2O) δ 60.7, 53.8, 53.5, 50.2, 46.9, 42.7, 40.2, 37.7, 29.4, 27.5, 27.3, 27.1, 24.7, 21.9, 18.9; MS (ESI) m/z calcd. for $[C_{38}H_{38}N_8O_7]^+$: 538.2863 $[M+H]^+$; found: 539.2543.

HPLC trace of compound 4.28

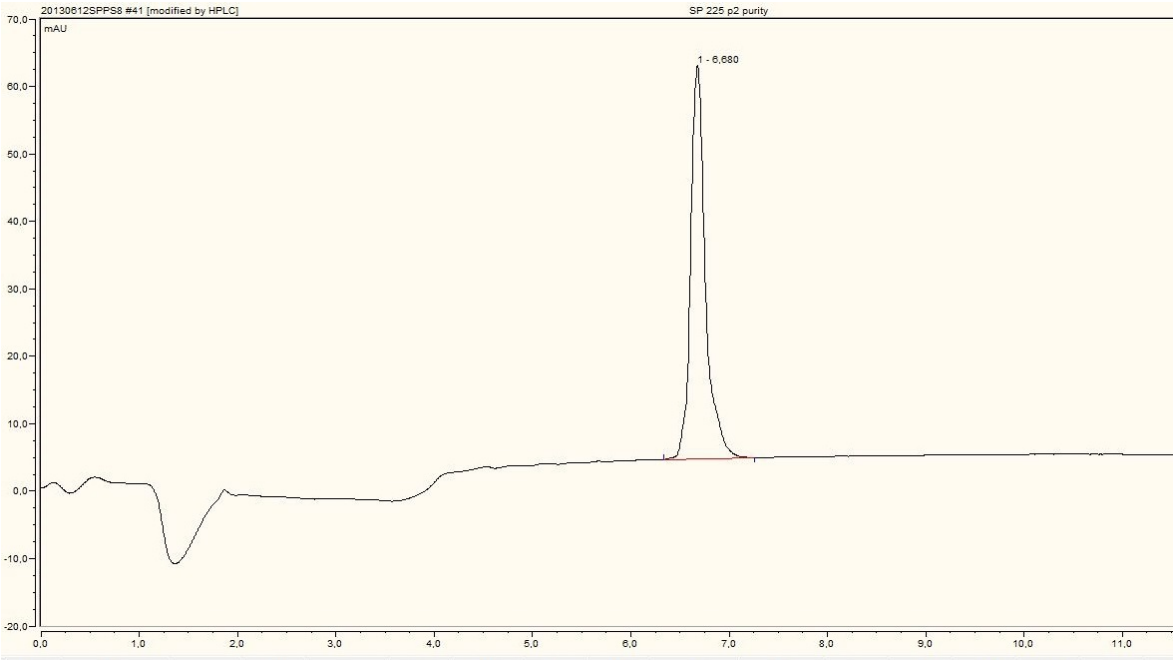

HPLC purity > 99%

***Cyclo*[Arg-(1*R*,2*S*)-β-ACPC-Val-*iso*Asp-Gly] (4.29)**

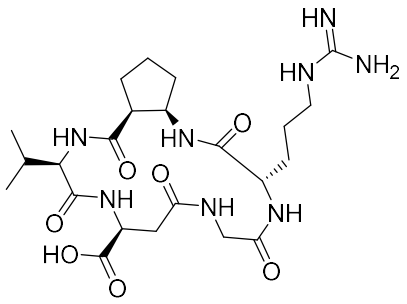

Compound **4.39** (73 mg, crude) was deprotected under the conditions described in **GP9**. The crude product was purified by RP-HPLC [gradient: 100% H_2O + 0.1% CF_3COOH/0% CH_3CN + 0.1% CF_3COOH to 50% H_2O + 0.1% CF_3COOH/50% CH_3CN + 0.1% CF_3COOH in 11 min; flow: 15 mL/min]. Pure fractions were concentrated and freeze-dried, affording 6.92 mg of a white solid. The characterization is ongoing.

APPENDIX

List of abbreviations:

AA	Amino acid
Ac	Acetyl
AcCN	Acetonitrile
Ac_2O	Acetic anhydride
All	Allyl
Amp	4-amino proline
aq.	Aqueous solution
Ar	Aril
Bn	Benzyl
Boc	*tert*-butoxycarbonyl
Boc_2O	di-*tert*-butyldicarbonate
BOC-ON	2-(*tert*-buttyloxycarbonyloxymino)-2-phenylacetonitrile
Bu	Butyl
c-	Cyclo
Cbz	Carboxybenzyl
CD	Circular Dichroism
Col.	Collagens
calcd.	Calculated
conc.	Concentrated
COSY	Correlation Spectroscopy
Co/C	Carbon-coated cobalt nanoparticles
CuAAC	Cu(I)-catalyzed Azide-Alkyne Click chemistry
DCC	*N*,*N*-Dicyclohexylcarbodiimide
DCM	Dicloromethane
DBU	1,8-diazabicyclo[5.4.0]undec-7-ene
DEG	Diethylene glycol
DIAD	diisopropylazadicarboxylate
DIC	*N*,*N*'-Diisopropylcarbodiimide
DIPEA	*N,N*-Diisopropylethylamine
DKP	Diketopiperazine
DMAP	4-Dimethylaminopyridine
DMF	*N*,*N*-Dimethylformamide
DMSO	Dimethylsulfoxide
EA	Elemental analysis
ECM	Extracellular matrix
EDC.HCl	1-ethyl-3-(3-dimethylaminopropyl)carbodiimide hydrochloride

EDT	1,2-ethanedithiol
EGF	Epidermal growth factor
eq.	Equivalents
ESI	Electrospray ionization
EtOAc	Ethyl acetate
Fbg	Fibrinogen
FBS	Fetal bovine serum
Fmoc	9-Fluorenylmethyloxycarbonyl
Fn	Fibronectin
h	hours
HATU	*O*-(7-Azabenzotriazol-1-yl)-*N*,*N*,*N*',*N*'-hetramethyluronium exafluorphosphate
HBTU	*O*-benzotriazole-*N*,*N*,*N*',*N*'-tetramethyl-uronium hexafluorphosphate
HMBC	Heteronuclear multiple bond correlation
HPLC	High performance liquid chromatography
HR-Ms	High resolution mass
HRTEM	High resolution transmission electron microscopy
HSQC	Heteronuclear single quantum correlation
HOAt	1-Hydroxy-7-azabenzotriazole
KHMDS	Potassium hexamethyldisilazane
LN	Laminin
LR-Ms	Low resolution mass
IC	Inhibitory Capacity
*i*PrOH	Propan-2-ol
IR	Infrared spectroscopy
J	Scalar coupling constant
KHMDS	Potassium hexamethyldisilazane
MC	Monte Carlo statistical mechanics
MD	Molecular dynamics
Me	Methyl
MeOH	Methanol
MIDAS	Metal ion dependent site
min	Minutes
MNPs	Magnetic nanoparticles
MRI	Magnetic resonance imaging
MS	Mass spectroscopy
Mtr	4-methoxy-2,3,6-trimethylbenzensulfonyl
MW	Molecular weight/Microwave

NMR	Nuclear magnetic resonance
NOE	Nuclear overhauser effect
Pbf	2,2,4,6,7-pentamethyldihydrobenzofuran-5-sulfonyl
PAA	Poly(acrylic acid)
PEG	Polyethylene glycol
PEI	Polyethyleneimine
PET	Positron Emission Tomography
PG	Protecting group
Ph	Phenyl
ppm	Part per million
Py	Pyridine
quant.	Quantitative
Rf	Retention factor
ROESY	Rotating frame NOE spectroscopy
r.t.	Room temperature
s	Seconds
SD	Stochastic dynamics
SPECT	Single-photon Emission Computed Tomography
SPPS	Solid phase peptide synthesis
SQUID	Superconducting quantum interference device
TEA	Triethyl amine
TIS	Triisopropylsilane
TBTU	*O*-(Benzotriazol-1-yl)-*N,N,N',N'*-tetramethyluronium tetrafluoroborate
*t*Bu	*tert*-butyl
TFA	Trifluoroacetic acid
THF	Tatrahydrofurane
TOCSY	Total correlation spectroscopy
tol	Toluene
TEM	Transmission electron microscopy
TLC	Thin-layer chromatography
TMS	Tetramethylsilane
UV	Ultraviolet spectroscopy
VN	Vitronectin
vWf	von Willebrand factor
XRD	X-ray diffraction
β-Acc	β-aminocyclopropanecarboxylic acid
β-ACPC	β-aminocyclopentanecarboxylic acid
δ	Chemical shift

Amino acids

Amino acid	Three-letter code	One-letter code
Alanine	Ala	A
Arginine	Arg	R
Asparagine	Asn	N
Aspartic acid	Asp	D
Cysteine	Cys	C
Glutamine	Gln	Q
Glutamic acid	Glu	E
Glycine	Gly	G
Histidine	His	H
Isoleucine	Ile	I
Leucine	Leu	L
Lysine	Lys	K
Methionine	Met	M
Phenylalanine	Phe	F
Proline	Pro	P
Serine	Ser	S
Threonine	Thr	T
Tryptophan	Trp	W
Tyrosine	Tyr	Y
Valine	Val	V
***iso*Aspartic acid**	*iso*Asp	*i*D

D-amino acids are described by D-Xaa in the three-letter code and with the small letter in the one-letter code. Where no indication is present, amino acids have to be intended as L-amino acids.

Acknowledgements

I would like to thank all the people who, during my whole PhD, contributed directly or indirectly to my growth as a person and also a chemist.

First, I sincerely acknowledge my supervisor Professor Umberto Piarulli for giving me the possibility of participating in this very interesting research topic, for the numerous opportunities, for the support and for all the teachings he offered to me during this period.

I would like to thank also Prof. Dr. Oliver Reiser for the chance to spend one year in his research group, for the teachings, and for the opportunities he gave me when I was in Regensburg.

I express my gratitude to the examiners, for having accepted to take part in the jury of my PhD thesis defence.

I want to acknowledge all the people at the University of Milan, at the CNR of Milan, at the University of Pavia, and at the University of Regensburg who contributed experimental data (NMR studies, conformational studies, binding tests, cell studies, mass spectrometry analysis, elemental analysis, and SQUID measurements) to my work.

I would like to express my very special thanks to all the Prof. Piarulli's research group current members, all the people who worked in the group in the past three years, and all the friends I met at the University in Como during my PhD. Thanks for the help, the advices, the fun and the time we spent together.

I owe a debt of gratitude to the whole Prof. Reiser's research group, especially my labmates and people with whom I directly collaborated on the two projects I developed in Regensburg.

Thank you very much also to all the European co-workers in the Mag(net)icFun Network and to all the people involved in the network.

Prof. Gennari's group past and current PhD students at the University of Milan who helped me in these years, especially people with whom I directly collaborated on my work, deserve my thanks too.

Last but not least, heart-felt thanks to my whole family and to Alessandro. Thanks for the support, the understanding, and the helpfulness that you proved me in these three years, especially in the more difficult moments. A warm thanks is certainly not enough compared to the love you displayed me, but it is really impossible to express in words my gratitude.